SUB-ARCTIC HYDROLOGY AND CLIMATE CHANGE
A CASE STUDY OF THE TANA RIVER BASIN
IN NORTHERN FENNOSCANDIA

SUBARCTISCHE HYDROLOGIE EN KLIMAATSVERANDERINGEN
EEN STUDIE IN HET STROOMGEBIED VAN DE TANA RIVIER
IN HET NOORDEN VAN FENNOSCANDIË

(met een samenvatting in het Nederlands)

PROEFSCHRIFT

ter verkrijging van de graad van doctor aan de Universiteit Utrecht op
gezag van de Rector Magnificus, Prof. dr. W. H. Gispen, ingevolge
het besluit van het College voor Promoties in het openbaar te
verdedigen op vrijdag 27 september 2002 des middags te 2:30 uur

door

Rutger Dankers

Geboren op 24 juli 1973 te Tilburg

Sub-arctic hydrology and climate change

"Als mijn proefschrift klaar is, zal er met geen woord gewag worden gemaakt van ontvelde schouders, geschaafde knieën, de beukende hoofdpijn, de muggen en de vleesetende vliegen."
W.F. Hermans: Nooit meer slapen.

"A lot of people like snow. I find it to be an unnecessary freezing of water."
Carl Reiner

CONTENTS

FIGURES

14

TABLES

16

VOORWOORD / PREFACE

" 's Winters sneeuw en 's zomers dichte wolken muggen." Zo omschreef W.F. Hermans het leven in het noordelijkste stukje van Scandinavië in zijn boek *Nooit meer slapen*. Lapland is in de ogen van veel mensen een land van extremen, woest, onherbergzaam en verlaten, in veel opzichten het tegenovergestelde van Nederland. Toch is dat maar gedeeltelijk waar: in feite is Noord-Scandinavië het meest toegankelijke en dichtstbevolkte gebied boven de poolcirkel, waar zelfs de mobiele telefoon het gewoon blijft doen, en je via internet op de hoogte kunt blijven van het weer in eigen land. Maar ook op andere manieren doet de westerse wereld zijn invloed gelden op deze "laatste wildernis van Europa". Klimaatsveranderingen, zoals die voorspeld worden voor de komende eeuw, en die het gevolg zijn van de uitstoot van fossiele brandstoffen, kunnen juist in dit soort gebieden grote gevolgen hebben. Veranderingen in temperatuur en neerslag zullen direct van invloed zijn op de duur van de sneeuwbedekking, en – wie weet? – ook op het aantal muggen in de zomer. Dit alles maakt het meer dan de moeite waard om het soort onderzoek te doen dat in dit proefschrift beschreven staat. Maar bovenal is Noord-Lapland een fascinerend gebied om onderzoek in te doen, vanwege de rust, de midzomernachtzon, de regen en sneeuw, de hitte en de kou. Net zo goed is het fascinerend om achter je pc in Utrecht via een reeks van satellietbeelden het verdwijnen van de sneeuw uit Scandinavië te kunnen volgen. Ik ben dan ook dankbaar voor de afgelopen jaren waarin ik met veel plezier aan dit proefschrift heb gewerkt.

Veel dank ben ik verschuldigd aan mijn promotoren Ward Koster ("jouw onderzoek heeft als geheel een onderkoelde toon") en Steven de Jong ("schrijf eens wat positiever man!"), en co-promotor Hans Middelkoop (op wiens gezag woorden als "rather", "quite", "fairly" en "reasonably" uit het manuscript zijn geschrapt). Bedankt voor jullie steun en vertrouwen, en de goede ideeën die jullie hebben aangedragen.

Furthermore, I am very much indebted to Richard Harding from the Centre of Ecology and Hydrology (Wallingford, UK) and his co-workers (especially Nick Jackson), as well as Seppo Neuvonen, the staff and supporting personnel of the Kevo Subarctic Research Institute (University of Turku, Finland). Without you much of the work presented here would not have been possible. I am not only grateful for all the data you shared with me, and the logistic support during the field campaigns in Northern Finland, but above all for your pleasant and inspiring cooperation, which I hope we can continue in the future. Seppo, I want to thank you in particular for your hospitality, your culinary efforts, and the trips in the surroundings of Kevo. The climate model data were provided by Ole Bøssing Christensen from the Danish Climate Center / Danish Meteorological Institute. Ole, thank you for all the time you spent on me, and I hope you will make backups more often now. Hopefully we will meet each other in person some day! Also I would like to thank Susan Lee, Mikhail Kozlov and Tarmo Virtanen for their support, and Eeva Huitu for the useful discussions, especially those that were not related to Skalluvaara. Hannu Nykänen and Juha Heikkinen and their co-workers from the University of Kuopio were very helpful by putting the data of their weather station from 2000 at my disposal.

18

1 INTRODUCTION: CLIMATE CHANGE AND HYDROLOGY IN SUB-ARCTIC ENVIRONMENTS

1.1 Climate change at high latitudes

Already in 1896 the Swedish chemist and Nobel Laureate Arrhenius was one of the first scientists to realise that combustion of fossil fuels will increase the level of carbon dioxide (CO_2) in the atmosphere, and that this may lead to a global warming of several degrees. Nowadays, more than a century later, there is general consensus among scientists that, due to this so-called enhanced greenhouse effect, global average temperatures could rise by more than 5°C by the end of the 21st century. Over the past century, the global average surface temperature has already increased by about 0.6 degrees (Houghton et al., 2001). The 1990s have been the warmest decade since the beginning of the record in 1860, and 1998 has probably been the warmest year of the last millennium (Jones et al., 1998; Hulme, 1999). Magnuson et al. (2000) analysed historical records on the dates of freezing and thawing of rivers and lakes around the Northern Hemisphere, and found a trend toward later freezing and earlier breakup dates over the last 150 years, corresponding to an increase in air temperature of 1.2°C per 100 years. However, due to the natural variability in climate it is difficult to attribute these changes unambiguously to human influence. In 1995, the Intergovernmental Panel on Climate Change (IPCC) concluded that: "the balance of evidence suggests a discernible human influence on global climate" (Houghton et al., 1996), which was confirmed again in 2001 (Houghton et al., 2001).

Predictions about future climate development by general circulation models (GCMs) are complicated due to uncertainties in the scenarios of emissions of CO_2 and other greenhouse gases, such as methane (CH_4) and nitrous oxide (N_2O). However, all emission scenarios adopted by the IPCC cause the global average temperature to rise when incorporated into various climate models. The projected increases in globally averaged surface temperatures range from 1.4 to 5.8°C for the period 1990-2100, but nearly all land areas are expected to warm more rapidly than the global average (Houghton et al., 2001). Furthermore, GCMs generally agree that warming will be most significant at northern high latitudes, particularly during the winter months. Previously, the degree of warming to be expected in the Arctic region had already been estimated to vary from 2-4°C in summer and 1-5°C in winter (Cattle & Crossley, 1995). The Arctic is therefore believed to be extremely vulnerable to projected changes in climate, and because of several feedback mechanisms, its response might be more rapid and more severe than in any other area of the world (Everett & Fitzharris, 1998).

Over the past century there has already been a trend towards higher temperatures in the Arctic, which was strongest over land areas in winter and spring (Chapman & Walsh, 1993). In winter this warming amounted to about 2°C in the last 100 years (Everett & Fitzharris, 1998), but there were considerable fluctuations (figure 1.1). In Scandinavia the first half of the 20th century was particularly warm, probably the warmest period of the
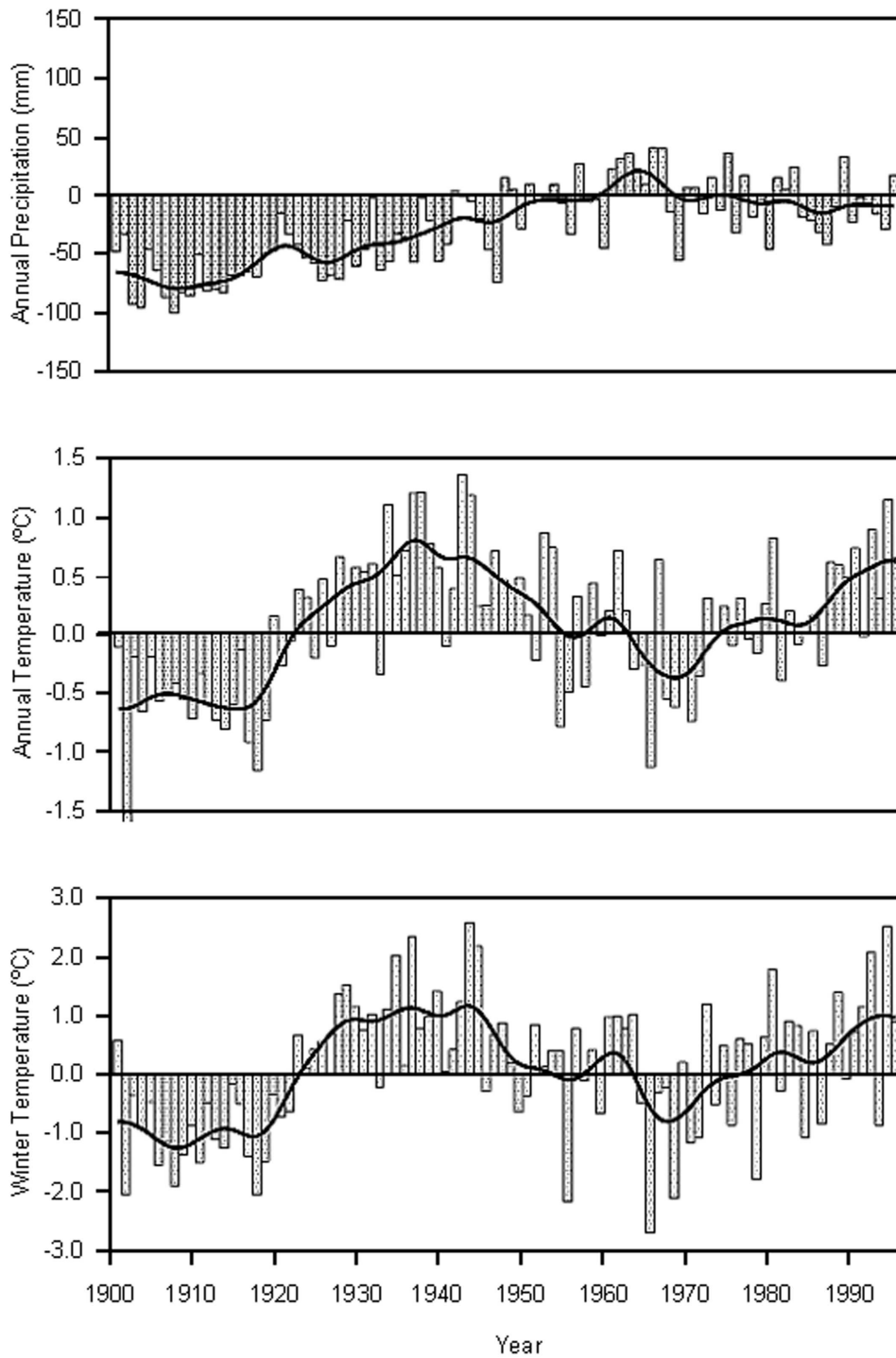
Figure 1.1 Anomalies in annual precipitation (above), mean annual temperature (middle) and winter temperature (below) in the Arctic region, relative to the means of 1961-1990. After Everett & Fitzharris (1998)

20

last millennium according to Timonen (1998), but little change or even a slight cooling has been observed since the 1960s (Jones & Briffa, 1992; Maxwell, 1997). Since 1990 there appears to be a current warming trend, mostly due to winter warming. A significant increase in precipitation has been observed as well in Finnish Lapland since 1879 (Lee et al., 2000).

A major implication of a rise in global temperature is most likely an intensification of the hydrological cycle (Houghton et al., 1992). A higher concentration of water vapour in the atmosphere will lead to an increase in precipitation, especially over northern mid- to high latitudes (Houghton et al., 2001). In the Arctic, changes in the extent and duration of the seasonal snow cover, depending on both temperature and precipitation, will have important consequences for the entire ecosystem. The presence of snow not only has a marked influence on the runoff regime of arctic and sub-arctic rivers, but also controls the length of the growing season for plants and lichens, the thermal regime and moisture conditions of the soil, and permafrost distribution (Koster, 1991). Coverage by snow furthermore affects the surface albedo, which controls the fraction of incident solar radiation that is reflected. Changes in the snow cover extent on the Northern Hemisphere therefore have a potential feedback effect on the global radiation budget, and, accordingly, on the global climate (Anisimov & Fitzharris, 2001). In summer, higher temperatures could result in higher evaporation rates, thereby increasing the risk of soil water stress and posing a threat to the existence of wetlands and shallow lakes. More precipitation in summer may however increase the soil moisture content, which in turn could stimulate plant growth (Callaghan et al., 1999). Changes in the discharge regime of arctic rivers will furthermore affect the formation of sea ice and the freshwater balance of the Arctic Ocean, which, because of its influence on the thermohaline circulation in the Atlantic, could have a profound impact on the global climate (Lewis et al., 2000). Because of this key role of hydrological processes in northern environments, the impact of climate change on arctic and sub-arctic hydrology needs to be studied in detail.

1.2   Studying the impact of climate change on hydrology

Predictions of future climate are usually based on GCMs that operate on a global, hemispheric or continental scale. In contrast, the focus of hydrological impact studies is usually on the local and regional consequences of climate changes. Unfortunately, the accuracy of any GCM output decreases at increasingly finer spatial scales, which is largely related to model resolution (Hostetler, 1994; Xu, 1999). A further problem is that the representation of hydrological processes in GCMs is simplistic and often incomplete as the lateral transfer of water on land is usually ignored (Kite et al., 1994). Studies that use GCMs directly to simulate river discharge generally show large discrepancies between simulated and observed annual or seasonal runoff (e.g. Kuhl & Miller, 1992; Miller & Russell, 1992; Van Blarcum et al., 1995). Regional climate models (RCMs) operate on a higher spatial resolution than GCMs, and may therefore be used to simulate changes in climate and hydrology at sub-continental scale, for example over the entire Fennoscandian region (e.g. SMHI, 1998). However, at present the grid size of RCMs is still too coarse to take account of the local and regional variability in hydrological

processes. Moreover, since they are usually driven by global models, the water balance of RCMs may not be any better.

As climate models are presently not able to give reliable estimates of the hydrological responses to climatic changes, most studies use hydrological models instead. In the past decades a wide range of hydrological models has been used to assess the impact of climate change on a variety of water resources. At sub-continental scales, or the scale of large drainage basins, conceptual water balance models are often believed to be appropriate (e.g. Kwadijk, 1993; Arnell, 1996, 1999). In terms of data demands, accuracy, flexibility and ease of use they offer significant advantages over process-based distributed parameter models (Gleick, 1986). Despite their simplicity, conceptual water balance models are generally capable of simulating river discharge reasonably well. However, the equations used in water balance models are often empirical, and based on relationships derived for current climate conditions. In exploring the consequences of changing environmental conditions, it is better to use physical descriptions of the processes involved in the transformation of precipitation into evaporation and runoff, such as snowmelt, interception, infiltration, and surface and groundwater flow. The applicability of so-called physically-based models is however limited by the availability and the quality of the input data that are required to run these models at the appropriate spatial and temporal resolution (Arnell, 1996). Moreover, most of their equations are based on small-scale[1] physics of homogeneous systems, and their application to heterogeneous catchments can be questioned (Beven, 1989). In practice, most physically-based models are lumped-conceptual models using effective parameter values at the grid scale (Beven, 1989).

Since data availability constrains the complexity of the model that can be applied, especially at larger scales, hydrological modellers have looked for strategies to deal with the major problems of data scarcity and relying on empirical relationships in climate change studies. Much attention has been paid to aggregation and disaggregation techniques (see for example Blöschl & Sivapalan, 1995), but in reality even a minimum of information required for reliable upscaling of, for example, meteorological observations to an entire river basin, may not be available. An alternative approach is to use regional meteorological or climate models (RCMs) as a data source for physically-based algorithms, such as full energy balance models of snowmelt (Melloh, 1999). Using the output of climate models as input in hydrological models has already proven to be successful in very large drainage basins, such as the Mackenzie Basin in Northwestern Canada (e.g. Kite & Haberlandt, 1999).

Most studies on the impacts of climate change in northern environments considered snow coverage, snowmelt and evapotranspiration in a lumped or semi-distributed way (e.g. Vehviläinen & Lohvansuu, 1991; Van Blarcum et al., 1995). Considering the importance of these processes for the entire arctic and sub-arctic ecosystem, hydrological impact studies should however not only concentrate on streamflow. Changes in the spatial and temporal distribution of snow coverage and evapotranspiration are important issues, that need to be addressed as well. Mostly, hydrological models are only validated with river discharge data, but a correct simulation of runoff at the catchment outlet, does not

22

necessarily imply that the spatial processes within the catchment are simulated correctly. In other words: a model may seem to work, but it may do so for the wrong reasons (Blöschl, 2001). Otherwise, if the spatial patterns in state variables, such as snow cover, are simulated correctly, the credibility of the model grows and the confidence in the results increases, also under different conditions. Spatial validation is therefore essential for any distributed model, and satellite sensors offer great potential in gathering the spatially distributed information required for this task.

1.3   Application of remote sensing in hydrological modelling

Remote sensing techniques have since long been identified as a useful and promising source of information for hydrological modelling. This is mainly because of the ability to provide spatially distributed data, rather than point measurements. In addition, there is a potential to measure hydrological variables that cannot be measured with conventional techniques, and to obtain global-wide data at a regular basis, even for remote regions (Engman, 1996). Remotely sensed data are especially believed to be appropriate for application in snow studies. However, hydrological variables such as snow water equivalent, snow depth, or evapotranspiration, are generally not measured directly by satellite or airborne sensors, and can only be estimated by relating them to vegetation properties, or by adopting certain algorithms. These are often highly empirical, and may not be applicable outside the range or extent for which they were developed. Further limitations may arise from the presence of clouds or vegetation, that may obscure the property of interest.

For these reasons, most applications of remote sensing data, particularly from sensors in the visible and near-infrared parts of the electromagnetic spectrum, concentrate on vegetation and snow cover extent (Kite & Pietroniro, 1996). Since 1998, several sensors have been launched that make observations in mid-infrared, which allows easy discrimination between clouds and snow. Moreover, because of their moderate spatial resolution of 1 km, these sensors are able to provide images of the global surface essentially on a daily basis. The data collected by these satellites may be very useful in observing and monitoring spatial patterns in snow coverage, but require straightforward and reliable algorithms for snow mapping. Several techniques have already been proposed for snow mapping in images of the Moderate Resolution Imaging Spectroradiometer (MODIS) (e.g. Hall et al., 1995), but it remains uncertain whether these apply to data from other sensors as well. Moreover, the performance of these techniques during snowmelt, when parts of the surface become snow-free, still needs to be assessed.

1.4 Climate change and hydrology in Northern Fennoscandia

The arctic and sub-arctic regions of Northern Europe belong to the last wilderness areas of the continent (Callaghan et al., 1999), and possess unique environmental values and natural beauty. The economic potential mainly consists of rich natural resources such as

natural gas and oil, mineral deposits, forestry and rich fishing grounds in the Barents Sea, while reindeer husbandry is still of importance for the indigenous Saami people. Climate change and anthropogenic perturbation are a potential threat to the fragile ecosystems, and can have serious consequences for the economy, social structure and culture of this region. The consequences of global change for the Barents Sea Region were investigated in the Barents Sea Impact Study (BASIS), a EU-funded research project that formed the onset of the present study.

This thesis discusses the potential impacts of human-induced climatic changes on the hydrology and water resources in Northern Fennoscandia (i.e. Scandinavia and Finland), more specifically in the drainage basin of the Tana River (in Finnish: Tenojoki), in northernmost Finland and Norway (see figure 1.2). The Tana is one of the largest rivers in Northern Fennoscandia that flows into the Barents Sea. In climate and vegetation the area belongs to the circumpolar sub-arctic zone. Although smaller than true macroscale river basins such as the Pechora in European Russia, the Ob, Yenisei and Lena in Siberia, and the Yukon and Mackenzie in North America, the catchment size of 16,000 km^2 implies a major challenge. The location in northernmost Finland and Norway leads to several advantages in accessibility and data availability over comparable drainage basins in Russia or North America. A more detailed description of the Tana river basin is given in chapter 2.

1.4.1   *Research objectives*

The main objective of this study is to assess the sensitivity of the hydrological system of the Tana River Basin to human-induced climatic changes. Because of their importance in sub-arctic hydrology and ecology, this study concentrates on snow coverage, snowmelt, and evapotranspiration, in addition to river discharge.

The following research objectives ensue from this major goal:
* To analyse current water balance characteristics and identify relevant hydrological processes in the Tana Basin, at both small and large scales.
* To monitor the spatial and temporal dynamics of snow cover with remote sensing techniques.
* To develop a physically-based hydrological model that is able to simulate spatial distributions in snow coverage and evapotranspiration in the Tana Basin, in addition to runoff
* To assess the impact of climate change scenarios on the water balance of the Tana Basin.

1.4.2   *Research questions*

The main objectives of this thesis were furthermore specified by formulating a number of research questions. These questions are discussed below:
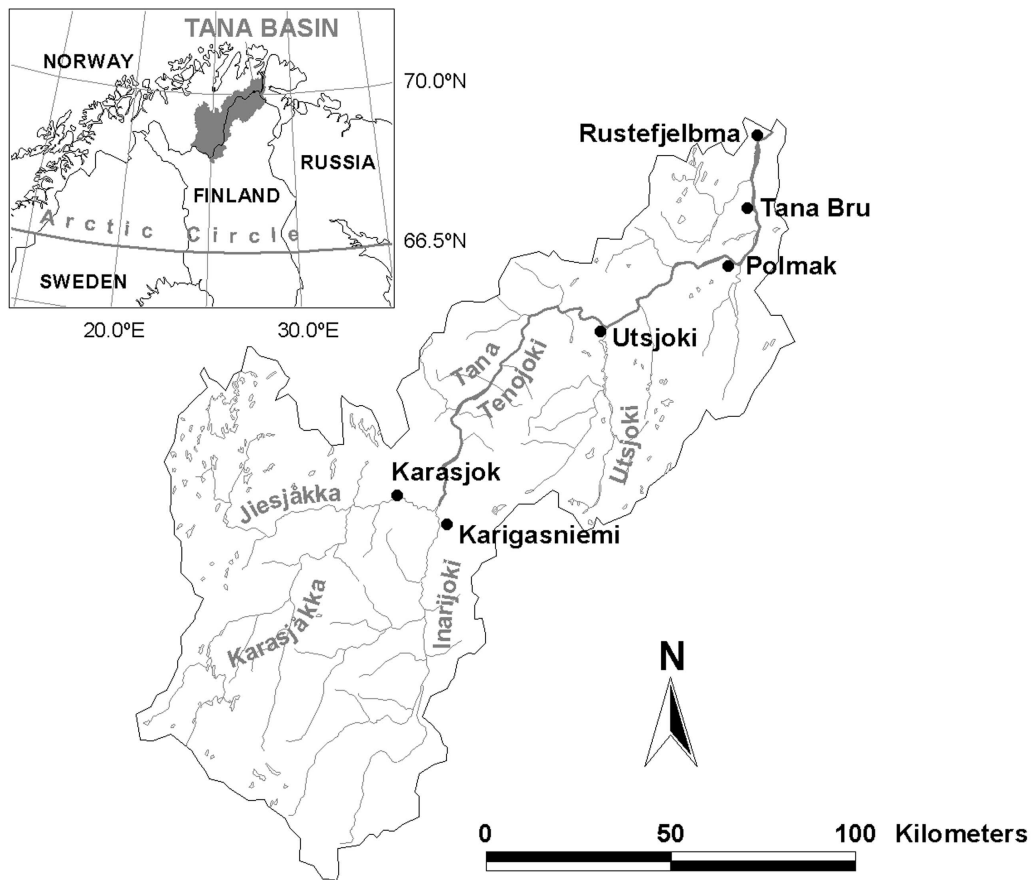
Figure 1.2 Location of the Tana River Basin in Northern Fennoscandia

1   *What trends have been observed in the water balance of the Tana Basin over the past century?*
In the Tana Basin, temperature and precipitation have been monitored since 1876, and river discharge 1911. Analysis of these long-term records may give a first indication of the sensitivity the discharge of the Tana River to changes in climate.

2   *What are the important hydrological processes in this sub-arctic environment?*
Hydrological processes in arctic and sub-arctic regions differ in intensity, magnitude and significance from more temperate environments (Mackay & Løken, 1974). Which processes dominate the hydrology of the Tana Basin in winter, spring and summer?

25

3   *What are the potentials and limitations of remote sensing techniques in*
           monitoring snow cover dynamics in this area?
           Since 1998 several satellite sensors have been launched that provide the
           opportunity to monitor snow cover dynamics at large-scale with short time
           intervals. In which way is it possible to infer the spatial and temporal
           distribution of snow from the data collected by these satellites, and what is the
           accuracy of this method?

4   *What are the spatial patterns in snow coverage and snowmelt in the Tana Basin*
           at the end of the winter?
           Observations on snow coverage are usually only available at a limited number of
           points, which give little information on the spatial patterns of snow cover
           depletion. If remote sensing techniques can be used to assess large-scale snow
           cover dynamics, what are the spatial patterns that can be discerned?

5   *Can a simple water balance modelling approach be used to simulate the water*
           balance of the Tana Basin, including the spatial patterns in snowmelt?
           Conceptual water balance have been successfully applied to large drainage
           basins, but most models are developed for temperate conditions. What is the
           performance of such a model in the sub-arctic Tana Basin? What is more, are
           these models capable to simulate the spatial patterns in snow cover depletion?

6   *Is it possible to improve the physical basis and generic character of such a*
           model, by using RCM data as an alternative source of model input?
           The empirical nature of many large-scale hydrological models is a fundamental
           problem if they are applied to different conditions than for which they were
           calibrated. Is it possible to adopt more physical process formulations and thereby
           improve the generic character of such a model, by combining meteorological
           observations, as far as available, with RCM data as input into the model?

7   *What are the differences between a simpler, conceptual water balance model,*
           and an advanced, physically-based model, in sensitivity to changes in climate?
           Theoretically, a physically-based model should retain its validity when applied
           to different climate conditions. However, does the use of such a model result in
           significantly different outcomes, compared with more empirical conceptual
           models, when analysing the sensitivity to climate change?

8   *What are the consequences of climate change for water balance components in*
           the Tana Basin?
           Once a hydrological model is able to describe the hydrological behaviour of the
           Tana Basin accurately and in sufficient detail, it can be used to assess the
           impacts of climate change by adopting climate scenarios. What are the
           consequences for snow cover dynamics, evapotranspiration and water
           availability, and runoff in the Tana Basin?

26

1.4.3   Outline

This thesis addresses the research questions mentioned above in a series of studies. Central in the approach is a large-scale hydrological model of the Tana Basin. Development and application of this model involved four steps:

1   First of all, the hydrological behaviour of the Tana Basin was analysed, at both small and large scales, using field measurements and satellite observations.
2   Subsequently an existing water balance model, developed for the River Rhine (Kwadijk, 1993), was applied to the Tana Basin and the model performance evaluated in order to identify areas for improvement.
3   Using physically-based process formulations of snowmelt and evapotranspiration it was tried to improve the generic character of the model, and to simulate the spatial and temporal distribution of these water balance components realistically.
4   Finally, this model, now suitable for sub-arctic conditions, was used to simulate the hydrological behaviour of the Tana Basin under scenarios of climate change.

The first step is described in chapters 2 to 4 of this thesis. Chapter 2 analyses datasets on hydrology and catchment characteristics of the Tana Basin, and identifies uncertainties and gaps in our knowledge of the water balance of sub-arctic catchments. A detailed analysis of the hydrological processes in the area, based on field observations in a small sub-catchment of the Tana Basin, is given in chapter 3. On a much larger scale, snow cover dynamics in the Tana Basin are monitored in chapter 4 by using satellite observations.

The second step mentioned above, concerning the first application of an existing water balance model to the Tana Basin, is described in chapters 5 and 6. Model performance is evaluated in chapter 5, while in chapter 6 the results are validated with satellite observations on snow cover depletion. Also in chapter 6, a first analysis is made of the sensitivity of the water balance to climate change. Chapter 7 describes the physically based algorithms of snow and evapotranspiration that were introduced in the water balance model. Meteorological observations on temperature and precipitation were combined with data from a RCM to run these algorithms. Finally, the impact of climate change on the hydrology of the Tana River Basin is assessed in chapter 8, by incorporating scenarios of climate change produced by a RCM into the hydrological model of chapter 7. The results of these studies are evaluated in chapter 9.

1.5   References

Anisimov, O. & B. Fitzharris (2001): Polar Regions (Arctic and Antarctic). In: J.J. McCarthy, O.F. Canziani, N.A. Leary, D.J. Dokken & K.S. White (eds.): Climate Change 2001: Impacts, Adaptation and Vulnerability. Cambridge: Cambridge University Press, pp. 801-841.
Arnell, N.W. (1996): Global warming, river flows and water resources. Chichester: Wiley.

Arnell, N.W. (1999): A simple water balance model for the simulation of streamflow over a large geographic domain. Journal of Hydrology 217, pp. 314-335.

Arrhenius, S. (1896): On the influence of carbonic acid in the air upon the temperature on the ground. Philosophical Magazine 41, pp. 237.

Beven, K. (1989): Changing ideas in hydrology - the case of physically based models. Journal of Hydrology 105, pp. 157-172.

Blöschl, G. (2001): Scaling in hydrology. Hydrological Processes 15, pp. 709-711.

Blöschl, G. & M. Sivapalan (1995): Scale issues in hydrological modelling: a review. In: J.D. Kalma & M. Sivapalan (eds.): Scale issues in hydrological modelling, advances in hydrological processes. Chichester: Wiley, pp. 9-48.

Callaghan, T.V., C. Körner, O.W. Heal, S.E. Lee & J.H.C. Cornelissen (1999): Global Change in Europe's cold regions: Scenarios for ecosystem responses to global change. In: M.A. Lange, B. Bartling & K. Grosfeld (eds.): Global Changes and the Barents Regions (Proceedings of the First International Basis Research Conference, St. Petersburg, Russia, February 22-25, 1998). Münster: Institute for Geophysics, University of Münster, pp. 17-50.

Cattle, H. & J. Crossley (1995): Modelling Arctic climate change. Philosophical transactions / Royal Society of London, Series A, Physical Sciences and Engineering 352, pp. 201-212.

Chapman, W.L. & J.E. Walsh (1993): Recent variations of sea ice and air temperature in high latitudes. Bulletin of the American Meteorological Society 74, pp. 33-47.

Engman, E.T. (1996): Remote sensing applications to hydrology: future impact. Hydrological Sciences Journal 41, pp. 637-647.

Everett, J.T. & B.B. Fitzharris (1998): The Arctic and Antarctic. In: R.T. Watson, M.C. Zinyowera & R.H. Moss (eds.): The regional impacts of climate change: an assessment of vulnerability (Special report of IPCC Working Group II). Cambridge: Cambridge University Press, pp. 85-103.

Gleick, P.H. (1986): Methods for evaluating the regional hydrologic impacts of global climatic changes. Journal of Hydrology 88, pp. 97-116.

Hall, D.K., G.A. Riggs & V.V. Solomonson (1995): Development of methods for mapping global snow cover using moderate resolution imaging spectroradiometer data. Remote Sensing of Environment 54, pp. 127-140.

Hostetler, S.W. (1994): Hydrologic and atmospheric models: the (continuing) problem of discordant scales. Climate Change 7, pp. 85-95.

Houghton, J.T., B.A. Callander & S.K. Varney (eds.) (1992): Climate Change 1992, The Supplementary Report to the IPCC Scientific Assessment. Cambridge: Cambridge University Press.

Houghton, J.T., L.G.M. Filho, B.A. Callander, N. Harris, A. Kattenberg & K. Maskell (eds.) (1996): Climate Change 1995: The Science of Climate Change. Cambride: Cambridge University Press.

Houghton, J. T., Y. Ding, D.J. Griggs, M. Noguer, P.J. van der Linden & D. Xiaosu (eds.) (2001): Climate Change 2001: The Scientific Basis. Cambridge: Cambridge University Press.

Hulme, M. (1999): Global Warming. Progress in Physical Geography 23, pp. 283-291.

Jones, P.D. & K.R. Briffa, (1992): Global surface air temperature variations during the twentieth century, 1. Spatial, temporal and seasonal detail. The Holocene 2, pp. 165-179.

Jones, P.D., K.R. Briffa, T.P. Barnett, & S.F.B. Tett (1998): High-resolution palaeoclimatic records for the last millennium: interpretation, integration and comparison with GCM control-run temperatures. The Holocene 8, pp. 455-471.

Kite, G.W. & A. Pietroniro (1996): Remote sensing applications in hydrological modelling. Hydrological Sciences Journal 41, pp. 563-591.

Kite, G.W. & U. Haberlandt (1999): Atmospheric model data for macroscale hydrology. Journal of Hydrology 217, pp. 303-313.

Kite, G.W., A. Dalton & K. Dion (1994): Simulation of streamflow in a macroscale watershed using general circulation model data. Water Resources Research 30, pp. 1547-1559.

Koster, E.A. (1991): Assessment of climate change impact in high-latitudinal regions. Terra 103, pp. 3-13.

Kuhl, S.C. & J.R. Miller (1992): Seasonal river runoff calculated from a global atmospheric model. Water Resources Research 28, pp. 2029-2039.

Kwadijk, J.C.J. (1993): The impact of climate change on the discharge of the River Rhine. Utrecht: Koninklijk Nederlands Aardrijkskundig Genootschap / Faculty of Geographical Sciences, University of Utrecht (Nederlandse Geografische Studies 171).

28

Lee, S.E., M.C. Press & J.A. Lee (2000): Observed climate variations during the last 100 years in Lapland, Northern Finland. International Journal of Climatology 20, pp. 329-346.

Lewis, E.L., E.P. Jones, P. Lemke, T.D. Prowse & P. Wadhams (eds.) (2000): The Freshwater Budget of the Arctic Ocean. Dordrecht, The Netherlands: Kluwer Academic Publishers.

Mackay, D.K. & O.H. Løken: Arctic Hydrology. In: J.D. Ives, & R.G. Barry (eds.): Arctic and Alpine Environments. London: Methuen, pp. 111-132.

Magnuson, J.J., D.M. Robertson, B.J. Benson, R.H. Wynne, D.M. Livingstone, T. Arai, R.A. Assel, R.G. Barry, V. Card, E. Kuusisto, N.G. Granin, T.D. Prowse, K.M. Stewart & V.S. Vuglinski (2000): Historical trends in lake and river ice cover in the northern hemisphere. Science 289, pp. 1743-1746.

Maxwell, B. (1997): Recent climate patterns in the Arctic. In: W.C. Oechel, T.V. Callaghan, T. Gilamnov, J.I. Holten, B. Maxwell, U. Molau U. & B. Sveinbjörnsson (eds.): Global Change and Arctic Terrestrial Ecosystems. New York: Springer (Ecological Studies 124), pp. 21-46.

Melloh, R.A. (1999): A synopsis and comparison of selected snowmelt algorithms. Hanover, New Hampshire, USA: US Army Corps of Engineers, Cold Regions Research & Engineering Laboratory (CRREL report 99-8).

Miller, J.R. & G.L. Russell (1992): The impact of global warming on river runoff. Journal of Geophysical Research 95, pp. 2757-2764.

SMHI (1998): Regional climate simulations for the Nordic region - First results from SWECLIM. Norrköping: Swedish Meteorological and Hydrological Institute.

Timonen, M (1998): Dendrochronological analysis at pine timberline. In: T. Tasanen (ed.): Research and management of the northern timberline region (Proceedings of the Gustav Sirén symposium in Wilderness Center Inari, September 4.-5. 1997). Helsinki: Metsäntutkimuslaitos (Finnish Forest Research Institute Research Papers 677), pp. 37-42.

Van Blarcum, S.C., J.R. Miller. & G.L. Russell (1995): High latitude runoff in a doubled CO_2 climate. Climate Change 30, pp. 7-26.

Vehviläinen, B. & J. Lohvansuu (1991): The effects of climate change on discharges and snow cover in Finland. Hydrological Sciences Journal 36, pp. 109-121.

Xu, C.-Y. (1999): From GCMs to river flow: a review of downscaling methods and hydrologic modelling approaches. Progress in Physical Geography 23, pp. 229-249.

1.6   Notes

[1] Throughout this thesis, the terms "small-scale" and "large-scale" will be used in their common meaning of referring to processes and models operating over small areas (i.e. field or plot scale), and over large areas (i.e. drainage basins), respectively; this in contrast to the cartographic denotation of the word "scale"

2 CLIMATE AND STREAMFLOW VARIABILITY IN THE TANA RIVER BASIN

2.1 Introduction

Changes in climate will ultimately affect river runoff. Since the last ice age climate in Northern Fennoscandia has fluctuated considerably. Paleoecological evidence suggests that during the mid Holocene (ca. 8000-5000 BP) summers were warmer and drier than today (Seppä & Hammarlund, 2000). There appears to be a general cooling trend throughout the rest of the Holocene, up to the 20th century (Eronen & Zetterberg, 1996; Seppä & Birks, 2002). Direct measurements on climate and discharge in Northern Fennoscandia are, however, only available for the last century. Lee et al. (2000) analysed data on temperature and precipitation for northern Lapland, and concluded that a significant warming occurred in the first half of the 20th century, while annual precipitation has increased since 1880. Few studies have analysed long-term trends in river discharge for northern Lapland. Hyvärinen & Leppäjärvi (1989) analysed observations on discharge in Finland, but could not find a clear trend for rivers in northern Lapland. Roald et al. (1997) reported a slight, though not significant, decreasing trend for rivers in northern Finland, Sweden and northeast Norway over the period 1930-1980. In this chapter, data series of temperature, precipitation and river discharge in the Tana Basin are analysed, in order to identify the variations in climate and hydrology that occurred over the past century. This analysis is preceded by a general description of the study area.

2.2 Study area

2.2.1 Location

The Tana River Basin is located in the northernmost part of Fennoscandia (i.e. Scandinavia and Finland, see figure 2.1), between 68º 28' and 70º 28' N and 23º 30' and 28º 30' E. The catchment area is approximately 16 000 km^2, of which 32 % belongs to Finland and the remaining 68 % to Norway (Mansikkaniemi, 1970). The Tana River (in Finnish Tenojoki) flows from the confluence of the Karasjåkka and Inarijoki rivers into the Tanafjord, and is one of the largest rivers in Scandinavia draining into the Barents sea. It drains an extensive upland area, including a large part of the Finnmarksvidda in Norway, and belongs to the sub-arctic zone of Fennoscandia.

2.2.2 Geology and topography

The Tana Basin is underlain by Precambrian bedrock, consisting mainly of granites, granulites, and various types of gneisses and schists. Eocambrian sedimentary rocks can be found in the northernmost part, consisting of siltstones, shales and sandstones

(Mansikkaniemi, 1970). Except for a few places the bedrock is covered with glacial tills, mainly deposited during the last glaciation (Weichselian), although in some areas deposits of pre-Weichselian age predominate (Olsen et al., 1996). Since the last glaciation extensive peat-bogs have been formed. Permafrost in Northern Fennoscandia is discontinuous, mainly occurring in palsa mires, and in bedrock on fell summits where it may reach a depth of several tens of meters (King & Seppälä, 1988; Seppälä, 1997, 1998; Kukkonen & Šafanda, 2001).

The topography of the upland area is generally smooth with gently sloping fells (treeless areas) and very flat summits (Seppälä & Rastas, 1980). This highland is cut through by several steep-sided fault valleys, such as the valleys of the Utsjoki and Tana, which are tectonic in origin (Mansikkaniemi, 1970). Although elevations are generally not higher than 500 m, some Norwegian mountain peaks in the northern part reach to just more than 1000 m above sea level. A digital elevation model of the Tana Basin, derived from the US Geological Survey (USGS) GTOPO30 global dataset (USGS, 2001), and a frequency distribution of the elevation classes, are shown in figure 2.2.
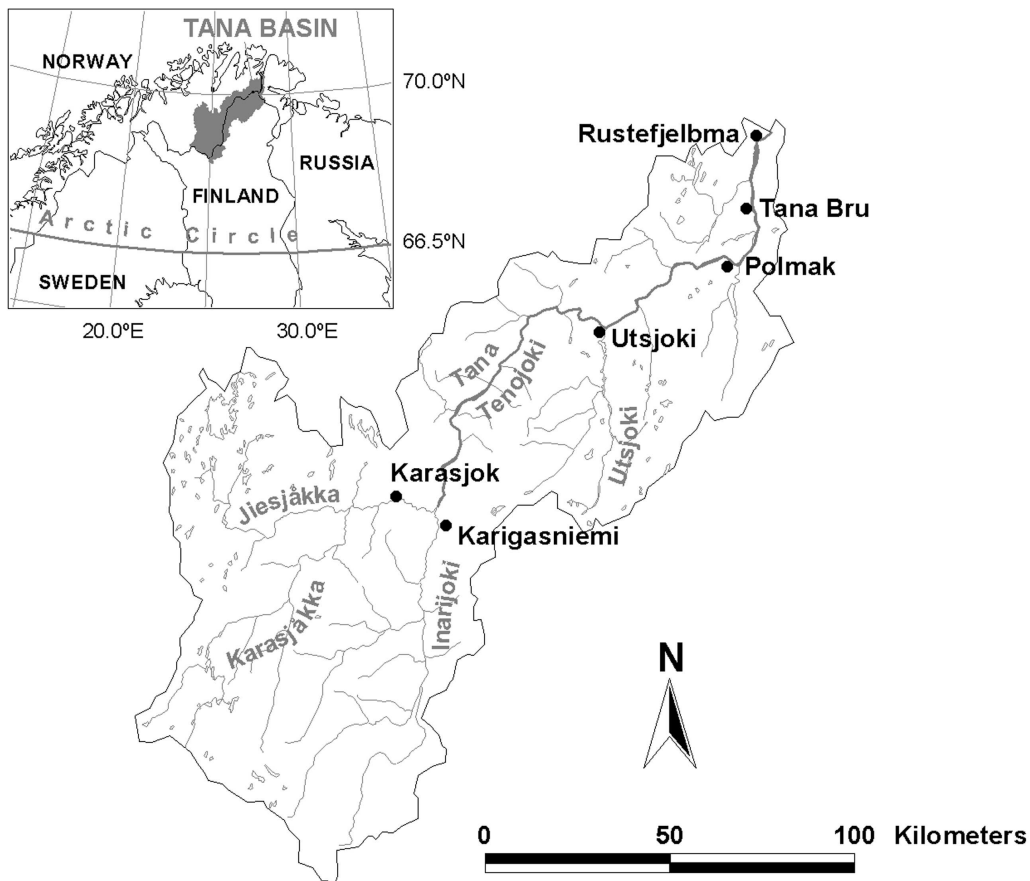
Figure 2.1 Location, topography and drainage network of the Tana River Basin

32

2.2.3   Climate

The climate of the Tana basin is influenced by the proximity of the Arctic Ocean and the Atlantic Gulf stream, and therefore relatively mild and maritime, considering its latitude. Several meteorological stations are located in and around the Tana basin, most of which have observation records since the 1950s or 1960s. These stations are listed in tables 2.1 and 2.2 (for locations see figure 2.3). Seasonal differences in temperature, precipitation and snow depth are illustrated in figure 2.4 for Karasjok, Norway. The climate of Kevo, Finland, has been described in more detail by Seppälä (1976). In the Köppen climate classification system this station belongs to the subpolar (Dfc) climates, with short, cool summers, severe winters, and no clear seasonality in precipitation. Polar tundra (ET) climates may be found at higher altitudes in the region (Seppälä, 1976).

Table 2.1 Mean annual temperatures for meteorological stations in and around the Tana basin

	Elevation	Mean annual temperature		Maximum annual temperature		Minimum annual temperature	
	m	ºC	period	ºC	period	ºC	
Rustefjelbma	9	-0.46	1957-1998	1.62	1990	-2.28	1971
Kevo (Finland)	107	-1.85	1962-1998	0.65	1974	-3.81	1966
Karasjok	129	-2.15	1957-1998	0.36	1974	-4.43	1966
Cuovddatmohkki	286	-2.46	1966-1998	-0.38	1974	-4.33	1985
Kautokeino	307	-2.54	1957-1970, 1996-1998	-0.52	1959	-4.83	1966
Kautokeino II	330	-1.79	1970-1996	-0.25	1989	-4.25	1985
Sihcajavri	382	-2.88	1957-1998	-0.76	1974	-5.10	1985

Annual precipitation is generally low for all weather stations, ranging from about 340-360 mm in Kautokeino (southwest of the Tana Basin) to 460 mm in Rustefjelbma in the northeast. There are significant differences between individual years, but in general the annual precipitation amount is not lower than 200 mm/year, or higher than 700 mm/year. Precipitation is usually highest in the summer months. However, it has long been recognised that gauge records in the Arctic may seriously underestimate actual precipitation amounts, especially in winter. Due to wind-induced undercatch, wetting and evaporation effects, measurement of snow using precipitation gauges has been shown to have systematic losses of up to 100 %, depending on gauge type and the observation site (Goodison et al., 1998; Yang et al., 2001).

Table 2.2 Mean annual precipitation for meteorological stations in and around the Tana basin.

	Elevation	Mean annual precipitation		Maximum annual precipitation		Minimum annual precipitation	
	m	mm	period	mm	year	mm	year
Rustefjelbma	9	459	1957-1998	600	1992	327	1980
Polmak	21	397	1968-1980	569	1975	291	1969
Sirbma	51	384	1968-1998	609	1992	210	1980
Skoganvarre II	74	424	1957-1997	586	1989	289	1969
Kevo (Finland)	107	407	1962-1998	582	1964	263	1980
Port	115	380	1981-1998	487	1982	289	1994
Karasjok	129	367	1957-1998	513	1964	252	1969
Valjok	132	444	1957-1998	681	1964	283	1969
Iskorasjohka	153	404	1974-1998	543	1982	308	1996
Jergol	230	362	1981-1998	484	1982	270	1994
Cuovddatmohkki	286	371	1966-1980, 1982-1998	494	1992	273	1986
Kautokeino II	307	361	1970-1996	497	1992	202	1980
Kautokeino	330	342	1957-1970	460	1961	226	1968
Mollesjohka	382	360	1974-1998	506	1992	248	1980
Sihcajavri	382	377	1957-1998	601	1957	199	1976
Jotkajavre	389	458	1957-1998	619	1959	320	1969

Mean annual temperatures range from -2.88 ℃ for Sihcajavri to slightly below 0 ℃ in Rustefjelbma, which is located close to the Tanafjord. Temperatures are usually below 0 ℃ from the middle of October until the end of May. Like in most sub-arctic environments, snowmelt in the Tana basin is usually a very rapid process. At Kevo, Finland, the depletion of the snow cover may amount to more than 20 cm of snow depth per day. Almost 50 % of the snow pack may disappear in only 10 days, and in 30 days on average 85 % of the snow pack is melted away. Most meteorological stations, usually located in the river valleys, become free of snow in May or occasionally in early June, but this can be several weeks later in the surrounding uplands.

2.2.4   Vegetation

In Northern Fennoscandia extensive forests of mountain birch (*Betula pubescens* ssp. *tortuosa*) extent beyond the arctic coniferous tree line. Most of the Tana basin therefore

(a)
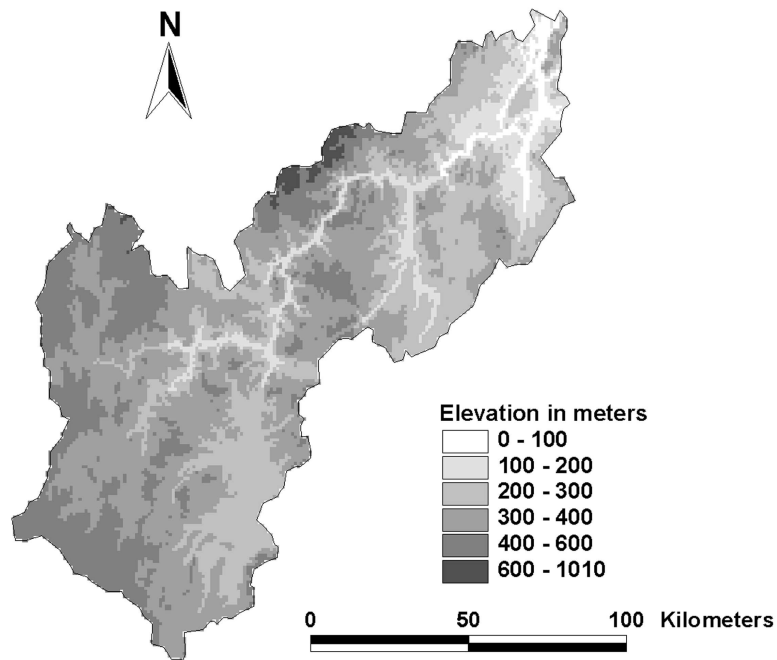
(b)
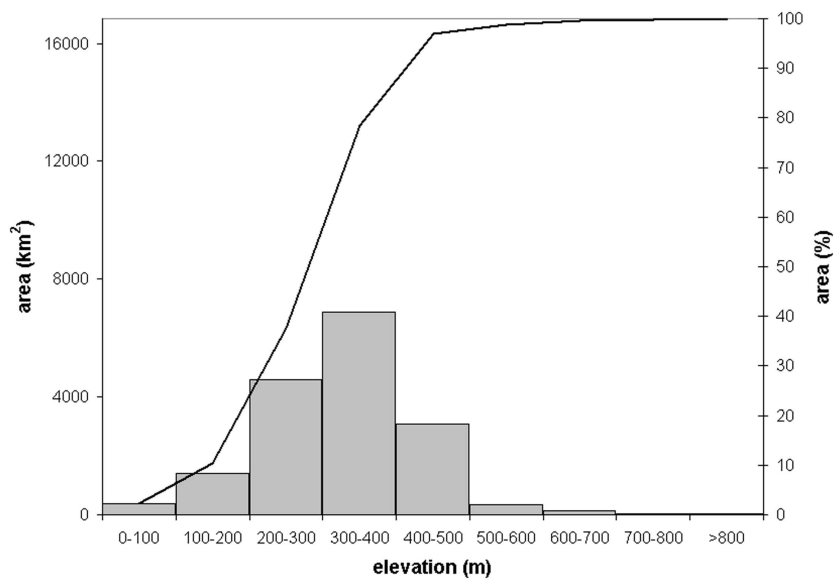
Figure 2.2 (a) Digital Elevation Model (DEM) of the Tana River Basin; (b) histogram and cumulative distribution of elevation classes. Data distributed by the EROS Data Center Distributed Active Archive Center (LP DAAC), located at the US Geological Survey's EROS Data Center in Sioux Falls, South Dakota, USA. See the appendix for a colour version

35
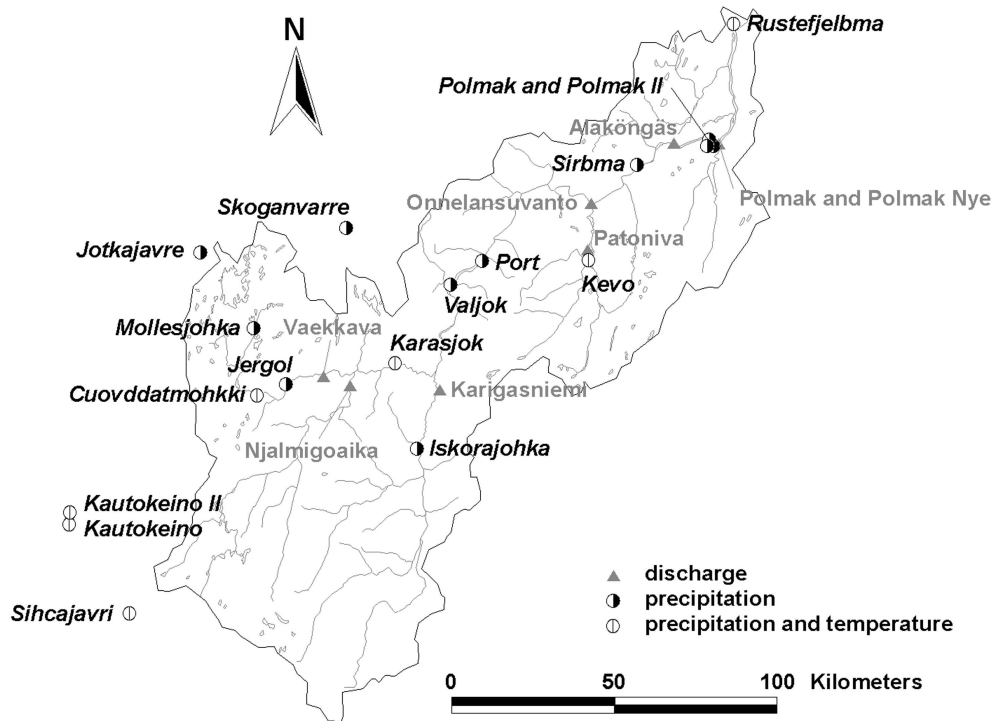
Figure 2.3 Meteorological and discharge stations in the Tana Basin

belongs to the sub-arctic deciduous birch zone (Hustich, 1961). Some isolated pine (*Pinus sylvestris*) forests can be found in the Inarijoki, Karasjåkka and Utsjoki valleys, which could be said to belong to the boreal coniferous region. Near the Arctic Ocean the upper limit of birch occurrence is only 20-30 m above sea level, but in the Karasjåkka valley the tree line is found at an altitude of nearly 400 m (Mansikkaniemi, 1970). Tundra heaths dominate the landscape above the birch forests; typical plant species here are *Betula nana*, *Empetrum hermaphroditum* and *Vaccinium myrtillus*. The highest fells and mountain tops are barren. Mires and peatlands in the area are characterised by willows (*Salix*), *Sphagnum*, and different grasses and sedges. Seppälä & Rastas (1980) distinguished a separate vegetation class for birch forests damaged by butterfly larvae of the geometrid *Oporinia autumnata*. Regular outbreaks of *Opirinia* are seen as one of the additional factors that determine the limits of birch occurrences. Human influence is believed to be insignificant (Mansikkaniemi, 1970). Some meadows and fields can be found in the main valleys, while in the rest of the area reindeer herding is the main land use.

A generalised vegetation map of the Tana basin is shown in figure 2.5. This map was made based on a Landsat TM satellite image of July 18th, 1987. This image was classified using field descriptions, collected during several field trips in 1999 and 2000. The classes resemble those of Seppälä & Rastas (1980). A mixed pine / birch class could

36

however not be discerned, as in mid-summer the spectral response of the fresh birch leaves is predominating the lower reflectivity of the pine trees. Spectral classes that could be separated include alpine heaths, block fields, sand and gravel, areas covered with reindeer lichens (which have a very characteristic, bright reflectance), and meadows in the river valleys. The classification procedure was complicated by several factors, such as shadowed steep valley slopes, the similar spectral response at pixel scale of pine forests and mires, and the high degree of mixing of vegetation species in the area, in particular of birch and pine trees. Nevertheless, it is believed that this map represents the general distribution of vegetation types in the Tana River Basin correctly.

2.2.5   River discharge

Mean annual runoff of the Tana River, as measured at Polmak, Norway, is 166 m^3/s. The interannual variability in discharge is high, ranging from 103 m^3/s (in 1941) to 269 m^3/s (1932). The stream flow regime of the Tana throughout the year (figure 2.6) is typical for rivers in sub-arctic environments. It is dominated by a high discharge peak in spring, caused by melting of the snow cover in combination with still frozen soils. Maximum runoff mostly occurs in the second half of May, but in some years it is delayed until late June. On average it amounts to 1304 m^3/s; the record stands for May 21, 1920, when 3844 m^3/s was measured. Snowmelt runoff may contribute as much as 65 % to the total annual discharge. During most of the summer discharge is steadily decreasing, interrupted by occasional rain storm peaks. In winter discharge is small, and the annual minimum, usually reached in April, is on average only 41 m^3/s.
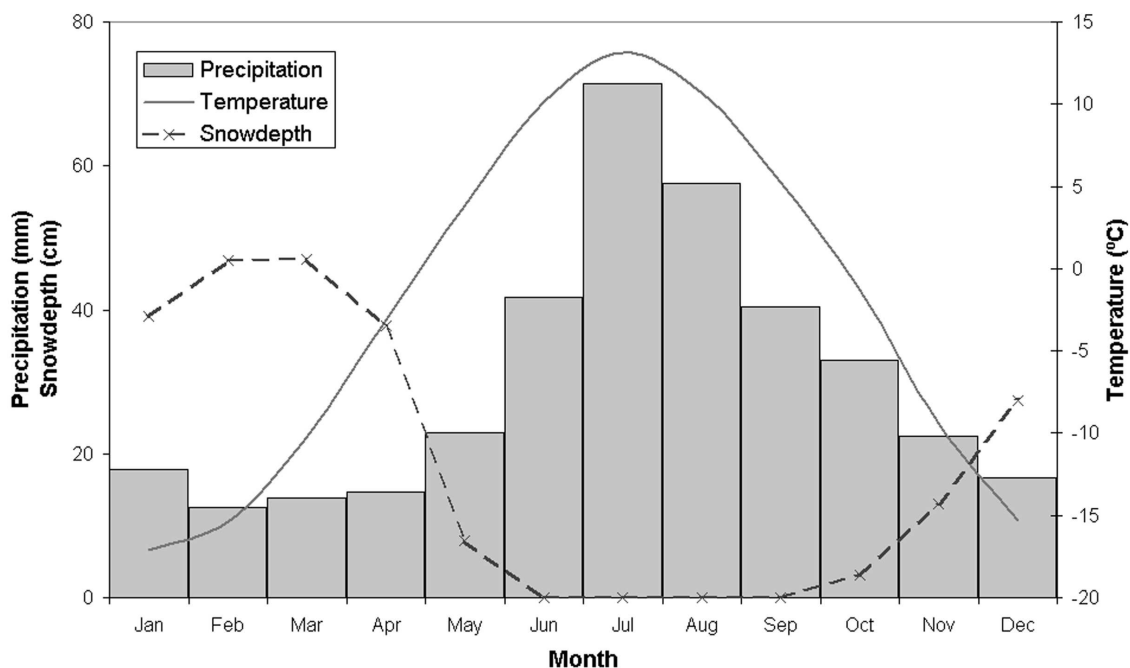
Figure 2.4 Monthly mean temperature, precipitation and snow depth in Karasjok, Norway, in 1961-1990
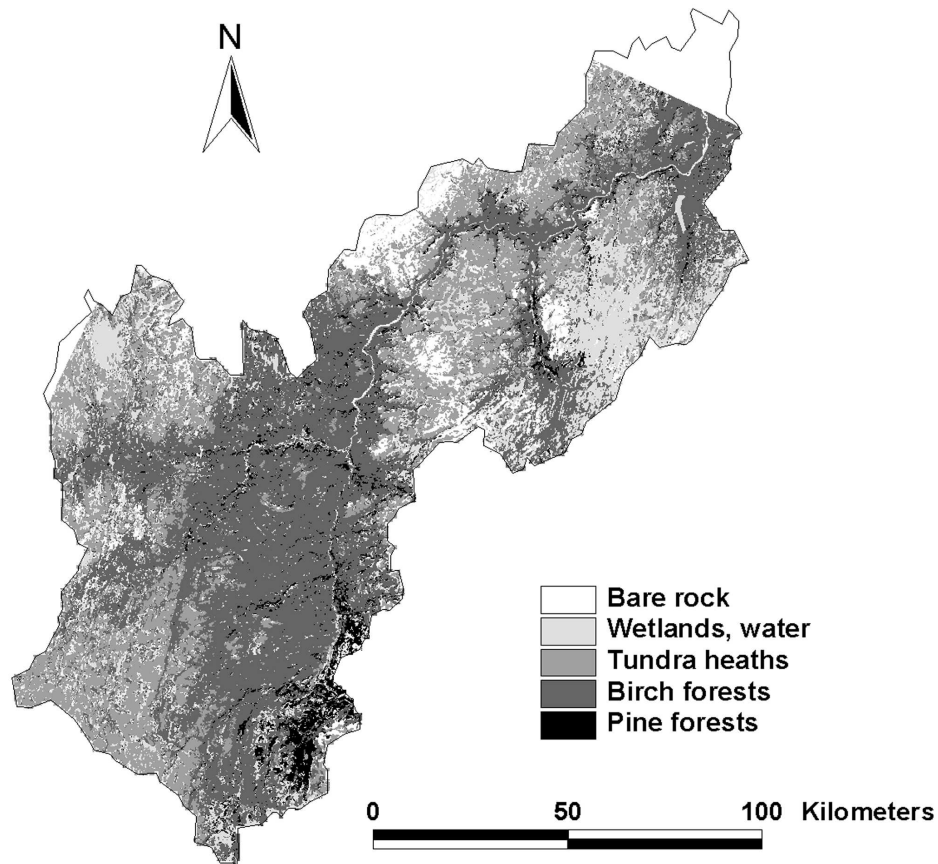
Figure 2.5 Generalised vegetation map of the Tana Basin, based on a Landsat TM image of 18 July 1987. For display purposes several classes have been grouped together. Please note that small parts of the Tana Basin in the north and west fall outside the image area. See the appendix for a colour version

2.3   Methodology

Discharge of the Tana River was observed at Polmak from 1911 to 1994, and in Karasjok temperature and precipitation have been recorded since 1870. These periods are considerably longer than in most sub-arctic river basins, and allow examination for trends over the last 100 years. The data of these stations were converted to annual values of hydrological years, starting in October, and were analysed for evidence of linear trends in precipitation, temperature and runoff over the period 1912-1993. In addition, separate trend lines were produced for years occurring in the first and in the second half of the century (i.e. 1912-1950 and 1951-1993). The data were furthermore analysed for trends in each (hydrological) season. Since all precipitation falling as snow accumulates during the winter, and is released in spring, temperature and precipitation in the winter season (defined here as October to April) were compared with river discharge in spring (April to June). Data from the summer season (July to September) were compared directly.

38
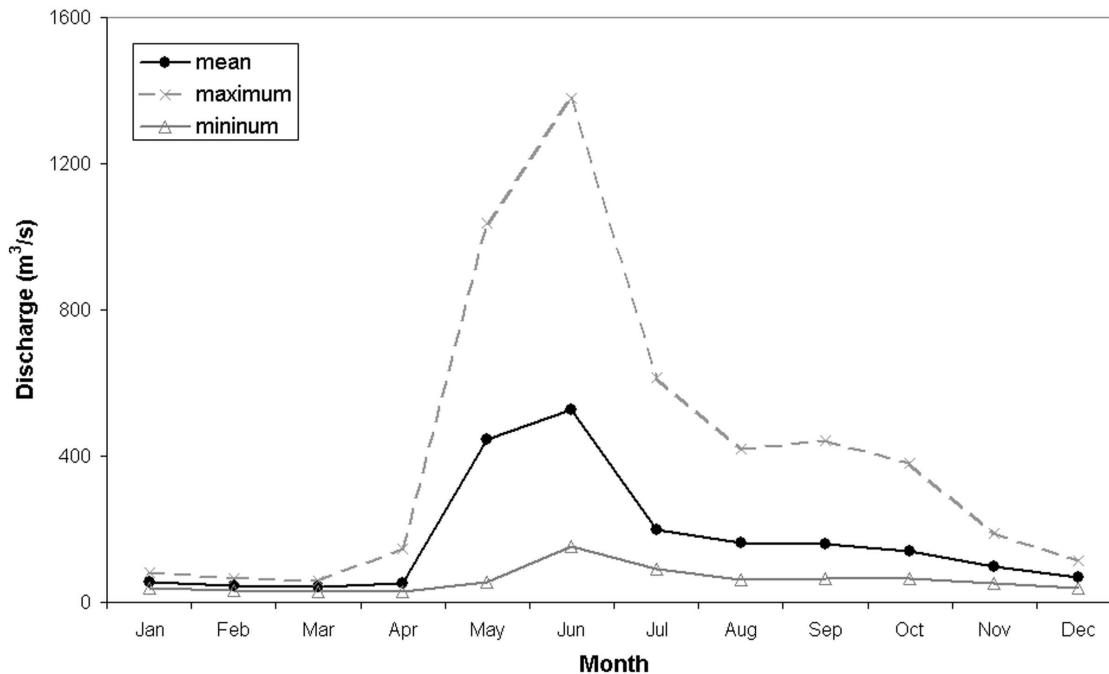
Figure 2.6 Monthly mean, maximum and minimum discharge of the Tana River at Polmak, Norway, in 1911-1992.

2.4   Results

The mean annual temperature in Karasjok in the period 1876-1999 is shown in figure 2.7, expressed as anomalies from the climate reference period 1961-1990. Figure 2.8 shows the anomalies in annual precipitation in the period 1902-1999. Between 1912 and 1993, precipitation at Karasjok increased significantly ($r = 0.35$, $p < 0.01$), corresponding to an average increase of about 1 mm per year (figure 2.9). Also the precipitation in winter ($r = 0.29$, $p < 0.01$) and summer ($r = 0.30$, $p < 0.01$) increased significantly between 1912 and 1993 (figures 2.10 and 2.11). Over the same period, there is no significant trend in annual temperature. However, in the first half of the century (1912-1950) there was a significant annual warming trend ($r = 0.43$, $p < 0.01$), as well as a significant trend in winter temperatures ($r = 0.33$, $p < 0.05$), with a maximum in the 1930s (figure 2.9). Although there was a slight positive trend in summer temperatures in the same period, it was not significant. The trends in seasonal and annual temperatures in the second half of the century were not significant as well.

Figure 2.9 also shows the mean annual discharge of the Tana River, expressed as anomalies from 1961-1990. Despite the increase in precipitation at Karasjok, there was no significant increasing trend in runoff at Polmak between 1912 and 1993. A significant decreasing trend occurred in the first half of the century ($r = 0.30$, $p < 0.1$), when a significant warming was found as well. Negative anomalies in discharge in the 1930s and 1940s correspond with lower precipitation totals in the same period, but this is not the
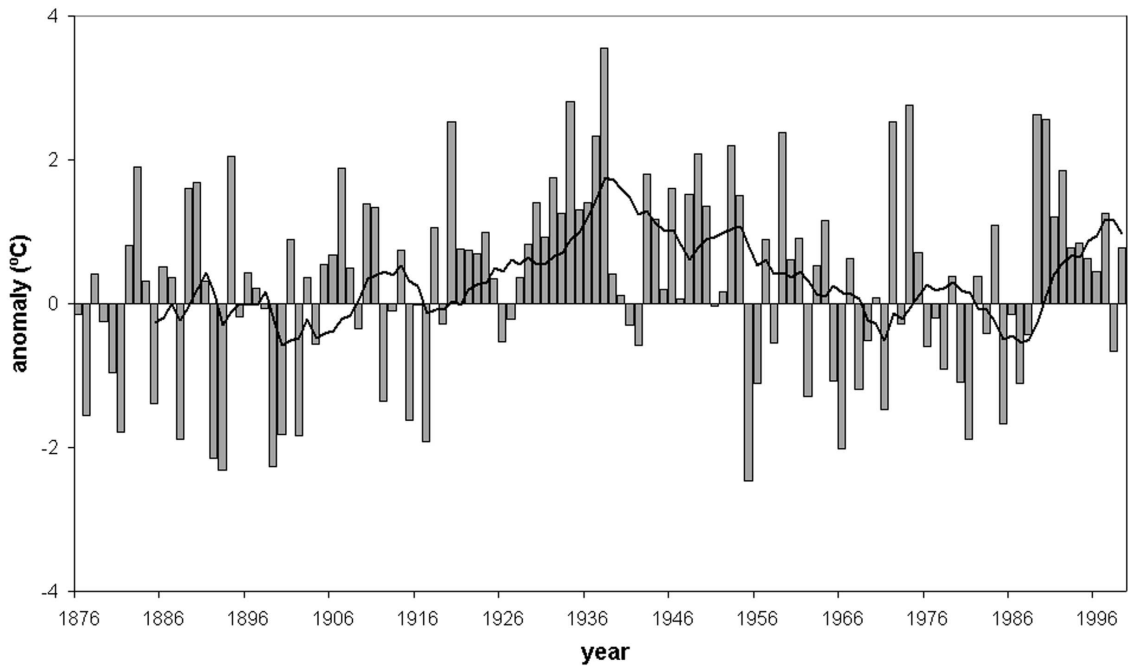
Figure 2.7 Mean annual temperature in Karasjok, Norway, in 1876-1999, expressed as anomalies in ℃ from 1961-1990. The smooth curve represents 10-year running means
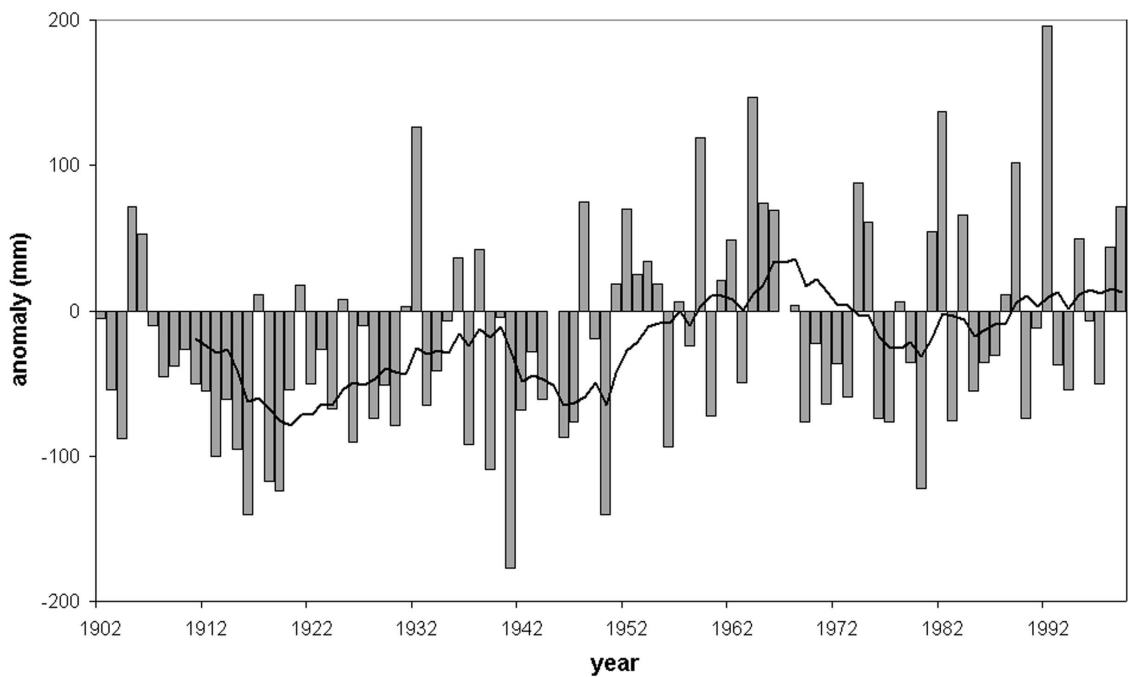
Figure 2.8 Annual (October to September) precipitation in Karasjok, Norway, in 1902-1999, expressed as anomalies in mm from 1961-1990. The smooth curve represents 10-year running means

40
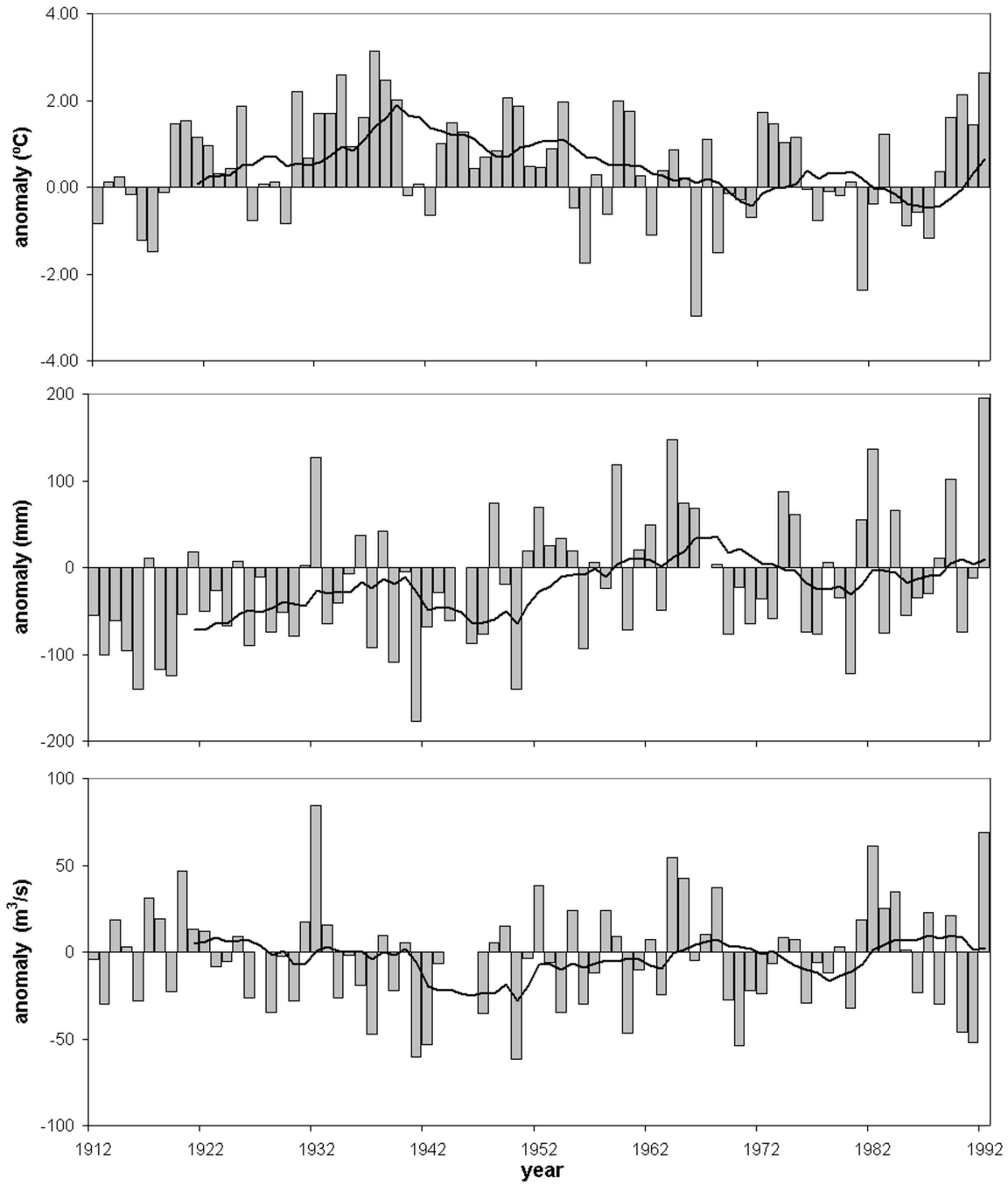
Figure 2.9 Mean annual (October to September) temperature (above) and precipitation (middle) in Karasjok, and discharge of the Tana River at Polmak (below), in 1912-1992, expressed as anomalies in ºC, mm and m³/s respectively from 1961-1990

case in the 1910s and 1920s. A wetter period in the 1960s is reflected by a slight increase in discharge in the same period (see figure 2.9), but the general increase in runoff in the second half of the century was not statistically significant.

As for annual discharge, the only significant (decreasing) trend in spring discharge occurred in the first half of the century ($r = 0.42$, $p < 0.01$). Anomalies in spring discharge can however not unambiguously be correlated with anomalies in winter precipitation at Karasjok (figure 2.10). For example, in the 1910s positive discharge anomalies occurred in years with strong negative precipitation anomalies. Also the increasing trend in summer precipitation since 1911 did not result in a significant increase in summer discharge (figure 2.11). Individual years with high anomalies, such as 1932, 1964, 1982 and 1992 are however correlated. As figure 2.12 shows, high summer discharge anomalies are related to high precipitation anomalies, and low discharge anomalies with low precipitation anomalies ($R^2 = 0.59$).
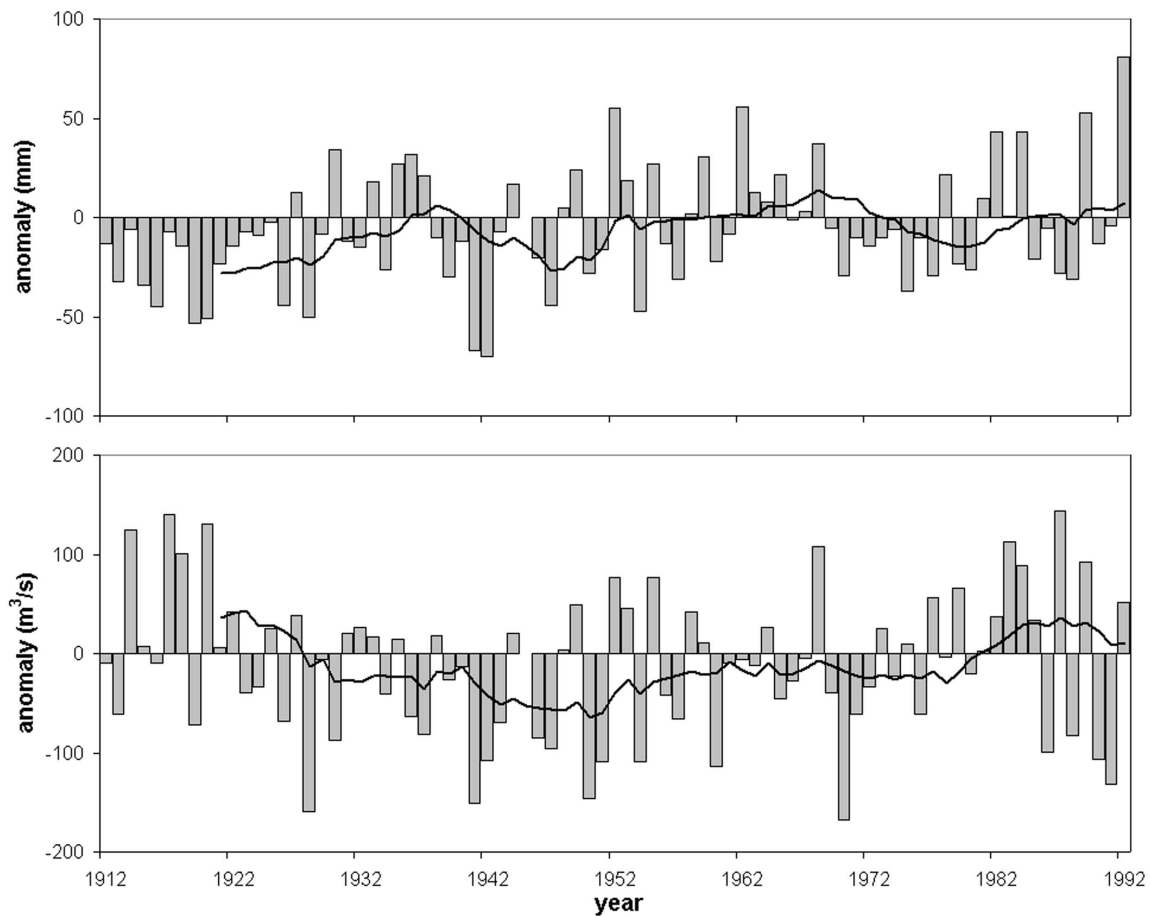
Figure 2.10 Winter (October to April) precipitation at Karasjok (above) and spring (April to June) discharge at Polmak (below) in 1912-1992, expressed as anomalies in mm and m^3/s respectively from 1961-1990
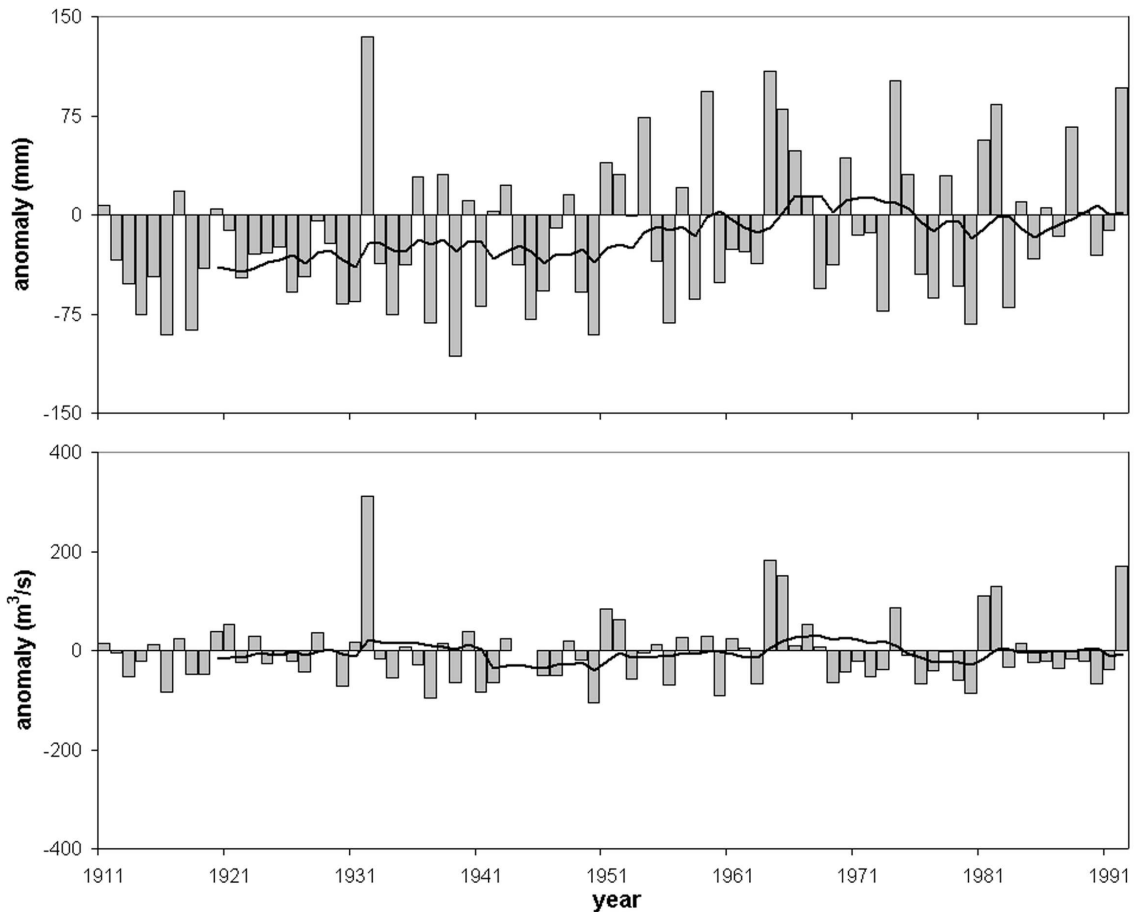
Figure 2.11 Summer (July to September) precipitation at Karasjok (above) and discharge at Polmak (below) in 1911-1992, expressed as anomalies in mm and m^3/s respectively from 1961-1990

It could be expected that changes in summer precipitation will be reinforced or counterbalanced by changes in summer temperature and hence evapotranspiration. If low precipitation is accompanied by high evaporation rates, the resulting discharge will be much lower than when low temperatures give rise to small evaporation losses. Likewise, high precipitation amounts may be counterbalanced by high temperatures, but will result in high discharges if evaporation losses are small. However, as shown in figure 2.12, the relationship between summer temperature and discharge anomalies is much weaker than for precipitation and discharge.

2.5 Discussion and conclusions

A thorough analysis of climate data from northern Finland is given by Lee et al. (2000). As in the present study, Lee et al. (2000) were unable to identify a significant warming

43

trend between 1876 and 1993, but they did find significant annual warming in the period 1901-1945, as well as a slight warming trend since the 1990s, mostly due to winter warming. Precipitation increased significantly between 1880 and 1993, and the period 1946-1990 was wetter than the period 1901-1945, with greater variability particularly in the summer months. In contrast to the present study, Lee et al. (2000) were not able to find a significant increase or decrease in summer precipitation since 1880, due to a particular wet period towards the end of the 19th century.

The increase in precipitation at Karasjok between 1912 and 1993 is however not reflected in discharge data of the Tana River. In fact, the only significant (decreasing) trend in runoff that could be found occurred in the first half of the 20th century (1912-1950), and seems to correspond to increasing temperatures rather than precipitation. However, this apparent correlation cannot be explained by higher evapotranspiration rates, since the trends in both summer temperature and summer discharge were not significant in the same period. A possibly explanation may therefore be that higher winter temperatures resulted in more sublimation during winter. Obviously, there are several processes that may have been counteracting, thereby obscuring the response of discharge to changes in precipitation. Any conclusions on the hydrological response to future climatic changes based on historical data would therefore be premature.
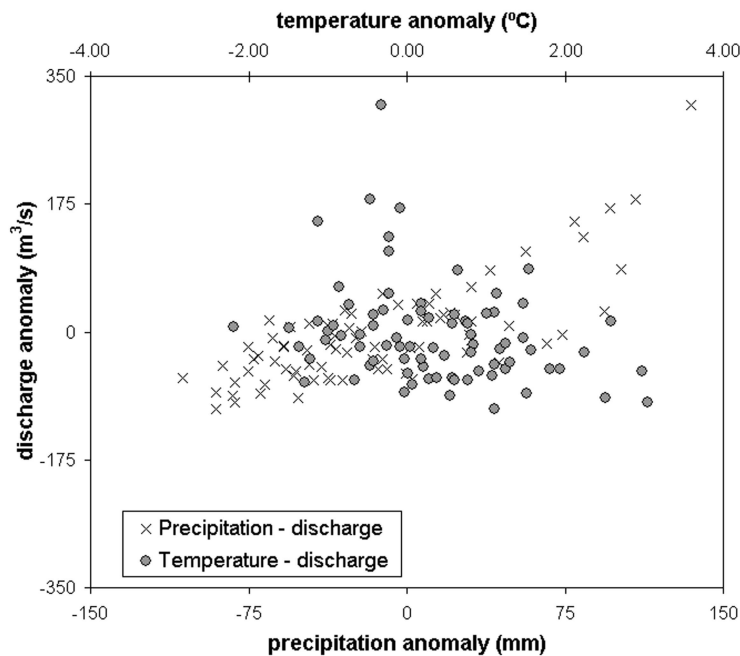
Figure 2.12 Scatterplot of anomalies in summer (July to September) precipitation (in mm) and temperature (in ºC) at Karasjok, and discharge (in m3/s) at Polmak, 1911-1992

2.6   References

Anisimov, O. & B. Fitzharris (2001): Polar Regions (Arctic and Antarctic). In: J.J. McCarthy, O.F. Canziani, N.A. Leary, D.J. Dokken & K.S. White (eds.): Climate Change 2001: Impacts, Adaptation and Vulnerability. Cambridge: Cambridge University Press, pp. 801-841.

Eronen, M. & P. Zetterberg (1996): Climatic changes in Northern Europe since Late Glacial times, with special reference to dendroclimatological studies in northern Finnish Lapland. Geophysica 32, pp. 35-60.

Goodison, B.E., P.Y.T. Louie & D. Yang (1998): WMO solid precipitation measurement intercomparison, final report. Geneva: World Meteorological Organization (WMO Instruments and Observing Methods Report No. 67, WMO/TD-No.872).

Hustich, I. (1961): Plant geographical regions. In: A. Sømme (ed.): A Geography of Norden. Oslo: Cappellen, pp. 54-62.

Hyvärinen, V. & R. Leppäjärvi (1989): Long-term trends in river flow in Finland. In: Proceedings of the Conference on Climate and Water, Helsinki, Finland, 11-15 September 1989 (Publications of the Academy of Finland 9/89), pp. 450-461.

King, L. & M. Seppala (1988): Permafrost thickness and distribution in Finnish Lapland - results of geoelectrical soundings. Polar-forschung 57, pp. 127–147.

Kukkonen, I.T. & J. Šafanda (2001): Numerical modelling of permafrost in bedrock in northern Fennoscandia during the Holocene. Global and Planetary Change 29, pp. 259-273.

S.E. Lee, Press, M.C. & Lee, J.A. (2000): Observed climate variations during the last 100 years in Lapland, Northern Finland. International Journal of Climatology 20, pp. 329-346.

Mansikkaniemi, H. (1970): Deposits of sorted material in the Inarijoki-Tana river valley in Lapland. Reports from the Kevo Subarctic Research Station 6, pp. 1-63.

Olsen, L., A. Reite, K. Riibe & E. Sørensen (1996): Finnmark county, Map of Quaternary Geology, scale 1:500,000, with description. Trondheim: Geological Survey of Norway.

Roald, L.A., H. Hisdal, T. Hiltunen, V. Hyvärinen, T. Jutman, K. Gudmundsson, P. Jonsson & N.B. Ovesen (1997): Historical runoff variation in the Nordic countries. In: A. Gustard, S. Blazkova, M. Brilly, S. Demuth, J. Dixon, H. Van Lanen, C. Llasat, S. Mkhandi & E. Servat (eds.): FRIEND'97 – Regional hydrology: concepts and models for sustainable water resource management. Wallingford: IAHS Publ. 246, pp.87-96.

Seppä, H. & H.J.B. Birks (2002): Holocene climate reconstructions from the Fennoscandian tree-line area based on pollen data from Toskaljavri. Quaternary Research 57, pp. 191-199.

Seppä, H. & D. Hammarlund (2000): Pollen-stratigraphical evidence of Holocene hydrological change in northern Fennoscandia supported by independent isotopic data. Journal of Paleolimnology 24, pp. 69-79.

Seppälä, M. (1976): Periglacial character of the climate of the Kevo region (Finnish Lapland) on the basis of meteorological observations 1962-71. Reports from the Kevo Subarctic Research Station 13, pp. 1-11.

Seppälä, M. (1997): Distribution of permafrost in Finland. Bulletin of the Geological Society of Finland 69, pp. 87-96.

Seppälä, M. (1998): New permafrost formed in peat hummocks (pounus), Finnish Lapland. Permafrost and Periglacial Processes 9, pp. 367-373.

Seppälä, M. & J. Rastas (1980): Vegetation map of northernmost Finland with special reference to subarctic forest limits and natural hazards. Fennia 158, pp. 41-61.

United States Geological Survey (USGS) (2001): GTOPO30 documentation. http://edcdaac.usgs.gov/gtopo30/README.html.

Yang, D., B.E. Goodison, J.R. Metcalfe, P.Y.T. Louie, E. Elomaa, C.L. Hanson, V.S. Golubev, Th. Gunther, J. Milkovic & M. Lapin (2001): Compatibility evaluation of national precipitation gauge measurements. Journal of Geophysical Research 106, p.1481-1492.

3   SMALL-SCALE WATER BALANCE CHARACTERISTICS

With contributions of Richard Harding and Seppo Neuvonen

3.1   Introduction

Modelling the impact of climate change on the sub-arctic hydrology of the Tana Basin requires an understanding of the hydrological processes that operate in this environment. Despite much research efforts - mainly in North America - the hydrology of sub-arctic regions and in particular of non-wetland areas is still not well understood. In particular, there is much confusion over the importance of evapotranspiration. The general perception is that evaporation rates are usually low, since there is only limited energy available (e.g. Seppälä, 1976; Henderson-Sellers & Robinson, 1992). Recent studies, however, suggest that evapotranspiration can be a significant component of the summer water balance (Rovansek et al., 1996; Harding et al., 2002). As a consequence, it can be of importance for the water availability for plants, and it may also be a significant factor in the generation of runoff during a considerable part of the year. Equally important for the summer water balance may be the supply of meltwater to the soil and groundwater reservoirs of a catchment in springtime. During snowmelt the hydrological system can be affected by ice layers in the snow pack and by frozen soils, which makes it difficult to predict to what extent meltwater runs off immediately, or can infiltrate into the soil.

The objective of this chapter is to analyse the water balance of a small sub-catchment of the Tana Basin in detail, with particular emphasis on the contribution of evapotranspiration to the summer water balance. For this purpose two field campaigns were undertaken in the summers of 1999 and 2000. Additional observations were made during the snowmelt season of 2001, in order to gain insight into the differences in runoff generation and water balance with mid-summer. The main objective of this field campaign was to establish the snow conditions at the end of the winter, and determine how much of the water stored in the snow pack is discharged immediately during the melt period. In this chapter we present measurements of the individual water balance components for these three study periods, and identify the hydrological processes that dominate the catchment response to precipitation. The results provide a framework for modelling of the water balance at the much larger scale of the entire Tana Basin.

3.2   Study area

The data for this study were collected in the small catchment of the Kidisjoki in Finnish Lapland, close to the Kevo Subarctic Research Institute of the University of Turku, with centre coordinates at 69º 48' N, 27º 06.5' E (see figure 3.1). The Kidisjoki flows into the Utsjoki, a tributary of the Tana River. The bottom of the Utsjoki river valley is at about 75 m a.s.l., while the highest fells in the region reach 640 m (Kallio et al., 1969). Geologically the region belongs to the Baltic Shield, and the bedrock consists mainly of

gneisses and granulite. Mean annual temperature at Kevo Meteorological Station (100 m a.s.l.) is –2 ℃ (January mean: –15 ℃, July mean: +13 ℃), and mean annual precipitation is 415 mm. The snow cover lasts generally from October to May. More climatic information is given in chapter 2, or by Seppälä (1976) and Lee et al. (2000). The dominating vegetation in the region is mountain birch woodland, while areas above 300-350 m are treeless alpine heaths; mires are also common (Heikkinen & Kalliola, 1989). The area belongs to the continental section of the subalpine mountain birch forest zone (Wielgolaski, 2001). Isolated Scots pine stands occur in the more favourable climate on the floor of Utsjoki and Kevojoki river valleys (Kallio et al., 1969).
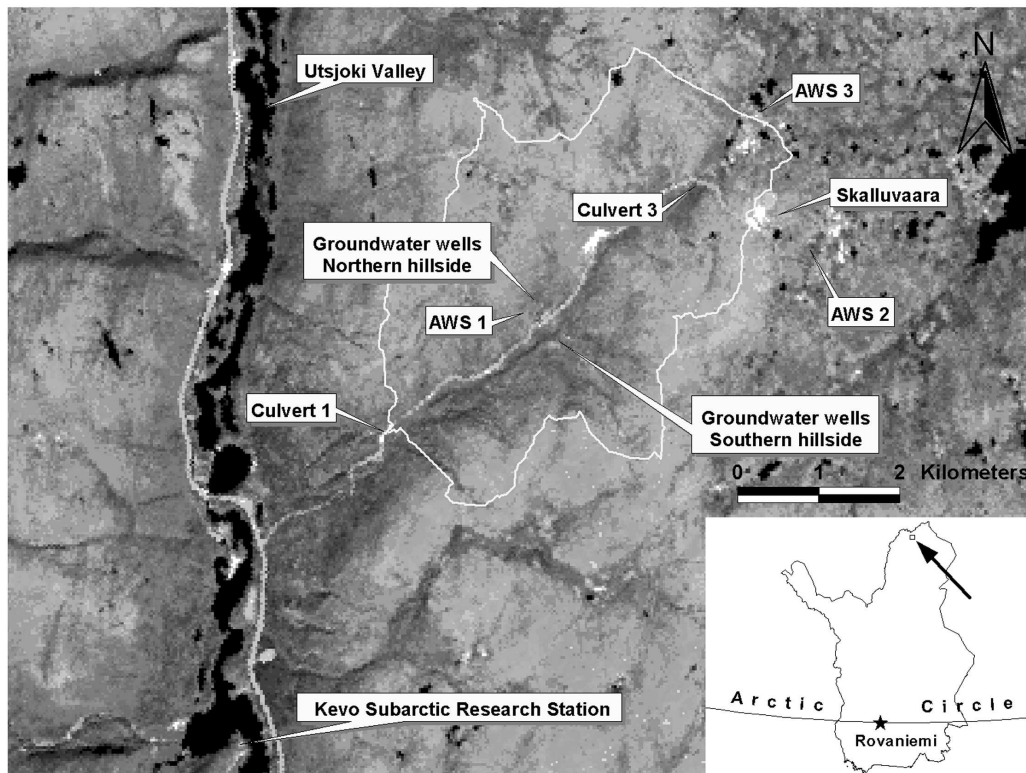
Figure 3.1 Location of the Kidisjoki catchment in northern Finnish Lapland. Background is a Landsat TM image of 30 June 1998. See the appendix for a colour version

The study area was defined by the catchment of the Kidisjoki upstream of a suitable discharge gauging point (see figure 3.1), and is 16.1 km^2 in size. It is characterised by a smooth topography, with elevations ranging from 160 to 360 m, and long and mostly gentle slopes of 6-8 % on the northern (south-east facing) hillsides, and 8-13 % on the southern (north-west facing) hillsides. Dry, convex sections and boulder fields with large amount of stones at the surface are usually located at the top of the hillslopes. These gradually change into humid slopes with mires, as well as some drier parts. Wetlands are often found at the lower end of the slopes and in depressions. At microscale most hillsides show a "hummocky" relief with many small depressions. The Kidisjoki has

48

incised itself into the valley floor, and runs in a narrow valley of 25 - 35 m wide and about 10 m deep in most places. Sediments at the surface are glacial till, consisting of poorly sorted sand and silt having a high degree of stoniness. Soils are poorly developed, and the shallow podsols are usually covered with a layer of mosses, plant roots and decomposing organic material. In this region permafrost is only found as small ice lenses in palsa mires (Seppälä, 1976).

In the lower parts of the catchment the vegetation mainly consists of forests of mountain birch (*Betula pubescens* ssp. *czerepanovi*), with occasionally scattered pine (*Pinus sylvestris*) stands near the catchment outlet (see figure 3.2). The birch trees are polycormic (multi-stemmed) as well as monocormic (single-stemmed), and have their highest densities near the stream. The shrub layer typically consists of dwarf birch (*Betula nana*) and juniper (*Juniperus communis*); in the field layer crowberry (*Empetrum hermaphroditum*), lingonberry (*Vaccinium vitis-idaea*), and bilberry (*V. myrtillus*) are common. In substantial parts of the study area the birch forests have been damaged by larvae of the moth *Epirrita autumnata* (*Lepidoptera, Geometridae*) in 1964-65, which caused many of the larger birch trees to die (Kallio & Lehtonen, 1973, 1975). Regular outbreaks of *Epirrita* are one of the factors that determine the limits of birch occurrence in northern Finland (Nuorteva, 1963; Seppälä & Rastas, 1980; Neuvonen et al., 1999). Wetlands and palsa mires are characterised by shrubs of *B. nana* and willow (e.g., *Salix glauca, S. lapponum*), hummocks of *Sphagnum fuscum*, and grasses and sedges. In total approximately 12 % of the catchment area consists of wetlands and mires. The higher parts of the catchment consist of treeless low alpine heaths, characterised by Ericales (*E. hermaphroditum, V. myrtillus*), *Betula nana* and various mosses and lichens. Occasionally some pioneer birches can be found over here.
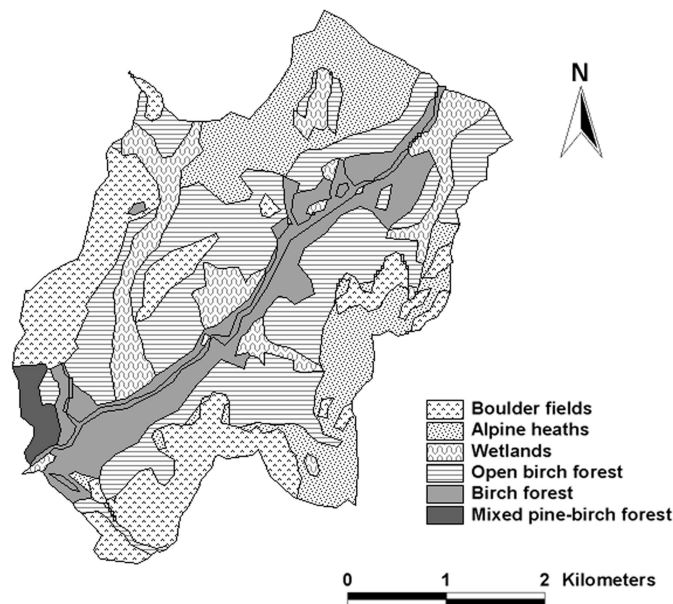
Figure 3.2 Vegetation map of the Kidisjoki catchment. The "open birch forest" class represents mainly birch forests defoliated by Epirrita autumnata; in species composition these areas nowadays resemble the low alpine heaths

3.3   Field measurements

Field data were collected in two summer periods in 1999 and 2000. For this study the research periods were determined by the runoff measurements, made from 22 June to 2 August 1999 (42 days), and 5 June to 23 July 2000 (49 days). Additional runoff measurements were made between 7 May and 3 June 2001 (27 days), following observations on snow coverage in the study area on 9 and 10 April of the same year.

3.3.1   Meteorological variables

In 1998 an automatic weather station (AWS 1) was set up at the northern hillside (figure 3.1) that continued measuring until 5 October 1999. The following climatic variables were measured every 10 seconds and averaged (or accumulated) to hourly values: air temperature and humidity, incoming solar and reflected radiation, net radiation, wind speed and direction, atmospheric pressure, rainfall and snow depth. Soil temperatures were measured every three hours at various depths between 25 and 250 mm below the surface. The equipment is described in more detail by Harding et al. (2002). Due to power failure data were not recorded during a three-week period (25 July to 18 August) in 1999. For this period the data were reconstructed using measurements at an identical weather station just outside the catchment (AWS 2 in figure 3.1; see Harding et al. (2002) for details). The data of 2000 were also lost due to battery failure. For this and the following year data were used from the meteorological station at the Kevo Institute (about 5 km away). For 2000 meteorological data were also available from a nearby experimental site on wetland carbon fluxes (AWS 3).

3.3.2   Evaporation

In 1999 evaporation from the same hillslope site was measured using a modified version of the portable eddy correlation system described by Shuttleworth et al. (1988). This system incorporates a three-dimensional anemometer which allows the calculation of surface fluxes perpendicular to the hillslope. In addition to measurements of heat and water vapour it also provides measurements of momentum flux, humidity and wind speed (Harding et al., 2002).

Evaporation measurements were not available for 2000, and therefore it was estimated with the Penman-Monteith equation (Monteith, 1965), which is described in more detail in chapter 7. Temperature, humidity, air pressure and wind speed data from Kevo were used as input, taking into account the average temperature difference with AWS 1 that was observed in 1999. Incoming solar radiation was calculated using the model POTRAD (Van Dam, 2000), which calculates the potential amount of radiation on a surface as a function of the latitude, altitude, slope and aspect of a given site. The results were corrected with observations on cloud cover. For tundra heaths a shortwave albedo of 0.15 was assumed (Lee, 1980). Longwave radiation was calculated as proposed by

Shuttleworth (1993). The aerodynamic and surface resistance were derived from Harding et al. (2002). This approach was validated against the data of 1999.

3.3.3   Soil moisture and groundwater

Soil moisture was monitored in 1999 using a surface capacitance insertion probe (SCIP), which is described by Dean (1994). This instrument provides a dielectric measurement of the soil permittivity, which is controlled by the amount of water in the soil and, to a lesser degree, by soil type. Readings at a depth of 5 or 10 cm can be converted to volumetric soil moisture content after calibration of the instrument (Robinson et al., 1999). In 2000 soil moisture was monitored by taking small soil samples of 98 cm^3 which were dried in ovens. The soil water retention curve was determined in the laboratory from soil samples.

For monitoring of the groundwater level 13 tube wells were installed on the northern hillslope site, of which 6 form a transect parallel to the slope. Five of these tubes were recorded automatically every hour during the 1999 study period, and the remaining tubes were measured manually at regular intervals in the summers of 1999 and 2000. In addition, four well tubes were installed in a transect along the strike of the slope in 2000, as well as five tubes in a transect parallel to the slope on the opposite southern hillside. Furthermore, a well tube was installed in a wetland in the upstream part of the catchment, close to AWS 3 (figure 3.1). All these tubes were recorded manually as well. All tubes on the northern hillside were also monitored in May 2001.

3.3.4   Discharge

Runoff was measured in the catchment at three culverts under the road running through the valley (see figure 3.1). Culvert 1 was taken as catchment outlet and yielded the discharge of the entire catchment area. In addition, culvert 2 allowed measurement of runoff from the instrumented hillslope site. Culvert 3 has a slightly higher proportion of wetlands in the upstream area than the rest of the catchment, namely 22 %, most of which is situated just above the culvert. At culverts 1 and 3 discharge was monitored on a daily basis by measuring stream velocity and water level in the culvert. For a number of precipitation events discharge was measured more frequently in order to obtain the exact height of the runoff peak. Culvert 2 was instrumented with a "V" notch weir on the outlet side, and water levels in 1999 were recorded every half hour using a pressure transducer. The water levels were rated against volumetric flow measurements.

3.4   Results: summer periods

3.4.1   Precipitation and temperature

In 1999, the winter snow cover disappeared at Kevo on 22 May, and in 2000 on 24 May. In both years the snow in the Kidisjoki catchment melted therefore in late May or early

June. In 1999 the remainder of June and July were relatively dry and warm (see figure 3.3), with two distinct dry periods: 25 – 29 June, and 14 – 20 July. From 6 to 22 July the total precipitation measured at AWS 1 was only 9.0 mm (0.5 mm/day). Over the entire study period the total precipitation was 124.0 mm (3.0 mm/day); the highest daily rainfall occurred on 24 June (19.0 mm). At AWS 2 the total rainfall in the study period was somewhat higher, 140.5 mm. Mean daily air temperature at AWS 1 was 12.1 °C, the highest temperature observed in the study period was 27.5 °C (on 27 July), the lowest 1.9 °C (on 5 July).
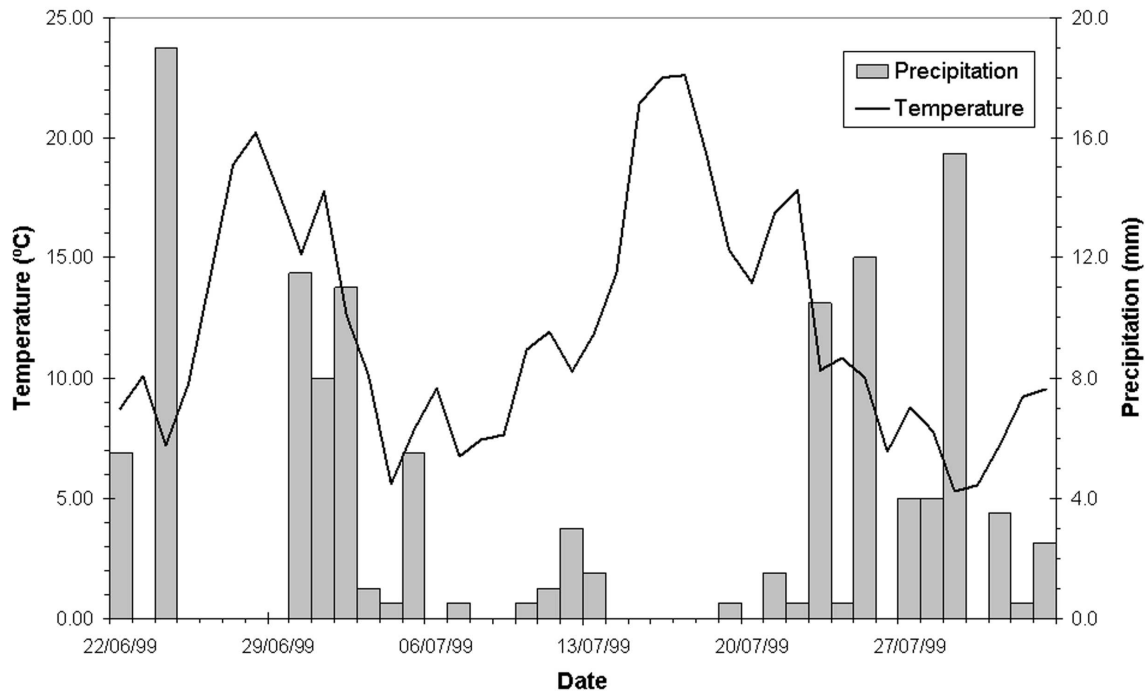
Figure 3.3 Precipitation and temperature at AWS 1 in the summer of 1999

For 2000 meteorological data collected within the catchment area were not available; the measurements of AWS 3 (figure 3.1) were therefore compared with the recordings at the Kevo Subarctic Research Institute. Precipitation and temperature at both locations are shown in figure 3.4. The temperature development is fairly consistent between the two sites; the average difference in mean daily temperature between Kevo and AWS 3 is 2.1 °C, which is somewhat larger than might be expected because of the elevation difference (about 200 m). The higher temperatures at Kevo can be explained by the sheltered location in the valley of the Utsjoki. Despite this different setting, also the precipitation measurements are generally in good agreement. On 6 days the difference between the two sites was larger than 2 mm, and on only 2 days it was larger than 3 mm. In total 86.2 mm

52

precipitation (1.8 mm/day) was measured at AWS 3, versus 100.9 mm (2.1 mm/day) at Kevo, the difference largely being produced on 10 and 14 July. Because the data are in good agreement for the rest of the days, and because AWS 3 is situated much closer to the catchment, these data were used in the rest of this study. Little rain fell in the beginning (6.2 mm in the first 10 days) and in the end of the study period (only 0.4 mm in the last 9 days); a third dry period occurred between 24 June and 4 July (7.4 mm in 11 days). The highest daily rainfall of 13.6 mm was measured this year on 23 June; the highest temperature (27.9 ℃) was observed on 19 July and the lowest (–0.2) on 17 June. In general the study period in 2000 was cooler but drier than in 1999.
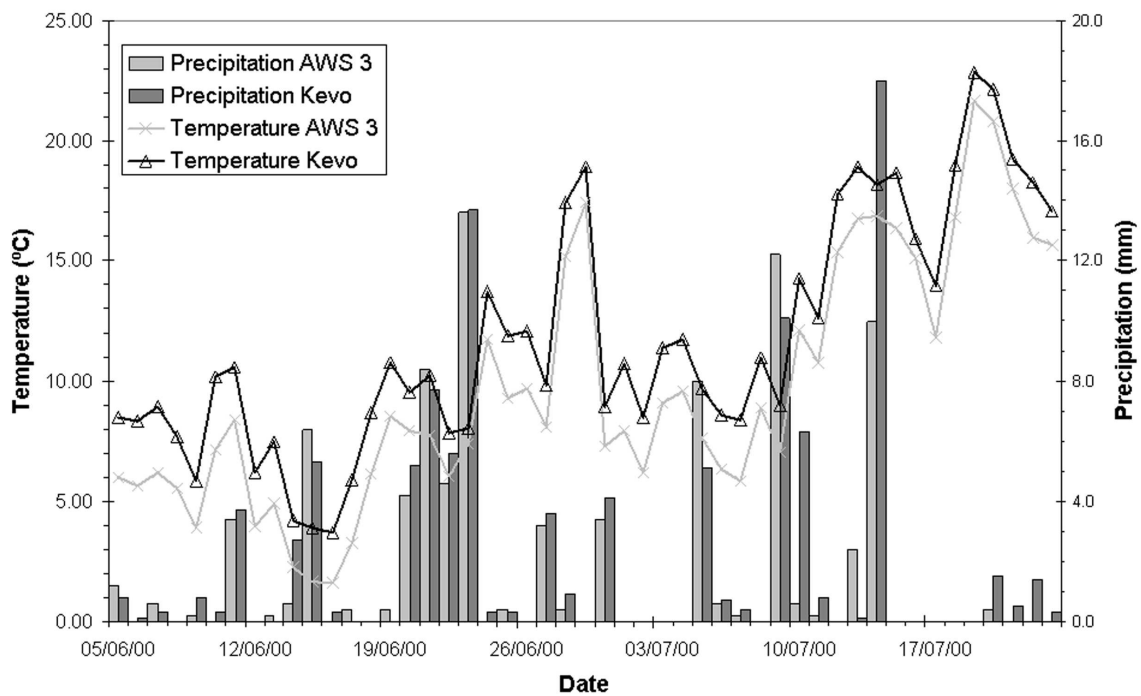
Figure 3.4 Precipitation and temperature at AWS 3 and Kevo in summer 2000

3.4.2   *Evapotranspiration*

From 23 June to 27 July 1999, 59 mm (1.7 mm/day) of evaporation was measured at the northern hillslope site, which is 64 % of the precipitation input in the same period. Since a significant number of hours of data are missing, this figure is probably an underestimate of the actual evaporation in this period. There were no indications that soil water deficit was limiting evaporation, even not during the drier periods. The Penman-Monteith estimate for the same period was slightly lower, namely 51 mm. Presumably this difference is mainly caused by the values of incoming solar radiation calculated with

POTRAD (Van Dam, 2000), that were significantly lower than observed at AWS 1 (figure 3.5). If the observed radiation is used as input, the Penman-Monteith evapotranspiration amounts to 66 mm, which agrees well with the measurements. If the estimates of incoming shortwave radiation of POTRAD are corrected for the average difference with the observed radiation at AWS 1, the evapotranspiration in the entire study period (22 June to 2 August) is calculated at 74 mm, or 60 % of the precipitation input. To a large extent daily evaporation seems to be controlled by air temperature (see figure 3.6).

For 2000, evaporation was modelled in the same way. When the same correction factor is applied to the POTRAD estimates of solar radiation, the evapotranspiration in the study period (5 June to 23 July) is calculated at 75 mm (1.5 mm/day), which is 86 % of the precipitation at AWS 3, and 74 % of the precipitation sum at Kevo. If no correction is applied to the solar radiation estimates, the total evaporation estimate is considerably lower (57 mm).

3.4.3 Soil moisture and groundwater

Measurements with the SCIP in 1999 (figure 3.7) revealed that soil moisture contents remained high throughout the study period, except for the two drier periods. In general the moisture content at 10 cm depth was higher than at 5 cm depth. In figure 3.7 it can
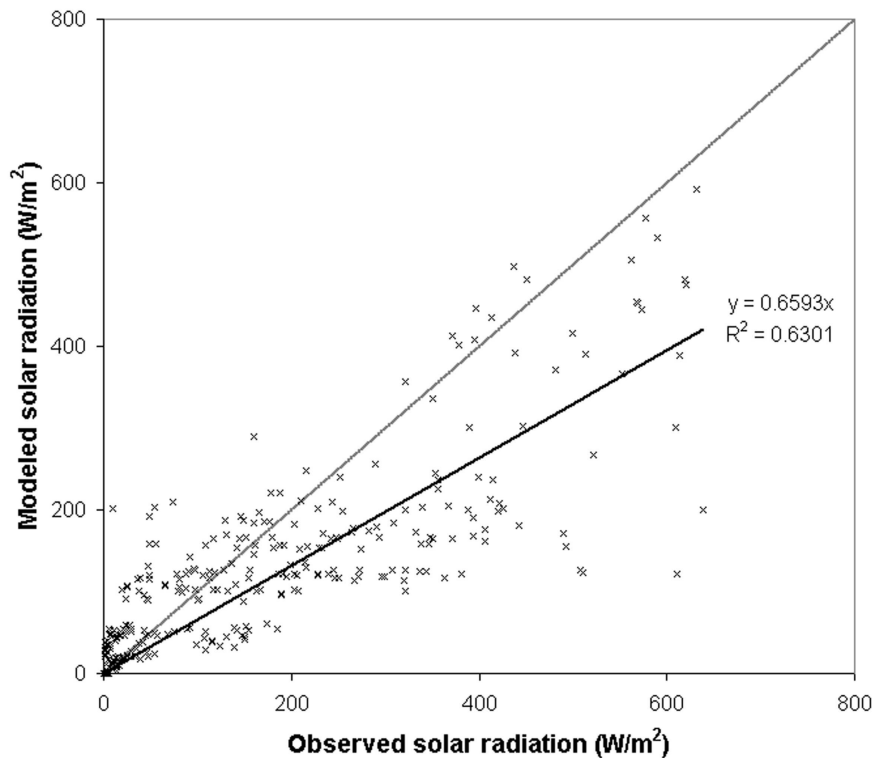
Figure 3.5 Observed and modelled incoming solar radiation at AWS 1 in 1999

54
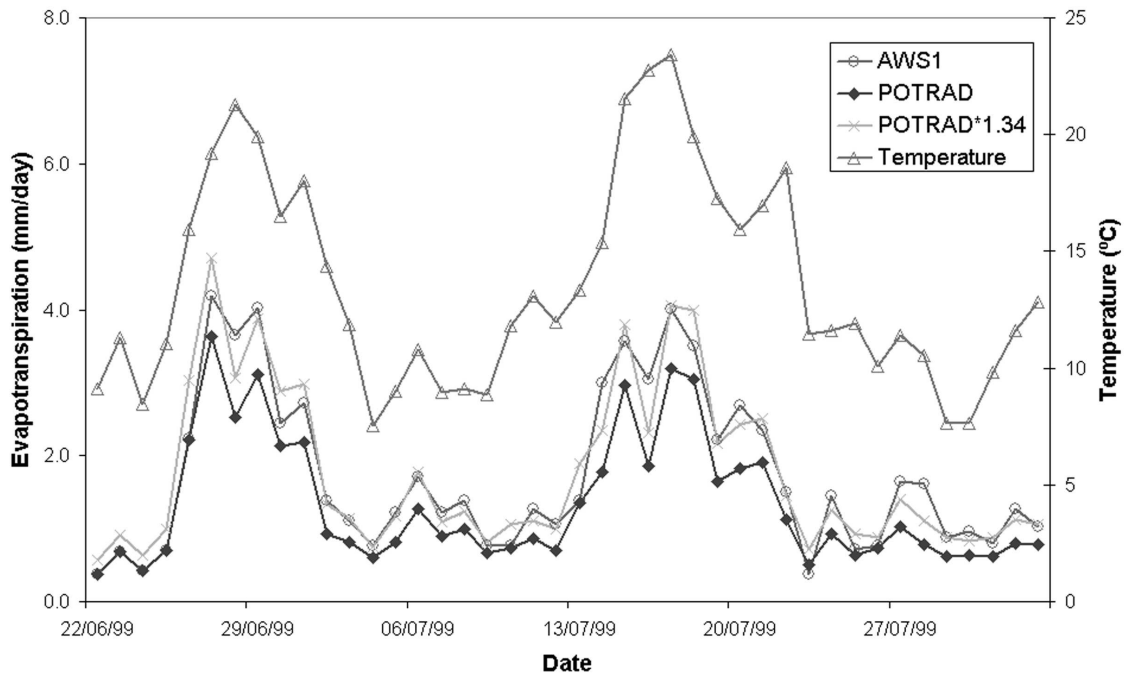
Figure 3.6 Evapotranspiration estimates according to Penman-Monteith, calculated with observed radiation data from AWS 1, as well as the uncorrected and adjusted POTRAD estimates of solar radiation. Also shown is the temperature course in the same period in 1999

also be seen that wetland sites remained near saturation during the whole period. Also the measurements of the moisture content of the soil samples in 2000 showed high moisture contents during most of the study period, gradually decreasing towards the end when precipitation inputs were small. This was furthermore confirmed by the soil water retention curve (not shown) that was determined from soil samples in the laboratory. Even at higher suctions the moisture contents remained relatively high.

Groundwater levels showed a similar pattern, but with large and rapid fluctuations, except for the wetland sites (figure 3.8). Striking are the sharp rises in the water table depth, for instance on 1 and 29 July 1999. During the latter event the water level at the automatically recorded tube well PT 5 rose more than 68 cm within 12 hours (from 29 July, 15:00 to 30 July, 03:00 h), in response to a rainstorm of 15 mm between 15:00 and 21:00 h (figure 3.9). In total 19.5 mm of rain fell between 28 and 30 July, causing the water levels in all non-wetland tube wells to rise 37 cm on average. In contrast, in the highest tube well of the transect across the slope, the increase was only 1 cm. Interestingly, the water level at all tubes responded much less pronounced to the precipitation that fell on 23 July (10.5 mm) and 25 July (12 mm), which were the first considerable rainfall events after a dry period of several weeks. Sharp rises in water level were less obvious in 2000, but did occur, e.g. on 5 July in response to 8.0 mm of rain. On other occasions, such as 9 July, the rise in water level may have been missed. In general water levels in 2000 showed a decreasing trend towards the end (figure 3.8.b).
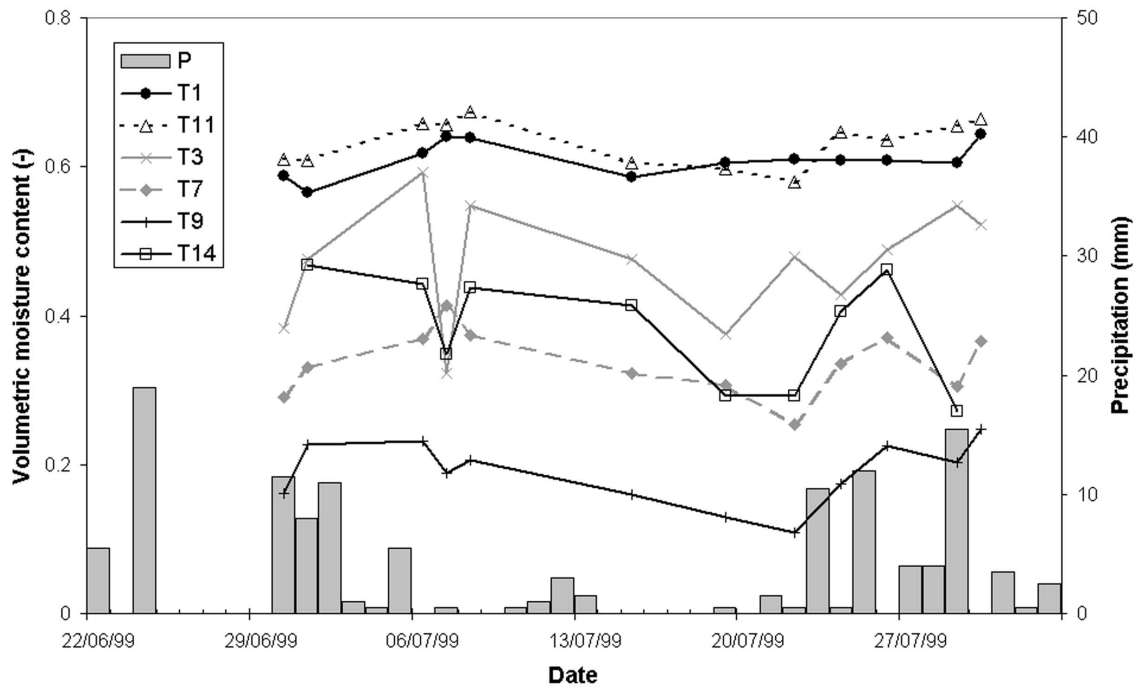
Figure 3.7 Soil moisture contents at 10 cm depth in 1999. T1 and T11 represent wetland sites, T3 the lower hillslope, and T7 and T9 are located uphill, all on the northern hillslope; T14 is located on the lower southern hillslope

The rise in the groundwater table of 37 cm on average, observed between 28 and 30 July 1999, is much higher than might be expected on account of the amount of rain (19.5 mm) and the soil porosity (on average about 40%). It can neither be explained by the lateral supply of water through the soil, considering the low saturated hydraulic conductivity of about 2 m/day. A similar effect has been described by Gillham (1984). If the capillary fringe (or tension saturated zone) extends from the water table close to the ground surface, an addition of a small amount of water may change the pressure potential in this zone from negative to positive, resulting in a large and sudden rise of the groundwater table. It seems that these findings are in line with our observations in the Kidisjoki catchment. Soil moisture contents remained high throughout most of the study period, but were lower after the dry period of mid-July. This explains why a similar rise in groundwater level was not observed after the rainfall events on 23 and 25 July. In addition, the fine soil material (silt mixed with sand and stones) results in a high capillary rise. These findings suggest that the effective specific yield is low (in other words, the field capacity is high), causing the groundwater table to rise rapidly in response to a relatively small precipitation event.

3.4.4   Runoff

Discharge in the Kidisjoki catchment showed a rapid response to rainfall events (see figure 3.10). At culvert 1, peak discharge occurred within a few hours after the end of a

56

(a)
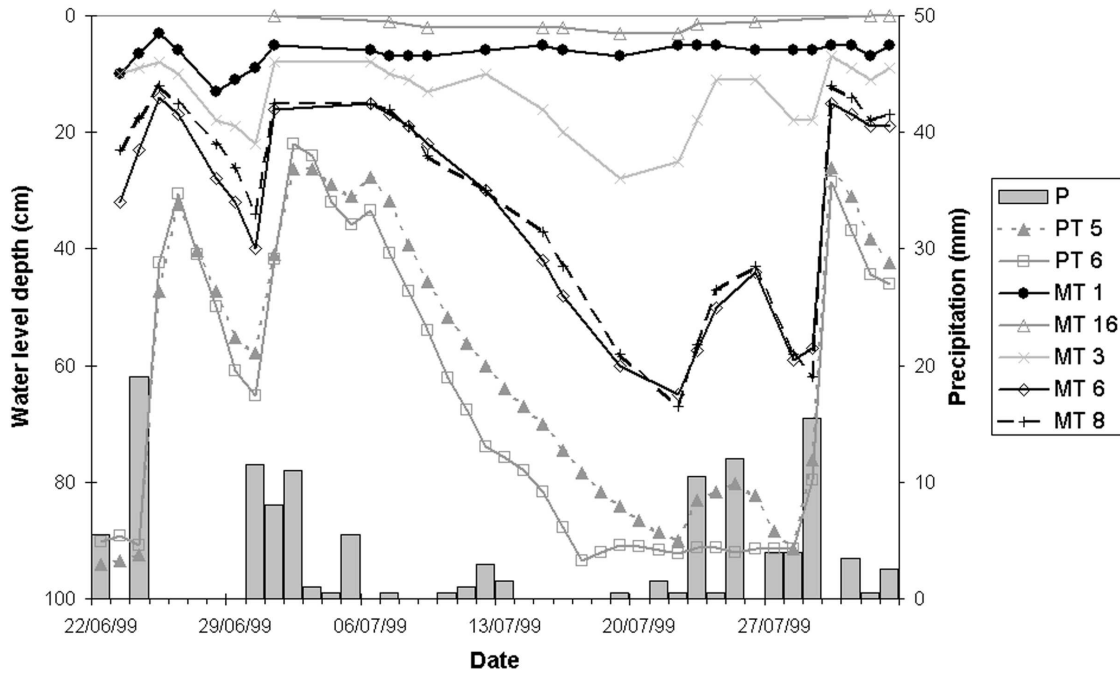
(b)
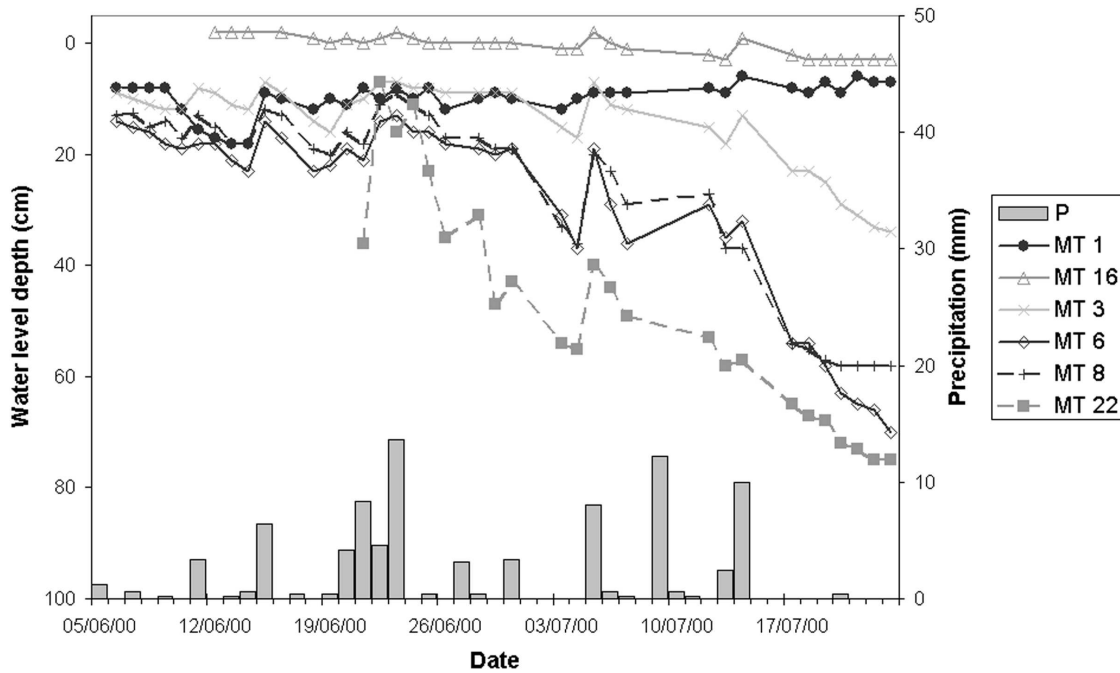
Figure 3.8 Water level at the tube wells, (a) in 1999; (b) in 2000. PT 5 and 6 are automatically recorded and located close to AWS 1; MT1 and MT16 are located in wetland areas, MT3 on the lower hillslope, and MT6, MT8 and MT22 higher on the hillslope. MT16 is located in the wetland area upstream of culvert 3, all other tube wells on the instrumented northern hillslope
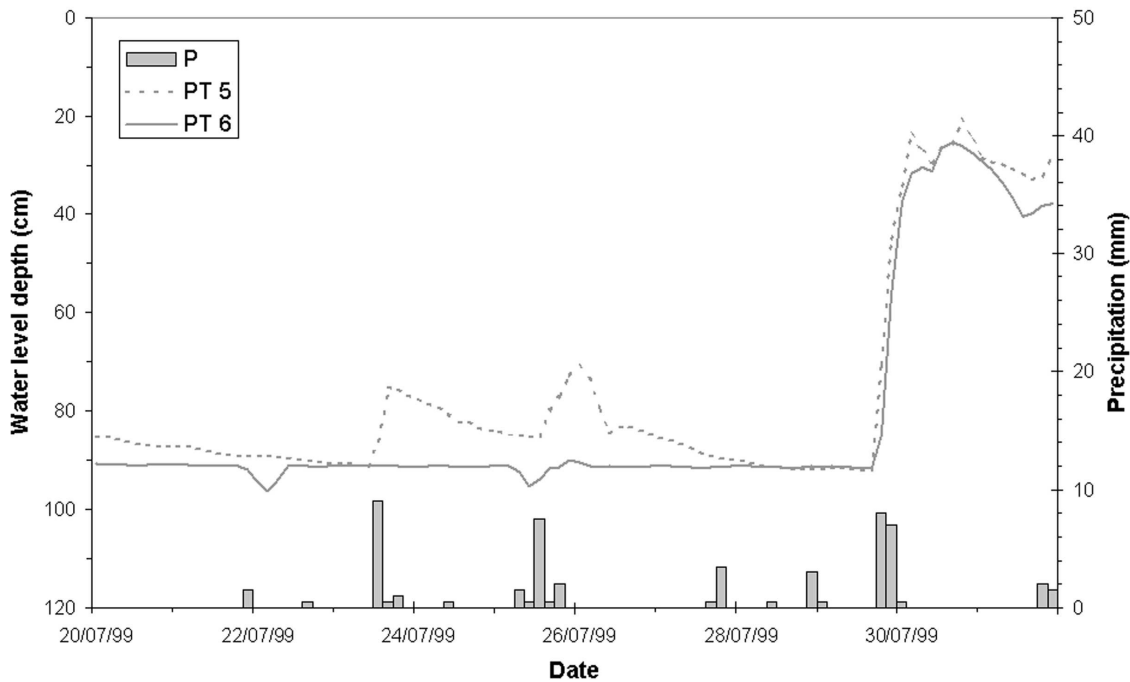
Figure 3.9 Water levels at the automatically recorded tube wells PT5 and PT6 on the northern hillslope, 20-30 July 1999 (3-hourly data)

rainstorm, after which water levels receded in one or two days. This rapid response implies that several peak flows may have been missed at culverts 1 and 3, that were measured only once or twice a day. Nevertheless, for a number of events, e.g. on 23 July 1999 and 23 June 2000, the actual peak flow was measured, and these cases confirm the rapid discharge response. On 23 July 1999 discharge at the catchment outlet rose from 0.15 m^3/s in the morning to 0.31 m^3/s in the afternoon, in response to 9.5 mm of rain earlier on the day, which was the first considerable rainfall event in several weeks. Maximum discharge was reached within 3 hours after precipitation had ceased. The highest discharge in 1999 was 0.48 m^3/s, measured on 30 July after 19.5 mm of rain in the preceding days. Meanwhile, the Kidisjoki maintained a stable baseflow in the drier periods, and discharge did not drop below 0.13 m^3/s, measured on 19 July.

Assuming a baseflow of 0.13 m^3/s, hydrograph separation allows an estimation of the quickflow component for the precipitation event on 23 July 1999. In total 10.5 mm of rain fell between 23 July, 9:30 and 24 July, 11:45; the total volume of quickflow (i.e. the area under the hydrograph minus the baseflow component) in the same period is 9789 m^3, or only 0.6 mm (6%) given the catchment size of 16.1 km^2. It is, however, unlikely that the entire catchment contributes to direct runoff, especially not after a dry period. Presumably most of the direct runoff is generated in the wetland areas, that are usually

58

(a)
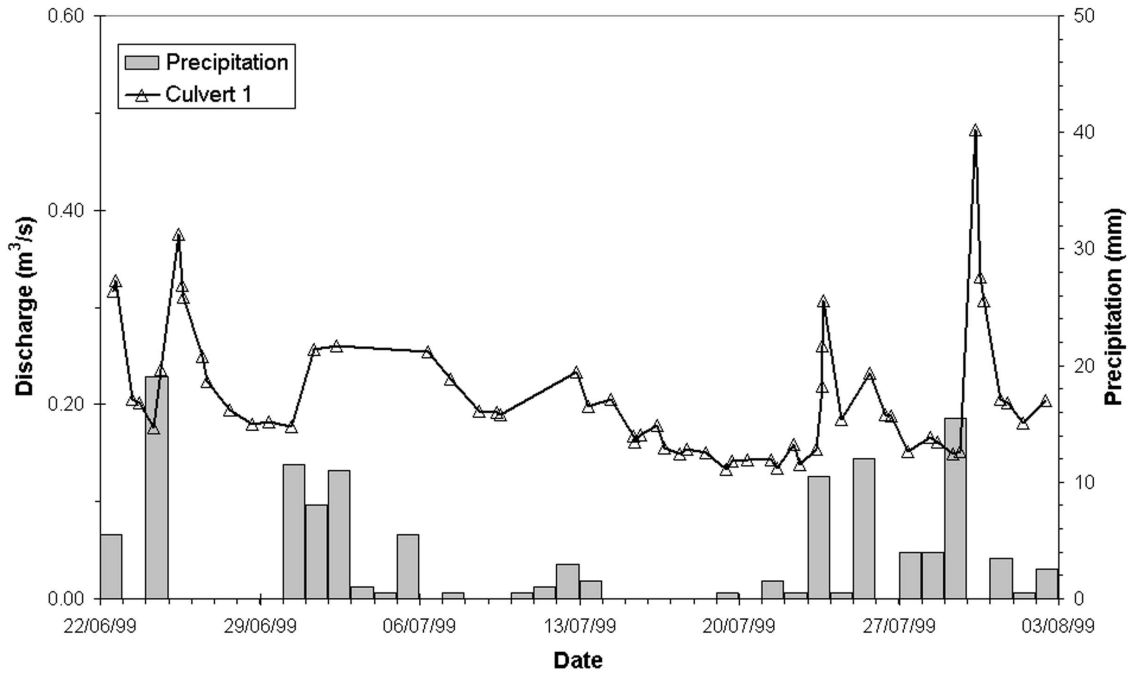
(b)
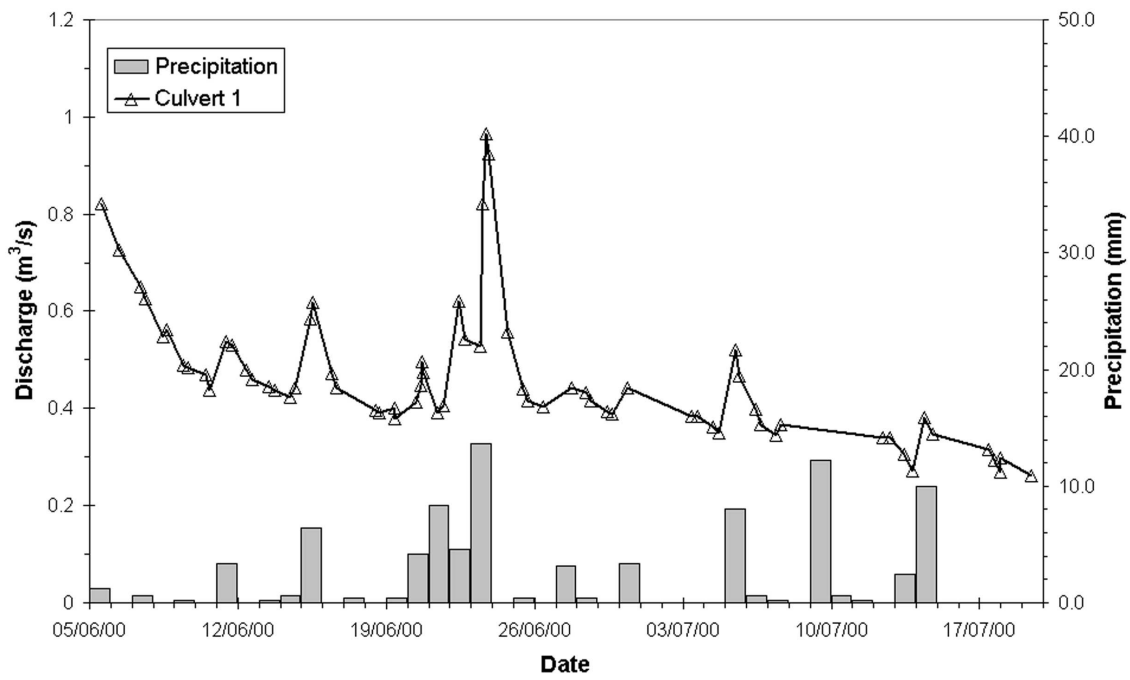
Figure 3.10 Runoff of the Kidisjoki at the catchment outlet (culvert 1), (a) in 1999; (b) in 2000

located close to the streams and have little storage capacity, considering the high groundwater levels that are maintained throughout the summer (figure 3.8). Others (e.g. Roulet & Woo, 1986[a]; Quinton & Roulet, 1998) have demonstrated that, due to the large volume of water that is already stored, the available storage capacity of arctic and sub-arctic wetlands can be very limited. In the subcatchment of culvert 3, where the proportion wetlands / non-wetland areas is higher than in the rest of the catchment, the fraction of precipitation that contributed to runoff in 1999 is therefore somewhat higher than at culvert 1, although the differences are small (37% at culvert 1, vs. 40% at culvert 3). Moreover, wetlands are the only places in the Kidisjoki catchment where overland flow has been observed during our study periods.

In 2000 field measurements started shortly after the snowmelt period, and in the first week the runoff was declining rapidly, as can be seen in figure 3.10. A trend towards recession can be observed throughout the entire study period, and is more apparent than in 1999. Lowest discharge was 0.26 m^3/s, measured at the end of the study period on 19 July. This recession was interrupted by occasional rainstorms, although some peak discharges might have been missed. The highest discharge was observed on 23 June, and amounted to 0.97 m^3/s. For the events on 20 and 23 June, the quickflow component was estimated by assuming the lowest point on the hydrograph before rising as baseflow. On 20 June, 4.2 mm of rain fell between 02:00 and 15:00 h. The highest discharge was measured at 16:15, and the quickflow component was estimated to be 0.14 mm (3 %), based on the catchment size of 16.1 km^2. Three days later 13.6 mm of rain was measured, and the quickflow component was estimated at 1.7 mm (12 %). This higher contribution of direct runoff can be explained by the larger rainfall amount and higher rainfall rates. Moreover, moisture conditions were higher on 23 June, as considerably more rain had fallen in the days before.

3.5 Results: snowmelt season

Additional measurements were made in the Kidisjoki area during the snowmelt season of 2001, in order to observe the differences in the water balance with early and mid-summer. Snow conditions in the catchment were examined on 9 and 10 April by measuring snow depth and density along four transects on the northern hillslope of the catchment, and one on the southern side (figure 3.11). The results (figure 3.12) give an indication of the variability of the snow cover at the end of the winter. Snow depths ranged from 13 to 100 cm, with an average of 48 cm and a standard deviation of 19 cm. In contrast with our expectations, there was no obvious correlation between snow depth and elevation, except for transect F on the southern hillslope. Also on transects A and B the smallest snow depth was recorded at highest elevation. Snow depth can however be highly variable, which is mostly related to microtopography. Due to this large variability, there is also no strong relation with vegetation type (figure 3.13). The variability seems to be smaller in birch and mixed pine / birch forests, but then the total number of sampling points is also smaller in these classes. Snow density was measured at 20 locations along the same transects. Mean snow water equivalent amounted to 118.7 mm, but here too the

variability was large ($\sigma = 53$ mm). The correlation between snow depth and water equivalent was strong (figure 3.14).

At Kevo, snow started to fall in late October 2000, but a continuous snow cover did not develop until December. Even at higher elevations there was little snow at that time, and snow-free patches could still be found (Esa Karpoff, personal communication). From December 2000 to 10 April 2001, 98.4 mm precipitation was recorded at Kevo. The snow depth measurements in the Kidisjoki catchment almost coincided with the moment of maximum snow depth in Kevo (figure 3.15), which amounted to 65 cm on 17 and 18 April. Since late April, temperatures were above zero, and the snow cover started to melt away. At Kevo, the snow cover disappeared on 9 May.
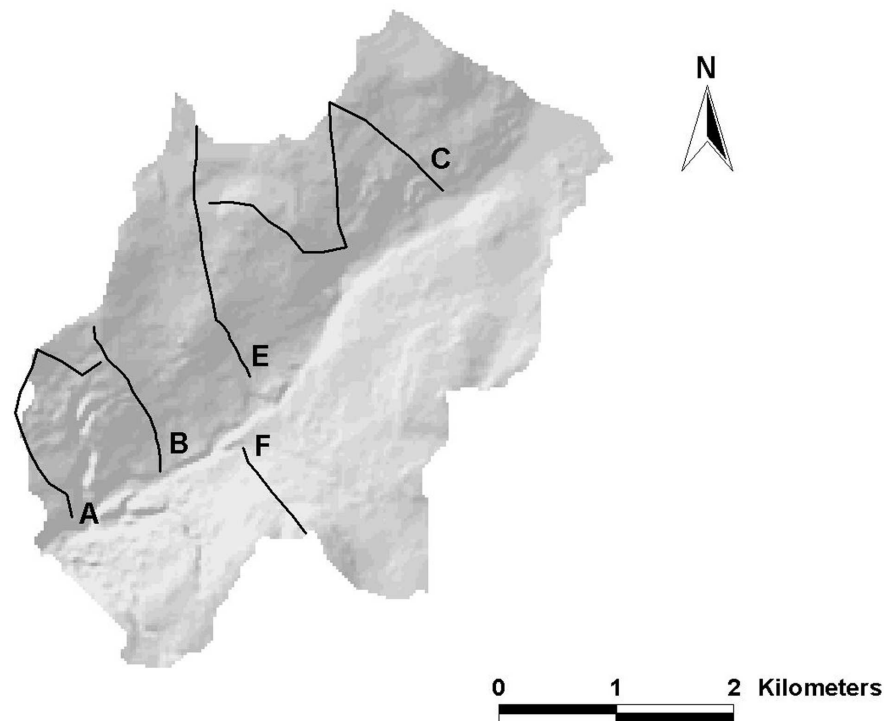
Figure 3.11 Location of the snow transects sampled in April 2001

Spring 2001 was characterised by more than average amounts of surface ice (in Finnish: paannejää), especially on peat bogs (Esa Karpoff and Seppo Neuvonen, personal observations). These ice formations usually melt later than the surrounding snow cover, and in this year they had still not completely disappeared at the end of the study period in early June. Runoff from the Kidisjoki catchment was monitored from 7 May onwards. However, due to icing in the culverts the readings of the first few days are not very accurate. The highest discharge was estimated at 3.1 m^3/s on 8 May. Little rain fell in the rest of the month, and the discharge curve consequently looks like a typical recession curve (figure 3.16). At the end of May, runoff had decreased to 0.14 m^3/s. Temperatures
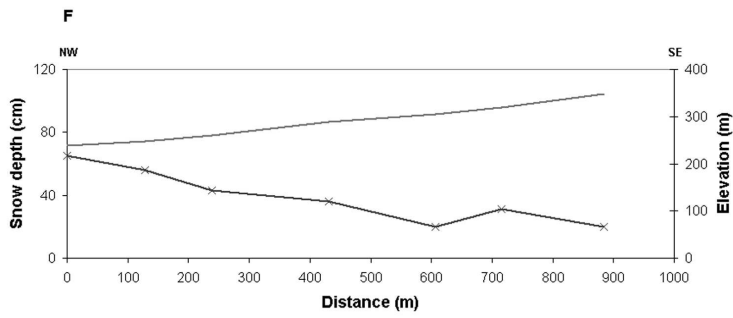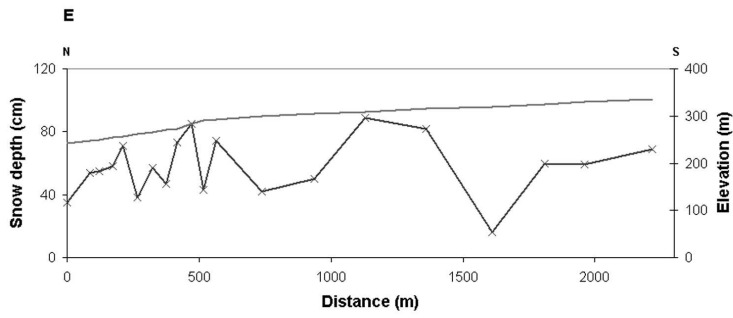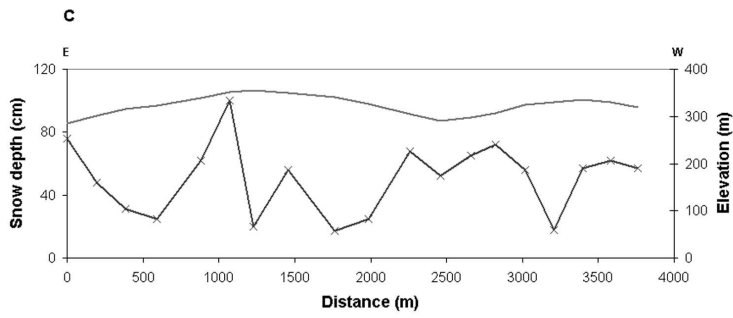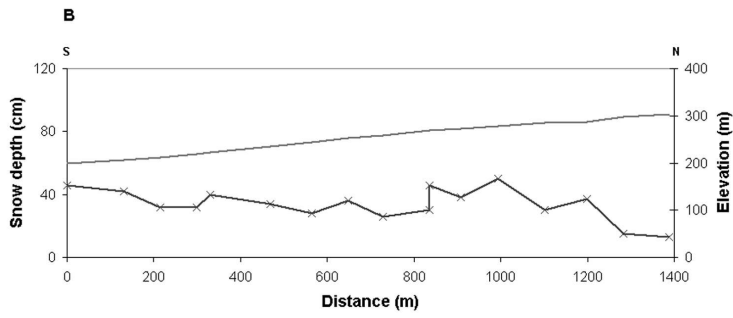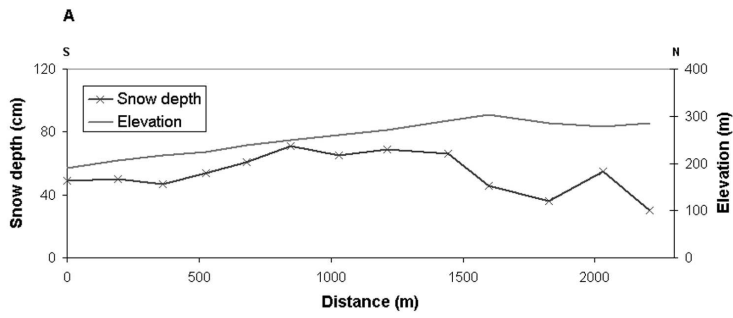
were also close to 0 ºC during most of this study period (figure 3.15), and since most trees had not developed leafs, it is believed that evapotranspiration was insignificant.

Also the tube wells show a decreasing groundwater table throughout the study period. However, most tubes were frozen at a certain depth below the groundwater level, which varied from one tube to another. Despite the low temperatures, the frost depth gradually decreased in most tubes, although some of them remained frozen to the surface until the end. The presence of frozen soil at varying depths complicates the calculation of any change in the groundwater storage. It appears however, that at the end of the winter season, a considerable variability in frost depth may occur, with consequences for the hydrological properties of the soil.
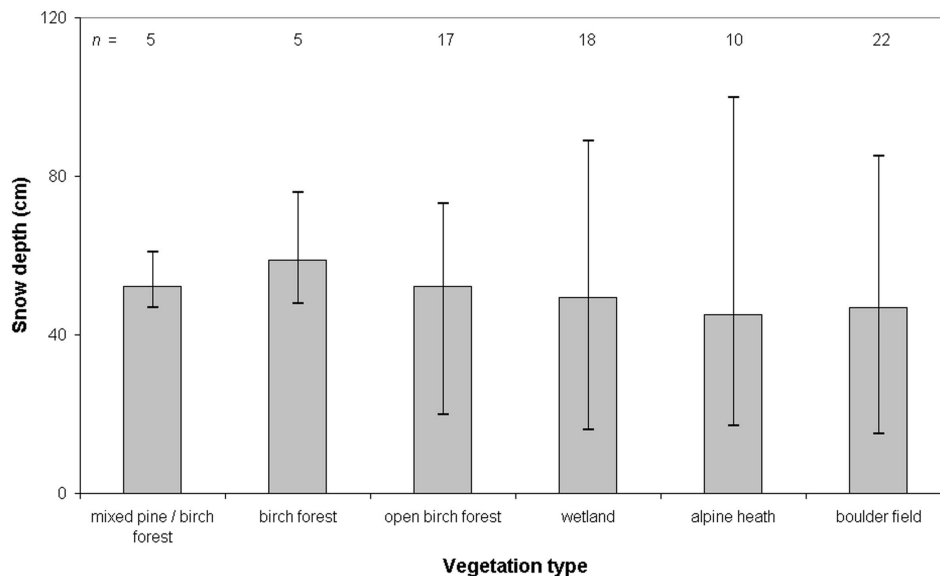
Figure 3.13 Mean, maximum and minimum snow depth per vegetation type

3.6 Water balance

The water balance of the two summer periods is summarised in table 3.1. In 1999 runoff accounted for 46 mm (37 %) of the precipitation input of 124 mm; total evaporation amounted to 74 mm (60 %). The net change is therefore close to zero: + 4 mm. It is difficult to relate this small storage increase to the observed groundwater levels, due to their rapid fluctuations. If the mean groundwater level of the first 10 days is compared with that of the last 10 days of the study period, the tube wells show a decline of 4.7 cm on average. Given a soil porosity of 40 % this would correspond with a change in storage of ‑18.8 mm. However, this figure is a combination of both wetland and non-wetland tube wells. On average the wetland tubes show a rise in water level of 5.6 cm, while the

non-wetland tubes dropped 7.9 cm. If these mean values can be considered as representative for the entire wetland and non-wetland area in the Kidisjoki catchment (roughly 12 and 88 % respectively), and a porosity of 0.8 is assumed for peat (Dingman, 1994), the change in storage can be calculated at –22 mm. However, as noted before the moisture content in the unsaturated zone remains high in general, and for extended periods the soil is close to saturation. The actual difference between measured and residual storage is therefore much smaller than the 26 mm calculated here, but its magnitude remains uncertain.

In 2000 measurements started shortly after snowmelt, and patches of snow were still present in the catchment. Soil moisture, groundwater levels and runoff were consequently high in the beginning, and decreased towards the end. In the water balance the total volume of runoff is therefore larger than the precipitation input during the measurement period (table 3.1). In total, runoff amounted to 116 mm or 134% of the precipitation sum of 86.2 mm. Evapotranspiration was estimated at 75 mm (87%), leading to a net change in storage of –104 mm (–121%). If the change in groundwater storage is calculated as described above, taking into account the differences between wetland and non-wetland areas, the result amounts to –122 mm (–142%). The difference between measured and residual storage (19 mm) is thus similar in magnitude to 1999, and for the same reason it is believed that the actual difference will be much smaller. Although the 2000 study period started earlier, there were no indications for soil frost that could influence the water balance. Some patches of snow however still existed in the beginning, and these may partly account for the storage difference as well.
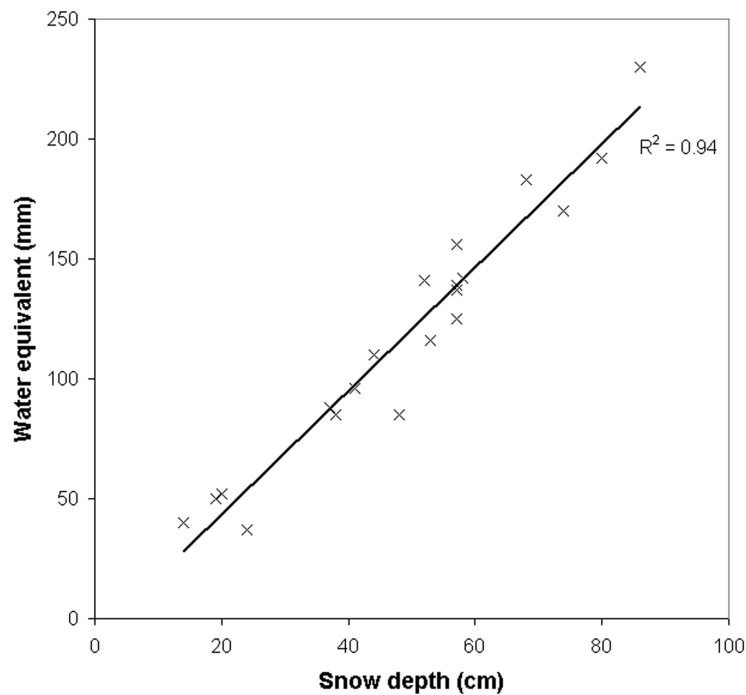
Figure 3.14 Snow depth and water equivalent at 20 points along the transects shown in figure 3.11
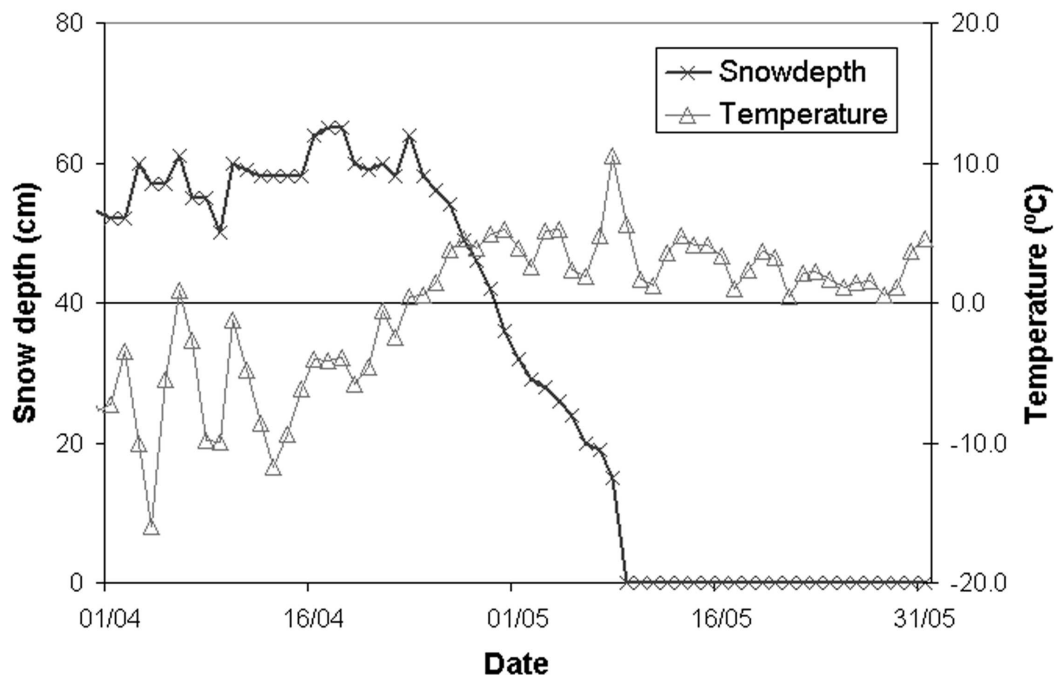
Figure 3.15 Temperature and snow depth at Kevo in spring 2001

For the snowmelt season in 2001 the water balance is summarised in table 3.2. As mentioned before, a lasting snow cover did not develop at Kevo before December 2000, which is unusually late. At higher elevations there were still some snow-free patches in December, but in places the accumulation of snow presumably began earlier. Between November 2000 and 10 April 2001, when the snow conditions in the Kidisjoki catchment were surveyed, 118.4 mm precipitation was recorded. After that, 19.4 mm was recorded until the start of the runoff measurements on 7 May. During the measurement period to 3 June, another 19.0 mm was measured. On 9 and 10 April, the mean snow water equivalent (SWE) in the catchment was119 mm, which corresponds well with the amount of precipitation since November 2000. The variability in water equivalent was however large, ranging from less than 40 to more than 200 mm. These differences can be explained by differences in the onset of the snow accumulation season, and – probably more important – by redistribution of snow by wind.

Mean discharge between 7 May and 3 June was 0.49 m^3/s, or 71 mm over the entire period. About 38 mm was discharged in the first few days, from 7 to 12 May. However, due to icing in the culverts this estimate is not very accurate. Moreover, water in the Kidisjoki was already running when the measurements started. On the other hand, when the data are compared with those of the Utsjoki, it seems that most of the snowmelt runoff peak has been captured (figure 3.17). This means that approximately 30% of the snow water equivalent, that was stored in the catchment at the end of the winter, was discharged as direct runoff in the first few days of the snowmelt period, and almost half of it ran off in the first month.

65

Table 3.1 Water balance of the Kidisjoki catchment for the two summer periods

	22 June – 2 August 1999		5 June – 23 July 2000	
	mm	%	mm	%
Precipitation	124.0	100.0	86.2	100.0
Evaporation	74.1	59.8	74.6	86.5
Runoff	46.3	37.3	115.6	134.8
Net change in storage	3.6	2.9	-103.9	-120.6
Soil storage	-22.3[a]	-18.0	-122.4[a]	-142.1

[a] Combination of wetland and non-wetland tube wells, see text for explanation
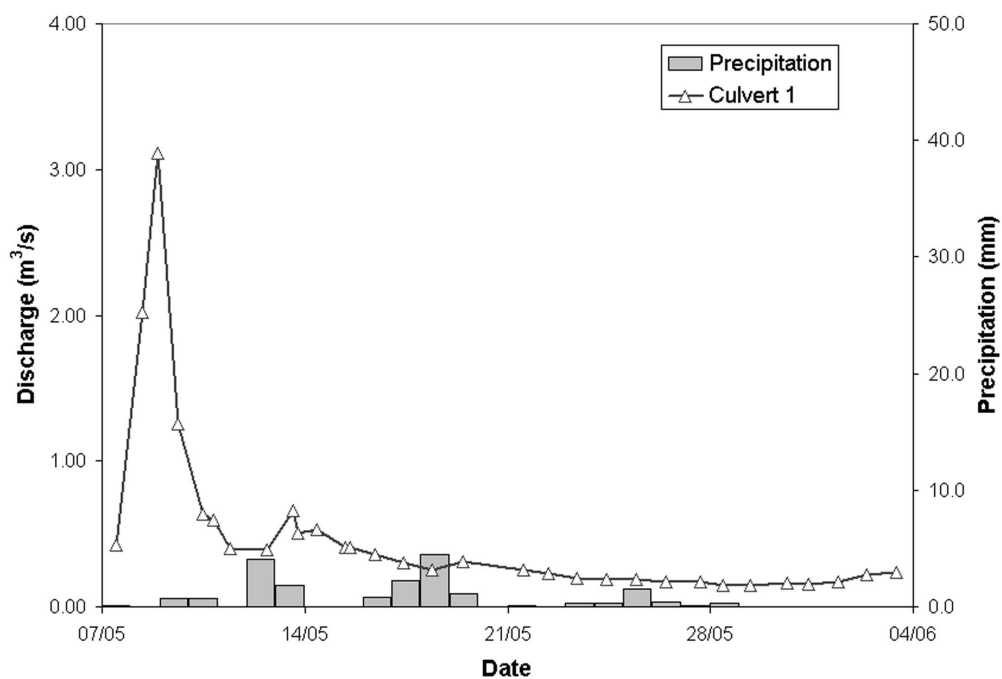
Figure 3.16 Runoff of the Kidisjoki at culvert 1, and precipitation at Kevo in spring 2001

66

3.7 Discussion

The water balance of the two summer periods showed considerable differences. In 1999, total evapotranspiration was larger than the total runoff volume; the sum of these two components was almost equal to the precipitation amount in the same period, which implies that the net storage change was close to zero. The 2000 study period however, was characterised by a large negative storage change, and although total precipitation was less than in 1999, runoff was considerably higher. Evapotranspiration were somewhat lower in 2000 than in 1999, which corresponds with the slightly lower temperatures. The differences between the two years can be explained by the different antecedent conditions. In 2000 the study period begin shortly after snowmelt, while the precipitation amount in the preceding winter was much higher than in the preceding year. At Kevo, 229 mm was recorded between October 1998 and May 1999, against 331 mm in the winter of 1999-2000. Consequently, the snow depths were higher in spring 2000, and much more water was stored in the catchment at the beginning of the study period, resulting in a total discharge that exceeded the precipitation input by one-third. This difference apparently has a lasting effect: even in late July 2000 the Kidisjoki discharge was on average about 1.6 times higher than in 1999, although the accumulated precipitation since the beginning of June was at that time similar for both years. In contrast with 2000, discharge of the Kidisjoki dropped rapidly in May 2001 after most of the snow had melted. This can be attributed not only to the small amount of precipitation during the measurement period, but also to the considerably smaller amount of snow that had accumulated in the winter before. In addition, in 2000 there were no indications of soil frost, while in 2001 several of the tube wells remained frozen at a certain depth, even several weeks after most of the snow had melted. It may well be that in 2000 a larger proportion of the meltwater could infiltrate into the soil, thereby extending the influence of snowmelt until mid-summer.

Table 3.2 Water balance of the Kidisjoki catchment for the spring 2001 period

	mm
Precipitation:	
- 1 December 2000 – 10 April 2001	98.4
- 10 April – 6 May 2001	19.4
- 7 May – 3 June 2001	19.0
- Total	136.8
Mean snow water equivalent 9/10 April 2001	118.7
Runoff (7 May – 3 June 2001)	71.0
Soil storage (7 May – 3 June 2001)	-22.3
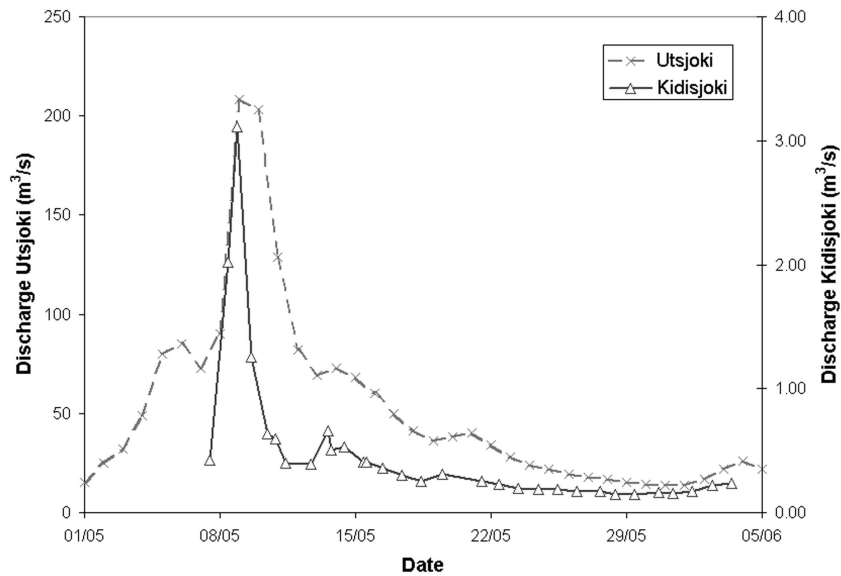
Figure 3.17 Runoff of the Utsjoki at Patoniva, and the Kidisjoki at culvert 1, in 2001. Discharge data of the Utsjoki provided by the Finnish Environmental Institute, Helsinki, Finland

Although much more precipitation had fallen in the winter before, the study period of 2000 itself was much drier than that of 1999. At Kevo the summer of 1999 was the wettest in almost 40 years (1962-2000), with more than 314 mm precipitation recorded in the months June to August. In 2000 the summer precipitation was close to normal (170 mm). Both summers were also about 0.3-0.5 ℃ warmer than the long-term average, but these differences are small compared with the range in summer (June to August) temperatures observed between 1962 and 2000 (from 8.7 to 14.2 ℃). In both summers the discharge of the Kidisjoki showed a rapid response to rainfall events, but the peak flows accounted for only a small part (12 % or less) of the total precipitation input. It seems that during these two study periods most of the direct runoff was generated in the wetland areas, that, considering the high groundwater levels throughout the summer, offer little storage capacity. During dry periods the available storage capacity may however increase and the following peak flows may be attenuated (cf. Quinton & Roulet, 1998). In our study, the quickflow component on 20 June 2000, when little rain had fallen in the days before, was considerably lower than for the event on 23 June, when the storage capacity of the wetlands had been replenished. After extended periods of rain, direct runoff may be more important than was found here. This was demonstrated on 13 and 14 August 1999, shortly after the fieldwork period, when a summer storm brought 74 mm of rain within a few days, causing a runoff peak in the Utsjoki that was almost as high as the snowmelt discharge peak of that year (see figure 3.18).

In non-wetland areas most of the precipitation in summer infiltrates into the soil. A low specific yield, bringing about high moisture contents throughout the summer season, explains the rapid fluctuations in groundwater level that were observed. The large amount of water that is stored in the soil results in a constant baseflow, that may however recede

68

during warmer and drier summers. Since much water is available for evaporation and transpiration by plants, the contribution of evapotranspiration to the summer water balance of non-wetland areas can be considerable, as this study demonstrates. The average daily evaporation rate of 1.7 mm/day that was measured at the northern hillslope site in 1999, was similar to what has been reported by others for comparable sites (e.g. Kane et al., 1990), and somewhat lower than reported for arctic and sub-arctic wetlands by Roulet & Woo (1986[b]) and Quinton & Roulet (1998). In vegetation and soil characteristics the hillside is representative for a large part of the catchment. For wetland areas Roulet & Woo (1986[b]) have demonstrated that over a period of several weeks mean evaporation is similar to lake evaporation. Evapotranspiration will be lower in the boulder fields due to sparse vegetation.

Vakkilainen (1986) estimated the yearly evaporation in northernmost Finland at approximately 150 mm, which corresponds well to the 124 mm measured at this site between late June and October 1999 (Harding et al., 2002). Compared with more temperate environments these quantities may seem small, but they make up a significant part of the annual precipitation input of approximately 400 mm. Almost all evapotranspiration takes place in a few summer months, in which on average about half of the annual precipitation falls. In this season the importance of evaporation is therefore even larger. In order to produce realistic estimates of the water balance of sub-arctic catchments, hydrological and climate models need to be able to realistically simulate evapotranspiration and soil moisture constraints. Unfortunately many models simulate both processes poorly (Robock et al., 1998; Walsh et al., 1998), especially at a large scale.

In the sub-arctic, summers are usually short, and most areas are covered with snow for eight months a year or more. In the winter of 2000-2001, a lasting snow cover did not develop at Kevo before December, which is exceptionally late. By April, the snow depth was only slightly less than the long-term average (mean maximum snow depth at Kevo in 1971-2000: 72 cm). According to Kallio et al. (1969) snow cover in the Kevo region can be much thinner on the fell summits, where it occasionally may disappear already towards the end of February. Shrub canopy may be an even more important control on snow depth than topographic relief (Clark et al., 1985; Sturm et al., 2001), although these two factors are of course interrelated. In our study we were unable to identify any significant correlation of snow depth, neither with vegetation type nor with elevation, except for transect F (figure 3.12). Even so, it seems that the variance is smallest in birch and mixed pine / birch forests (figure 3.13), which is in agreement with findings of Kärenlampi (1972) in the same region. Especially on the alpine heaths, small microtopographical features, often related to shrubs and peat hummocks, may lead to a considerable variation in snow depth over short distances.
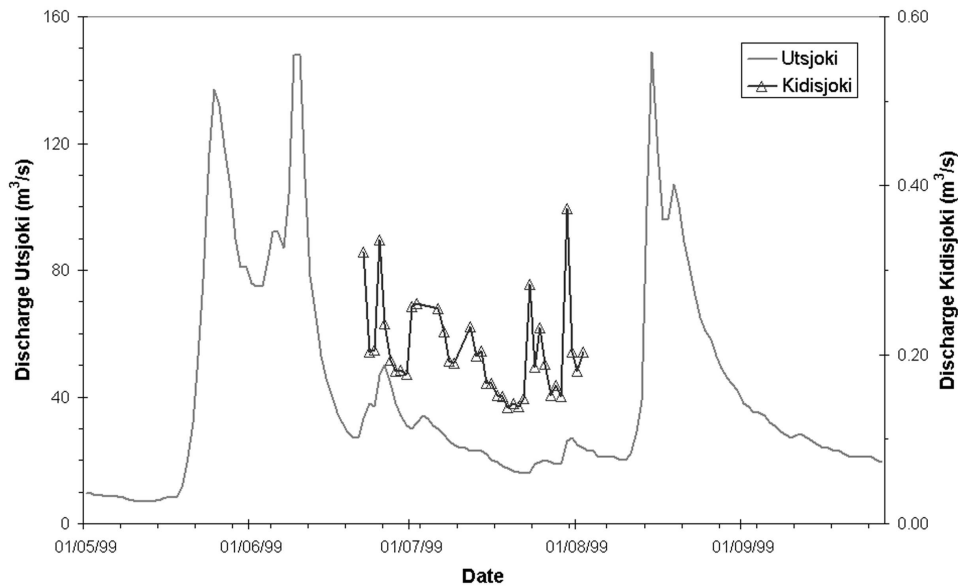
Figure 3.18 Runoff of the Utsjoki at Patoniva, and the Kidisjoki at culvert 1, in 1999. Discharge data of the Utsjoki provided by the Finnish Environmental Institute, Helsinki, Finland

3.8 Conclusions

Using a combination of measurements and evapotranspiration modelling we were able to determine the water balance components of the Kidisjoki catchment in northernmost Finland for two summer periods. In both years there was a difference between the residual of precipitation, evaporation and runoff, and the storage change derived from the groundwater observations. However, although the groundwater levels did drop during both study periods, the soil moisture contents generally remained high, and it is therefore believed that the actual difference between measured and residual storage will be much smaller than calculated. Remnants of snow and ice in the beginning may also have influenced the water balance of the 2000 study period.

In both summer periods evapotranspiration accounted for a large part of the precipitation input into the catchment: 60 % in 1999, and 87 % in 2000. The actual evaporation rates were slightly lower in 2000, which corresponds to slightly lower temperatures. Daily evaporation is largely controlled by air temperature, but is promoted by the low specific yield of the soil, which results in relatively high moisture contents throughout most of the summer. Considering the contribution of evapotranspiration to the summer water balance of both wetland and non-wetland areas, and considering its supposed sensitivity to changes in climate, there is a need for physical models that can simulate summer evapotranspiration in the sub-Arctic at a large scale.

Due to the low specific yield of the soil, the groundwater levels in the non-wetland areas in the catchment showed rapid fluctuations in response to the moderate precipitation events that occurred during both study periods. Although the discharge of the Kidisjoki

70

responded rapidly to rainfall events, the quickflow component was very small in most occasions. Direct runoff therefore played only a minor part in the water balance, and originated in the wetland areas only. During extreme summer rainstorms however, as well as during snowmelt, it can be of more importance, and may not be restricted to wetlands.

Snow depth and density in the Kidisjoki catchment showed considerable variability at the end of the winter in April 2001. A clear correlation between snow depth and elevation or vegetation type could not be found, and it seems that most of the variability is related to small-scale features such as peat hummocks. Mean snow water equivalent was however in agreement with the total precipitation amount recorded at Kevo since November 2000. Although the runoff estimates in the first few days were hampered by icing, it seems that a significant part (about 30 %) of the volume of water stored in the snow pack was discharged in the first few days of the snowmelt season, and approximately 50 % was discharged in the first month. Depending on the extent of soil frost, these proportions may however differ from year to year.

3.9   References

Clark, M.J., A.M. Gurnell, E.J. Milton, M. Seppälä & M. Kyöstilä (1985): Remotely-sensed vegetation classification as a snow depth indicator for hydrological analysis in sub-arctic Finland. Fennia 163, pp. 195-216.

Dean, T.J. (1994): The IH capacitance probe for measurement of soil water content. Wallingford, United Kingdom: Institute of Hydrology (IH Report 125).

Dingman, S.L. (1994): Physical Hydrology. New York: Macmillan.

Gillham, R.W. (1984): The capillary fringe and its effect on water table response. Journal of Hydrology 67, pp. 307-324.

Harding, R.J., N.A. Jackson, E.M. Blyth & A. Culf (2002): Evaporation and energy balance of a sub-Arctic hillslope in northern Finland. Hydrological Processes 16, pp. 1419-1436.

Heikkinen, R.K. & R.J. Kalliola (1989): Vegetation types and map of the Kevo nature reserve, northernmost Finland. Kevo Notes 8, pp. 1-39 + map.

Henderson-Sellers, A. & Robinson, P.J. (1992): Contemporary Climatology. Harlow, United Kingdom: Longman.

Kallio, P., U. Laine, & Y. Mäkinen, (1969): Vascular flora of Inari Lapland. 1. Introduction and Lycopodiaceae - Polypodiaceae. Reports from the Kevo Subarctic Research Station 5, pp. 1-108.

Kallio, P. & J. Lehtonen (1973): Birch forest damage caused by Oporinia autumnata (Bkh.) in 1965-66 in Utsjoki, N Finland. Reports from the Kevo Subarctic Research Station 10, pp. 55-69.

Kallio, P. & J. Lehtonen (1975): On the ecocatastrophe of birch forests caused by Oporinia autumnata (Bkh.) and the problem of reforestation. In: F.E. Wielgolaski (ed.): Fennoscandian tundra ecosystems. Part 2: animals and systems analysis. Berlin: Springer Verlag (Ecological Studies 17), pp. 174-180.

Kane, D.L., R.E. Gieck & L.D. Hinzman (1990): Evapotranspiration from a small Alaskan arctic watershed. Nordic Hydrology 20, pp. 253-272.

Kärenlampi, L. (1972): Comparisons between the microclimates of the Kevo ecosystem study sites and the Kevo Meteorological Station. Reports from the Kevo Subarctic Research Station 9, pp. 50-65.

Lee, R. (1980): Forest Hydrology. New York: Columbia University Press.

Lee, S.E., M.C. Press & J.A. Lee (2000): Observed climate variations during the last 100 years in Lapland, northern Finland. International Journal of Climatology 20, pp. 329-346.

Monteith, J.L. (1965): Evaporation and environment. Proceedings of the 19th Symposium of the Society for Experimental Biology. New York: Cambridge University Press, pp. 205-234.

Neuvonen, S., P. Niemelä & T. Virtanen, T. (1999): Climatic change and insect outbreaks in boreal forests: the role of winter temperatures. Ecological Bulletins 47, pp. 63-67.

Nuorteva, P. (1963): The influence of Oporinia autumnata (Bkh.) (Lep., Geometridae) on the timber-line in subarctic conditions. Annales Entomologici Fennici 29, pp. 270-277.

Quinton, W.L. & N.T. Roulet (1998): Spring and summer runoff hydrology of a subarctic patterned wetland. Arctic and Alpine Research 30, pp. 285-294.

Robinson, D.A., C.M.K. Gardner & J.D. Cooper (1999): Measurement of relative permittivity in sandy soils using TDR, capacitance and theta probes: comparison, including the effects of bulk soil electrical conductivity. Journal of Hydrology 223, pp. 198–211.

Robock, A., C.A. Schlosser, K.Y. Vinnikov, N.A. Speranskaya, J.K. Entin & S. Qiu (1998): Evaluation of the AMIP soil moisture simulations. Global and Planetary Change 19, pp. 181–208.

Rovansek, R.J., L.D. Hinzman & D.L. Kane, D.L. (1996): Hydrology of a tundra wetland complex on the Alaskan Arctic coastal plain, U.S.A. Arctic and Alpine Research 28, pp. 311-317.

Roulet, N.T. & M.-K. Woo (1986[a]): Hydrology of a wetland in the continuous permafrost region. Journal of Hydrology 89, pp. 73-91.

Roulet, N.T. & M.-K. Woo (1986[b]): Wetland and lake evaporation in the low Arctic. Arctic and Alpine Research 18, pp. 195-200.

Seppälä, M. (1976): Periglacial character of the climate of the Kevo region (Finnish Lapland) on the basis of meteorological observations 1962-71. Reports from the Kevo Subarctic Research Station 13, pp. 1-11.

Seppälä, M. & J. Rastas (1980): Vegetation map of northernmost Finland with special reference to subarctic forest limits and natural hazards. Fennia 158, pp. 41-61 + appendix.

Shuttleworth, W.J. (1993): Evaporation. In: D.R. Maidment (ed.): Handbook of Hydrology. New York: McGraw-Hill, pp. 4.1-4.53.

Shuttleworth, W.J., J.H.C. Gash, C.R. Lloyd, D.D. McNeil, C.J. Moore & J.S. Wallace, J.S. (1988): An integrated micrometeorological system for evaporation measurement. Agricultural and Forest Meteorology 43, pp. 295-317.

Sturm, M., J.P. McFadden, G.E. Liston, F.S. Chapin III, C.H. Racine & J. Holmgren (2001): Snow-shrub interactions in Arctic tundra: a hypothesis with climatic implications. Journal of Climate 14, pp. 336-344.

Vakkilainen, P. (1986): Haihdunta. In: S. Mustonen (ed.): Sovellettu hydrologia. Mänttä, Finland: Mäntän Kirjapaino Oy, pp. 64-79.

Van Dam, O. (2000): Modelling incoming Potential Radiation on a land surface with PCRaster. POTRAD5.MOD manual. Utrecht: Utrecht Centre for Environment and Landscape dynamics, Utrecht University.

Walsh, J.E., V. Kattsov, D. Portis & V. Meleshko (1998): Arctic precipitation and evaporation: model results and observational estimates. Journal of Climate 11, pp. 72-87.

Wielgolaski, F.E. (2001): Vegetation sections in Northern Fennoscandian mountain birch forests. In: F.E. Wielgolaski (ed.) Nordic Mountain Birch Ecosystems. Paris: UNESCO, and New York: Parthenon (Man and the Biosphere Series 27), pp. 23-33.

4 MONITORING SNOW COVER DYNAMICS IN NORTHERN FENNOSCANDIA WITH SPOT VEGETATION IMAGES

Rutger Dankers & Steven M. de Jong
Submitted to International Journal of Remote Sensing

Abstract

In order to monitor snow cover dynamics in the Tana River Basin in Northern Fennoscandia, SPOT VEGETATION (VGT) images of the snowmelt seasons of 1998 and 1999 were used to identify snow covered areas, employing an algorithm that has originally been developed for data from the Moderate Resolution Imaging Spectroradiometer (MODIS). This algorithm is based on the Normalized Difference Snow Index (NDSI), which usually is calculated from the green and mid-infrared bands. Since the VGT sensor does not have a green band, the applicability of this algorithm to VEGETATION data from the red and mid-infrared bands was tested by comparing NDSI values and snow cover estimates with a corresponding Landsat Thematic Mapper (TM) image. The best agreement was found with slightly lower threshold values for the NDSI, when calculated from the red instead of the green band. By applying the NDSI-based algorithm to 10-day syntheses of VGT images the moment of snow disappearance could be registered for each 1 by 1 km pixel in the study area. The results were largely consistent with the observed first snow-free date at meteorological stations in the area, which confirms the effectiveness of VGT images in monitoring snow cover depletion patterns.

4.1 Introduction

Climate simulation models generally agree that the most significant changes in climate due to the so-called enhanced greenhouse effect are to be expected at high latitudes (Houghton et al. 2001). In these arctic and sub-arctic environments seasonal snow coverage plays an essential role in the hydrological cycle. It not only controls the length of the growing season, the soil thermal regime and the exchange of greenhouse gases with the atmosphere, but it is also a major source for river discharge in spring. Controlled by both precipitation and temperature, changes in climate may have important consequences for the extent and duration of the snow cover, that, considering the high albedo of snow, may ultimately have a feedback effect on the global radiation budget (McCarthy et al. 2001). Knowledge on snow cover dynamics in arctic and sub-arctic environments is therefore of major importance (Koster 1991).

Earth observation by satellites offers great potential in monitoring snow dynamics at various levels of scale. Unfortunately most sensor systems are not designed to measure snow water equivalent (SWE) nor snow depth. Snow cover extent can however easily be identified in the visible and near-infrared wavelength bands due to its high reflectance.

However, in this spectral range it is difficult to discriminate between snow and clouds. Including the mid-infrared part of the spectrum, around 1.6 μm, helps to separate clouds from snow (Dozier 1984). Since 1998 several sensors have been launched that make observations in this wavelength region, and that, because of their moderate spatial resolution of 1 km, are able to provide daily images of the global surface (table 4.1): the SPOT VEGETATION (VGT) sensor (Saint 1996), launched in March 1998; the Advanced Very High Resolution Radiometer (AVHRR/3), on board of the National Oceanic & Atmospheric Administration (NOAA) KLM satellites (Goodrum et al. 2000), of which the first was launched in May 1998; and the Moderate Resolution Imaging Spectroradiometer (MODIS, see Barnes et al. 1998), that was launched on the Terra platform in December 1999.

Table 4.1 Specifications of the Landsat TM, SPOT VGT, MODIS and AVHRR/3 sensors

Spectral region	TM	VGT	MODIS	AVHRR/3 (NOAA-15,16, M)
Blue	0.45-0.52 (b1)	0.43-0.47 (b0)	0.46-0.48 (b3)	
Green	0.52-0.60 (b2)		0.55-0.57 (b4)	
Red	0.63-0.69 (b3)	0.61-0.68 (b2)	0.62-0.67 (b1)	0.58-0.68 (ch1)
Near-infrared	0.76-0.90 (b4)	0.78-0.89 (b3)	0.84-0.88 (b2)	0.73-1.00 (ch2)
Mid-infrared	1.55-1.90 (b5)	1.58-1.75 (SWIR)	1.63-1.65 (b6)	1.58-1.64 (ch3A)
Spatial resolution	30 m	1 km	250 m (b1-2) 500 m (b3-6)	1.1 km
Revisit time	16 days	daily [a]	daily	twice each day

[a] At latitudes higher than 35º N and S

With the arrival of these new sensors that make frequent observations world-wide, there is a need for straightforward and reliable algorithms for snow mapping. Hall et al. (1995) proposed to use the Normalized Difference Snow Index (NDSI) for the identification of snow in MODIS imagery with a simple thresholding method. An enhanced MODIS algorithm, that was proposed by Klein et al. (1998), was found to be able to map snow cover accurately, also in dense forests (Hall et al. 1998). The accuracy of this algorithm was determined in an area in central Alaska that was completely covered by snow. However, this procedure checks for omission errors, but not for errors of inclusion. For many applications the performance during snowmelt, when parts of the surface become snow-free, will be much more relevant.

The objective of the study we present in this paper was to monitor snow cover depletion in the Tana River Basin in Northern Fennoscandia using SPOT VEGETATION images. For this purpose we used a similar algorithm as described by Klein et al. (1998), and

74

evaluated its performance and applicability to VGT images with Landsat TM images from the snowmelt season.

4.2 Snow Cover Mapping using the NDSI

In snow cover mapping the Normalized Difference Snow Index (Dozier 1989) takes advantage of the fact that the reflectance of snow decreases sharply in the mid-infrared part of the spectrum, while the reflectance of clouds remains relatively high. The NDSI is analogous to the well-known Normalized Difference Vegetation Index (NDVI) (Tucker 1979), and for Landsat TM image data it is calculated as follows:

$$NDSI = \frac{(TM\,2 - TM\,5)}{(TM\,2 + TM\,5)} \tag{4.1}$$

Where TM 2 = reflectance in TM band 2 (green band)
       TM 5 = reflectance in TM band 5 (mid-infrared band)

Due to the low reflectance in mid-infrared, pixels covered with snow will show a high NDSI-value, while clouds and bare rock will have much lower values. A NDSI threshold of 0.4 was proposed by Hall et al. (1995) to identify pixels that are covered with snow for at least 50%. An additional criterion of more than 11% reflectance in near-infrared (TM band 4) was necessary in order to distinguish snow from water, that may also have high NDSI values. Hall et al. (1998) tested this algorithm in an area in central Alaska that was completely covered with snow, and found that in tundra areas with low vegetation densities 96% of the pixels was identified as snow. In areas with high vegetation densities however, the classification accuracy was only 71%. An enhanced algorithm was therefore developed by Klein et al. (1998) that uses the NDVI in combination with the NDSI to discriminate between snow-covered and snow-free forests. An NDVI-NDSI field was added to the classification algorithm to include forested pixels with NDSI-values lower than the threshold of 0.4, yet lower NDVI-values than would be expected for snow-free conditions (see Klein et al. 1998). Furthermore, an additional threshold of 10% in green wavelengths (TM band 2) was added to exclude pixels with very low visible reflectances. In the same test area in central Alaska this enhanced algorithm correctly identified 98% of the forested pixels as snow-covered (Hall et al. 1998).

Although the algorithm has been developed for MODIS data, snow cover mapping with the NDSI should be possible with all sensor systems that make observations in visible and mid-infrared wavelengths (see table 4.1). The VGT sensor does not have a green band, but Xiao et al. (2001) found that an index calculated with red and mid-infrared data (TM band 3 and 5) gives similar results. Xiao et al. (2001) called this index the Normalized Difference Snow and Ice Index (NDSII), but to avoid confusion we will refer to it as $NDSI_{red}$, and use $NDSI_{green}$ for the original index. For a Landsat TM image of the Qinghai-Xizang (Tibetan) plateau in China Xiao et al. (2001) found that $NDSI_{green}$ and

NDSI$_{red}$ are highly correlated, especially at higher index values, and concluded that the VGT sensor has the potential to map snow cover at regional to global scales.

A thorough test of the ability of the VGT sensor to map snow coverage with the NDSI-based algorithms would require extensive field data, which have to be collected under difficult circumstances. Alternatively, the accuracy may be explored by applying different algorithms, and comparing VGT-based snow cover estimates with those of other sensors. In the present study the following approach was adopted to monitor snow cover dynamics in the Tana River Basin in Northern Fennoscandia (see figure 4.1):

1)   Like Xiao et al. (2001), we started by comparing NDSI$_{green}$ and NDSI$_{red}$ in a Landsat TM image of 30 June 1998. We also compared snow cover estimates of the original (Hall et al. 1995) and enhanced (Klein et al. 1998) NDSI algorithms, applied to this image.
2)   The next step involved a comparison of TM-NDSI$_{red}$ values and TM-NDSI-based snow cover estimates with NDSI$_{red}$ values in a corresponding VGT image.
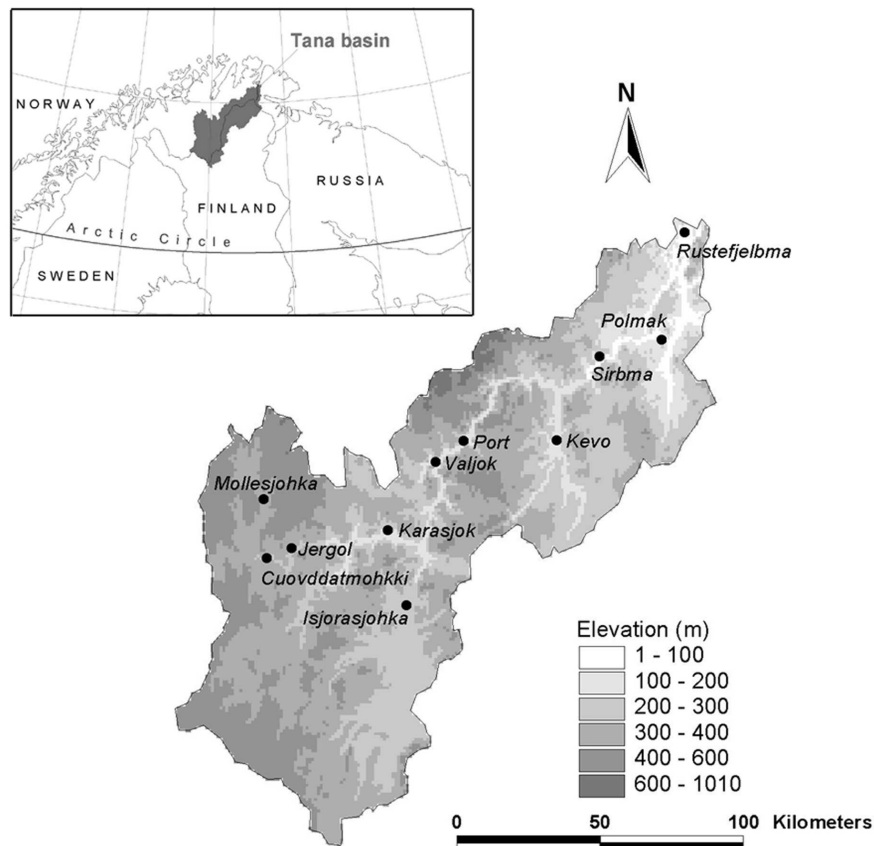
Figure 4.1 Map of the Tana Basin in Northern Fennoscandia showing the location of meteorological stations

3)	Subsequently the NDSI-based snow mapping algorithm was applied to the VGT image, using both the original and the enhanced version, and testing several threshold values. The results were compared with the snow cover estimates in the Landsat TM image.

4)	Finally, a slightly modified version of the enhanced algorithm (Klein et al. 1998) was used to monitor snow cover depletion in the Tana Basin in 1998 and 1999 with 10-day syntheses of VGT images.

In this way we were able to test the usefulness of NDSI-based snow mapping algorithms for application to VGT images of areas at high latitudes, and during the late snowmelt season.

## 4.3	Study area

The Tana River (in Finnish Tenojoki) in northernmost Finland and Norway is one of the largest rivers in Northern Fennoscandia that flows into the Barents Sea. The catchment area of 16,000 km^2 is situated between 68º 28' and 70º 28' N and 23º 30' and 28º 30' E (figure 4.1). The Tana Basin belongs to the circumpolar sub-arctic zone, and is characterised by gently sloping fells (treeless areas), cut by several deep fault valleys (Seppälä and Rastas 1980). Elevations are generally not higher than 500 m, but some mountain peaks in the northern part reach to just more than 1000 m above sea level.

Snowmelt in the Tana Basin usually takes place in late May or early June, but on the higher parts in the north the snow cover may persist until early July. Both in 1998 and 1999 the timing of snowmelt did not differ much from normal. At meteorological stations in the area temperatures came about 5 days earlier above zero in 1999 than in 1998, but due to a colder period in late April and the first half of May the snow cover disappeared 3-7 days later at most stations (figure 4.2).

## 4.4	Images used

Four Landsat TM 5 images were used in this analysis, in addition to the 10-day syntheses of SPOT VEGETATION images from 1998 and 1999 (table 4.2). Two of them were acquired in 1999, on 21 and 30 June, when snow coverage was limited to the mountainous areas in the north of the Tana Basin. The third image was acquired on 21 May 1995 and, although partly covered with clouds, it represents almost completely snow-covered conditions. Furthermore, a TM image of 18 July 1987 was used to map vegetation classes in the Tana Basin. Following Markham & Barker (1986) the digital numbers of all images were converted to "Top of the Atmosphere" reflectances. Next, band 2 (green), 3 (red) and 5 (mid-infrared) were used to calculate the NDSI. The VGT syntheses contain for each location the data of the image with the highest NDVI value within a period of 10 days, i.e. from the 1st to 10th, from the 11th to 20th, and from 21st to the end of each month (VEGETATION User Guide, 2002). All VGT data have been
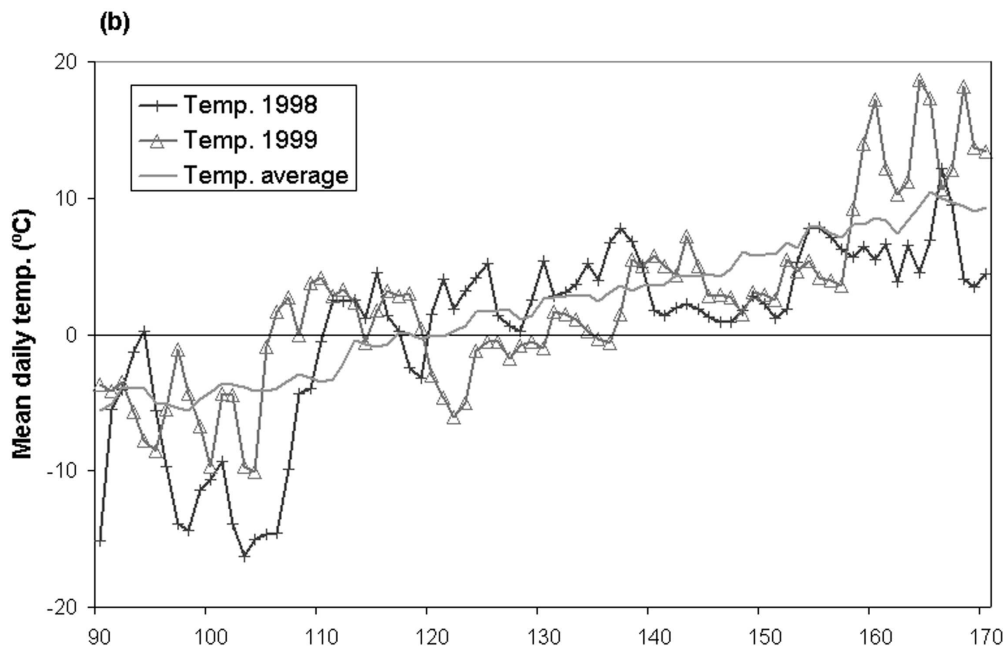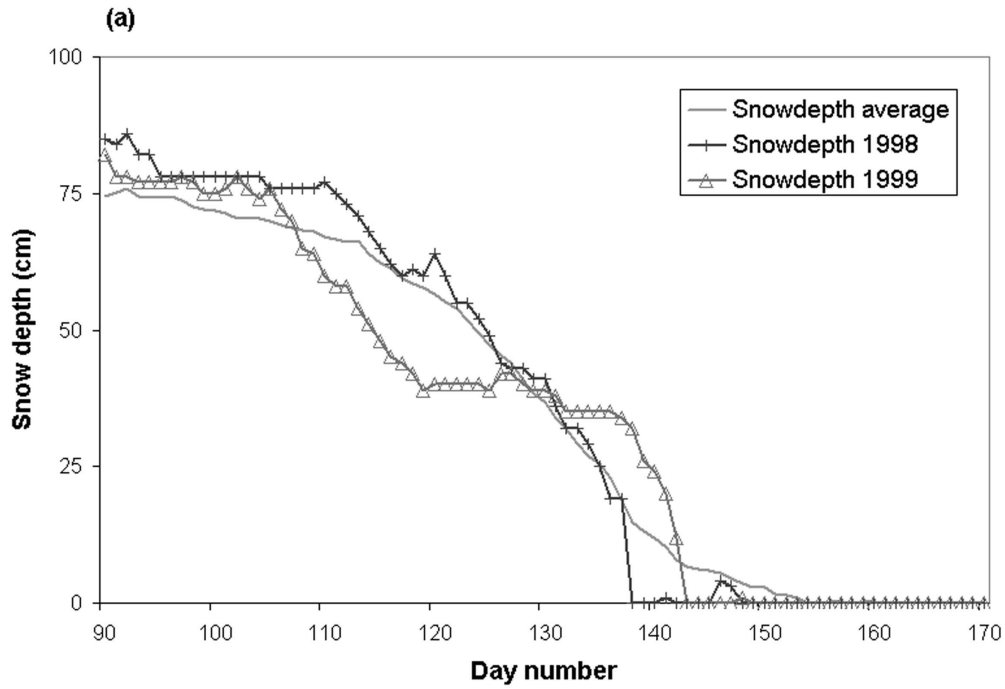
Figure 4.2 (a) Snow depths and (b) daily temperatures measured during snowmelt at Kevo, Finland, in 1998 and 1999. Averages were calculated for 1980-1999

Table 4.2 Overview of Landsat TM images used in this study

Acquisition date	Path	Row	Sun elevation angle (degrees)
18-7-1987	193	11	41.14
21-5-1995	193	11 [a]	39.58
21-6-1998	194	11 [b]	43.21
30-6-1998	193	11 [b]	42.91

[a] shifted southwards with 10%
[b] shifted northwards with 20%

calibrated to reflectances and atmospherically corrected, and have a spatial resolution of 1 km. In the synthesis of 21-30 June 1999, 98% of the pixels in the Tana Basin has been collected on 29 June, which allows a suitable comparison with the Landsat TM image of 30 June 1999.

4.5 Results

4.5.1 Comparison between $NDSI_{green}$ and $NDSI_{red}$ in Landsat TM images

The $NDSI_{red}$ in the three TM images from the snowmelt season was compared with the $NDSI_{green}$ at 2500 randomly selected points throughout the Tana Basin; points that fell outside the image area were omitted. Like Xiao et al. (2001) we found that the $NDSI_{red}$ is highly correlated to $NDSI_{green}$ (figure 4.3). This correlation is particularly strong at higher NDSI-values, which explains why the correlation coefficient is highest in the May 1995 image (see table 4.3). Regression analysis suggests that the threshold value of 0.4, used in the MODIS snow mapping algorithm, should be somewhat lower if the $NDSI_{red}$ is used. Based on these images the $NDSI_{red}$–threshold would be in the range 0.36-0.38.

For this reason several threshold values were applied to the $NDSI_{red}$–images and the results compared with $NDSI_{green}$–images, classified into snow / no-snow areas using a threshold of 0.40, as suggested by Hall et al. (1995). Although the differences are small,

Table 4.3 Correlation coefficients and regression equations between $NDSI_{green}$ and $NDSI_{red}$ in the Landsat TM images

Landsat TM image	R^2	Regression equation	n
21-5-1995	1.00	$NDSI_{red} = 1.0299 * NDSI_{green} - 0.0327$	2340
21-6-1998	0.99	$NDSI_{red} = 0.9838 * NDSI_{green} - 0.0123$	1936
30-6-1998	0.98	$NDSI_{red} = 0.9953 * NDSI_{green} - 0.0364$	2234
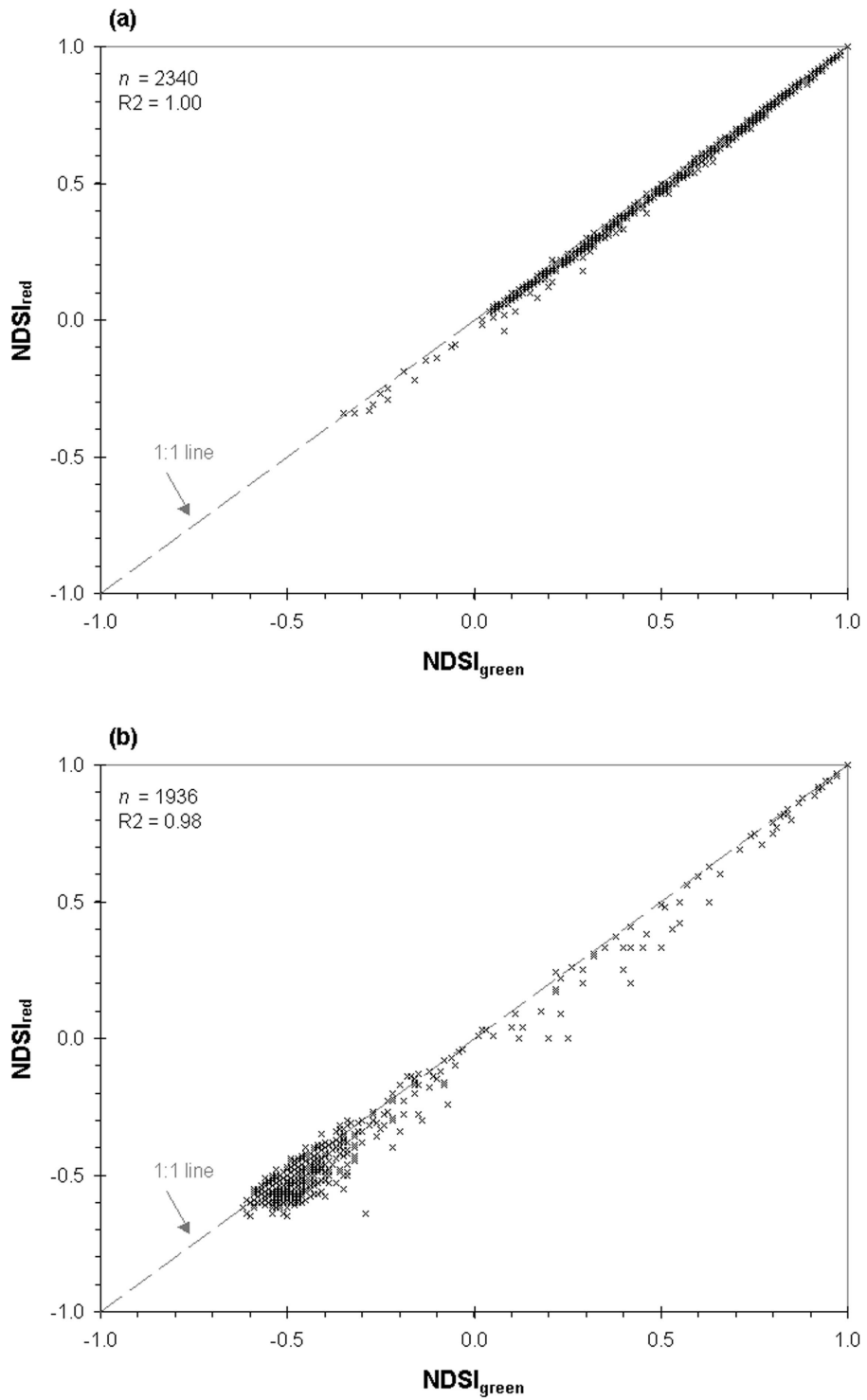
Figure 4.3 Relation between NDSI$_{green}$ and NDSI$_{red}$ in the Landsat TM image of (a) 21 May 1995, representing almost completely snow-covered conditions, and (b) 30 June 1998, representing the late snowmelt season. The comparison was based on 2500 random points in the Tana Basin, but points outside the respective image areas were omitted

the best match of the area covered by snow is generally obtained with a $NDSI_{red}$–threshold value between 0.37 and 0.39 (table 4.4). The late snowmelt images of 1998 appear to be relatively more sensitive to changes in the threshold value than the May 1995 image, that is almost completely covered with snow.

Table 4.4 Estimates of snow covered area (in km^2) in Landsat TM images using the original algorithm of Hall et al. (1995) with different threshold values

Algorithm	Threshold value	Snow covered area		
		21-5-95	21-6-98	30-6-98
$NDSI_{green}$	0.40	11969	487	134
$NDSI_{red}$	0.40	11879	479	132
$NDSI_{red}$	0.39	11912	485	134
$NDSI_{red}$	0.38	11943	491	135
$NDSI_{red}$	0.37	11976	497	137
$NDSI_{red}$	0.36	12010	504	139

Klein et al. (1998) proposed to include a NDVI/NDSI field in the snow mapping algorithm, and a similar algorithm was applied to the Landsat TM images of the Tana Basin. Compared with the original algorithm this results in slightly higher estimates of the snow covered area (table 4.5). Again, several threshold values were used for theNDSI$_{red}$–images, and the best agreement was found with slightly lower threshold values of about 0.37 (see table 4.5).

Table 4.5 Estimates of snow covered area (in km^2) in Landsat TM images using an enhanced algorithm similar to Klein et al. (1998) with different threshold values

Algorithm	Threshold value	Snow covered area		
		21-5-95	21-6-98	30-6-98
$NDSI_{green}$	0.40	12062	554	146
$NDSI_{red}$	0.40	11970	544	144
$NDSI_{red}$	0.39	11994	547	145
$NDSI_{red}$	0.38	12017	549	146
$NDSI_{red}$	0.37	12064	555	148
$NDSI_{red}$	0.36	12090	558	149

Comparison VGT-NDSI$_{red}$ with TM-NDSI$_{red}$ and snow cover estimates

The high-resolution Landsat TM image of 30 June 1998 was used as a reference for the VGT synthesis image of 21-30 June 1999. For this purpose, NDSI$_{red}$-values and snow cover estimates in the TM image were compared with NDSI$_{red}$-values in the VGT image. This was done by determining mean NDSI-values and fractional snow coverage in the TM image for each NDSI-class in the VGT image. Plotted against each other, a linear relation is visible between NDSI$_{red}$-values higher than about –0.3 (coefficient of determination $R^2 = 0.81$ in figure 4.4). Interestingly, most pixels in this range plot below the 1:1 line, in other words the mean TM NDSI$_{red}$-values are slightly lower than the corresponding VGT-classes. Below –0.5 however, the TM means are considerably higher than the VGT-classes. It is a well-known phenomenon in upscaling of remote sensing data, that larger pixel sizes result in smaller variations of measured reflectances (Curran and Atkinson 1999). Smaller visible reflectance values in the VGT image result therefore in lower (i.e. more negative) NDSI-values than in the TM image. It is however unlikely that pixels in this range will influence the identification of snow covered areas.

Comparing the fractional snow coverage in the TM image with the NDSI-classes in the VGT image shows a relatively large scatter, regardless of the algorithm used to map snow cover in the TM image (figure 4.5). For NDSI-classes higher than 0.0 the NDSI$_{red}$ correlates well with TM snow coverage ($R^2 = 0.71$). The regression line suggests that for
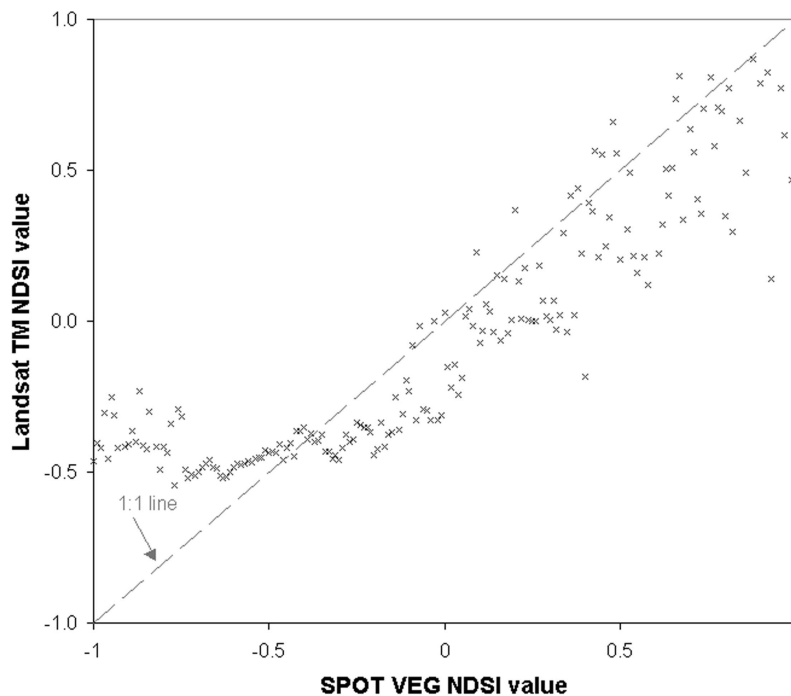
Figure 4.4 Comparison between NDSI$_{red}$-values in the Landsat TM image of 30 June 1998 and the VGT syntheses of 21-30 June 1998.

VGT images the threshold for NDSI-values needs to be much higher (about 0.6) to identify pixels that are covered with snow for 50% or more. Likewise, using a threshold of 0.4 will include areas that are covered with snow for only 36%. Figure 4.5 also shows that almost all VGT pixels that are covered with snow even for only a small part, have a NDSI-values higher than about –0.1, suggesting that this threshold value may be used to identify even small amounts of snow within the 1 by 1 km grid cells. The non-perfect correlation is caused by shaded and vegetated pixels in the TM image, of which the spectral signals are blurred in the VGT image.

4.5.3   *Comparing snow cover estimates in VGT and TM images*

The original algorithm of Hall et al. (1995) and an enhanced version (after Klein et al. 1998) were both applied to the VGT image of 21-30 June 1998 to map snow covered areas, using different threshold values (see figure 4.6). Good agreement with the TM-based estimates of snow covered area are obtained with $NDSI_{red}$-thresholds of 0.37 in the original algorithm, and 0.36 in the enhanced version (table 4.6). In the Landsat image of 30 June, the $NDSI_{green}$-based estimates of the area covered with snow were 134 km^2 using the original algorithm, and 146 km^2 using the enhanced algorithm (both with a threshold value of 0.40). Using the threshold values mentioned above, the VGT estimates are 135 and 147 km^2 respectively. Spatially the VGT sensor is able to identify the broad snow cover characteristics, but fails to recognise the detailed patterns related to topographical features, that are visible in the TM image (figure 4.6).
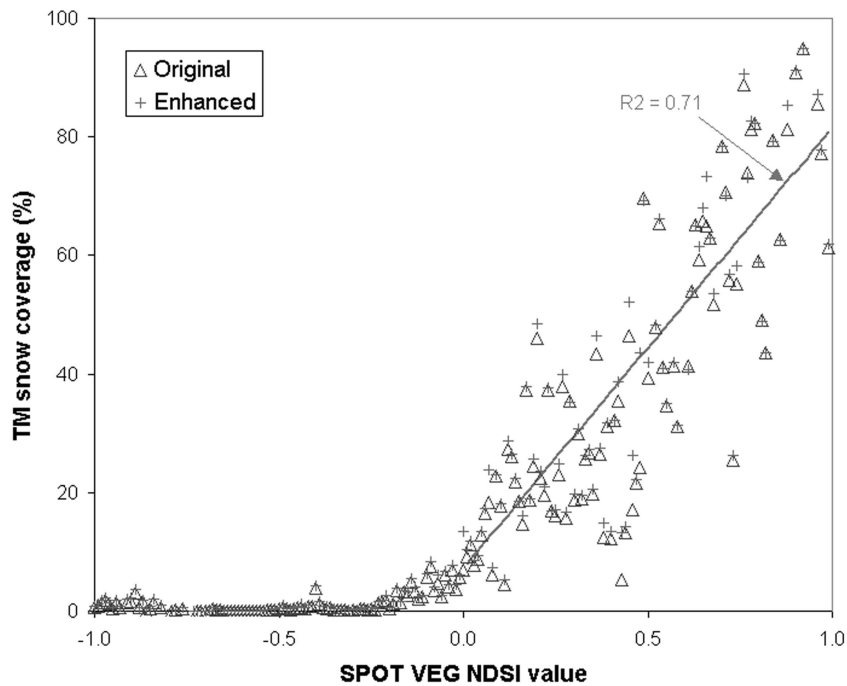
Figure 4.5 Comparison between $NDSI_{red}$-values in the VGT synthesis of 21-30 June 1998 and the mean fractional snow coverage in the TM image of 30 June 1998, mapped with both the original and the enhanced algorithm using the $NDSI_{green}$
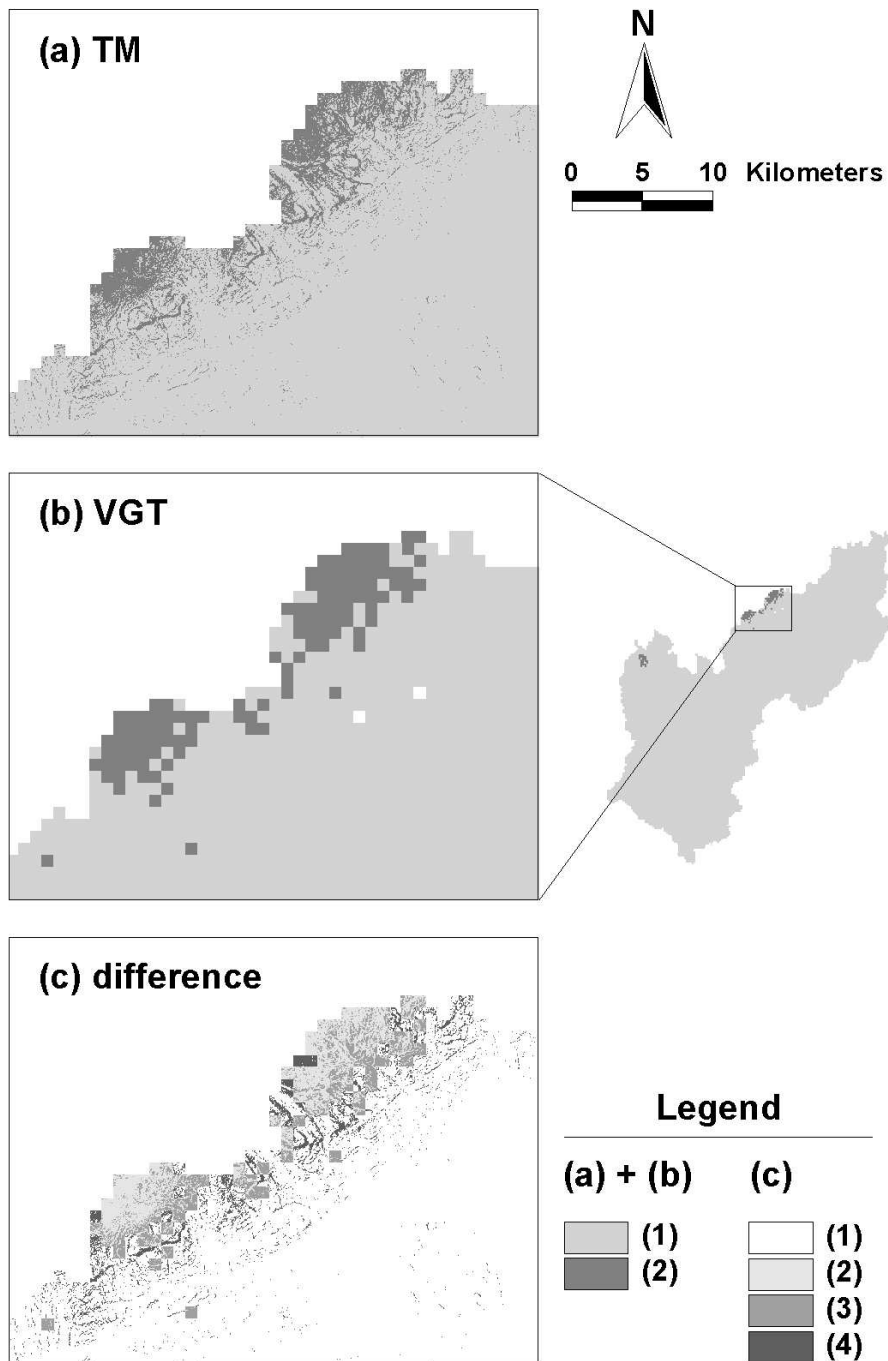
Figure 4.6 (a) Mapped snow cover in the TM image of 30-6-98; (b) mapped snow cover in the corresponding VGT image; (c) differences between (a) and (b). Legend: figure (a) + (b): 1 = snow-free, 2 = snow-covered; figure (c): 1 = snow-free in both images, 2 = snow-covered in both images, 3 = snow-free in TM and snow-covered in VGT image, 4 = snow-covered in TM and snow-free in VGT image. See the appendix for a colour version

84

Table 4.6 Estimates of snow covered area (in km^2) in the VGT image of 21-30 June 1998 using both the original and the enhanced algorithm with different threshold values

Threshold value	Snow covered area	
	Original	Enhanced
0.40	123	130
0.39	129	131
0.38	132	137
0.37	135	143
0.36	140	147

4.5.4   *Monitoring snow cover depletion with VGT images*

The enhanced snow mapping algorithm with a NDSI$_{red}$-threshold of 0.36 was finally applied to the time series of all VGT-syntheses of the snowmelt season in 1998 and 1999. Subsequently the moment was registered at which each pixel was first mapped as snow-free. This was done by comparing snow-free pixels in each image with their counterparts in the preceding one; by working backwards through the snowmelt season the effect of clouds in the earlier images was limited. The result (figure 4.7) shows the patterns of snowmelt in the Tana Basin in 1998 and 1999. In both years snow melted first in the river valleys in the southern half around mid-May. On the higher plateau areas snow cover lasted until early June, while on the mountainous areas in the north it continued to exist until late June or early July. In 1998 snowmelt started earlier, but it was more rapid in 1999 (figure 4.8). As most meteorological stations are situated in the river valleys, they became snow-free earlier in 1998 than in 1999, while the higher parts remained covered with snow for a longer period (figure 4.9). For the same reason meadows became free of snow earlier than vegetation types that are only found in the higher parts, such as alpine heaths, boulder fields and areas of bare rock (table 4.7).

In order to analyse to what extent the results depend on the snow mapping algorithm that is used, the original algorithm was applied to the images of 1999 with a NDSI$_{red}$-threshold of 0.38, and the moment of snow disappearance was registered in the same way. The resulting map of snow cover depletion appeared to be very similar to the previous one, and differs only on minor details. This means that this methodology to map the timing of snow disappearance is robust: the employed algorithm nor the NDSI-threshold value that was chosen led to significantly different results in this case.

Furthermore, there is good agreement between the observed first snow-free date at the meteorological stations in the Tana Basin, and the first snow-free period of their corresponding pixels in the VGT synthesis images (table 4.8). At most stations the pixels are flagged as snow-free in the same period as observed or in the period after that, which may be due to the date of imaging for that particular pixel. These results are encouraging,

a) 1998

N

21-30 April
1-10 May
11-20 May
21-31 May
1-10 June
11-20 June
21-30 June
1-10 July or later

b) 1999

0   25   50 Kilometers
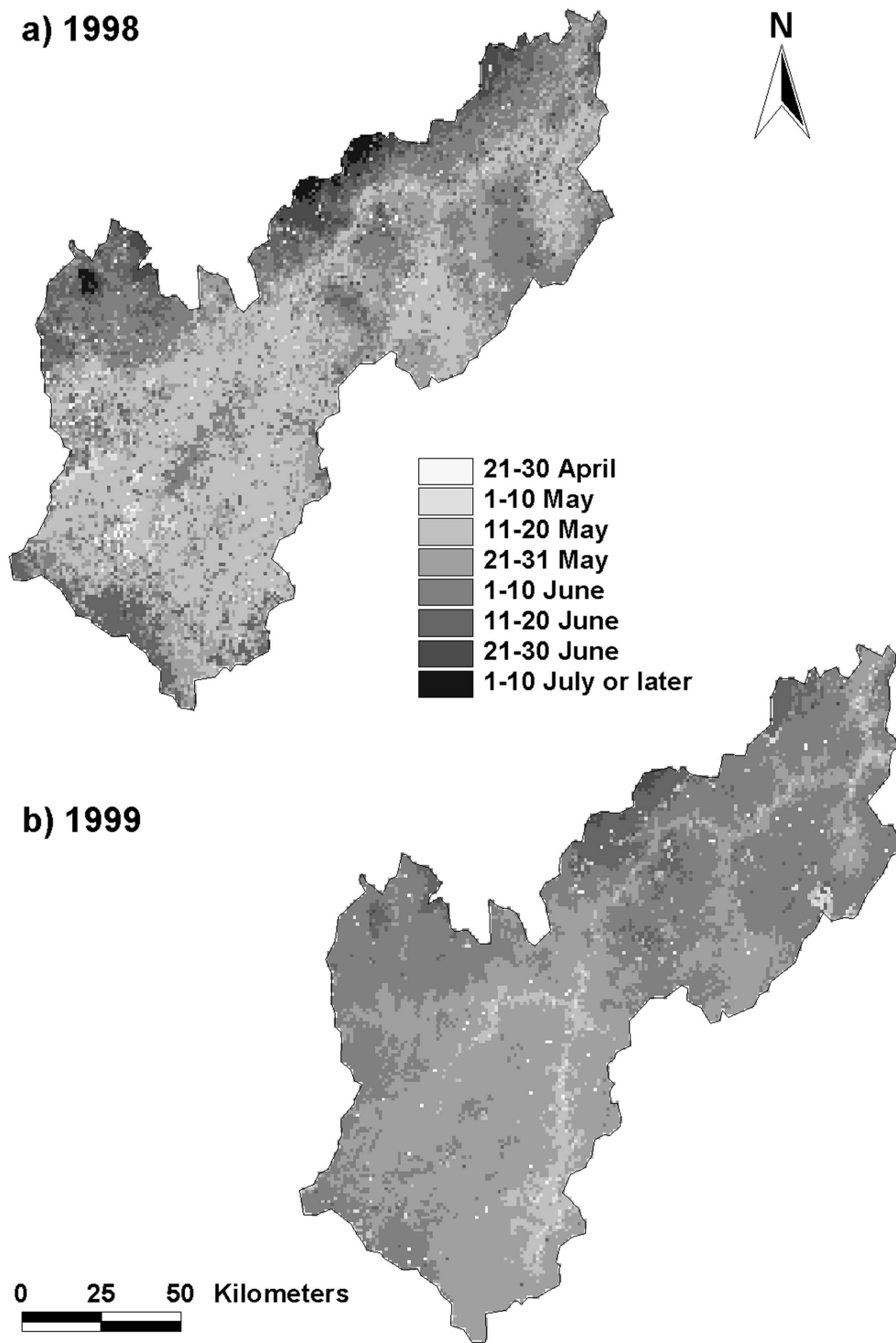
Figure 4.7 Disappearance of snow in the Tana Basin, based on 10-day VGT syntheses of (a) 1998 and (b) 1999. See the appendix for a colour version
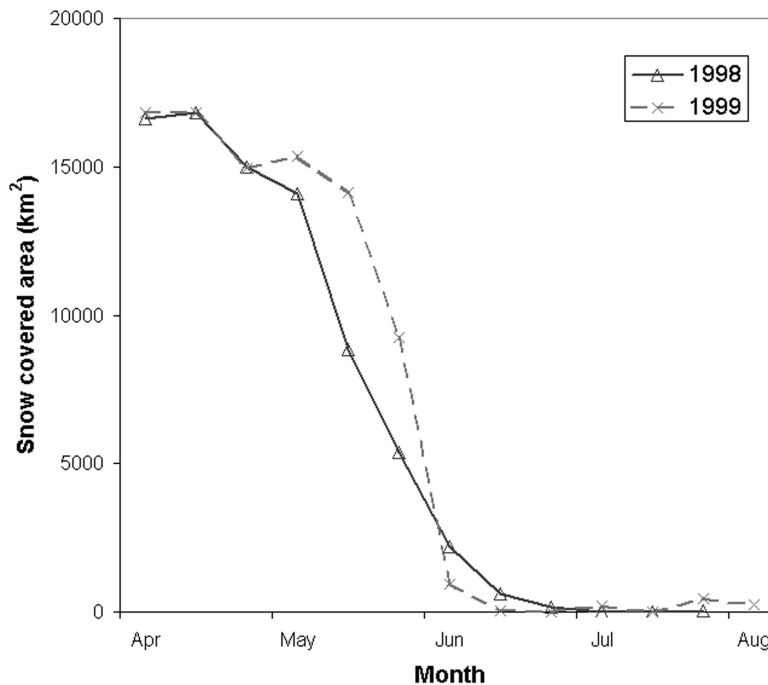
Figure 4.8 Mapped snow cover extent in the Tana Basin in 1998 and 1999

considering the fact that the VGT pixels represent a spectral response over 1 by 1 km, while the station data are point observations. At only one station, Mollesjohka, the observed first snow-free date is much later than the VGT estimate, both in 1998 and 1999; the reason for this is unknown.

4.6   Discussion

Remote sensing of the spatial and temporal extent of snow is helpful for a number of hydrological applications. Depletion curves of the snow covered area, similar to figure 4.8 but plotted against cumulative degree-days or cumulative melt depth, are used as input in the Snowmelt Runoff Model (SRM) (Martinec et al. 1994) to predict melt runoff from snow-covered catchments (Ferguson 1999). Dankers et al. (2002) used the observations of snow cover depletion in the Tana Basin, shown in figure 4.7, to validate a hydrological model in a spatially distributed way. For all these applications it is essential to obtain frequent observations during the snowmelt season. This is particularly true at high latitudes, where cloud cover can be persistent. Medium-resolution sensors such as the AVHRR, MODIS and the VGT sensor on the SPOT 4 satellite essentially make observations in the visible and mid-infrared region on a daily or near-daily basis, and are therefore suitable to monitor snow cover dynamics in spring. Sensors such as the Landsat TM may have a much higher spatial resolution, but their revisit time is too long for reliable mapping of snowmelt. Landsat TM images however are able to give much more detailed information on snow cover patterns, that are not recognisable in a VGT image

(see figure 4.6). The linear relation between NDSI-values in the VGT syntheses of 21-30 June 1998 and snow cover in the Landsat TM image of 30 June 1998 (figure 4.5) indicates that the NDSI can be used to map fractional snow coverage at sub-pixel level in VGT images. Due to the scattering of points around the regression line classification accuracies may be modest. Linear spectral unmixing may prove to be a more promising approach for partly snow covered pixels (cf. e.g. Fortin et al. 2000).

A prerequisite for the operational use of satellite imagery is an algorithm that correctly identifies snow-covered areas. Hall et al. (1998) validated both the original and the enhanced NDSI-based algorithm in Alaska under completely snow-covered conditions. However, this is only a valid test for underestimation of the snow covered area at the beginning of the snowmelt season, but not for overestimation at the end. We tested a similar algorithm for VGT images during late spring, and found that the best agreement with Landsat TM-based estimates of the snow covered area is obtained with slightly lower NDSI-threshold values than in the MODIS algorithm. This may be due to the use of the red, and not the green band, to calculate the NDSI. Since the VGT, TM and MODIS spectral bands do not completely overlap, the threshold values found in this study are not necessarily the same for other sensors. Moreover, it should be noted that the

Table 4.7: Mean and standard deviation (SD) of the moment of snow disappearance per vegetation class in the Tana Basin, in 1998 and 1999. Vegetation types were mapped by classifying the Landsat TM image of 18 July1987

| | 1998 | | 1999 | |
	Mean	SD (10-day periods)	Mean	SD (10-day periods)
Water	1-10 June	1.48	1-10 June	0.89
Snow	1-10 July	0.73	11-20 June	0.49
Meadows	11-20 May	0.68	11-20 May	0.69
Birch forest, high density	21-30 May	0.90	21-31 May	0.58
Birch forest, low density	21-30 May	1.08	21-31 May	0.61
Pine	21-30 May	1.02	21-30 May	0.74
Wetlands	21-30 May	1.09	21-30 May	0.74
Alpine heaths	1-10 June	1.10	1-10 June	0.66
Lichen areas	21-30 May	1.40	1-10 June	0.71
Boulder fields	1-10 June	1.41	1-10 June	0.77
Bare rock, gravel	1-10 June	1.87	1-10 June	1.09
Areas in shadow	21-30 May	0.89	21-30 May	0.66

88
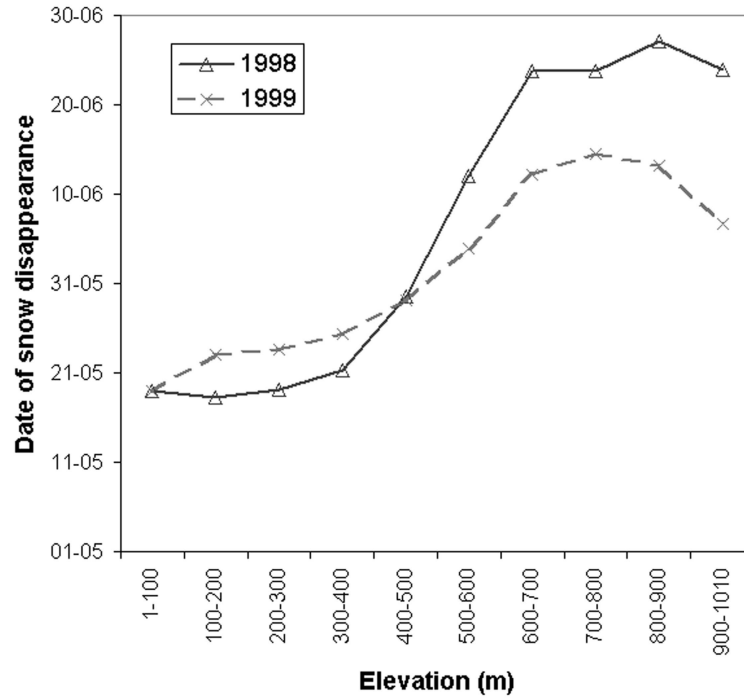
Figure 4.9 Mean date of snow disappearance per elevation class in the Tana Basin, 1998 and 1999

Table 4.8 Observed first snow-free date at meteorological stations in the Tana Basin, and first snow-free period of the corresponding pixels in the VGT 10-day syntheses

	Elevation in m	1998		1999	
		Observation	VGT	Observation	VGT
Rustefjelbma	9	17/5	21-31/5	15/5	21-31/5
Polmak	21	20/5	11-20/5	-	21-31/5
Sirbma	51	14/5	11-20/5	19/5	21-31/5
Kevo	107	18/5	11-20/5	23/5	21-31/5
Port	115	17/5	21-31/5	23/5	1-10/6
Karasjok	129	12/5	11-20/5	18/5	21-31/5
Valjok	132	18/5	11-20/5	21/5	21-31/5
Iskorasjohka	153	10/5	11-20/5	16/5	11-20/5
Jergol	230	16/5	11-20/5	22/5	21-31/5
Cuovddatmohkki	286	14/5	11-20/5	21/5	21-31/5
Mollesjohka	382	10/6	21-31/5	1/6	21-31/5

89

differences in snow cover estimates are only small, and that a higher threshold value had little influence on the final estimate of snow cover disappearance. Klein et al. (1998) developed the NDVI-NDSI field in the enhanced algorithm using a snow reflectance model in conjunction with a canopy reflectance model, and it is recommended to investigate if the relations they found are exactly similar for VGT images.

4.7   Conclusions

In the Tana River Basin in Northern Fennoscandia a time series of SPOT VEGETATION images appeared to be useful in monitoring the snow cover dynamics during spring. Since the $NDSI_{red}$ was found to correlate well with the $NDSI_{green}$, the MODIS snow-cover mapping algorithm proposed by Hall et al. (1995) and Klein et al. (1998), can be applied to 10-day VGT syntheses using the red and mid-infrared spectral bands. The best agreement with snow covered area, mapped using a Landsat TM image of almost the same date, is found with slightly lower threshold values (0.36 – 0.37) than in the original algorithm. The actual choice for a different threshold-value in the VGT-syntheses has however little influence on the final estimate of the moment of snow cover disappearance.

Applying the algorithm to 10-day VGT-syntheses of the snowmelt season in 1998 and 1999 resulted in good agreement with the first snow-free date observed by meteorological stations in the area. The time series of VGT images revealed snowmelt patterns that are not apparent in the data from these stations, that are mostly located in river valleys. Over the entire Tana Basin, snowmelt started earlier in 1998 but lasted longer. Therefore, the river valleys became snow-free earlier in 1998 than in 1999, while the opposite happened on the highest parts. Satellite-based observations of snow cover dynamics in spring are therefore a useful tool in hydrological studies of northern environments.

4.8   Acknowledgements

4.9   References

Barnes, W.L., T.S. Pagano & V.V. Salomonson (1998): Prelaunch characteristics of the Moderate Resolution Imaging Spectroradiometer (MODIS) on EOS-AM1. IEEE Transactions on Geoscience and Remote Sensing 36, pp. 1088–1100.
Curran, P.J. & P.M. Atkinson (1999): Issues of scale and optimal pixel size. In: A. Stein, F.D. van der Meer & B. Gorte (eds.): Spatial Statistics for Remote Sensing. Dordrecht: Kluwer, pp. 115-134.

Dankers, R., O.B. Christensen & H. Middelkoop, H. (2002): Climate change impact on snow cover dynamics in the Tana River Basin, Northern Fennoscandia. Submitted to Nordic Hydrology.

Dozier, J. (1984): Snow reflectance from Landsat-4 Thematic Mapper. IEEE Transactions on Geoscience and Remote Sensing GE-22, pp. 323-328.

Dozier, J. (1989): Spectral signature of Alpine snow cover from the Landsat Thematic Mapper. Remote Sensing of Environment 28, pp. 9-22.

Ferguson, R.I. (1999): Snowmelt runoff models. Progress in Physical Geography 23, pp. 205-227.

Fortin, J.P., M. Bernier, A. El Battay & Y. Gauthier (2000): Estimation of surface variables at the sub-pixel level for use as input to climate and hydrological models. Québec, Canada: INRS-Eau (Rapport de recherche INRS-Eau 564).

Goodrum, G., K.B. Kidwell & W. Winston (2000): NOAA KLM user's guide, September 2000 revision. Suitland, Maryland: National Oceanic and Atmospheric Administration (NOAA), available from http://www2.ncdc.noaa.gov/docs/klm/, accessed on 30 July 2002.

Hall, D.K., G.A. Riggs & V.V. Salomonson (1995): Development of methods for mapping global snow cover using moderate resolution imaging spectroradiometer data. Remote Sensing of Environment 54, pp. 127-140.

Hall, D.K., J.L. Foster, D.L. Verbyla, A.G. Klein & C.S. Benson (1998): Assessment of snow-cover mapping accuracy in a variety of vegetation-cover densities in central Alaska. Remote Sensing of Environment 66, pp. 129-137.

Houghton, J. T., Y. Ding, D.J. Griggs, M. Noguer, P.J. van der Linden & D. Xiaosu (2001): Climate Change 2001: The Scientific Basis. Cambridge: Cambridge University Press.

Klein, A.G., D.K. Hall & G.A. Riggs (1998): Improving snow cover mapping in forests through the use of a canopy reflectance model. Hydrological Processes 12, pp. 1723-1744.

Koster, E.A. (1991): Assessment of climate change impact in high-latitudinal regions. Terra 103, pp. 3-13.

Markham, B.L. & J.L. Barker (1986): Landsat MSS and TM post-calibration dynamic ranges, exoatmospheric reflectances and at-satellite temperatures. EOSAT Technical Notes 1, pp. 3-8.

Martinec, J., A. Rango & R. Roberts (1994): Snowmelt runoff model (SRM) user's manual, edited by M.F. Baumgartner. Bern: Department of Geography, University of Bern (Geographica Bernensia P29).

Mccarthy, J.J., O.F. Canziani, N.A. Leary, D.J. Dokken & K.S. White (2001): Climate Change 2001: Impacts, Adaptation and Vulnerability. Cambridge: Cambridge University Press.

Saint, G. (1996): SPOT 4 VEGETATION system: Association with high resolution data for multiscale studies. Advances in Space Research 17, pp. (1)107-(1)110.

Seppälä, M. & J. Rastas (1980): Vegetation map of northernmost Finland with special reference to subarctic forest limits and natural hazards. Fennia 158, pp. 41-61 + appendix.

Tucker, C.J. (1979): Red and photographic infrared linear combinations for monitoring vegetation. Remote Sensing of Environment 8, pp. 127-150.

VEGETATION User Guide. Available from http://www.spotimage.fr/data/images/vege/VEGETAT/home.htm, accessed on 29 July 2002.

Xiao, X., Z. Shen & X. Qin (2001): Assessing the potential of VEGETATION sensor data for mapping snow and ice cover: a Normalized Difference Snow and Ice Index. International Journal of Remote Sensing 22, pp. 2479-2487.

5 APPLICATION OF A LARGE-SCALE WATER BALANCE MODEL TO THE TANA RIVER BASIN

5.1 Introduction

Conceptual water balance models are often believed to be useful in assessing the impact of climatic changes on regional hydrology, and have successfully been applied at larger scales (Arnell, 1999; Kwadijk, 1993). In terms of data demands, accuracy, flexibility and ease of use they have significant advantages over lumped empirical models or physically-based models (Xu, 1999). Most models currently in use have been developed for temperate climatic conditions. However, sub-arctic environments, such as the Tana Basin in Northern Fennoscandia (see chapter 2), are very distinct in their hydrological behaviour. The water balance of these areas is dominated by a long-lasting snow cover in winter, while in summer evapotranspiration may predominate in many areas (Mackay & Løken, 1974; Rovansek et al., 1996; see also chapter 3). Moreover, many models are designed to simulate river discharge, and may not be able to simulate spatial patterns in snow coverage or evaporation realistically. The objective of this chapter is therefore to explore the performance of a GIS-based water balance model, developed for the Rhine, in the sub-arctic Tana Basin. This model, named RHINEFLOW (Kwadijk, 1993), was applied to the Tana Basin without significant changes in the model concept. The data that were used and the assumptions that had to be made, are discussed in this chapter. In evaluating the model performance, attention is paid those processes that dominate the water balance of this area. Finally, some suggestions for model improvement are given.

5.2 The concept of water balance

The water balance of an area describes the relation between input, storage and output of water. While input in the form of precipitation is mainly dependent on climate, the output, either in the form of river discharge or evapotranspiration, also depends on vegetation and catchment characteristics. In the longer term, i.e. on a yearly basis or longer, changes in storage can usually be neglected, and the water balance can be written as:

$$Q = P - E \tag{5.1}$$

where Q = river discharge
        P = amount of precipitation
        E = amount of evapotranspiration

According to Woo (1990), however, year-to-year changes in water storage may not be negligible in (non-glacial) permafrost basins. Theoretically the annual partitioning of precipitation into evapotranspiration and runoff is controlled by the temporal distribution

of water supply (precipitation) and demand (evapotranspiration), which are balanced by water storage in the soil (Milly, 1994). At smaller than annual time scales – monthly, daily or even hourly – the changes in and interactions between the storages that can be identified in a catchment, have to be taken into account:

$$Q = P - E \pm \Delta S \qquad (5.2)$$

where ΔS = change in storage

These storages include water storage in vegetation, surface detention, storage in snow and glaciers, soil storage, groundwater storage, and storage in lakes and channels (Kwadijk, 1993). The importance of each component differs in time and in space. In sub-arctic catchments for example, storage of precipitation in snow is much more important than in temperate environments.

5.3   Water balance of the Tana Basin

Annual water balance characteristics of the Tana Basin (chapter 2) were analysed for a period of 20 years: October 1979 through September 1999 (referred to as 1980-1999). For this purpose, daily temperature and precipitation data from the meteorological stations listed in table 5.1 were extrapolated to the entire river basin using Thiessen polygons. Mean annual precipitation in this period amounted to 401 mm, and the mean annual temperature was −2.0ºC. The second half of this period (1990-1999) was considerably warmer than in the first (−1.51ºC vs. −2.50ºC in 1980-1989. The second half also received slightly more precipitation (405 vs. 398 mm/year). Due to the large interannual variability, a significantly drier or wetter period could not be identified.

A first indication of the water balance was obtained by comparing the basin-averaged precipitation with observations on river runoff. The ratio of observed discharge and precipitation (Q / P ratio) in the Tana basin and several subcatchments is given in table 5.2. Obviously, these ratios are too high. Considering the fact that a significant proportion of the annual rainfall in the area is lost to evapotranspiration, the average Q / P ratio should be less than 1.0. However, in several subbasins it is even higher than 1.0, which is theoretically impossible. According to equation (5.1), the difference between input (P) and output (Q) indicates the amount of evapotranspiration (E) in the entire basin. Upstream of Polmak, Norway, this difference is only 3 mm/year in the period 1980-1989. This estimate is not realistic. As demonstrated in chapter 3, the actual amount of evapotranspiration in this area is much higher.

There are two possible explanations for the unrealistic Q / P ratios in table 5.2: the observed discharge of the Tana River is too high, or the precipitation measurements are too low. Most precipitation stations are located in the river valleys (see figure 5.1), and may not be representative for the surrounding upland areas, that constitute the greatest part of the Tana Basin. Moreover, it is a well-known problem that precipitation gauges

94

Table 5.1 Meteorological stations in the Tana Basin used in this chapter, and their observation period of temperature and precipitation between October 1979 and September 1999. For locations, see figure 5.1

	Precipitation	Temperature
Rustefjelbma	10/79 – 9/99	10/79 – 9/99
Kevo	10/79 – 9/99	10/79 – 9/99
Karasjok	10/79 – 9/99	10/79 – 9/99
Cuovddatmohkki	10/79 – 9/99	10/79 – 9/99
Sihcajavri	10/79 – 9/99	10/79 – 9/99
Polmak, Polmak II	10/79 – 7/98	
Sirbma	10/79 – 9/99	
Skoganvarre	10/79 – 12/79	
Port	8/81 – 9/99	
Valjok	10/79 – 9/99	
Iskorajohka	10/79 – 9/99	
Jergol	8/81 – 9/99	
Mollesjohka	10/79 – 9/99	
Jotkajavre	10/79 – 9/99	

systematically underestimate snowfalls (Goodison et al., 1998; Yang et al., 2001). In addition, point snow data are not representative for the snow cover of an area (Yang & Woo, 1999). Assuming that the discharge measurements are correct, it appears that precipitation in the catchment area is seriously underestimated by direct extrapolation of the observations.

5.4   Model description

In a previous study, Kwadijk (1993) developed a water balance model of the Rhine Basin, and used it to study the impact of climate change on the discharge of the River Rhine. This model, named RHINEFLOW, is a GIS-based, conceptual water balance model that uses standard meteorological input variables, and geographical data on topography, land cover, soil type and groundwater flow characteristics. Parameters and variables are stored in a raster Geographical Information System (GIS) called PCRaster, and the model itself is implemented in PCRaster using a scripting language (Van Deursen, 1995). Considering its limited data demands and ease of use, this model was applied to the Tana River Basin. A brief introduction to the concept of the model is given in this section.
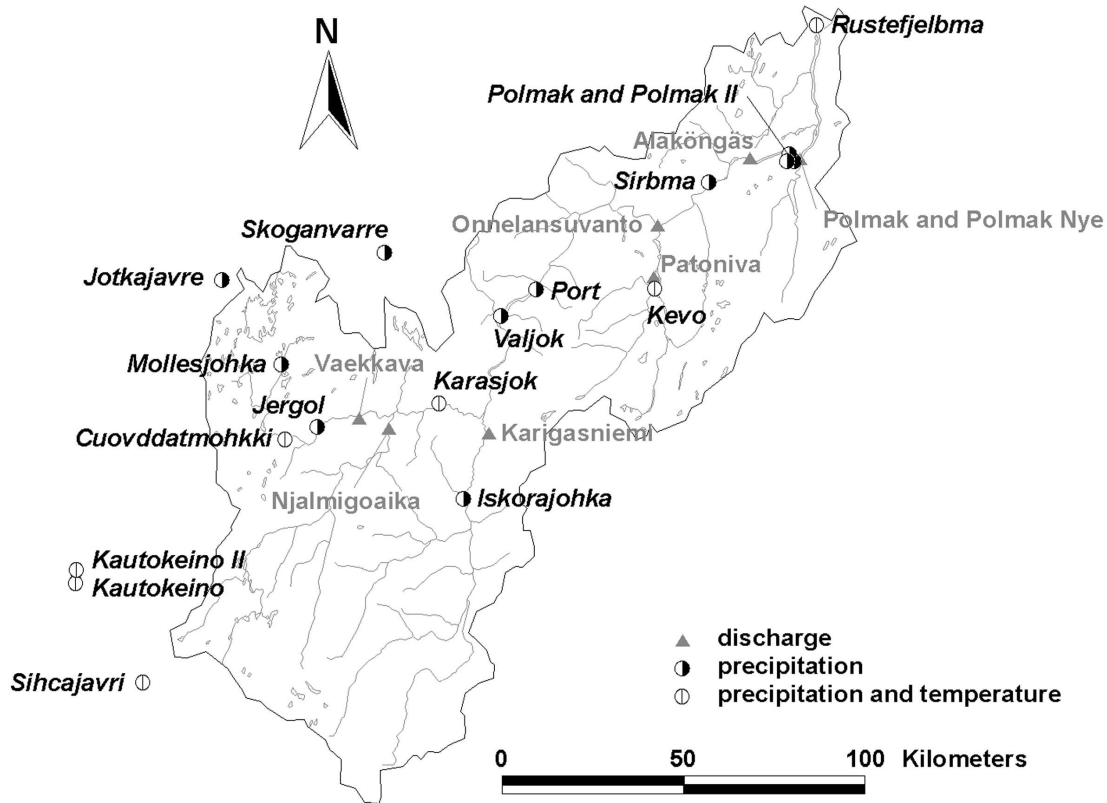
Figure 5.1 Location of meteorological stations and discharge stations in the Tana Basin

5.4.1   Model concept

Following the water balance equation (5.2), RHINEFLOW calculates runoff as a function of precipitation, actual evapotranspiration and changes in water storage. The model identifies four storages: snow, soil, groundwater and lakes. For each time step the input, storages and losses are calculated for each cell, and the produced discharge is accumulated over a digital elevation model (DEM) of the catchment to determine runoff at the outflow point (figure 5.2). A hydraulic routing scheme, that calculates travel times of runoff, is not included in the model. The water balance calculations of RHINEFLOW are based on the concept of Thornthwaite & Mather (1957). This approach takes possible soil water deficiencies into account when calculating actual evapotranspiration. Snow accumulation and snowmelt are simulated using the temperature-index method; discharge is a combination of rapid runoff (a fraction of the water surplus of the soil compartment) and baseflow from the groundwater store. Originally designed for monthly timesteps and grid cells of 3 by 3 km, the model has later been applied to the Rhine Basin at 1 by 1 km cells with 10-day timesteps (Van Deursen, 1999[a]). The main components of the model are described below.

96

Table 5.2 Runoff / rainfall (Q/P) ratios of observed runoff for the Tana Basin and several sub-catchments in the period 1980-1999. For locations, see figure 5.1

Discharge station	River	Q/P ratio		
		1980-1989	1990-1999	1980-1999
Vækkava	Jiesjåkka	0.93		
Njalmigoaika	Karasjåkka	0.94		
Karigasniemi	Inarijoki	1.06	0.95	1.01
Patoniva	Utsjoki	0.97	0.99	0.98
Onnelansuvanto	Tana (Tenojoki)	1.12	1.03	1.07
Alaköngäs	Tana (Tenojoki)	1.10	1.03	1.06
Polmak	Tana	0.95		

5.4.2 Snow storage and melt

Similar to many other hydrological models, such as the Snowmelt Runoff Model (SRM) (Martinec et al., 1994) and the HBV model (Bergström, 1995), RHINEFLOW uses a temperature-index approach to estimate snow accumulation and melt. In this approach a degree-day factor (*DDF*) is used to convert air temperature above a certain threshold to snowmelt in mm (Ferguson, 1999):

$$M = (T_a - T_0) \times DDF \tag{5.3}$$

where　M　= amount of snowmelt (mm.month^{-1})
　　　　T_a　= air temperature (ºC)
　　　　T_0　= threshold temperature (ºC)
　　　　DDF = degree-day factor (mm.ºC^{-1}.month^{-1})

The degree-day coefficient implicitly represents all terms of the energy budget that account for the mass balance of a snow pack, and is therefore highly variable over time (Melloh, 1999). For this reason, several models allow the *DDF* to vary in time, instead of using a constant value. Martinec et al. (1994) recommend to increase the *DDF* twice a month, to account for lower albedo, higher aerodynamic roughness and higher liquid water content as the snowpack ages. In the HBV model season- and weather-dependent degree-day factors were tested, but without much success (Lindström et al., 1997). The melt rate may also differ between vegetation types. Wind speed and turbulent heat transfer in forests for example are generally lower than in open areas. Several models such as HBV and the Semi-distributed Land Use-based Runoff Processes (SLURP) model (Kite, 1995) have therefore been applied with different snowmelt rates for several

land use classes (see e.g. Kite & Kouwen, 1992). In the latest version of RHINEFLOW (Van Deursen, 1999[a]), minimum and maximum temperatures, instead of the mean temperature, may be used to calculate snowmelt. In this case snowfall is triggered by the minimum temperature, and the fraction of precipitation falling as snow is equal to the fraction of the temperature interval between minimum and maximum temperature that is below the snowfall-threshold temperature. Likewise, snowmelt is triggered by the maximum temperature, but decreased for the fraction of the temperature interval that is below the snowmelt-threshold temperature.
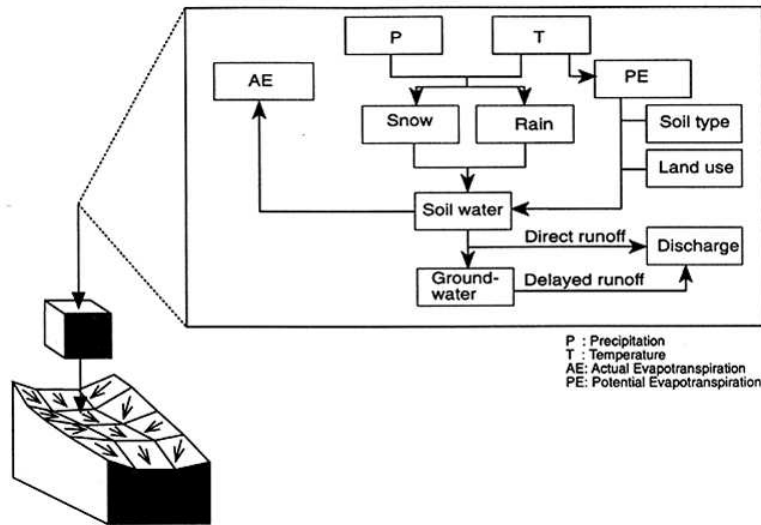
Figure 5.2 Flowchart of RHINEFLOW (after Kwadijk, 1993)

In many areas the temperature-index method may perform well but it is dependent on an appropriate degree-day factor (*DDF*). This factor can be determined by field experiments, or will have to be obtained by calibration otherwise. Singh et al. (2000) list several *DDF*s reported by researchers, ranging from 1.3 to 8.0 mm.°C^{-1}.day^{-1} for snow and from 5.0 to 13.8 mm.°C^{-1}.day^{-1} for ice. Kwadijk (1993) used a much lower value of 18 mm.°C^{-1}.month^{-1} for the Alpine regions of the Rhine basin. Kite & Kouwen (1992) used different factors for different land use classes, ranging from 1.04 mm.°C^{-1}.month^{-1} for bare soil to 3.78 mm.°C^{-1}.day^{-1} for forested areas.

5.4.3   Evapotranspiration

The Thornthwaite method of estimating potential evapotranspiration (E_p) (Thornthwaite & Mather, 1955; 1957) is based on air temperature and day length only. Expressed on a monthly basis it reads (Ward & Robinson, 1990; Sellinger, 1996):

$$E_{pi} = 16 \times d_i \left(\frac{10 T_i}{I} \right)^a \tag{5.4}$$

where E_{pi} = potential evapotranspiration in month i (mm.month^{-1})
          d_i = day length correction factor (Rosenberg et al., 1983):

$$d_i = \left(\frac{L_i}{12} \right) \times \left(\frac{N_i}{30} \right) \tag{5.5}$$

          L_i = mean actual day length (h)
          N_i = number of days in the month under consideration
          T_i = mean air temperature (ºC)
          I = heat index, which is a summation of the monthly heat indexes:

$$I = \sum_{i=1}^{12} \left(\frac{T_i}{5} \right)^{1.514} \tag{5.6}$$

          a = a cubic function of I, namely:

$$a = 0.49 + 0.179\ I + 7.71 \times 10^{-5}\ I^2 + 6.75 \times 10^{-7}\ I^3 \tag{5.7}$$

Thornthwaite & Mather (1957) recommend to use the day length correction factors of 50º N also for higher latitudes.

The Tornthwaite method requires only temperature and hours of daylight, and these two variables are relatively easy to obtain. Consequently, it has been applied in many studies in a wide range of climatological conditions, often with reliable results (Penman, 1956; Pereira & Camargo, 1989). Less good results can be expected over very short periods of time (when mean temperature is not a suitable measure of incoming radiation) and in environments with rapidly changing air temperature and humidity resulting from advection effects, such as the British Isles (Ward & Robinson, 1990). According to Rosenberg et al. (1983) E_p is likely to be underestimated at the time of annual maximum radiation reception during summer.

In RHINEFLOW the potential evapotranspiration is modified with a crop factor to obtain potential evapotranspiration rates for different land use types (Kwadijk, 1993). If the combined input of precipitation and snowmelt exceeds this potential evapotranspiration, the actual evapotranspiration is assumed to be equal to the latter. Otherwise, the actual evapotranspiration is a combination of the available precipitation and a change in soil moisture:

$$E_{ai} = E_{pi} \qquad\qquad \text{if } (P_i + M_i) \geq E_{p_i}$$
$$E_{ai} = P_i + M_i + (SM_{i-1} - SM_i) \quad \text{if } (P_i + M_i) < E_{p_i} \tag{5.8}$$

where E_{ai} = actual evapotranspiration in month i (mm.month^{-1})
        P_i = amount of rain (mm)
        SM_i = amount of water stored in the soil (mm)

Instead of calculating evapotranspiration rates with the Thornthwaite method, Van Deursen (1999[a]) used reference crop evapotranspiration data as input data in RHINEFLOW. In climate change studies, an empirically derived relationship between temperature change and reference evaporation change was used to estimate changes in evaporation.

Since the Thornthwaite method was developed for temperate environments in the USA, the performance in the sub-arctic Tana basin was tested separately. Figure 5.3 shows the Penman-based evapotranspiration estimations for the Kidisjoki catchment near Kevo, Finland (see chapter 3). Also shown are potential evaporation estimates based on the Thornthwaite method, using day length correction factors of this specific site (equation 5.5), as well as those for 50° N, as recommended by Thornthwaite & Mather (1957). As can be seen the Thornthwaite-based estimates of potential evapotranspiration are much higher than those predicted by Penman-Monteith. According to the latter the overall evaporation in the period 22 June – 2 August 1999 is 74 mm or 1.8 mm/day, which corresponds to flux measurements in the same area (chapter 3). The Thornthwaite estimates amount to 5.2 mm/day using local day length correction factors, and 3.5 mm/day using the correction of 50° N. If no day length correction is applied at all, the evaporation estimate is still 2.7 mm/day. Assuming that the estimates of Penman-Monteith – being one of the most advanced evapotranspiration models currently available (Shuttleworth, 1993) – are correct, the Thornthwaite model appears to overestimate evaporation in this sub-arctic environment considerably.

5.4.4   Soil and groundwater storage

Soil moisture is calculated as a function of the maximum water holding capacity of the soil and the accumulated potential water loss:

$$SM_i = MWC \times e^{(-APWL_i / MWC)}$$
$$APWL_i = APWL_{i-1} - (P_i + M_i) + E_{pi} \quad \text{if } (P_i + M_i) < E_{p_i} \tag{5.9}$$

where MWC = maximum water holding capacity (mm)
        $APWL_i$ = accumulated potential water loss (mm)
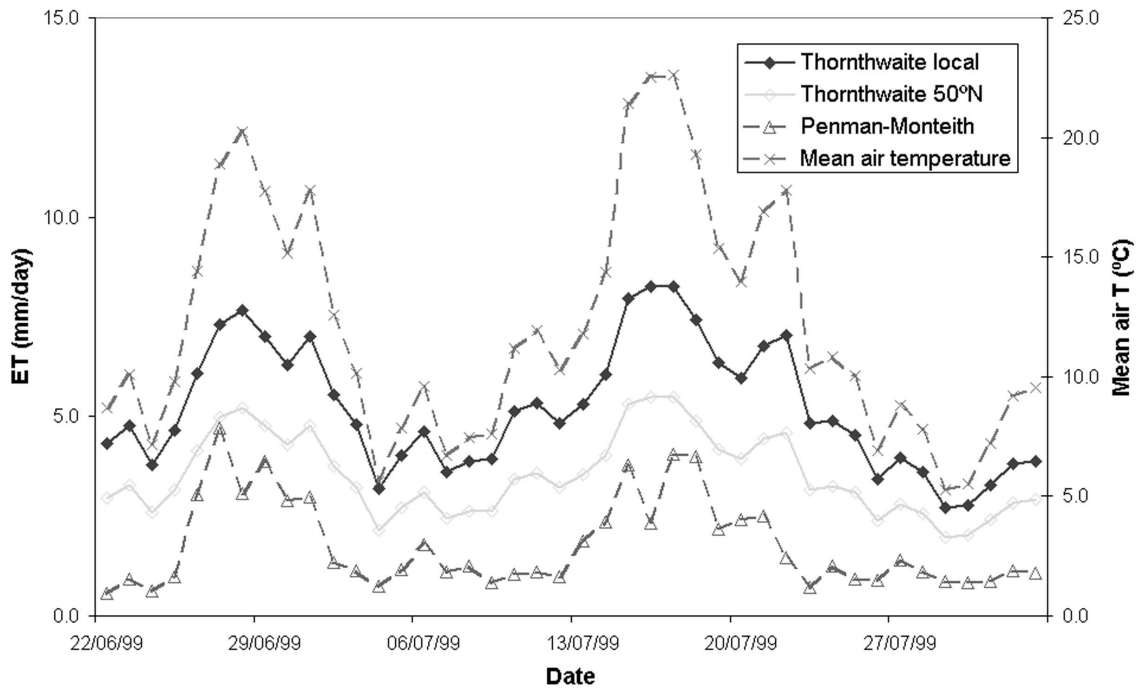
Figure 5.3 Evapotranspiration estimates for the Kidisjoki catchment near Kevo, Finland, in the summer of 1999, based on Penman-Monteith (see chapter 3), and based on the Thornthwaite method using both local and 50ºN day length correction factors. Also shown is the temperature course in the study period

Any water surplus (i.e. $SM_i > MWC$) is separated into rapid runoff, that contributes to the discharge of the month under consideration, and a volume of water that is added to the groundwater reservoir. This is controlled by a separation ratio χ that has to be obtained by calibration:

$$\chi = \frac{Q_r}{Q_{gw} + Q_r}$$ (5.10)

where Q_r = rapid runoff (mm.month^{-1})
$\quad\quad\quad Q_{gw}$ = amount of water added to groundwater (mm.month^{-1})

In the Rhine Basin, Kwadijk (1993) found a value for χ of 0.2, meaning that 20% of the water surplus from the soil compartment is discharged directly as rapid runoff, and 80% is drained to the groundwater reservoir. Baseflow from the groundwater reservoir is calculated with a recession equation:

$$Q_b = \frac{GWS}{C}$$ (5.11)

101

where Q_b = baseflow (mm.month^{-1})
         GWS = amount of water stored as groundwater (mm)
         C = recession parameter (months)

The recession parameter was calibrated for the main tributaries of the Rhine, using observed discharges of low flow months. According to Kwadijk (1993) low values of C and high values of the separation ratio χ represent catchments with a short response time (relatively steep hydrographs), while high values of C and low values of χ represent a long response time (relatively flat hydrographs). Kwadijk also assumed that C is mainly dependent on the geohydrological properties of a catchment and will not change under changing climatic conditions. By calibrating on discharge data the recession parameter is however dependent on present reservoir storage, which may not correspond with the catchment storage capacity. The latter is mainly dependent on the dimensions and lithological characteristics of the catchment. The ratio of present reservoir storage to the catchment storage capacity is an indication of the sensitivity of the catchment to climate variability or change (Van der Wateren – de Hoog, 1997).

5.5   Application to the Tana Basin

In order to test its performance in a sub-arctic environment, the RHINEFLOW model of Kwadijk (1993), that is described in the previous section, was applied to the Tana River Basin in Northern Fennoscandia. The model was consequently called TANAFLOW, and was applied on a 10-day basis, without further modifications to the model concept. This section describes the input data that were used, the procedure that was followed, as well as the performance of the model.

5.5.1   Modelling period

The model was applied to the period October 1979 – September 1999 (or 1980-1999, see section 5.3). Each month in this period was divided into three parts: the first and second period of 10 days, and the remaining period of 8, 9, 10 or 11 days. The dataset was furthermore split into two equal parts, the first half (1980-1989) was used for calibration and second half (1990-1999) for validation of the model. Before each model run, the calculations of the first 5 years were repeated, in order to reduce initialisation effects.

5.5.2   Input data

The data that were used in the application of the model to the Tana Basin, are listed below. All spatial data were stored as raster maps with a resolution of 1 by 1 km.

102

-       *Precipitation and temperature*
        Data on precipitation and temperature were interpolated from the meteorological
        stations listed in table 5.1 with Thiessen polygons, as in section 5.3.
        Meteorological observations were however not continuous for all stations used
        and even within the periods of observation some missing data occurred. The
        spatial interpolation of the meteorological data was therefore incorporated in the
        dynamic section of the model. This means that the interpolation with Thiessen
        polygons was repeated in each time step, using only those stations for which
        data were available. Temperature values were corrected for elevation differences
        using a DEM of the Tana Basin, assuming a 0.57°C temperature decrease per
        100 m elevation increase.

-       *Thornthwaite coefficients*
        The annual heat index I and coefficient a (equations 5.6 and 5.7) were calculated
        for each temperature station that was used in the model run (table 5.3). The
        evapotranspiration estimates were corrected for day length, which was
        calculated for each station using software from Lammi (2001).

        As discussed in section 5.4.3, estimates of evapotranspiration based on the
        Thornthwaite method are too high in sub-arctic environments. The Thornthwaite
        estimates were therefore adjusted to meet the long-term water balance the Tana
        Basin (see section 5.3). In 1980-1999, the ratio of observed runoff and observed
        (basin-averaged) precipitation ranged between 0.95 and 1.12 (table 5.2). To
        obtain a similar ratio of simulated runoff and rainfall, the evapotranspiration
        estimates of the model need to be scaled by a factor 0.01 – 0.03 (table 5.4).
        However, in section 5.3 it was argued that the Q / P ratios in table 5.2 are too
        high, and that the observations at the meteorological stations underestimate
        precipitation over the entire catchment area. In other words, a Q / P ratio of 0.95
        does not reflect the actual proportion between rainfall and runoff in the
        catchment. As an alternative, a reduction factor of 0.1 resulted in a lower runoff
        / precipitation ratio of 0.88 (see table 5.4), and appeared to yield slightly higher

Table 5.3 Annual heat index (I) and Thornthwaite coefficient a for temperature stations in the Tana Basin,
calculated for the period 1980-1999

	I	a
Rustefjelbma	9.84	0.66
Kevo	11.26	0.68
Karasjok	12.16	0.70
Cuovddatmohkki	10.60	0.67
Sihcajavri	11.25	0.68

modelling efficiencies as well. It was therefore decided to apply this scaling factor to the modelled evapotranspiration rates.

- *Digital Elevation Model (DEM)*
  A digital elevation model (DEM) of the Tana Basin was obtained from the GTOPO30 data set of the US Geological Survey's EROS Data Centre. This data set provides elevation data with a nominal cell size of 1 km, and is derived from various vector and raster data sets. The vertical accuracy varies by location according to the source data; for the Tana basin an accuracy of $\pm$ 30 m at the 90 % confidence level is indicated (Defense Mapping Agency, 1986). This corresponds with a root mean square error of 18 m, assuming that the errors show a Gaussian distribution with a mean of zero (US Geological Survey, 2000). The catchment of the Tana river was delineated following a procedure outlined by Wesseling et al. (1997).

- *Vegetation map*
  A Landsat TM satellite image of 18 July 1987 was used to map vegetation types in the Tana Basin (see section 2.3.3 and figure 2.5). This map was converted into crop factors, that were used in the calculation of evapotranspiration rates for each specific land cover type. Unfortunately, no crop factors have been published for the specific vegetation types occurring in the Tana basin. The crop factors that were used are therefore based on comparable vegetation types in the Rhine Basin, as published by Brechtel & Scheele (1982) (see table 5.5).

- *Soil map*
  According to the FAO-UNESCO soil map of the world (Zobler, 1986) medium coarse soils (orthic podsols, texture class sandy loam) and organic soils

Table 5.4 Simulated runoff / rainfall (Q / P) ratios with several adjustments of the evapotranspiration estimates

Day length correction factor	Evaporation reduction factor	Q / P ratio
-	1	0.39
50ºN	1	0.27
Local	1	0.15
Local	0.5	0.47
Local	0.1	0.88
Local	0.05	0.93
Local	0.03	0.95
Local	0.01	0.97

predominate in Northern Fennoscandia. This dataset has a spatial resolution of only 1 by 1 degree latitude / longitude. Quarternary geology maps of the area (e.g. Olsen et al., 1996) show much more detail, and indicate that most of the Tana Basin is covered by glacial till, except for open water, wetlands and those areas where bedrock is exposed. The vegetation map was therefore used as a basis for the soil map, by re-labelling the vegetation classes into soil types according to table 5.5.

The maximum soil water capacity of the glacial till was estimated based on published data from Bouwman et al. (1993) and Vörösmarty et al. (1989). According to the latter the saturation capacity of sandy loam is 41.3 %, and for silty loam (medium, coarse-fine and coarse-medium-fine) 46.8 %. The actual amount of water that can be stored is furthermore dependent on rooting depth. Observations on rooting depth were made in the Kidisjoki catchment near Kevo, Finland (see chapter 3). Here, rooting depth at non-forested sites (such as alpine heaths) was in general not more than 20 cm, and soil development usually did not reach below 30 cm depth. The saturation capacity of non-forested sites with a sandy loam texture may therefore be estimated at $(41.3\% \times 200 =)$ 83 mm, assuming a root depth of 20 cm, or 124 mm based on 30 cm soil development. For silty loam these values are 94 and 140 mm respectively. In forested and semi-forested areas the maximum soil water capacities can expected to be higher because of the larger rooting depth. As an average, the maximum soil water capacity of all areas (both forested and non-forested) consisting of glacial tills was therefore estimated at 150 mm. As argued in chapter 3, the storage capacity of arctic wetlands may be limited (see also Quinton & Roulet, 1998), and a much lower value was therefore chosen for this land cover type. The maximum soil water holding capacity of bare rock is based on Groenendijk (1989). To allow for temporary storage of water in lakes by fluctuations in the water table, a storage capacity of 10 mm was assumed.

Table 5.5 Recoding of vegetation types in the Tana Basin into crop factors, soil types and maximum soil water capacities (*MWC*)

	Crop factor	Soil type	*MWC* mm
Lakes	1.0	Water	10
Wetland	1.0	Peat	10
Sand / gravel, bare rock, boulder fields	0.4	Bare rock	30
Birch forests (high density), pine forests	1.1	Glacial till	150
Alpine heaths, meadows, birch forests (low density)	0.9	Glacial till	150

5.5.3   Calibration

The model was calibrated using observed discharge at several stations in the Tana Basin (table 5.6). The calibration was carried out by adjusting the values of the degree-day factor (*DDF*) for snowmelt, the separation ratio (χ) of quick runoff and groundwater flow, and the recession parameter (*C*) for baseflow calculation. As calibration procedure a "brute force" Monte Carlo technique was used, meaning that all possible combinations of *DDF*, χ, and *C* were calculated, within a given range of parameter values and with fixed increments. The results were compared with the observed discharge for all locations, and several error statistics were calculated: the Nash & Sutcliffe (1970) coefficient of efficiency, the mean bias error (Barr et al., 1997), the mean difference between measurement and simulation (Addiscott et al., 1995) and the product moment-correlation (*r*) (Addiscott et al., 1995).

The most downstream discharge gauging station available is Polmak, Norway. In terms of the Nash-Sutcliffe coefficient the best results for this station were obtained with the following parameter combination: $DDF = 14$ mm.$^{\circ}$C^{-1} per 10-day period, $\chi = 0.7$ and $C = 30$ 10-day periods (figure 5.4). In the Rhine basin these values were 18 mm.$^{\circ}$C^{-1} per *month*, 0.20 and 1 to 6 *months* respectively (Kwadijk, 1993). The higher value of χ indicates a much shorter response time of the Tana basin (section 5.4.4), while the higher *DDF* may represent the high snowmelt rates in the Tana Basin. The Nash-Sutcliffe coefficient of this parameter set is 0.59 in the calibration period 1980-1989, and the product-moment correlation (*r*) is 0.77. In the various sub-basins different parameter combination give the best results (see table 5.7). It is interesting to note that in the smaller subcatchments the best results were obtained with higher *DDF* values of about 20 mm.$^{\circ}$C^{-1}.period^{-1}, except for the Jiesjåkka river in Norway.

Table 5.6 Discharge stations used in the calibration of TANAFLOW, and period of observation. For locations, see figure 5.1

Discharge station	River	Catchment size km^2	Period of observation
Polmak	Tana	14386	1911 - 1992
Polmak Nye	Tana	13601	1991 - 1994
Alaköngäs	Tana (Tenojoki)	13457	1963 - present
Onnelansuvanto	Tana (Tenojoki)	10505	1959 - present
Patoniva	Utsjoki	1458	1963 - present
Karigasniemi	Inarijoki	2868	1961 - present
Vækkava	Jiesjåkka	2071	1973 - 1995
Njalmigoaika	Karasjåkka	2264	1966 – 1991

Figure 5.4 Simulated and observed discharge at Polmak, Norway, in the calibration period 1980-1989 (10-day periods). The parameter combination used here is: $DDF = 14$ mm ${}^{\circ}C^{-1}$ period^{-1}, $\chi = 0.7$, and $C = 30$ 10-day periods

It appears that the modelling efficiency, as described by the Nash-Sutcliffe coefficient, is least influenced by the recession parameter, and most by the degree-day factor. If the DDF was too low, say less than 10 mm.${}^{\circ}C^{-1}$.period^{-1}, the simulated snowmelt discharge peaks were too late and too low, compared with the observed ones. Similarly, if the DDF was 20 mm.${}^{\circ}C^{-1}$.period^{-1} or higher, the discharge peaks at Polmak were sometimes simulated too early. For good results a DDF in the range of 10-20 mm.${}^{\circ}C^{-1}$.period^{-1} had to be accompanied by a high separation ratio of 0.6-0.8; with lower values of χ the simulated peak discharges were too low. Apparently the DDF is of particular importance for determining the timing of the snowmelt peak, and χ for adjusting the height of the peak discharge, although it can be seen in figure 5.4 that the runoff peaks are still too low in general.

At the same time the recession parameter primarily controls the shape - and more specifically the slope - of the recession limb of the hydrograph during winter. The higher the value for C, the more horizontal the recession curve will be, simply because the drainage of the groundwater reservoir is slower. A value of 10 periods of ten days for C gave the best results. Correct simulation of the recession limb is however not only dependent on C, but also on χ. The separation ratio determines how much water will drain to the groundwater reservoir, and in consequence the position of the simulated recession curve above or below the observed discharge. In general, a χ of 0.3-0.5 resulted in a simulated recession limb that coincided with the observed one.

107

Table 5.7 Best parameter combinations in the calibration period in terms of the Nash-Sutcliffe coefficient, for the Tana River and several sub-basins. For locations, see figure 5.1

Discharge station	River	DDF [a]	χ	C [b]	Nash-Sutcliffe
Polmak	Tana	14	0.7	30	0.59
Alaköngäs	Tana	14	0.8	30	0.65
Onnelansuvanto	Tana	14	0.8	30	0.63
Patoniva	Utsjoki	20	0.6	20	0.63
Karigasniemi	Inarijoki	20	0.8	20	0.58
Vækkava	Jiesjåkka	14	0.6	5	0.60
Njalmigoaika	Karasjåkka	20	0.7	30	0.64

[a] Units mm $°C^{-1}$ period^{-1}
[b] Units 10-day periods

The Nash-Sutcliffe coefficient describes how well seasonal variations in the stream flow are simulated. When the model is calibrated on this coefficient, it is optimised to simulate the snowmelt discharge peaks. A high Nash-Sutcliffe value therefore does not necessarily mean that the performance of the model in the rest of the year is satisfying, as can be seen in figure 5.4. This diagram shows clearly that the parameter combination that gives the highest possible Nash-Sutcliffe value, results in a significant overestimation of the discharge peaks in summer, and an underestimation of the discharge in fall and winter. It seems that for the rest of the year a different parameter with lower χ values and a C of about 10 or 20 would be more appropriate.

For that reason it was decided to calculate a mean absolute bias error separately for three periods: the spring snowmelt peak (May and June), the summer period (July - September) and the winter recession period (October - April). The mean absolute bias error was also calculated for the combined summer, fall and winter period (July - April, i.e. all months except May and June). The mean absolute bias error (MABE) is similar to the mean bias error used by Barr et al. (1997), but is based on absolute differences between measured and simulated discharge. In this way periods in which the simulated runoff is higher than the observed, are not averaged out by periods in which the opposite is the case. It is calculated as follows:

$$MABE = \frac{\sum_{i=1}^{k} |Q_i - Q_{si}|}{\sum_{i=1}^{k} Q_i} \tag{5.12}$$

where Q_i = observed discharge in time period i (m^3 s^{-1})
        Q_{si} = simulated discharge (m^3 s^{-1})
        k = number of time steps

MABE values close to 0 indicate good agreement between measurement and simulation, while a value of 1 indicates that the total accumulative differences are equal in size to the sum of the measurements.

The smallest MABE value for the snowmelt period was obtained with a *DDF* of 14 mm.°C^{-1}.period^{-1}, and χ equal to 0.7 or 0.8 (see table 5.8); the value that was chosen for *C* had little influence on the performance of the model in May and June. For the summer period however, the best results were obtained with χ between 0.2 and 0.4, and *C* ranging between 30 and 40. In the winter period somewhat higher values for χ (between 0.3 and 0.5) and similar values for *C* (between 20 and 50) gave the lowest error values. The *DDF* had little influence on the model performance in both the summer and winter periods.

Figure 5.5.a shows the simulation of the parameter combination that gave the best results in the summer period. Indeed the discharge in summer is simulated well and the peaks that could be seen in figure 5.4 have disappeared. However, the snowmelt peak in spring is almost completely missed, and in winter the discharge is too high. Due to the lower separation ratio the amount of rapid runoff is lower, and more water is added to the groundwater storage, which is then drained slowly throughout the winter. The best parameter combination for the winter period is shown in figure 5.5.b. The recession limb of the annual hydrograph is now simulated very well, but the discharge peaks in summer are too high, which is caused by the higher separation ratio and more rapid groundwater drainage. Also the snowmelt peaks in spring are still too low.

In conclusion, the parameter combinations that give the best results for the summer or winter period, are different from those for the snowmelt period in spring. Only in the

Table 5.8 Best parameter combinations at Polmak in the calibration period, in terms of the mean absolute bias error (MABE), for the spring (May and June), summer (July-September) and winter (October-April) seasons, as well as the combined summer-winter season (July-April)

Season	DDF [a]	χ	C[b]	MABE
Spring	14	0.8	5	0.34
Summer	20	0.3	40	0.33
Winter	14	0.5	20	0.35
Summer + winter	14	0.5	20	0.40

[a] Units mm °C^{-1} period^{-1}
[b] Units 10-day periods

(a)
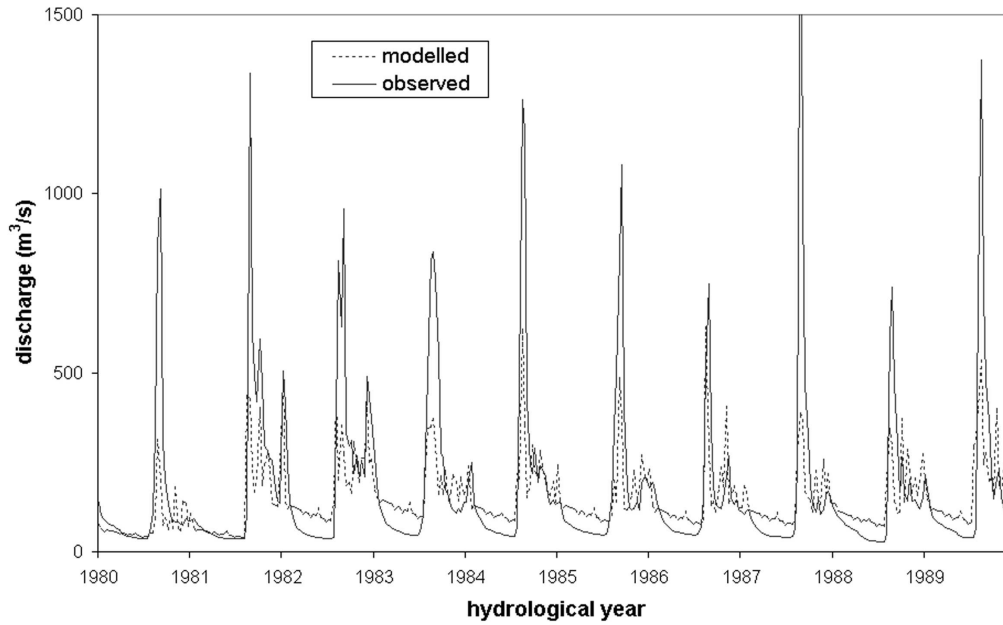
(b)

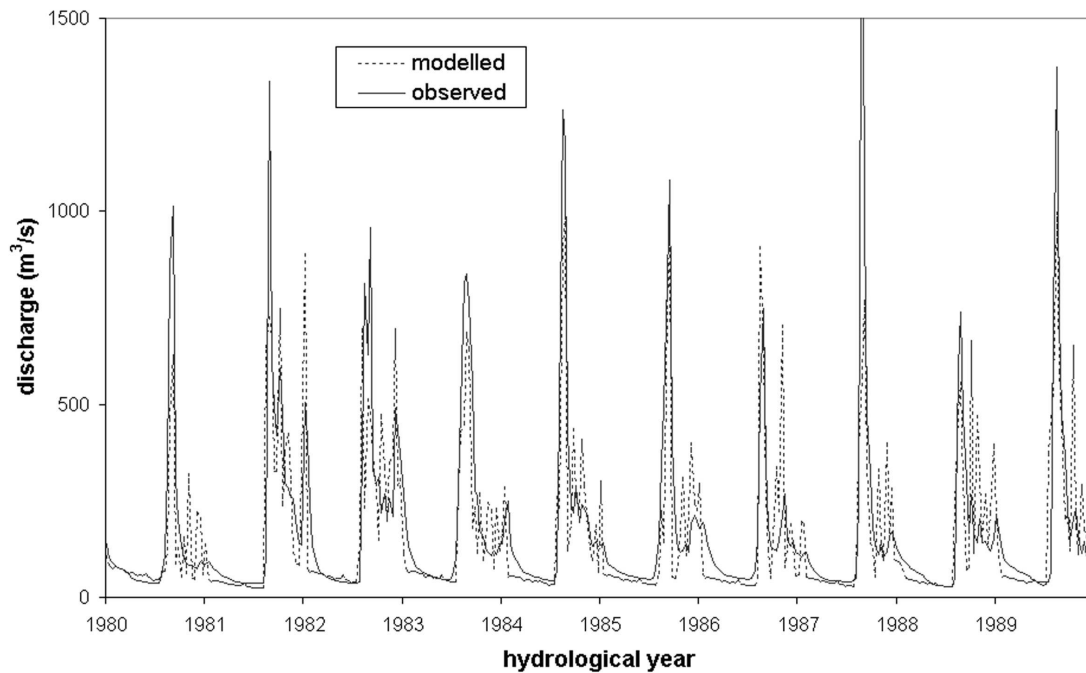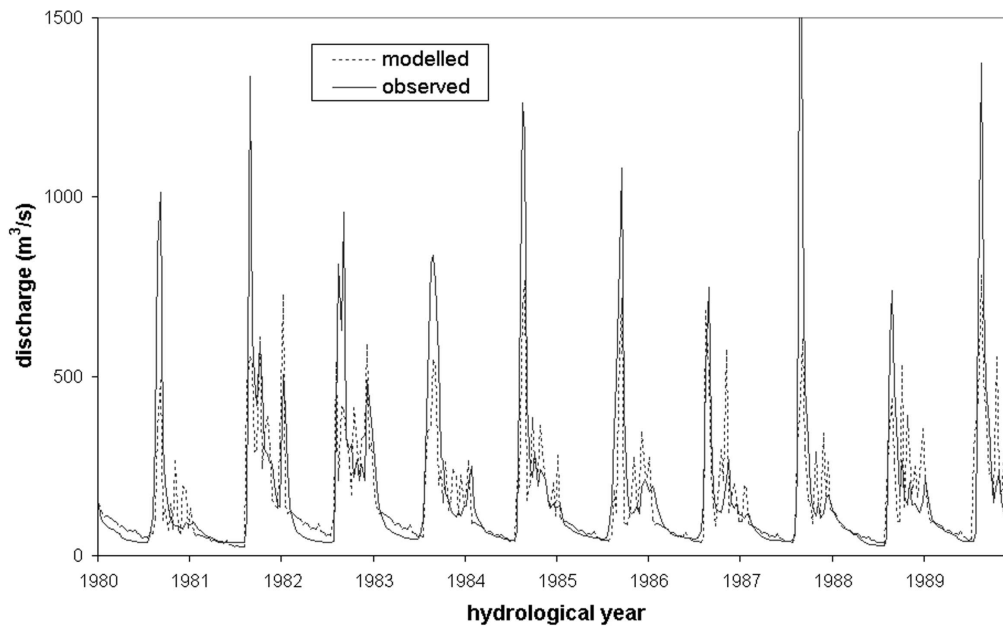**Figure 5.5** Simulated and observed discharge at Polmak, Norway, in the calibration period 1980-1989, (a) for the parameter combination DDF = 20 mm °C^{-1} period^{-1}, χ = 0.3, and C = 40 10-day periods, and (b) for the parameter combination DDF = 14 mm °C^{-1} period^{-1}, χ = 0.5, and C = 20 10-day periods.

110

latter case the best parameter combination was similar to what was found by calibration on the Nash-Sutcliffe coefficient. Moreover, it seems that the separation parameter χ has the largest influence on the model performance.

5.5.4 Validation

The model was validated for the period 1990-1999. Discharge measurements in Polmak stopped in 1992, and in nearby Polmak Nye in 1994 (table 5.6). The results for Alaköngäs, Finland, are summarised in table 5.9 for the three parameter combinations listed in table 5.8. In general the simulation results are better in the validation period than in the calibration period, which is probably because the of the lower peak discharges (figure 5.6). At Polmak the highest Nash-Sutcliffe coefficient in the calibration period (0.59) was obtained with the parameter combination $DDF = 14$, $\chi = 0.7$ and $C = 30$. The water balance characteristics of the Tana Basin upstream of Alaköngäs for this parameter combination are summarised in table 5.10, for both the calibration and the validation period, as well as the total simulation period of 20 years (1980-1999). At Alaköngäs this combination results in a Nash-Sutcliffe coefficient of 0.63 in the calibration period, 0.71 in the validation period and 0.67 for the total period (figure 5.6). Also the parameter combinations in table 5.9 result in higher Nash-Sutcliffe coefficients and lower spring MABE values in the validation period. There is little difference in MABE values of the summer and winter periods between calibration and validation period, and sometimes the

Table 5.9 Model performance at Alaköngäs, Finland, for the calibration (1980-1989), validation (1990-1999) and total (1980-1999) simulation period, for the parameter combinations in table 5.8

Parameter combination			Period	Error statistics			
DDF [a]	χ	C [b]		Nash-Sutcliffe	MABE spring	MABE summer	MABE winter
14	0.8	5	1980-89	0.64	0.39	0.56	0.85
			1990-99	0.66	0.38	0.52	0.84
			1980-99	0.66	0.38	0.54	0.84
20	0.3	40	1980-89	0.39	0.64	0.29	0.61
			1990-99	0.51	0.57	0.32	0.79
			1980-99	0.44	0.61	0.30	0.70
14	0.5	20	1980-89	0.56	0.53	0.36	0.35
			1990-99	0.70	0.42	0.35	0.35
			1980-99	0.62	0.47	0.35	0.35

[a] Units mm °C^{-1} period^{-1}
[b] Units 10-day periods

error values have even increased. This supports the idea that the improved model performance can be attributed to lower peak discharges in the validation period. In this respect it is interesting to remind that the average temperature was higher in the validation period than in the calibration period (−1.51 and −2.50°C respectively).
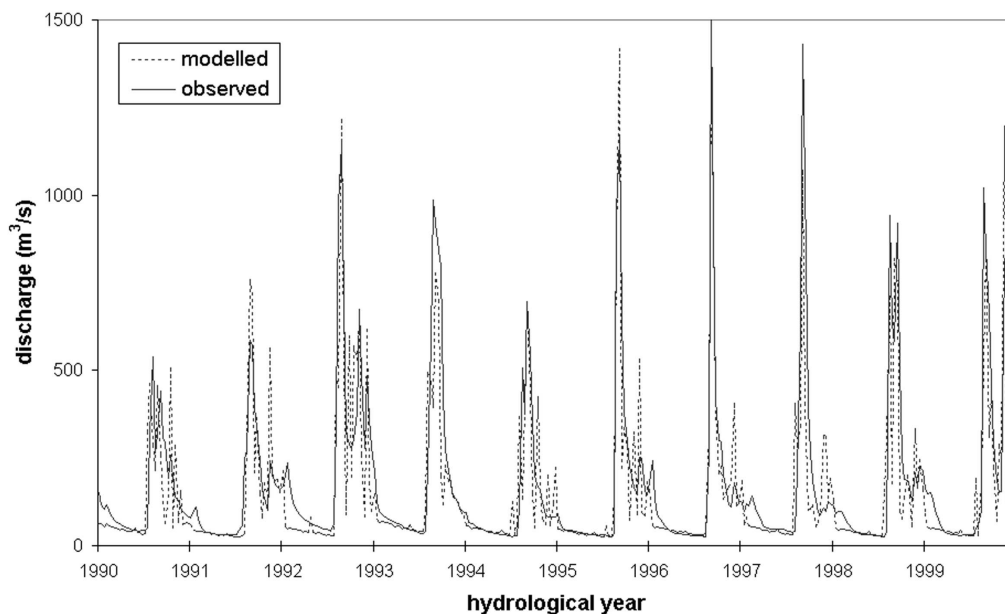
Figure 5.6 Simulated and observed discharge at Alaköngäs, Finland, in the validation period 1990-1999, for the parameter combination $DDF = 14$ mm °C^{-1} period^{-1}, $\chi = 0.7$, and $C = 30$ 10-day periods

5.6   Discussion

Although the hydrological regime of the Tana river is different from the Rhine, the model performance of TANAFLOW was similar or even somewhat better than reported by Van Deursen (1999[b]). This justifies the conclusion that conceptual water balance models can successfully be applied to sub-arctic regions. Analysis and simulation of the water balance of the Tana Basin is however complicated by uncertainties about the actual amount of precipitation in the catchment. Presumably, precipitation amounts at the meteorological stations in the area, mostly located in river valleys, are significantly lower than in the surrounding uplands. As a consequence, it is not possible to derive the actual amount of evapotranspiration in the Tana Basin from the water balance. Measurements in the area suggest that total evapotranspiration in summer is much higher than the remainder of precipitation and runoff of about 3 mm/year (cf. Harding et al., 2002). The model estimate of 40 mm/year is unfortunately not based on a physical algorithm, but on the highly empirical method of Thornthwaite & Mather (1955; 1957), adjusted with an arbitrary reduction factor to meet the long-term ratio of runoff and precipitation. Realistic simulation of the water balance therefore requires better estimates of evaporation losses, either by analysis of small-scale measurements (chapter 3), or at a larger scale by using evaporation models that are more physically based (chapter 7).

112

Table 5.10 Water balance of the Tana Basin upstream of Alaköngäs in the simulation period (1980-1999), for the parameter combination DDF = 14 mm $°C^{-1}$ period^{-1}, χ = 0.7, and C = 30 10-day periods. Explanation: Q = observed discharge, Q_s = simulated discharge, P = precipitation, E_a = actual evapotranspiration

	1980-1989	1990-1999	1980-1999
Total Q ($\times 10^{10}$ m^3)	5.9	5.6	11.5
Mean Q (m^3/s)	185.6	176.3	182.1
Total Q_s ($\times 10^{10}$ m^3)	4.8	4.9	9.6
Mean Q_s (m^3/s)	150.3	152.9	151.6
$Q - Q_s$ (mm/year)	83.9	55.4	69.6
Q / P ratio	1.10	1.03	1.06
Q_s / P ratio	0.89	0.89	0.89
$(Q_s + E_a) / P$ ratio	0.99	0.99	0.99
Mean E_a (mm/year)	40.4	39.8	40.1

Since all precipitation in the winter months accumulates as snow, the uncertainties about the actual amounts of precipitation also affect the simulation of the spring discharge peak resulting from snowmelt. As a consequence, TANAFLOW had in particular difficulties in accurately simulating the height of the peak runoff. For this reason the model performed better in the validation period, when peak discharges were generally lower than in the calibration period. Moreover, in TANAFLOW snow accumulation and snowmelt are simulated using a temperature-index approach, which is essentially a black box model as well. Although practical and straightforward, it lacks a sufficient physical basis for applications such as predicting the spatial distribution of melt in heterogeneous terrain, or transferring the model to different climatic conditions (Williams & Tarboton, 1999). Especially in climate change studies it would be better to use an energy balance model, that is applicable to a wide range of climatic conditions, and independent of calibration (see chapter 7). In the present study, the degree-day factor (*DDF*) was obtained by calibrating the model on river discharge data. However, this does not necessarily imply that the model is able to simulate spatial patterns in snow coverage realistically. In chapter 6, the spatial model performance is therefore tested by comparing the simulations with remotely sensed observations on snow cover depletion.

The Nash & Sutcliffe (1970) criterion that is widely used to the performance of hydrological models, is particularly sensitive to peak discharges, that dominate the hydrograph of sub-arctic rivers. However, a high efficiency coefficient does not mean that the simulation is acceptable throughout the year. In the present study, it appeared useful to calculate several error statistics, such as the mean absolute bias error (MABE) (equation 5.12), for different seasons. In this way, the performance of the model in the summer and winter periods could be evaluated. The different optimal parameter combinations that were found in this way correspond to the distinct hydrological regime

of sub-arctic environments. All precipitation falling in winter is accumulated in the snow pack, although sublimation can be significant for blowing snow, or snow intercepted on a forest canopy (Pomeroy & Gray, 1995; Lundberg et al., 1998). In spring this volume of water is released within a short period of time. Since infiltration and storage of meltwater may be limited by ice horizons in the snow pack and by frozen soils, most of it will contribute to rapid runoff. In the Tana Basin, as much as 65 % of the total annual runoff may be discharged in the spring months April to June. Later in summer, when the soil has thawed and an active layer has formed, storage of water in the soil becomes more important. In this season evapotranspiration can also be significant. As a consequence, rapid runoff will be much less important, except maybe for extreme rainfall events. In winter, discharge is very low and consists primarily of baseflow. Currently, not all of these processes are properly represented in TANAFLOW. For example, during winter and spring there is no constraint on infiltration, that would account for underlying snow layers and frozen soils. This explains why the best results in the spring period were obtained with a high value for the separation ratio (χ), while in summer a lower value performed better. By introducing a conceptual representation of soil frost in the model, it may be possible to simulate the hydrological behaviour of the Tana Basin more realistically.

5.7   Conclusions

In this study it was demonstrated that a conceptual water balance, originally developed for the Rhine, can successfully be applied to the sub-arctic Tana River Basin. However, before such a model can be used in hydrological impact studies of climate change in sub-arctic environments, several issues may need to be improved. First of all, the simulations were complicated by uncertainties about the actual amount of precipitation over the catchment. As a result, the actual amount of evapotranspiration cannot be derived from the water balance, nor can it safely be deduced from the empirical algorithm that is currently employed in the model. Secondly, snowmelt in spring, that dominates the hydrological regime of the Tana River, is simulated by using a highly empirical method as well. Since the temperature-index model is calibrated on river runoff, it remains uncertain whether it is able to simulate spatial patterns in snow coverage realistically. Finally, it may be necessary to include a representation of soil frost in the model, in order to take account of the differences in hydrological behaviour between winter, spring and summer. In chapter 7, physically-based algorithms for snowmelt and evapotranspiration, will be introduced into TANAFLOW, in combination with a conceptual representation of the effect of frozen soils on the infiltration during snowmelt. Before that, the simulation of spatial patterns in snow cover depletion is evaluated in chapter 6, and a first assessment is made of the sensitivity of snow cover dynamics to changes in climate.

5.8   References

Addiscott, T., J. Smith & N. Bradbury (1995): Critical evaluation of models and their parameters. Journal of Environmental Quality 24, pp. 803-807.

114

Arnell, N. (1999): A simple water balance model for the simulation of streamflow over a large geographic domain. Journal of Hydrology 217, pp. 314-335.

Barr, A.G., G.W. Kite, R. Granger & C. Smith (1997): Evaluating three evapotranspiration methods in the SLURP macroscale hydrological model. Hydrological Processes 11, pp. 1685-1705.

Bouwman, A.F., I. Fung, E. Matthews & J. John (1993): Global analysis of the potential for nitrous oxide (N$_2$O) production in natural soils. Global Biochemical Cycles 7, pp. 557-597.

Bergström, S. (1995): The HBV model. In: V.P. Singh (ed.): Computer Models of Watershed Hydrology. Highlands Ranch, Colorado: Water Resources Publications, pp. 443-476.

Brechtel, H.M. & G. Scheele (1982): Erwirtschaftung von Grundwasser durch Land- und Forstwirtschafliche Massnahmen. Hannover: Hessische Forstliche Versuchsanstalt.

Defense Mapping Agency (1986): Defense Mapping Agency product specifications for digital terrain elevation data (DTED). St. Louis: Defense Mapping Agency Aerospace Center.

Ferguson, R.I. (1999): Snowmelt runoff models. Progress in Physical Geography 23, pp. 205-227.

Harding, R.J., N.A. Jackson, E.M. Blyth & A. Culf (2002): Evaporation and energy balance of a sub-arctic hillslope in northern Finland. Hydrological processes 16, pp. 1419-1436.

Goodison, B.E., P.Y.T. Louie & D. Yang (1998): WMO solid precipitation measurement intercomparison, final report. Geneva: World Meteorological Organization (WMO Instruments and Observing Methods Report No. 67, WMO/TD-No.872).

Groenendijk, H. (1989): Estimation of waterholding-capacity of soils in Europe: the compilation of a soil dataset. Wageningen: Centre for Agrobiological Research, Department of Theoretical Production Ecology, Agricultural University (Simulation reports CABO-TT 19).

Kite, G.W. (1995): The SLURP model. In: V.P. Singh (ed.): Computer Models of Watershed Hydrology. Highlands Ranch, Colorado: Water Resources Publications, pp.521-562.

Kite, G.W. & N. Kouwen (1992): Watershed modelling using land classifications. Water Resources Research 28, pp. 3193-3200.

Kwadijk, J.C.J. (1993): The impact of climate change on the discharge of the River Rhine. Utrecht: Koninklijk Aardrijkskundig Genootschap / Faculteit Ruimtelijke Wetenschappen Universiteit Utrecht (Netherlands Geographical Studies 171).

Lammi, J. (2001): Online photoperiod calculator and sunrise / sunset calculator for MS Excel. Available from http://www.nic.fi/~benefon/sun.php3, accessed on 30 July 2002.

Lindström, G., B. Johansson, M. Persson, M. Gardelin & S. Bergström (1997): Development and test of the distributed HBV-96 model. Journal of Hydrology 201, pp. 272-288.

Lundberg, A., I. Calder & R.J. Harding (1998): Evaporation of intercepted snow: measurement and modelling. Journal of Hydrology 206, pp. 151-163.

Mackay, D.K. & O.H. Løken (1974): Arctic Hydrology. In: J.D. Ives & R.G. Barry (eds.): Arctic and Alpine Environments. London: Methuen, pp. 111-132.

Martinec, J., A. Rango & R. Roberts (1994): Snowmelt runoff model (SRM) user's manual (M.F. Baumgartner, ed.) Bern: Department of Geography, University of Bern (Geographica Bernensia P29).

Melloh, R.A. (1999): A synopsis and comparison of selected snowmelt algorithms. Hanover, New Hampshire: US Army Corps of Engineers, Cold Regions Research & Engineering Laboratory (CCREL report 99-8).

Milly, P.C.D. (1994): Climate, interseasonal storage of soil water, and the annual water balance. Advances in Water Resources 17, pp. 19-24.

Nash, J.E. & Sutcliffe, J.V. (1970): River flow forecasting through conceptual models; Part 1 -a discussion of principles. Journal of Hydrology 10, pp. 282-290.

Olsen, L., A. Reite, K. Riibe & E. Sørensen (1996): Finnmark county, Map of Quaternary Geology, scale 1:500,000, with description. Trondheim: Geological Survey of Norway.

Penman, H.L. (1956): Evaporation: an introductory survey. Netherlands Journal of Agricultural Science 4, pp. 9-29.

Pereira, A.R. & A.P. Camargo (1989): An analysis of the criticisms of Thornthwaite's equation for estimating potential evapotranspiration. Agricultural and Forest Meteorology 46, pp. 149-157.

Pomeroy, J.W. & D.M. Gray (1995): Snow cover accumulation, relocation and management. Saskatoon: National Hydrology Research Institute (NHRI Science Report 7).

Quinton, W.L. & N.T. Roulet (1998): Spring and summer runoff hydrology of a subarctic patterned wetland. Arctic and Alpine Research 30, pp. 285-294.

Rosenberg, N.J., B.L. Blad & S.B. Verma (1983): Microclimate, The Biological Environment. New York: Wiley.

Rovansek, R.J., L.D. Hinzman & D.L. Kane, D.L. (1996): Hydrology of a tundra wetland complex on the Alaskan Arctic Coastal Plain, U.S.A. Arctic and Alpine Research 28, pp. 311-317.

Sellinger, C.E. (1996): Computer program for estimating evapotranspiration using the Thornthwaite method. Ann Arbor, Michigan: National Oceanic and Atmospheric Administration (NOAA), Great Lakes Environmental Research Laboratory (NOAA Technical Memorandum ERL GLERL-101).

Shuttleworth, W.J. (1993): Evaporation. In: D.R. Maidment (ed.): Handbook of Hydrology. New York: McGraw-Hill, pp. 4.1-4.53.

Singh, P., N. Kumar & M. Arora (2000): Degree-day factors for snow and ice for the Dokriani Glacier, Garhwal Himalayas. Journal of Hydrology 235, pp. 1-11.

Thornthwaite, C.W. & J.R. Mather (1955): The water balance. Centerton: Drexel Institute of Technology, Laboratory of Climatology (Publications in Climatology 8).

Thornthwaite, C.W. & Mather, J.R. (1957): Instructions and tables for computing potential evapotranspiration and the water balance. Centerton: Drexel Institute of Technology, Laboratory of Climatology (Publications in Climatology 10), pp. 183-243.

United States Geological Survey (USGS) (2002): GTOPO30 documentation. Available from http://edcdaac.usgs.gov/gtopo30/README.html, accessed on 30 July 2002.

Van der Wateren – de Hoog, B. (1997): Quantification of catchment discharge sensitivity to climate variability. Utrecht: Koninklijk Aardrijkskundig Genootschap / Faculteit Ruimtelijke Wetenschappen Universiteit Utrecht (Netherlands Geographical Studies 233).

Van Deursen, W.P.A. (1995): Geographical Information Systems and Dynamic Models. Development and application of a prototype spatial modelling language. Utrecht: Koninklijk Aardrijkskundig Genootschap / Faculteit Ruimtelijke Wetenschappen Universiteit Utrecht (Netherlands Geographical Studies 190).

Van Deursen, W.P.A. (1999[a]): RHINEFLOW-2: Development, calibration and application. Rotterdam: Carthago Consultancy (report of the NRP project 952210).

Van Deursen, W.P.A. (1999[b]): Impact of climate change on the river Rhine discharge regime. Rotterdam: Carthago Consultancy (report of the NRP project 952210).

Vörösmarty, C.J., B. Moore, M.P. Gildea, B. Peterson, J. Melillo, D. Kicklighter, J. Raich, E. Rastetter & P. Steudler (1989): A continental-scale model of water balance and fluvial transport: application to South America. Global Biogeochemical Cycles 3, pp. 241-265.

Ward, R.C. & M. Robinson (1990): Principles of Hydrology. London: McGraw-Hill.

Wesseling, C.G., W.P.A. Van Deursen & M. De Wit, M. (1997): Large scale catchment delineation: a case study for the River Rhine basin. In: S. Hodgson, M. Rumor & J.J. Harts (eds.): Geographical Information '97 (Third Joint European Conference & Exhibition on Geographical Information, Vienna, Austria), pp. 487-496.

Williams, K.S. & D.G. Tarboton (1999): The ABC's of snowmelt: a topographically factorized energy component snowmelt model. Hydrological Processes 13, pp. 1905-1920.

Woo M.-K. (1990): Permafrost Hydrology. In: T.D. Prowse & C.S.I. Ommanney (eds.): Northern Hydrology, Canadian Perspectives. Saskatoon: National Hydrology Research Institute (NHRI Science Report 1), pp. 63-76.

Xu, C.-Y. (1999): From GCMs to river flow: a review of downscaling methods and hydrologic modelling approaches. Progress in Physical Geography 23, pp. 229-249.

Yang, D. & M.-K. Woo (1999): Representativeness of local snow data for large scale hydrologic investigations. Hydrological Processes 13, pp. 1977-1988.

Yang, D., B.E. Goodison, J.R. Metcalfe, P.Y.T. Louie, E. Elomaa, C.L. Hanson, V.S. Golubev, Th. Gunther, J. Milkovic & M. Lapin (2001): Compatibility evaluation of national precipitation gauge measurements. Journal of Geophysical Research 106, pp. 1481-1492.

Zobler, L.(1986): A world soil file for global climate modelling. New York: NASA Goddard Institute for Space Studies (NASA Technical Memorandum 87802).

6   SENSITIVITY OF SNOW COVER DYNAMICS
         AND RIVER RUNOFF TO CLIMATE CHANGE

Based on: Dankers, R., O.B. Christensen & H. Middelkoop: Climate Change impact on snow cover dynamics in the Tana River Basin, Northern Fennoscandia. Submitted to Nordic Hydrology.

6.1   Introduction

At high latitudes, the terrestrial ecosystem is predominated by the presence of a seasonal snow cover. The extent and duration of snow coverage determine the length of the growing season of shrubs and lichens, and influence water availability for plants later in summer. Snow also controls the soil thermal regime, and snowmelt dominates the hydrological regime of northern rivers (Koster, 1991). Changes in the spatial and temporal extent of snow coverage, that may be caused by human-induced climatic changes, will undoubtedly have consequences for the vegetation, permafrost and water balance of northern areas, but may also have important feedback effects on the global climate because of the high albedo of snow (Anisimov & Fitzharris, 2001).

Analysis of the impact of climate change on snow cover therefore requires models that are able to simulate spatial and temporal patterns of snow coverage. At a larger (regional or landscape) scale, most hydrological models consider snow only in a lumped or semi-distributed way, and concentrate on runoff for calibration and validation. Moreover, as noted in the previous chapter, snow accumulation and snowmelt are often simulated using a highly empirical temperature-index approach. As a consequence, it is uncertain whether these models are able to simulate spatial snow cover dynamics, and whether or not these models can be applied to different climatic conditions.

Aim of the present chapter is to test the ability of the water balance model TANAFLOW (presented in chapter 5) to simulate the spatial distribution of snowmelt in the Tana Basin. This was done by comparing the model results with satellite observations of snowmelt patterns. Furthermore, the sensitivity of snow cover dynamics, river runoff and the water balance of the Tana Basin to changes in climate was tested by assuming increases in temperature and precipitation in the model. In this way, a first estimate was obtained of the magnitude of changes that can be expected for future climate conditions.

6.2   Snowmelt in the Tana Basin

Like in most sub-arctic environments, late-spring snowmelt in the Tana Basin (see chapter 2) is usually a very rapid process. At Kevo, Finland, the depletion of the snow cover may amount to more than 20 cm per day, and in only 10 days almost 50 % of the original maximum snow thickness may disappear (figure 6.1). Most meteorological stations become free of snow in May, or occasionally in late April or early June (figure

117

6.2). However, as noted in the previous chapter, these stations are mostly located in the river valleys, where the snow cover usually disappears a few weeks earlier than in the surrounding uplands. As was demonstrated in chapter 4, this time difference varies from year to year (see e.g. figure 4.9).
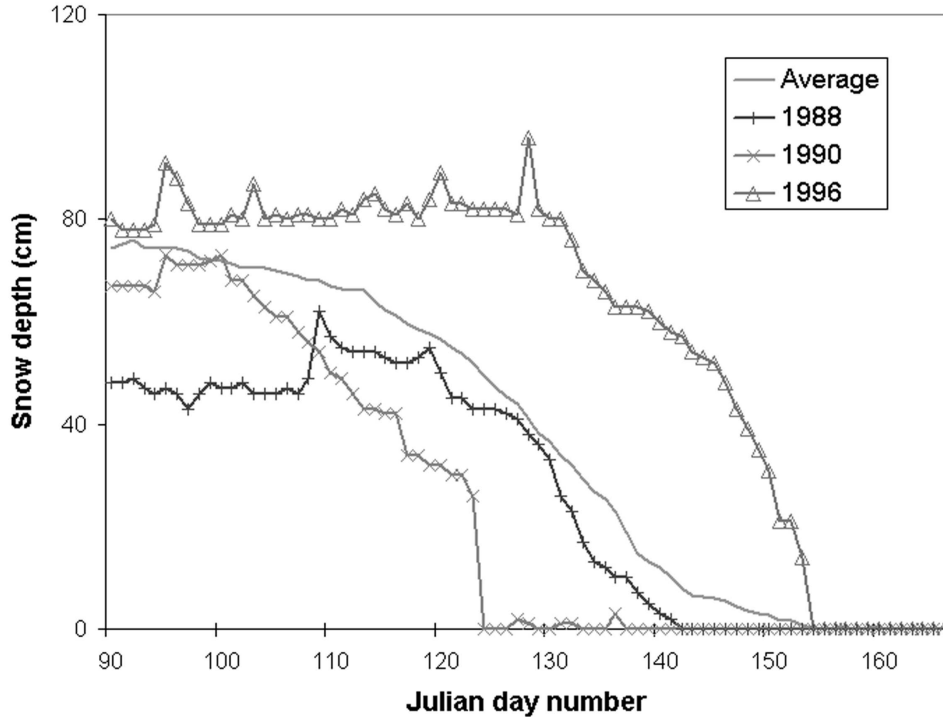
Figure 6.1 Late-winter snow depth at Kevo, Finland, in three typical years: 1988 (relatively little snow), 1990 (early snowmelt), and 1996 (late snowmelt). Also shown is the average snow depth in the period 1980-1999

Earth observation techniques offer the opportunity of monitoring spatial and temporal patterns in snowmelt (chapter 4). With the arrival of new sensors such as NOAA-15 and onwards, SPOT VEGETATION and MODIS, that all make observation in the mid-infrared part of the spectrum around 1.6 μm, the spatial and temporal extent of the snow cover can effectively be monitored over large areas, such as the Tana Basin (Dankers et al., 2001). In the present study 10-day syntheses of SPOT VEGETATION images were used, that were acquired during the spring seasons of 1998 and 1999. The spatial resolution of these images is 1 km by 1 km. As described in chapter 4, snow cover extent in each 10-day synthesis image was mapped using a similar algorithm as developed by Klein et al. (1998). Using data from the red and mid-infrared bands, a normalised difference snow index (NDSI) was calculated, and a threshold value was used to identify pixels that are covered with snow for more than 50% (see chapter 4 for more details). Subsequently the moment of snow disappearance was registered for each pixel (figure

6.3). In the river valleys snowmelt started earlier in 1998, but it was more rapid in 1999. In this year, almost 80% of the Tana Basin became free of snow in only 20 days, from mid-May to early June. The snow cover disappeared latest on the plateau uplands and mountain areas in the north, where it continued to exist until early June. In 1998 snow coverage at these high elevations lasted until late June (figure 4.9).
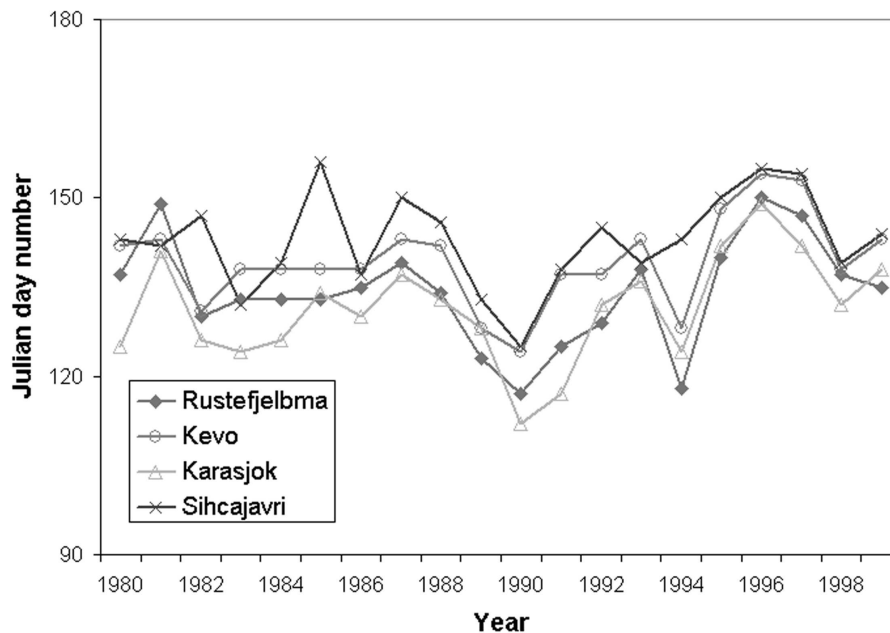
Figure 6.2 First observed snow-free day at selected meteorological stations in the Tana Basin, in 1980-1999. For locations, see figure 2.3

Rapid melting of snow, combined with frozen soils, causes a high runoff peak in a relatively short period of time, which is typical for rivers in the Arctic and sub-Arctic (figure 2.6). In the Tana Basin snowmelt runoff may contribute as much as 65% to the total annual runoff. In this period discharge can be higher than 3000 m^3/s, while the mean annual runoff of the Tana River is only 166 m^3/s. Maximum runoff is usually reached in the second half of May, but can be delayed until the second half of June.

6.3   Model application and performance

Snowmelt and runoff in the Tana Basin were simulated using the conceptual water balance model TANAFLOW, that is described in more detail in chapter 5. Being fully distributed, this model calculates the water balance on a 10-day basis for grid cells of 1

a) 1998

N

21-30 April
1-10 May
11-20 May
21-31 May
1-10 June
11-20 June
21-30 June
1-10 July or later

b) 1999

0   25   50 Kilometers
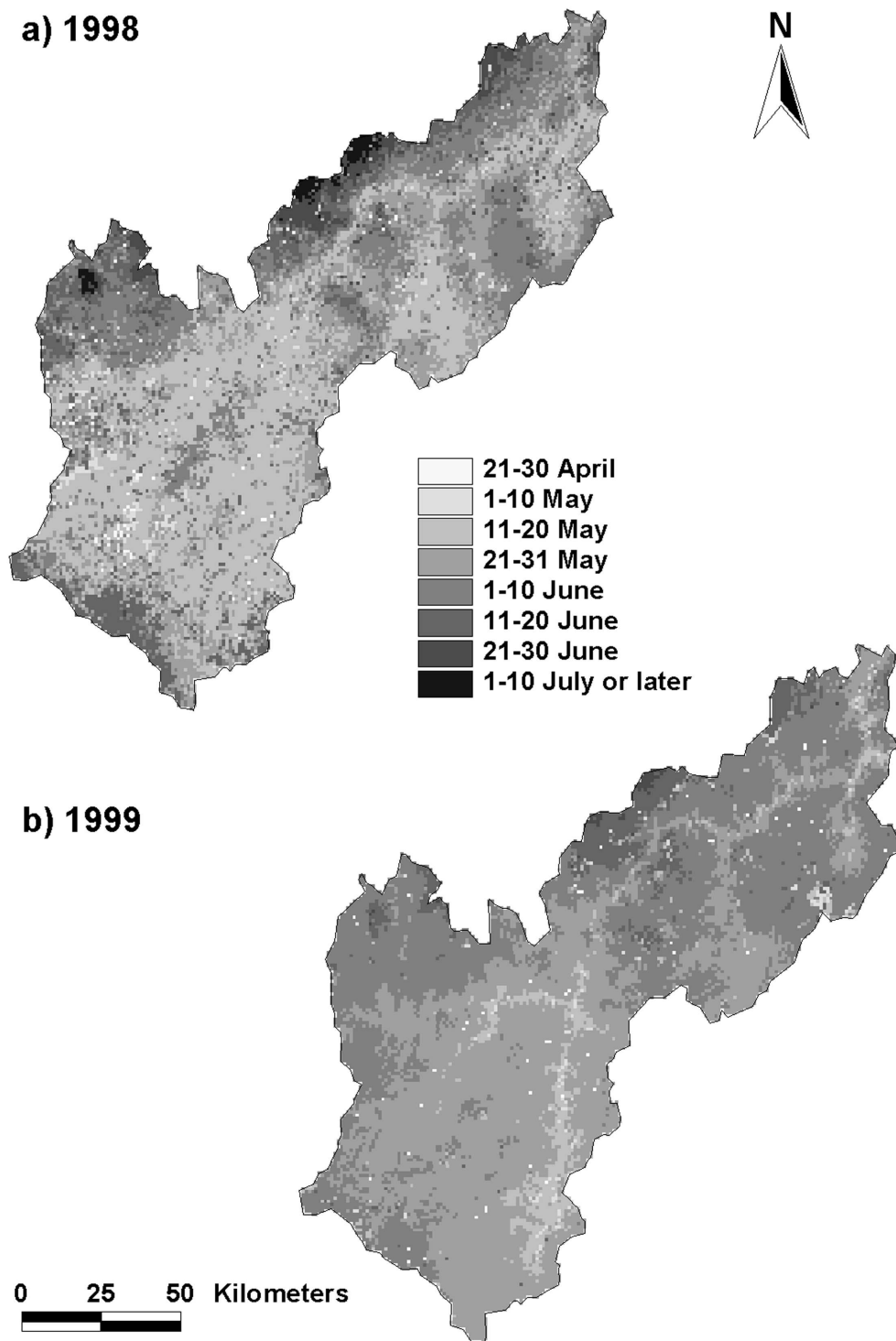
Figure 6.3 Disappearance of snow cover in the Tana Basin, based on SPOT VEGETATION data: (a) in 1998; (b) in 1999. Original image data distributed by SPOT IMAGE and produced by VITO, Belgium, copyright CNES, 1999. See the appendix for a colour version

km by 1 km, as a function of temperature, precipitation, vegetation and soil characteristics. Temperature and precipitation data are interpolated from meteorological stations in the study area. Snowmelt is estimated with a temperature index approach, using a degree-day factor to convert air temperature above a certain threshold to snowmelt in mm (Ferguson, 1999). The amount of runoff that is produced in each cell, is subsequently accumulated over a digital elevation model (DEM) of the area, and compared with observed runoff at the catchment outlet.

Using discharge data of the Tana River, the model was calibrated for the period October 1979 to September 1989, by adjusting three parameters: the degree-day factor (*DDF*) for snowmelt estimation, the separation ratio of runoff into direct and delayed runoff (χ), and the recession parameter (*C*) for baseflow from the groundwater reservoir. The model was validated for October 1989 to September 1999 (section 5.5). The parameter combination that yielded the highest efficiency coefficient (Nash & Sutcliffe, 1970) for the entire basin was used in this chapter (table 5.7).

In the 10 years of the validation period, the TANAFLOW model appeared to simulate the timing of the snowmelt runoff peak correctly (figure 6.4). The total peak runoff volume was on average about 20% too low, although in some individual years the simulated runoff peak was higher than actually measured (figure 6.4.b). However, the capability of the model to predict the snowmelt runoff peak at the catchment outlet, does not mean that it simulates the snow cover depletion within the catchment correctly. This became evident when comparing the moment of snow disappearance in the catchment, as simulated by the model, with the SPOT VEGETATION satellite observations (figure 6.5 and figure 6.6). Both in 1998 and 1999 the simulated snow cover depletion is later than inferred from the VEGETATION images in about 80% of the catchment area, while in only a small part (4 and 1% respectively) it is earlier than observed by satellite. Those areas where the depletion of the snow cover is more or less in agreement with the satellite observations, are mainly situated at higher altitudes along the northern boundary of the Tana Basin, where snow usually melts latest (figure 6.5).

In part this difference can be attributed to the algorithm used to map snow cover in the SPOT VEGETATION images, that only classifies pixels as snow if they contain at least 50 % snow cover (Klein et al., 1998). During snowmelt however, the snow cover can become very patchy, and considerable amounts of snow may occur in pixels that are not mapped as snow-covered any more. In contrast, a pixel in TANAFLOW is still flagged as snow-covered even if it contains a small amount of snow water equivalent. In chapter 4 it was noted that the same algorithm as used here, may also be used to identify pixels that are covered with snow for only a small part, if a lower NDSI threshold is used (cf. figure 4.5). The same procedure was therefore repeated using a NDSI-threshold of –0.1, and the results were again compared with the model estimates of snow cover depletion (figure 6.6). Assuming that a lower threshold value in the VEGETATION images results in correct identification of pixels that are covered with snow for only a small part, the

(a)
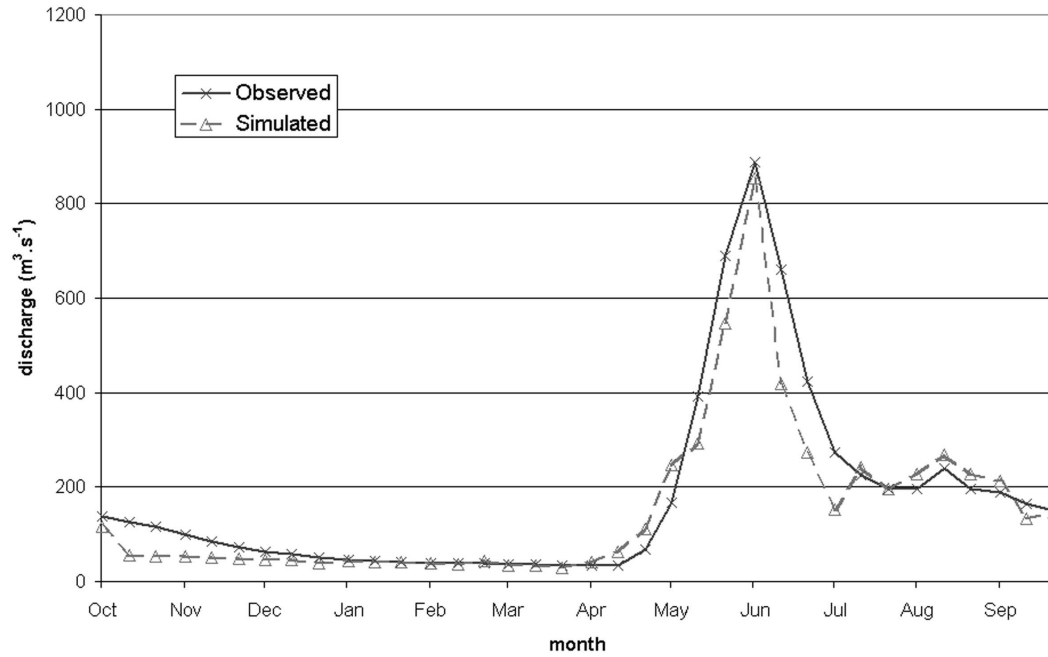
(b)
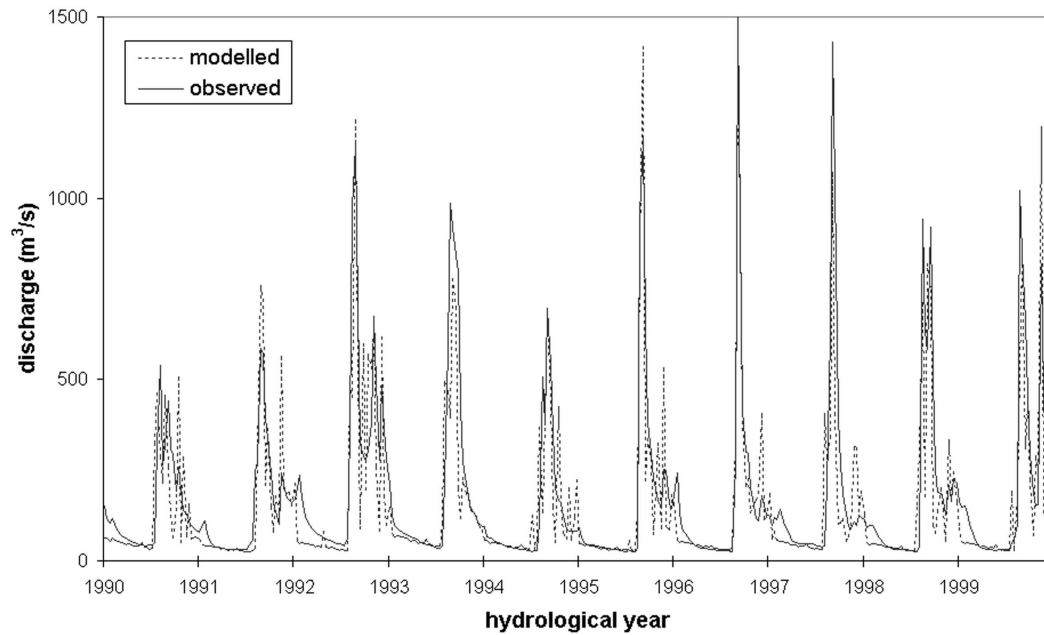
Figure 6.4 Observed and simulated discharge of the Tana River at Alaköngäs, Finland: (a) averaged over the validation period 1990-1999; (b) for all individual years in the validation period
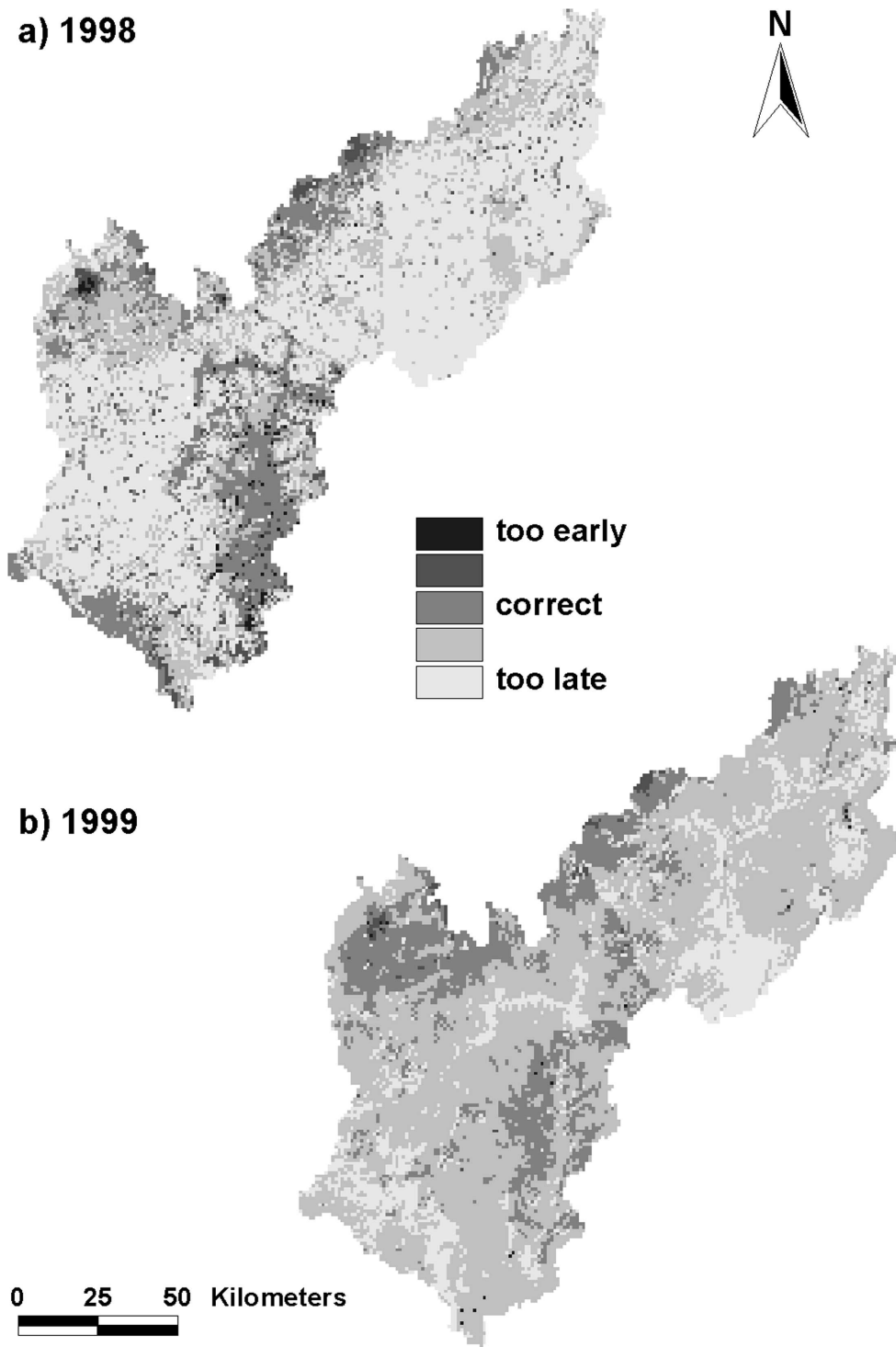
122

Figure 6.5 Disappearance of snow as predicted by TANAFLOW, compared with satellite observations of pixels covered by snow for more than 50%: (a) in 1998; (b) in 1999. See the appendix for a colour version

(a)
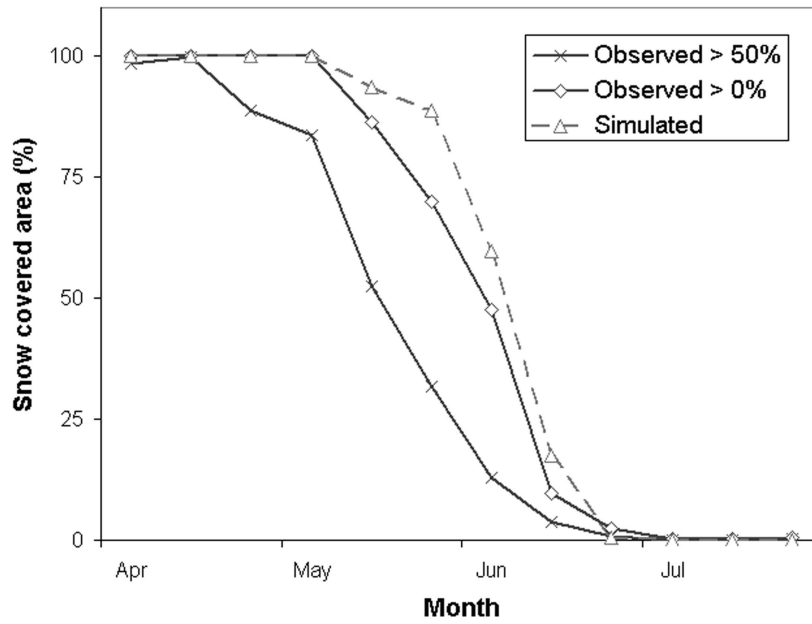
(b)
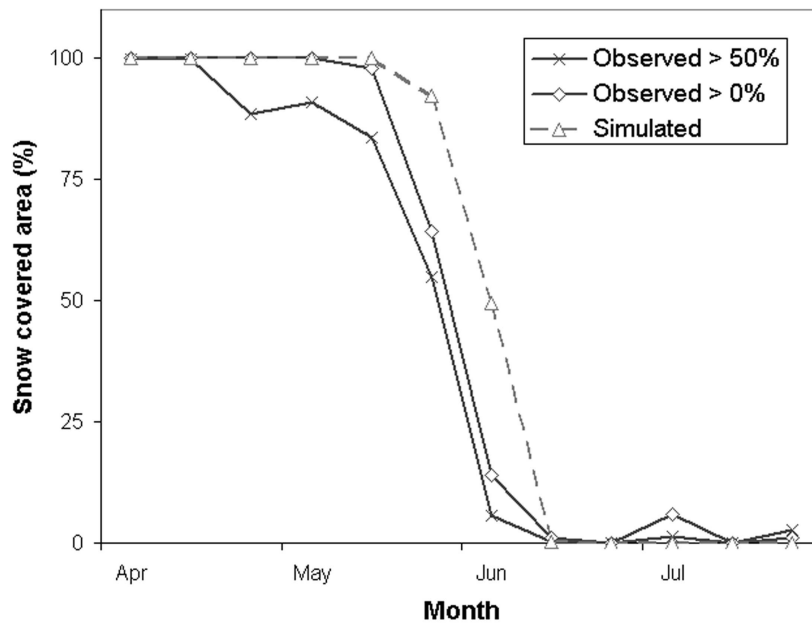
Figure 6.6 Fractional snow coverage in the Tana basin as predicted by TANAFLOW, compared with satellite observations of pixels covered by snow for more than 50 %, and more than 0 %: (a) in 1998; (b) in 1999

124

simulated snow cover depletion still appears to be somewhat too late. The rate of rate of decline in snow coverage is however more or less similar (figure 6.6).

6.4　Sensitivity of snow coverage and melt to climate change

Under conditions of a doubled CO_2 content in the atmosphere, temperatures in Northern Fennoscandia may rise by 3-4ºC and precipitation may increase by 20-50 % (SMHI, 1998). The sensitivity of snow coverage and river discharge in the Tana Basin to changes of these magnitudes was analysed by applying changes in precipitation of +10, +20 and +50 % and changes in temperatures of +1, +2 and +5 degrees Celsius to the data from the meteorological stations that were used in the model. A temperature rise results in an earlier onset of the snowmelt season, and reduces the total snow mass considerably (see figure 6.7). An increase in precipitation may compensate for the latter effect, but it cannot prevent that the snow disappears about one month earlier if the temperature rises 5ºC as well. For current climate conditions, the model estimates the total length of the snow-free season in the Tana Basin to be between about 150 days in the valleys and in the southwestern part, and less than 100 days in the mountains in the north (figure 6.8.a). A temperature rise of 5ºC extends the snow-free season by 45-65 days in the southwest, to more than 80 days in the northeast, close to the Barents Sea (figure 6.8.b). If this rise in temperature coincides with a precipitation increase of 50 %, this prolongation of the snow-free season is less, but still considerable (figure 6.8.c). It is important to note that snow cover may be reduced significantly in spring, when levels of photosynthetically active radiation are at maximum. For the vegetation in the area this might have important consequences (Callaghan et al, 1998).

Because of the earlier snowmelt, the spring runoff peaks earlier in the year. However, the magnitude of the maximum runoff is considerably lower, unless the rise in temperature is accompanied by a large precipitation increase (see figure 6.9). A precipitation increase also results in higher discharges in summer. In fall, river discharge can be higher if part of the precipitation is falling as rain, instead of snow (figure 6.9).

Table 6.1 Change (in %) in mean annual runoff of the Tana River compared to the control run

Change in Temperature	Change in precipitation			
	no change	+10%	+20%	+50%
no change		+11.4	+22.6	+56.2
+1ºC	-0.9	+10.2	+21.4	+54.8
+2ºC	-1.9	+9.2	+20.3	+53.7
+5ºC	-5.1	+6.1	+17.2	+50.8
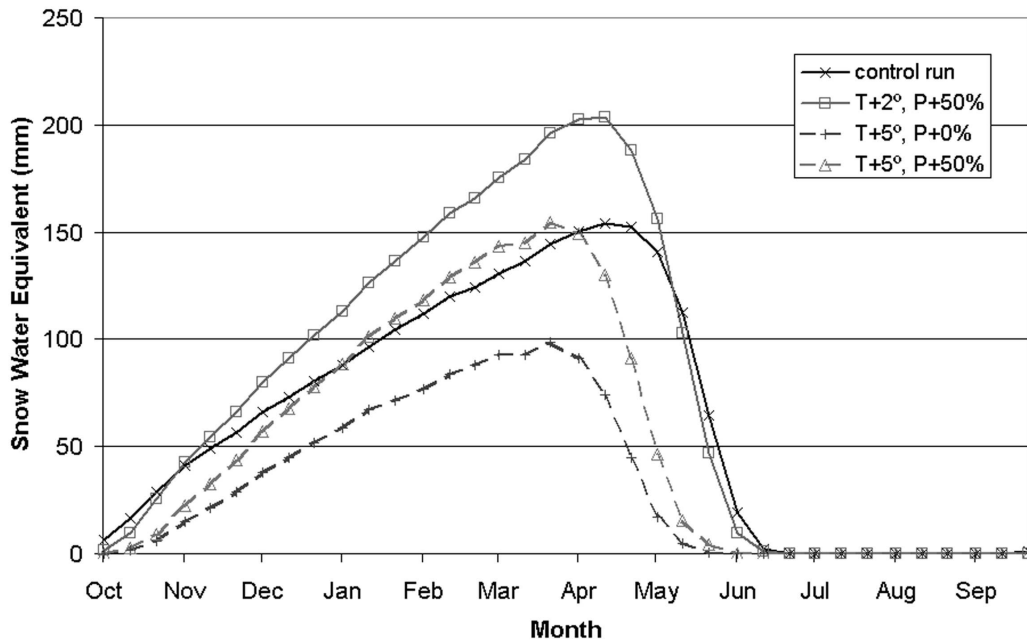
Figure 6.7 Sensitivity of basin-averaged snow water equivalent to increases in temperature (T) and precipitation (P). The control run represents the simulation for current climate conditions

The effect of changing temperature and precipitation on the water balance is summarised in table 6.1. A precipitation increase of for example 50 % increases the annual runoff more than proportionally. This is due to the relative decrease in evapotranspiration losses: the additional snowfall in winter is discharged during snowmelt, instead of being evaporated in summer. It seems that the annual water balance is much less influenced by changes in temperature than by precipitation changes. However, especially for the summer period these results should be interpreted with care, considering the uncertainties associated with the estimates of evapotranspiration (see chapter 5).

6.5   Discussion

Once calibrated against river discharge data, the hydrological model used in this study, TANAFLOW, was able to predict the timing of the snowmelt discharge peak accurately. At the same time the depletion of the snow cover appeared to be one or two timesteps of 10 days too late in comparison with satellite observations. This difference is partly due to the fact that the algorithm used to map snow cover in the VEGETATION images, was originally developed to identify pixels that are covered with snow for 50% or more. Since the model does not consider sub-grid variability, a pixel in TANAFLOW is mapped as snow-covered even if it contains only a small amount of snow water equivalent. However, even after the snow mapping algorithm for the satellite images was adjusted by using a lower NDSI-threshold value, so that also pixels that are covered with snow for
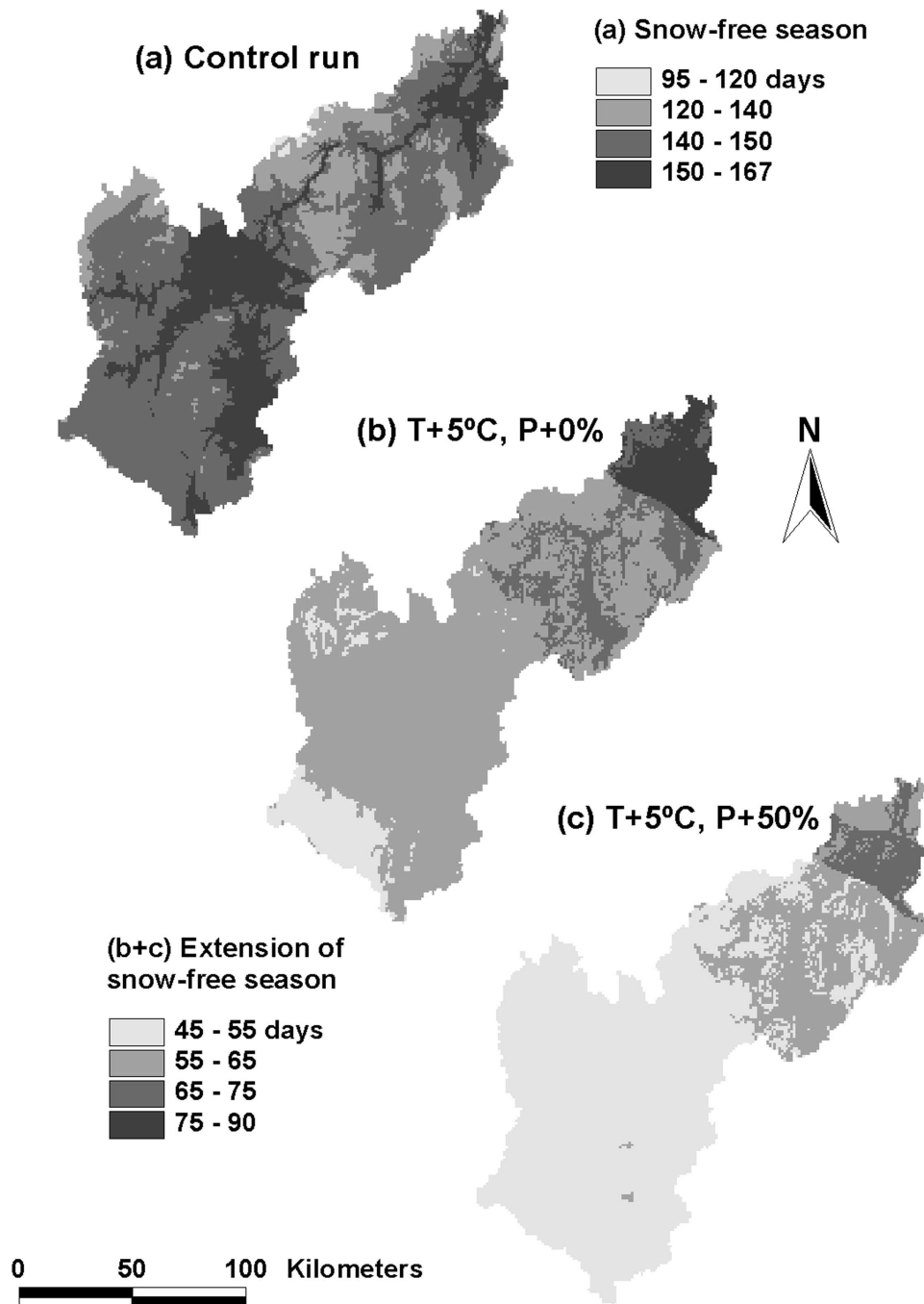
126

Figure 6.8 Length of the snow-free season in the Tana Basin, predicted by TANAFLOW: (a) for current climate conditions; (b) prolongation after a temperature rise of 5ºC; (c) prolongation after a combined increase in temperature and precipitation of 5ºC and 50 % respectively. See the appendix for a colour version
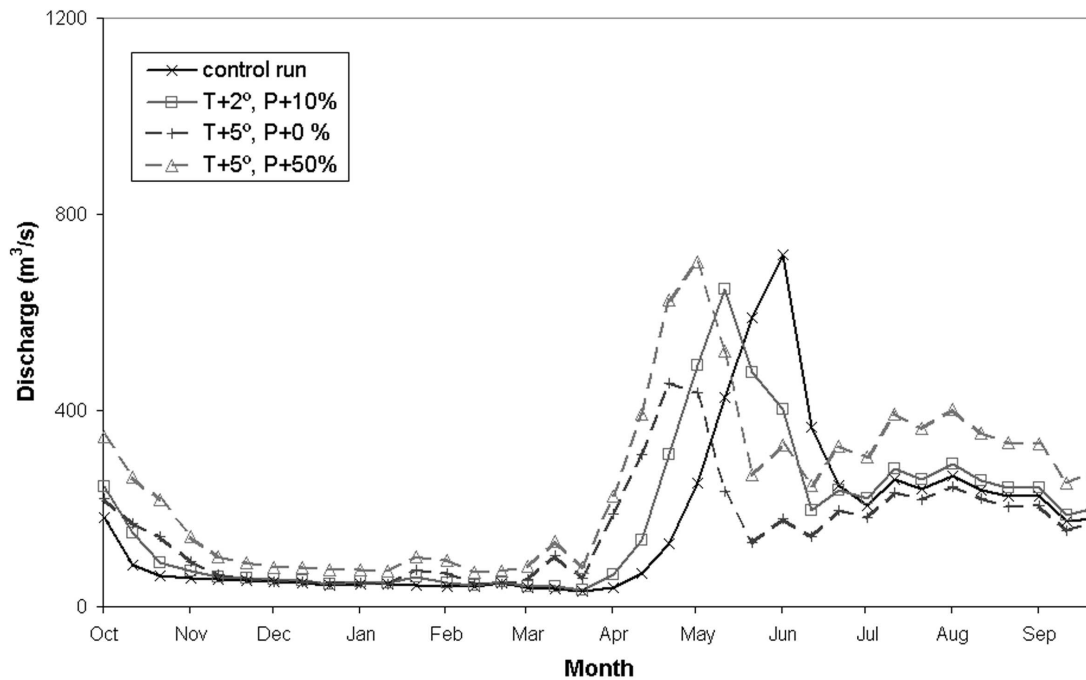
Figure 6.9 Sensitivity of discharge of the Tana River to increases in temperature (T) and precipitation (P). The control run represents the simulation for current climate conditions

only a small part would be identified, the simulated snow cover depletion was still somewhat too late (figure 6.6). It should be noted that the degree-day factor for snowmelt in TANAFLOW was obtained by calibration against river discharge data. Apparently the discharge peak at the catchment outlet is not a suitable indicator of the date of snowmelt for pixels within the catchment. However, the differences in snow cover disappearance were not larger than one or two timesteps, and the depletion rate was similar.

As noted in the chapter 5, the empirical nature of the temperature index method to estimate snowmelt rates may be an additional problem in climate change studies. Although only artificial climate changes have been considered in this chapter, the results are generally consistent with those of other studies. For example, Vehviläinen & Lohvansuu (1991) predicted increases in mean annual runoff of 20-50 % for Finland under conditions of a doubled CO_2 content in the atmosphere. According to their simulations winter discharge will increase considerably, while spring high flows will generally decrease, due to a smaller snow storage. The smallest changes were found for the summer period, when evapotranspiration counterbalanced the increase in precipitation (Vehviläinen & Lohvansuu, 1991). According to TANAFLOW evapotranspiration remains an insignificant part of the water balance, even if temperatures rise. As argued in chapter 5, this process is however indefinite even with regards to its actual value. A more physically-based simulation method is therefore

128

necessary to evaluate the actual contribution of evapotranspiration to the water balance of the Tana Basin, and to assess the possible impacts of climatic change.

In the present study, a temperature rise of 5ºC had a significant impact on the timing of snowmelt and the magnitude of the spring peak runoff (figure 6.7 and 6.9). Periods of intermittent winter thaw may however affect the snowmelt process by leading to the formation of ice layers in the snow pack (Callaghan et al., 1998), and by reducing the heat deficit of the snow pack. This may affect runoff generation and accelerate the onset of snowmelt in spring. On the other hand, if snowmelt takes place one month earlier indeed, as suggested by figure 6.7, the radiation conditions will be different. In mid-April, the potential solar radiation at these latitudes is only 58 % of the radiation in mid-May, when snowmelt presently occurs (figure 6.10).

The empirical temperature-index method fails in making allowances for these different conditions. Obviously, the best method to estimate snowmelt rates would be to solve the energy balance of the snow pack, but it is virtually impossible to obtain enough measurements for a distributed energy balance model. According to Melloh (1999) climate model data could be used to drive physically-based snowmelt algorithms in hydrological models. A similar procedure, using data from a Regional Climate Model (RCM), will be tested in the Tana Basin in the next chapter.
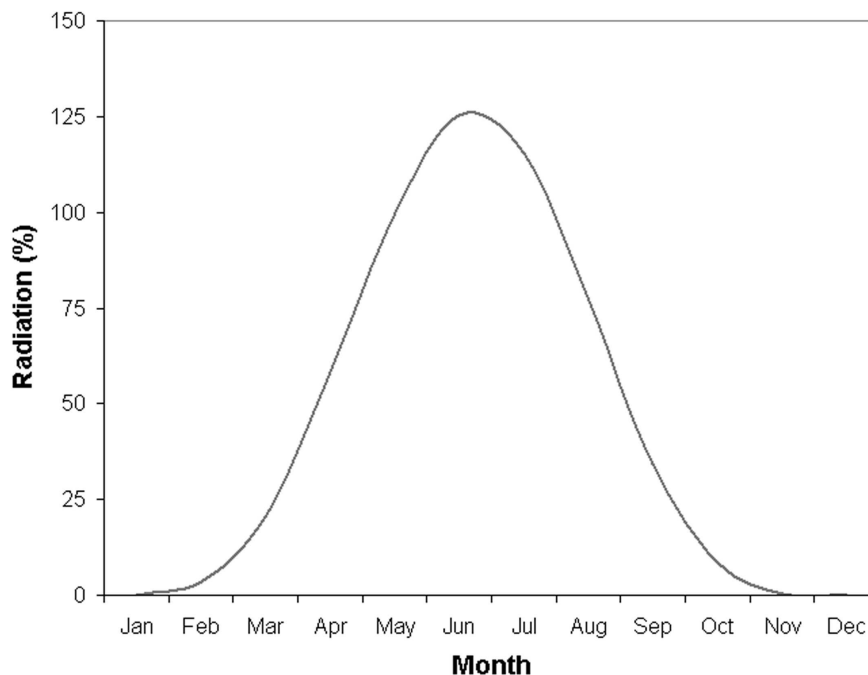
Figure 6.10 Potential solar radiation at Kevo, Finland, expressed as a fraction of the potential solar radiation in mid-May. Radiation was modelled using the program POTRAD (Van Dam, 2000)

6.6   Conclusions

In this chapter the ability of TANAFLOW to simulate snowmelt patterns and runoff in the Tana Basin was evaluated. The model was able to simulate the timing of the annual discharge peak correctly, but compared with satellite observations the depletion of the snow cover was too late in large parts of the area. This difference could only partly be attributed to the algorithm that was used to map snow cover in the satellite images. Since the model was calibrated on runoff data, it appears that the discharge peak at the catchment outlet is not a reliable indicator of the timing of snowmelt for pixels within the catchment. A more physically-based snowmelt model may therefore improve the simulation of spatial patterns in snow coverage.

Despite all uncertainties still associated to the model predictions, it becomes clear that snow accumulation and snowmelt, being dependent on temperature and precipitation, are highly sensitive to changes in climate. By introducing changes in temperature and precipitation into the model simulations, the sensitivity of snow cover dynamics in the Tana Basin to climatic changes could be analysed. The model simulations suggest that a rise in temperature results in a smaller snow mass and a considerably earlier snowmelt. In case of a temperature rise of 5°C the snow-free season may be extended by 50 to more than 80 days (figure 6.8). The largest changes in snow cover duration occurred in the Northeast, close to the Barents Sea. Although a concurrent increase in precipitation may compensate for the reduction in winter snow mass, it seems to have little effect on the timing of the snowmelt. Considering the fact that in spring levels of photosynthetically active radiation are at maximum, changes of these magnitudes will certainly have important consequences for the ecology of the area.

6.7   References

Anisimov, O. & B. Fitzharris (2001): Polar Regions (Arctic and Antarctic). In: J.J. McCarthy, O.F. Canziani, N.A. Leary, D.J. Dokken & K.S. White (eds.): Climate Change 2001: Impacts, Adaptation and Vulnerability. Cambridge: Cambridge University Press.

Callaghan, T.V., C. Körner, O.W. Heal, S.E. Lee & J.H.C. Cornelissen (1998): Scenarios for ecosystem response to global change. In: O.W. Heal, T.V. Callaghan, J.H.C. Cornelissen, C. Körner & S.E. Lee (eds.): Global Change in Europe's cold regions. Luxembourg: Office for Official Publications of the European Communities (Ecosystems Research Report No. 27), pp. 11-63.

Dankers, R., H. Middelkoop & S.M. De Jong (2001): Observation and modelling of water balance components in Northern Fennoscandia with NOAA-AVHRR and SPOT VEGETATION imagery. In: M. Owe, K. Brubaker, J. Ritchie & A. Rango (eds.): Remote Sensing and Hydrology 2000. Wallingford: IAHS Publication 267, pp. 123-125.

Ferguson, R.I. (1999): Snow melt runoff models. Progress in Physical Geography 23, pp. 205-227.

Klein, A.G., D.G. Hall & G.A. Riggs, G.A. (1998): Improving snow cover mapping in forests through the use of a canopy reflectance model. Hydrological Processes 12, pp. 1723-1744.

Koster, E.A. (1991): Assessment of climate change impact in high-latitudinal regions. Terra 103, pp. 3-13.

Melloh, R.A. (1999): A synopsis and comparison of selected snowmelt algorithms. Hanover, New Hampshire: US Army Corps of Engineers, Cold Regions Research & Engineering Laboratory (CCREL report 99-8).

Nash, J.E. & J.V. Sutcliffe (1970): River flow forecasting through conceptual models; Part 1 -a discussion

of principles. Journal of Hydrology 10, pp. 282-290.

SMHI (1998): Regional climate simulations for the Nordic region - First results from SWECLIM. Norrköping: Swedish Meteorological and Hydrological Institute.

Van Dam, O. (2000): Modelling incoming Potential Radiation on a land surface with PCRaster. POTRAD5.MOD manual. Utrecht: Utrecht Centre for Environment and Landscape dynamics, Utrecht University.

Vehviläinen, B. & J. Lohvansuu (1991): The effects of climate change on discharges and snow cover in Finland. Hydrological Sciences Journal 36, pp. 109-121.

7 A LARGE-SCALE, PHYSICALLY-BASED MODEL OF SNOWMELT AND EVAPOTRANSPIRATION IN SUB-ARCTIC ENVIRONMENTS

With a contribution of Ole Bøssing Christensen

7.1 Introduction

In the water balance of sub-arctic environments, seasonal snow coverage in winter and evapotranspiration in summer play an important role. Most areas at high latitudes are covered with snow for up to 8 months per year or more, and the timing of snowmelt is of utmost importance for the start of the growing season in these fragile ecosystems. Although summers are short, the contribution of evapotranspiration to the water balance can be considerable, since total radiation amounts can be high and ample water is generally available after snowmelt (see chapter 3).

It is generally expected that changes in climate, caused by the so-called enhanced greenhouse effect, will be largest at high latitudes (Houghton et al., 2001). In order to estimate the impact of these changes on large-scale hydrology and water resources, most hydrological models rely on empirical or semi-empirical descriptions of evapotranspiration and snowmelt. Snowmelt for example, is frequently modelled using a degree-day factor that relates melt rates to air temperature only, and that often has to be determined by calibration (Ferguson, 1999). However, since it is likely that a changing climate will lead to a shift of the snowmelt season to earlier in the year (chapter 6), the input of solar radiation and hence the entire snowmelt process may become different (see figure 6.10). Physically-based models of snowmelt and evapotranspiration, that are independent of calibration and applicable to a wide range of climatic conditions, are therefore preferable in climate change impact studies.

The application of physically-based models over large areas is however impeded by the large amount of data they require, data that are often not available (Arnell, 1996; Kite et al., 1996). Climate or weather prediction models may serve as an alternative source of data for hydrological models (Melloh, 1999). However, few studies have actually accomplished this approach successfully. Kite & Haberlandt (1999) used data from several general circulation models (GCMs) and numerical weather prediction models (NWPs) as input for a hydrological model of the Mackenzie River Basin in northwestern Canada. They concluded that these resulted in better model performance than the sparsely available observations from meteorological stations in the area. Direct use of GCM data may therefore be advantageous especially in very large and remote drainage basins, such as the Mackenzie Basin. In general, it is however believed that particularly the water balance of GCMs is not accurate enough to give satisfying results in hydrological modelling. Not only is precipitation usually overestimated, also its seasonal distribution is often inaccurate (Kite & Haberlandt, 1999). Van Blarcum et al. (1995) accumulated runoff calculated by GCM of the Goddard Institute of Space Studies (GISS) (Hansen et

al., 1983), and compared it with observed discharge for nine of the largest northern rivers in the world. The model results deviated significantly from observed runoff, sometimes by several orders of magnitude; the changes in runoff patterns that were found for doubled CO_2 conditions were nevertheless consistent with other studies (Van Blarcum et al., 1995).

In order to estimate the consequences of climate change for the hydrology and water resources in the Tana River Basin in Northern Fennoscandia (figure 2.1), the main aim of the study presented in this chapter was to increase the robustness of the hydrological model TANAFLOW, that was introduced in chapter 5. The original version of this model was developed for the Rhine Basin in Western Europe by Kwadijk (1993). The temperature-index approach to estimate snowmelt, and the Thornthwaite method of estimating potential evapotranspiration (Thornthwaite & Mather, 1957), were replaced by physically-based models for snowmelt and evapotranspiration in this sub-arctic environment. In view of the considerations discussed above, these models were driven by observations on temperature and precipitation from meteorological stations in the area, in combination with data from a regional climate model (RCM) for those input variables of which no observations were available. By combining these different sources of data it appeared to be possible to run physically-based models of snowmelt and evapotranspiration over the large area of the Tana Basin. This chapter introduces the procedure that was followed, describes the models for snowmelt and evapotranspiration that were developed, and discusses the model performance when compared with observed snow cover depletion and river discharge.

7.2   Outline

The main purpose of this study was to develop physically-based models of snowmelt and evapotranspiration for use in TANAFLOW. These models should be applicable to a wide range of climatic and radiation conditions, but at the same time not too complex for application to the entire catchment of the Tana River. Moreover, they should be driven by observations on temperature and precipitation from meteorological stations in the area (figure 7.1), while all other input variables (net radiation, humidity and wind speed) are taken from the RCM HIRHAM4 (Christensen et al., 1998).

For the simulation of snow accumulation and snowmelt, a simplified energy balance model was developed, based on a lumped representation of the snow pack as a single layer. Energy content and water equivalence are the main state variables that describe the snow pack. The energy exchange at the snow surface is simulated using physically-based descriptions, and is balanced by a net heat flux into the snow pack. Similar to the Utah Energy Balance Snow Accumulation and Melt Model (UEB) of Tarboton & Luce (1996) an equilibrium approach is used to solve for the snow surface temperature. The model, named TANASNOW, is based on UEB and similar models as described by Price & Dunne (1976), USACE (1956, 1998), Anderson (1976), Kustas et al. (1994), and Koivusalo et al. (2001). The model runs on a daily time step since daily data are commonly available from meteorological stations. Despite the marked diurnal variation

134

of the components of the energy balance (see e.g. Gray & Prowse, 1993), an energy balance model should give reasonable results with time steps up to 24 hours, as in this range the components are linear or nearly linear functions of meteorological and other independent variables (Dingman, 1994).

In order to simulate evapotranspiration, a model was chosen that is generally accepted and has been proven to be applicable to a wide range of conditions. The Penman-Monteith model of evapotranspiration, originally developed by Penman (1948) and later modified by Monteith (1965), takes into account the meteorological influences on evaporation, as well as the aerodynamic and physiological influences of the vegetation cover (Ward & Robinson, 1990). A major disadvantage of this approach is that the aerodynamic and surface resistances are generally unknown for the natural vegetation types occurring in the Tana Basin. For this reason, a reference evapotranspiration is calculated for an idealised crop type with specific characteristics, which is then converted to vegetation-dependent evapotranspiration by using a crop factor, as described in section 7.5.

Both models were programmed in the dynamic modeling language of the raster geographical information system (GIS) package PCRaster (Van Deursen, 1995), and were incorporated as separate modules within TANAFLOW. In addition, some minor modifications were introduced into the model structure of TANAFLOW, that were believed to lead to a better representation of the hydrological system in this sub-arctic environment. These modifications are discussed in section 7.6.
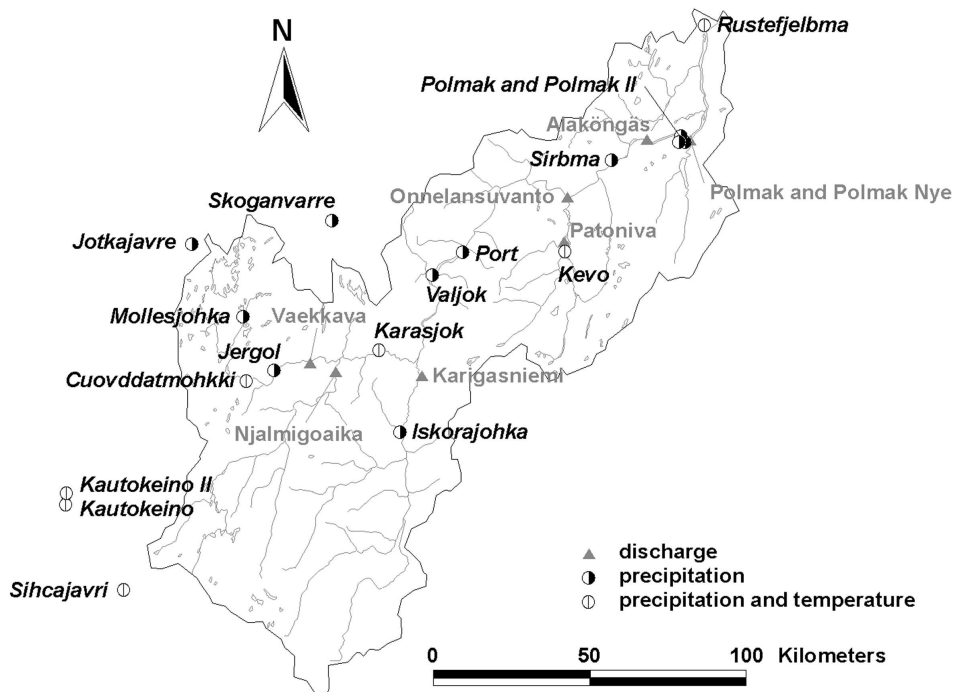
Figure 7.1 Location of meteorological stations and discharge measurement stations in the Tana Basin

135

7.3 The HIRHAM4 Regional Climate Model

The regional climate model employed is HIRHAM4, which is based on the HIRLAM (Källén, 1996) numerical weather forecast model but using the physical parameterization schemes of the ECHAM4 global climate model (Roeckner et al. 1996). HIRHAM4 is documented in detail by Christensen et al. (1996). The HIRHAM model was developed by the Danish Meteorological Institute (DMI) and the Max Planck Institute (MPI) for Meteorology in Germany, and has also been used extensively at the Dutch and Norwegian meteorological institutes, and, aimed at polar regions, at the Alfred-Wegener Institute in Potsdam. HIRHAM has been used in several EU projects concerned with regional climate modelling. Applications of HIRHAM include both observation-based experiments, like the one used in the present study, and experiments driven by global model output with the aim of describing possible regional effects of anthropogenic greenhouse warming. Data from these experiments will be used in chapter 8.

During the EU project MERCURE (ENV4-CT97-0485) a 15-year experiment has been performed with boundary conditions given by the 15-year reanalysis from the European Centre for Medium-range Weather forecasts (ECMWF). This reanalysis covers the period 1979-1993 and consists of 6-hourly global data in 19 vertical levels and a spectral resolution of T106, corresponding to approximately 150 km grid distance. All available observations have been used to make this reanalysis as close to reality as possible. At the time of the experiment (1998-1999) This data set was the most realistic boundary data available in terms of resolution, homogeneity and general quality.

The HIRHAM integration area consists of 19 vertical levels and 110 by 104 points with a distance of about 50 km in a domain covering Europe and surrounding ocean. From the ECMWF reanalysis 6-hourly atmospheric data were applied in a 10 points wide relaxation zone, Sea surface temperatures were also taken from the reanalysis. As part of the MERCURE project the HIRHAM model was improved in order to reproduce observed temperatures and precipitation. These improvements included implementation of satellite-based high-resolution land surface parameters and an improvement of the coupling between land surface and atmosphere.

In the present study, data from HIRHAM4 were used for the 14 hydrological years that were covered by the ECMWF reanalysis period, i.e. from October 1979 to September 1993 (referred to as 1980-1993). In this period, the modelled temperature in the Tana Basin agreed well with the observed temperatures at meteorological stations in the area (figure 7.2.a). Winter temperatures were somewhat higher than observed, while in summer the modelled temperature was slightly lower. As a result the annual average was the same as observed: -2.0ºC. Precipitation from HIRHAM4 was significantly higher than observed in the Tana Basin, although the RCM reproduced the seasonal pattern (figure 7.2.b). According to the model mean annual precipitation in the Tana Basin in 1980-1993 amounted to 635 mm, the observation-based estimate was only 402 mm per year. However, the latter value is based on extrapolation from meteorological stations, that are

(a)
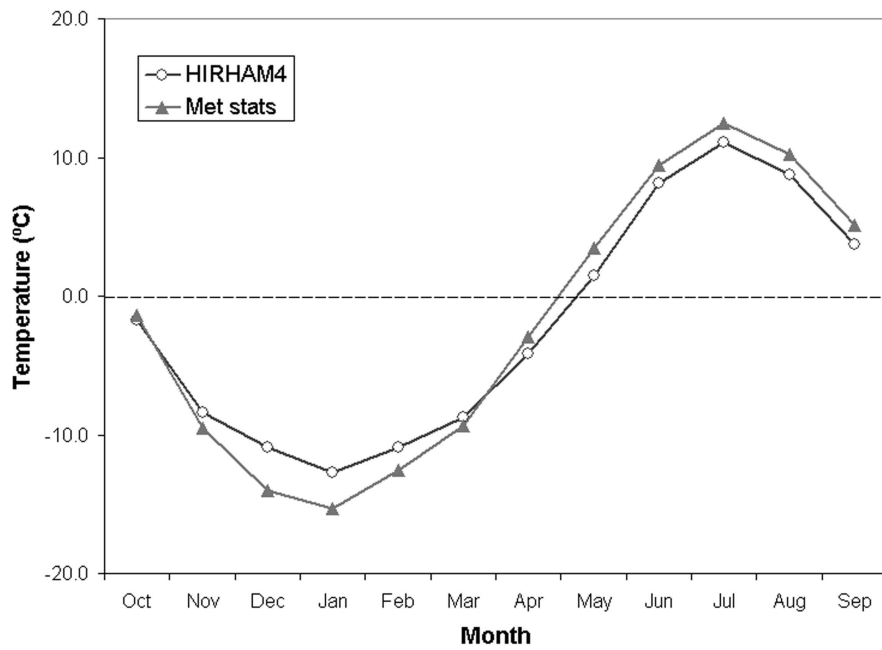
(b)
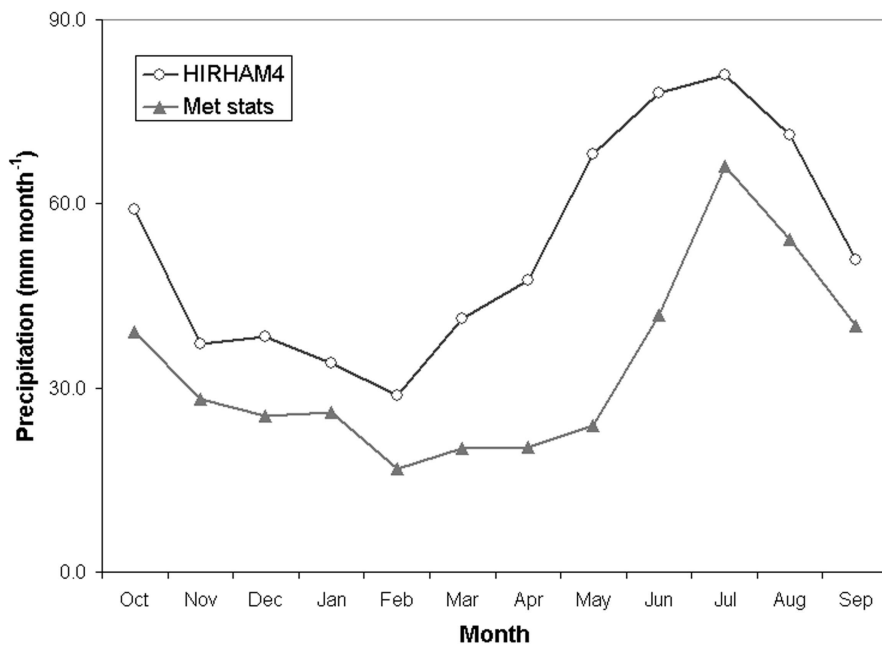
Figure 7.2 Basin-averaged temperature (a) and precipitation (b) in 1980-1993, obtained from the HIRHAM4 RCM and by extrapolation of observations at meteorological stations in the Tana Basin

137

mainly situated in river valleys, to the catchment area. As discussed in chapter 5 these stations are supposedly not representative for the surrounding highlands.

7.4 TANASNOW: an energy balance model of snowmelt for use in TANAFLOW

Melting of snow is caused by input of energy (or heat) into the snow pack. A net energy input may come from a variety of sources: shortwave and longwave net radiation, convection from the air (or sensible heat exchange with the atmosphere), condensation of water vapour (or latent heat exchange), heat input by precipitation, and conduction of heat from the ground. These energy fluxes are balanced by a change in the internal energy content of the snow pack, or, if the snow is isothermal at 0ºC, by melting of ice. Thus, following the common notation:

$$Q_m = Q_{sw} + Q_{lw} + Q_h + Q_e + Q_p + Q_g - \Delta Q_i \qquad (7.1)$$

where Q_m = energy available for melt
$\quad\quad Q_{sw}$ = net shortwave radiation
$\quad\quad Q_{lw}$ = net longwave radiation
$\quad\quad Q_h$ = sensible heat exchange
$\quad\quad Q_e$ = latent heat exchange
$\quad\quad Q_p$ = heat advected from precipitation
$\quad\quad Q_g$ = ground heat input
$\quad\quad \Delta Q_i$ = rate of change in the internal energy of the snow pack

All components in equation (7.1) are generally expressed in energy per unit surface area per unit time (cf. Anderson, 1976; Price & Dunne, 1976; Gray & Prowse, 1993). During the accumulation period of a seasonal snow pack the net inputs of energy are generally negative, leading to a heat deficit, sometimes referred to as the "cold content" of the snow, and to a decreasing average snow pack temperature. Before melting can occur, a (positive) net energy input is required to warm the snow pack. Once the heat deficit has been accounted for, any further input of energy will lead to melting. Initially, meltwater will be retained in the snow pack until the latter is saturated. At that point the snow pack is said to be "ripe", and any further input of energy will result in an output of water (Dingman, 1994; USACE, 1998). The physical descriptions of each component in equation (7.1) are discussed in the following sections. More details can be found in USACE (1956, 1998), Gray & Prowse (1993), and Dingman (1994).

7.4.1 Net radiation

Radiation is the prime source of energy to the snow pack. Net radiation can be divided into two components: net solar or shortwave radiation Q_{sw}, with wavelengths between 0.2 and 4.0 µm, and terrestrial or longwave radiation Q_{lw} at greater wavelengths (up to 100

138

μm). The amount of incident shortwave radiation depends on latitude, season, time of the day, and atmospheric conditions. Local influences include topography and, if present, the density of the vegetation cover. The net input of shortwave energy is the difference between the incident radiation, and the proportion that is reflected. The reflectivity or albedo of snow varies over a wide range, depending on snow particle size, density and composition, surface roughness, wetness, and the presence of impurities and vegetation, but is generally higher than for snow-free surfaces. The albedo is an important determinant of the net energy input into the snow pack (Dingman, 1994).

The net input of shortwave radiation can be written as:

$$Q_{sw} = Q_{sw\ in} \times (1 - \alpha) \tag{7.2}$$

where Q_{sw} = net shortwave radiation, kJ m^{-2} day^{-1}
         $Q_{sw\ in}$ = incoming shortwave radiation, kJ m^{-2} day^{-1}
         α = shortwave albedo (-)

Various models exist to calculate the potential incident shortwave radiation flux if measurements are not available, such as POTRAD (Van Dam, 2000). The actual amount of incident radiation is however strongly influenced by clouds and vegetation. To simulate the decrease of the albedo of an aging snow surface, several empirical or conceptual decay functions have been proposed, e.g. by the USACE (1956).

In TANASNOW shortwave radiation data from the RCM are taken as an approximation of the actual net shortwave radiation in the area. These data allow for the effects of cloudiness, but not for local topography and vegetation. The latter effect is assumed to be of relatively minor importance during the winter season, except for the relatively small area of pine forests. For practical reasons only, this study uses *net* radiation data from the RCM; theoretically it is however feasible to use incoming radiation fluxes, and calculate net shortwave radiation according to equation (7.2), with some decay function for the albedo.

Net longwave radiation is the difference between incident radiation, emitted by the atmosphere, clouds and vegetation canopy, and radiation emitted by the snow surface. The flux of longwave radiation is described by the Stefan-Boltzmann law:

$$Q_{lw} = \varepsilon\ \sigma\ T_s^4 \tag{7.3}$$

where Q_{lw} = net longwave radiation, kJ m^{-2} s^{-1}
         ε = emissivity (-)
         σ = Stefan-Boltzmann constant, 5.67×10^{-8} W m^{-2} K^{-4}
         T_s = surface temperature, K

Since the emissivity of snow is generally very high, between 0.97 and 0.99, the snow surface acts as a near-perfect blackbody (USACE, 1998). Opposed to the longwave

radiation emitted by the snow surface, is radiation emitted by the atmosphere and, if present, the vegetation canopy. Both may be calculated using the Stefan-Boltzmann equation by using an effective emissivity and effective radiating temperature of the atmosphere and canopy. Under clear skies this "back-radiation" is usually less than the radiation emitted by the snow surface, leading to a heat loss from the snow pack. In these conditions the longwave radiation emitted by the atmosphere is largely dependent on the content of carbon dioxide and water vapour. The presence of clouds or vegetation has a large influence on the effective emissivity of the atmosphere, and may lead to a net heat gain. Empirical formulae that correct for atmospheric humidity and the degree of cloudiness can be found in Gray & Prowse (1993) and Dingman (1994). In forest environments the situation is more complex. Incident longwave radiation increases with increasing canopy coverage; however, the incoming shortwave radiation will decrease. In general, snowmelt under a forest canopy due to net radiation exchange is less than in open environments (Gray & Prowse, 1993).

7.4.2   Turbulent heat transfer

Turbulent exchange of heat between snow and atmosphere involves two processes. Sensible heat transfer (or convection) is due to a temperature difference between the snow surface and the overlying air. Latent heat exchange results from condensation or sublimation of water vapour. The sensible heat exchange is mainly driven by the temperature gradient between the snow surface and the overlying atmosphere, and the wind speed. It is described by the following aerodynamic equation (Price & Dunne, 1976; Kustas et al., 1994):

$$Q_h = \rho_a c_a \frac{k^2 U_z}{[\ln(z/z_0)]^2} \times (T_a - T_s) \times C_h \qquad (7.4)$$

where Q_h = sensible heat flux, kJ m^{-2} s^{-1}
  ρ_a = air density, 1.293 kg/m^3
  c_a = specific heat of air at constant pressure, 1.00 kJ kg^{-1} K^{-1}
  k = Von Karman's constant, 0.4
  U_z = wind speed at height z, m s^{-1}
  z = measurement height, usually 2 m
  z_0 = aerodynamic roughness length snow surface, m
  T_a = air temperature, K or ºC
  T_s = snow surface temperature, K or ºC
  C_h = correction factor for atmospheric stability

The roughness length of the snow surface, z_0, is highly variable over a wide range; a value of 0.5 cm is typically used (e.g. Price & Dunne, 1976; Tarboton & Luce, 1996), and was also assumed in this study. Protruding vegetation for example, may however increase z_0 considerably (Dingman, 1994). The correction factor C_h is required for application of

equation (7.4) to stratified (either stable or lapse) conditions. In TANASNOW this correction is based on the Richardson number, following Price & Dunne (1976).

The exchange of latent heat is primarily dependent on the difference in vapour pressure between the air and the snow surface, as well as wind speed. The aerodynamic formula to describe the latent heat flux resembles that for sensible heat (Dingman, 1994; Williams & Tarboton, 1999):

$$Q_e = \frac{0.622\lambda}{R_d T_a} \frac{k^2 U_z}{[\ln(z/z_0)]^2} \times (e_a - e_{ss}) \times C_h \tag{7.5}$$

where Q_e = latent heat flux, kJ m^{-2} s^{-1}
λ = latent heat, kJ kg^{-1}
R_d = dry gas constant, 0.2871 kJ kg^{-1} K^{-1}
e_a = vapour pressure of the air, kPa
e_{ss} = saturated vapour pressure of the snow surface, kPa

The latent heat λ to be used in equation (7.5) depends on the phase changes that are involved. If condensation takes place on a melting snow pack, water vapour changes into liquid, but it will not freeze; in this case the latent heat of vaporisation (2470 kJ kg^{-1}) should be used in equation (7.5). In all other cases, two phase changes are involved, namely from vapour to liquid, and from liquid to solid, or vice versa, and the latent heat in equation (7.5) is the sum of the latent heat of vaporisation and that of fusion (334.9 kJ kg^{-1}) (Dingman, 1994). The vapour pressure deficit ($e_a - e_s$) can be derived from data on air temperature, snow surface temperature and relative humidity using the following relations:

$$e_a = RH \times e_s \tag{7.6}$$

and (Tetens, 1930):

$$e_s = 0.61078 \times e^{(17.27 * T)/(T + 237.3)} \tag{7.7}$$

where e_s = saturated vapour pressure at the temperature of the air, kPa
T = air temperature in °C
RH = relative humidity (-)

The saturated vapour pressure of the snow surface, e_{ss} can be found by using the snow surface temperature in equation (7.7). Note that equation (7.5) gives the evaporation or sublimation rate if the right-hand side is divided by the latent heat λ (Dingman, 1994).

7.4.3   Advected heat from precipitation

Rain that is falling on a snow pack will be cooled to the snow temperature, according to (Dingman, 1994; USACE, 1998)

$$Q_p = c_p \rho_w P(T_r - T_s) \qquad (7.8)$$

where Q_p = heat convected from precipitation, kJ m^{-2} day^{-1}
           c_p = specific heat of precipitation, kJ kg^{-1} K^{-1}
           ρ_w = density of water, 1000 kg m^{-3}
           P = amount of rain, m day^{-1}
           T_r = temperature of the rain, K or °C
           T_s = temperature of the snow, K or °C

If the snow temperature is below freezing, the rain will also freeze, liberating latent heat. In this case the equation becomes:

$$Q_p = c_p \rho_w P(T_r - T_s) + \rho_w \lambda_f P \qquad (7.9)$$

where λ_f = latent heat of fusion, 334.9 kJ kg^{-1}

The specific heat c_p is equal to 4.20 kJ kg^{-1} K^{-1} for rain, and 2.09 for snow (USACE, 1998). The temperature of the rain T_r is assumed to be equal to the dewpoint temperature, which can be found by inverting equation (7.7) and solving with the actual vapour pressure of the air, e_a. The contribution of Q_p to the energy budget of the snowpack is usually very small (Dingman, 1994).

7.4.4   Ground heat

Conduction of heat from the ground is usually a very small component of the overall energy budget and therefore it is often neglected over shorter periods of time. However, since it is a continuous process, its contribution can be significant over an entire snow season. Calculation of the ground heat input requires information on the thermal conductivity of the soil, as well as the vertical temperature gradient into the soil, information that is usually not available. Based on USACE (1998), a constant heat flux of 2 J m^{-2} s^{-1} is therefore assumed in TANASNOW.

7.4.5   Melt and mass balance of the snow pack

A positive energy budget in equation (7.1) will initially be used to diminish the heat deficit or cold content of the snow pack. In other words, the average snow pack temperature will be raised. This temperature can be calculated with the following equation:

142

$$T_m = \frac{Q_i}{d_s(\rho_i c_i + \rho_w c_w)} \qquad (7.10)$$

where T_m = average snow pack temperature, ºC below freezing
           Q_i = internal energy content, kJ m^{-2}
           d_s = snow depth, m
           ρ_i = density of ice, 922 kg m^{-3}
           c_i = specific heat of ice, 2.09 kJ kg^{-1} K^{-1}
           c_w = specific heat of water, 4.20 kJ kg^{-1} K^{-1}

In the above equation the vapour phase term is neglected (Gray & Prowse, 1993). By definition, the temperature of the snow pack cannot rise above the freezing point. If the snow pack is isothermal at 0 ºC, any further input of energy will lead to melting. The amount of melt is calculated with (USACE, 1998):

$$M = \frac{Q_m}{\rho_w \lambda_f B} \qquad (7.11)$$

where M = amount of melt, m
           Q_m = energy available for melt, kJ m^{-2}
           B = thermal quality of the snow (-)

The thermal quality of the snow is typically between 0.95 and 0.97 for melting snow packs (USACE, 1998). Initially melting will increase the liquid water content of the snow pack. The maximum amount of water that can be retained depends on the depth, density and structure of the snow pack, but is approximately 2 to 5 % of the snow water equivalent (SWE) at 0 ºC (USACE, 1956). According to Kuusisto (1984) the liquid water retention capacity decreases during snowmelt. Once the snow is saturated, any further melting will lead to a loss of water.

In addition to outflow of meltwater, the mass balance of the snow pack also depends on input of precipitation, and the amount of sublimation. The latter can be calculated by dividing equation (7.5) by the latent heat. In TANASNOW precipitation is considered as snow if the dewpoint temperature is less than or equal to 0 ºC. Rain falling on snow only contributes to the snow mass if the surface temperature or the average temperature of the snow pack is below freezing; otherwise, it is added to the liquid water content.

7.4.6   Snow surface temperature

Using the equations discussed in the previous sections, the energy and mass balance of a snow pack can be calculated if the required meteorological variables are known, and proper estimates are made for the various parameters. In TANASNOW meteorological

observations on temperature and precipitation are used as input variables. In addition, radiation, humidity and wind speed data are obtained from a RCM. Similar to UEB (Tarboton & Luce, 1996), the snow surface temperature T_s is obtained by iteration, based on the assumption that the energy fluxes at the snow surface are balanced by the conduction of heat into the snow pack. In general T_s is different from the average temperature from the snow T_m, and the heat flux into the snow can be calculated with (Tarboton & Luce, 1996):

$$Q_{in} = K_s \rho_s c_s (T_s - T_m) \tag{7.12}$$

where Q_{in} = heat flux into the snow pack, kJ m^{-2}
        K_s = snow surface conductance, 0.48 m day^{-1}
        ρ_s = density of snow, 450 kg m^{-3}
        c_s = specific heat of snow, 2.09 kJ kg^{-1} K^{-1}

The values for K_s and ρ_s are derived from Tarboton & Luce (1996). The value of T_m depends on the internal energy content of the snow pack in the previous timestep, and is calculated with equation (7.10). T_s is found by iterating the calculation of the surface heat fluxes, with the dewpoint temperature as an initial estimate for the snow surface temperature. If the resulting snow surface temperature is above freezing, the energy exchange at the snow surface cannot be balanced by heat conduction into the snow. In this case surface melt will occur; the infiltrating meltwater will subsequently refreeze, and by liberating latent heat it will account for the energy difference (Tarboton & Luce, 1996).
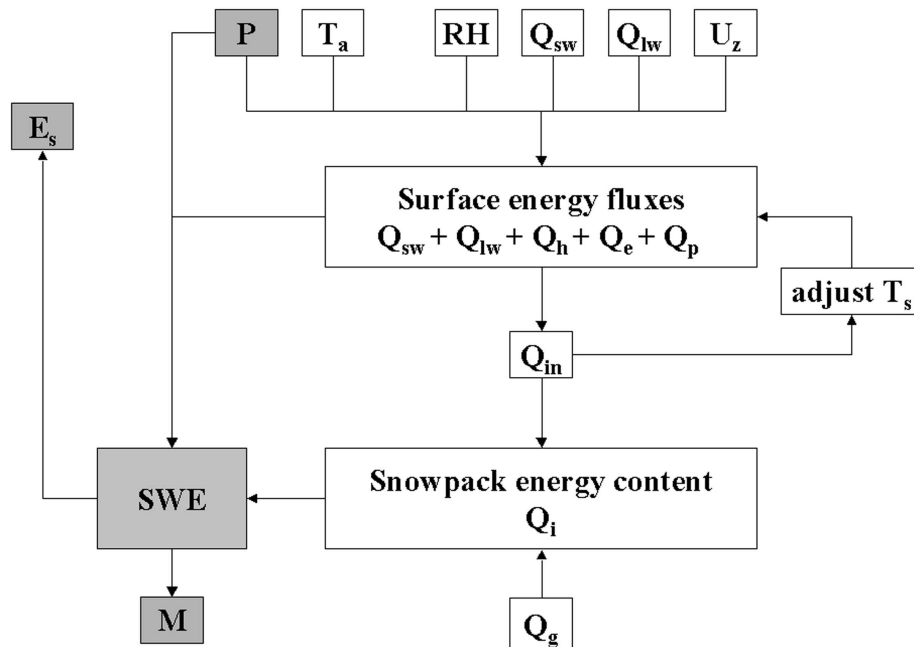

Figure 7.3 Flowchart of TANASNOW. See text for explanation of the symbols, E_s = sublimation

144

7.4.7   *Importance of energy balance components*

The relative importance of each term in equation (7.1) varies considerably, both in space and time, depending on location and weather conditions. Kuusisto (1984) reviewed several energy balance studies and deduced several generalisations. In general, the contribution of heat convected from precipitation or conducted from the ground is small or negligible; the most important sources of energy are therefore net radiation and turbulent exchange of sensible and latent heat. During snowmelt the radiation balance and sensible heat exchange are generally positive, leading to a net heat gain. The latent heat flux however can be positive or negative, as both evaporation and condensation conditions may prevail. On cloudy or rainy days turbulent heat exchange dominates the energy balance, and extremely high snowmelt rates are usually caused by a large turbulent heat flux. In forest environments however net radiation is generally the most important component of the energy balance (Kuusisto, 1984).

7.4.8   *Structure of TANASNOW*

The structure of TANASNOW consists of four major components: (1) input and interpolation of the variables and parameters; (2) calculation of the surface energy balance by solving the snow surface temperature T_s by iteration; (3) calculation of the snow pack energy content, as a function of heat conducted from the surface, infiltration of rain or surface meltwater, and ground heat; and (4) output of sublimation and – if the average temperature of the snow pack is equal to 0ºC – melted snow (see figure 7.3). The model runs with daily time steps, and for each time step the model requires data on precipitation and temperature (obtained by interpolation from meteorological stations in the Tana Basin), and radiation, humidity and wind speed (that are obtained from the HIRHAM4 regional climate model). Fixed parameter values that are used in the calculations, are listed in table 7.1.

7.5   **Evapotranspiration modelling according to Penman-Monteith**

7.5.1   *Reference evaporation*

The Penman-Monteith model of evapotranspiration, based on the combination equations of Penman (1948), and later adjusted to account for vegetation controls by Monteith (1965), is one of the best-known and advanced evaporation models currently available (Shuttleworth, 1993). The original Penman (1948) equation for potential evaporation combines the energy-balance approach to estimate the net radiation available for evaporation, with a turbulent transfer theory describing the diffusion of water vapour from the surface. Monteith (1965) allowed for the important aerodynamic and physiological influences that a vegetation cover has on the evapotranspiration process, by incorporating the aerodynamic and surface resistance of the vegetation to evaporation.

Table 7.1 Parameter values in TANASNOW

	Symbol	Value
Measurement height (m)	z	2.0
Von Karmann's constant	k	0.4
Aerodynamic roughness (m)	z_0	0.005
Latent heat of vaporisation (kJ kg^{-1})	λ_v	2470
Latent heat of fusion of ice (kJ kg^{-1})	λ_f	334.9
Ground heat flux (kJ m^{-2} s^{-1})	Q_g	0.002
Gas constant air (kJ kg^{-1} K^{-1})	R_d	0.2871
Snow surface heat conductance (m day^{-1})	K_s	0.48
Air density (kg m^{-3})	ρ_a	1.293
Water density (kg m^{-3})	ρ_w	1000
Snow density (kg m^{-3})	ρ_s	450
Ice density (kg m^{-3})	ρ_i	922
Specific heat air (kJ kg^{-1} K^{-1})	c_a	1.00
Snow heat capacity (kJ kg^{-1} K^{-1})	c_i, c_s	2.09
Specific heat water (kJ kg^{-1} K^{-1})	C_p	4.02
Maximum liquid water content (%)		5

The general form of what has become know as the Penman-Monteith model is (Shuttleworth, 1993):

$$
E = \frac{1}{\lambda} \left[\frac{\Delta\,(Q_n - Q_g) + \rho_{air}\,C_p\,\dfrac{(e_s - e_a)}{(r_a)}}{\Delta + \gamma\left(1 + \dfrac{r_s}{r_a}\right)} \right]
\tag{7.13}
$$

where E = crop evaporation, mm day^{-1}
λ = latent heat of vaporisation, kJ kg^{-1}
Δ = slope of the saturation vapour pressure curve, kPa °C^{-1}
Q_n = net radiation, kJ m^{-2} day^{-1}
Q_g = soil heat flux, kJ m^{-2} day^{-1}
ρ_a = air density, kg m^{-3}
C_p = specific heat of moist air, kJ kg^{-1} °C^{-1}
e_s = saturated vapour pressure, kPa
e_a = actual vapour pressure, kPa
γ = psychrometric constant, kPa °C^{-1}

146

$$r_a \quad = \text{aerodynamic resistance, s m}^{-1}$$
$$r_s \quad = \text{surface resistance, s m}^{-1}$$

With some assumptions, this model can be used to calculate reference crop evapotranspiration, i.e. evaporation from an idealised grass crop with an uniform height of 0.12 m, an albedo of 0.23, and a surface resistance of 69 s m^{-1}, actively growing, completely shading the ground, and not short of water (Shuttleworth, 1993). The equation for estimating reference crop evaporation can then be written as:

$$E_{rc} = \frac{\Delta \dfrac{(Q_n - Q_g)}{\lambda} + \gamma \dfrac{900}{(T_{air} + 273)} U_2 (e_s - e_a)}{\Delta + \gamma (1 + 0.33\, U_2)} \tag{7.14}$$

where E_{rc} = reference crop evaporation, mm day^{-1}
           U_2 = wind speed at 2 m, m s^{-1}
           T_{air} = air temperature, °C

Apart from air temperature, this model requires information on net radiation, humidity and wind speed. The vapour pressure deficit (e_s-e_a) can be calculated as a function of air temperature and humidity using the following equations:

$$e_s = 0.6108 \exp\left(\frac{17.27\, T_{air}}{237.3 + T_{air}} \right) \tag{7.15}$$

$$e_a = e_s \times \left(\frac{RH}{100} \right) \tag{7.16}$$

where RH = relative humidity, %

Alternatively, the actual vapour pressure may be calculated by using the dew point temperature for T_{air} in equation (7.15). The slope of the saturation vapour pressure curve, Δ, is also a function of temperature:

$$\Delta = \frac{4098\, e_s}{(237.3 + T_{air})^2} \tag{7.17}$$

The psychrometric constant, γ, is not strictly a constant, but a function of atmospheric pressure (which varies slightly over time, and with altitude), and the latent heat of vaporisation of water, λ, which varies slightly with temperature (Dingman, 1994). It is calculated as follows:

$$\gamma = \frac{C_p\, P}{\varepsilon \lambda} \qquad (7.18)$$

where C_p = specific heat of moist air = 1.013 kJ kg^{-1} °C^{-1}
         P = atmospheric pressure, kPa
         ε = ratio of the molecular weight of water vapour to that of dry air = 0.622

The latent heat can be calculated with:

$$\lambda = 2501 - 2.361 \times T_s \qquad (7.19)$$

where T_s = temperature of the evaporating surface, °C

The magnitude of the soil heat flux may be estimated from the soil heat capacity, but since it is relatively small over 10- to 30-day periods, it is often neglected for hydrologic applications (Shuttleworth, 1993).

7.5.2 Crop factor

Evaporation from a certain crop may be estimated from equation (7.13) if the aerodynamic and surface resistance for that specific vegetation type are known. This is rarely the case. In practice the reference crop evaporation is often estimated from equation (7.14), which is then multiplied by a crop coefficient or crop factor K_c:

$$E = K_c \times E_{rc} \qquad (7.20)$$

The crop factor implicitly represents differences in the canopy resistance relative to the reference crop, but also in vegetation height, that controls the aerodynamic resistance. To some extent the crop factor is also dependent on temperature, wind speed and rainfall, and it will vary according to the seasonal development of the vegetation type under consideration (Shuttleworth, 1993). Inevitably these considerations are often neglected in the absence of any relevant information, especially on natural vegetation types.

Based on flux measurements in 1999, Harding et al. (2002) determined the surface resistance r_s for the hillslope site in the Kidisjoki catchment near Kevo, Finland, where the vegetation mainly consists of dwarf shrubs, lichens, and a few solitary birch trees (see chapter 3). By inverting the Penman-Monteith equation on an hourly basis, a mean r_s value of 245 s m^{-1} was obtained. The results showed however a considerable variability, ranging from 0 to 1000 s m^{-1}. The highest values were obtained during warmer periods (Harding et al., 2002). This illustrates the uncertainties associated with the application of Penman-Monteith to natural conditions. For this reason, it was decided to calculate reference crop evaporation using equation (7.14), which is then modified using the crop coefficients used in chapter 5.

7.5.3   Incorporation of Penman-Monteith in TANAFLOW

The Penman-Monteith model (equation 7.14) replaced the Thornthwaite method
(Thornthwaite & Mather, 1957) of estimating potential evapotranspiration in
TANAFLOW. The new evaporation scheme runs on daily time steps, and requires data
on air temperature, net radiation, humidity and wind speed. Of these variables, the first
was obtained from meteorological stations in the Tana Basin (figure 7.1), while the last
three were derived from HIRHAM4. Conduction of heat into the soil was neglected,
which may be a reasonable assumption in most hydrological applications (Shuttleworth,
1993).

Under natural conditions the amount of evapotranspiration may be limited by the
availability of soil moisture. Several curves have been proposed that describe the relation
between decreasing soil water and the actual evapotranspiration (see e.g. Ward &
Robinson, 1990). Similar to for example Macro-PDM (Arnell, 1999), the actual
evaporation rate in TANAFLOW is reduced linearly as a function of residual soil
moisture storage. The actual form of the soil moisture extraction function may have little
influence on the estimates, since the cumulative error is set to zero each time the soil
becomes saturated, or dries completely (Shuttleworth, 1993).

7.6   Modifications to the model structure of TANAFLOW

The physically-based models for snowmelt and evapotranspiration, described in the
previous sections, were included in the TANAFLOW model. Although both models
operate on a daily resolution, runoff is accumulated over periods of 10 days, so that a
hydraulic routing scheme is not necessary. In addition, several modifications were
introduced in the model, that are believed to provide a better representation of the
specific hydrological behaviour of the Tana Basin.

First of all, in order to correct the underestimation of precipitation in the catchment, a
precipitation lapse rate was included in the model, in addition to the lapse rate for
temperature. As discussed in chapter 5, most meteorological stations in the Tana Basin
are situated in river valleys, and their precipitation record is supposedly not
representative for the surrounding upland areas. This results in unrealistically high ratios
of observed runoff and precipitation in the Tana Basin (table 5.2). The actual value of the
precipitation lapse rate was obtained by comparing long-term observed and simulated
runoff, which is described in more detail in section 7.7. Furthermore, the extrapolation of
observations on precipitation and temperature to the catchment area with Thiessen
polygons, was replaced with an inverse distance interpolation. This should result in
spatial patterns that are more realistic, and no longer dominated by the shape of the
Thiessen polygons.

In chapter 5, it was argued that during snowmelt the hydrological system of the Tana
Basin is different from that later in summer. Due to frozen ground and ice layers in the

snow pack, the infiltration of meltwater into the soil may be limited. For this reason, the model formulation was changed in such a way that infiltration is impeded as long as a pixel is still covered with snow. This means that all meltwater produced during snowmelt, contributes to rapid runoff, except for the last time step in which the snow cover disappears. Later in summer, infiltration is no longer limited and the hydrological system may act as normal.

Finally, the soil moisture compartment of the model was changed in order to generate more rapid runoff during snowmelt and extreme rainfall events. In the original model, rapid runoff is produced only if the input of rain and snowmelt is larger than the evaporation rate, and if the soil moisture storage is filled to its capacity. When these conditions are met, rapid runoff is only a fixed portion of the water in excess of the soil storage, controlled by the separation ratio χ, which has to be obtained by calibration (Kwadijk, 1993). For the Tana Basin, it was believed to be physically more realistic if rapid runoff would be more prominent during snowmelt and extreme rainfall events, but less important during periods of low flow in summer and winter. For this reason, the model was changed in such a way that, when the soil moisture storage is filled to its capacity, all excess water contributes to rapid runoff. Simultaneously, percolation to the groundwater reservoir takes place as a function of soil moisture storage. This concept is similar to many other models (e.g. Arnell, 1999). This modification eliminates the separation ratio χ from the model. In exchange, a new parameter, the seepage coefficient S, is introduced, describing how percolation to the groundwater reservoir depends on soil moisture:

$$Q_{gw} = S \times SM \tag{7.21}$$

where Q_{gw} = percolation to the groundwater reservoir, mm day^{-1}
          S = seepage coefficient (day^{-1})
         SM = soil moisture storage (mm)

In this study, the value of S was obtained by calibration as well.

7.7   Model application

In this modified form, the TANAFLOW model was applied to the Tana River Basin by running it for the period October 1979 to September 1993 (referred to as 1980-1993), for which the HIRHAM4 RCM data were available. This period was split up into two equal parts, one for calibration (1980-1986) and one for validation of the model (1987-1993). Before each simulation run, the model was initialised by repeating the calculations of the first five years. In contrast with the previous model version (chapter 5), the model ran at daily time steps, but runoff was only accumulated and reported every 10-day period. The spatial resolution was maintained at 1 by 1 km. Values of precipitation and temperature were obtained by inverse distance interpolation from meteorological stations in and around the Tana Basin. Elevation differences were taken into account by using the lapse

rates for temperature and precipitation. All other meteorological input variables (radiation, humidity and wind speed) were taken from the HIRHAM4 regional climate model, that operates on grid cells of approximately 50 by 50 km. No specific downscaling techniques were applied to these data. Other input parameters like elevation, maximum soilwater storage, and crop parameters, were the same as described in section 5.5. The values of the seepage coefficient *S* and the recession parameter *C* were obtained by calibrating the model against observed discharge data. Before that however, the performance of the snow module TANASNOW was evaluated independently using observed snow depth data.

7.7.1   *Evaluation of the snow module TANASNOW*

The performance of TANASNOW was tested by comparing the simulated snow water equivalent with observed snow depths at four meteorological stations in and around the Tana Basin (figure 7.1): Rustefjelbma, Kevo, Karasjok and Sihcajavri. These stations represent different snow conditions: Rustefjelbma is located close to the Barents Sea, and receives relatively much precipitation, while Sihcajavri is situated on the Finnmarksvidda plateau, just southwest of the Tana Basin, at an elevation of 382 m. The other two stations are located in the valleys of two tributaries of the Tana River. Due to compaction and snow metamorphism the density of a snow pack usually increases progressively throughout the season (Dingman, 1994), and for this reason snow depth is not a proper indicator of water equivalent. Measurements of snow density or water equivalent were not available for these four stations. In comparing measured snow depth and simulated water equivalent, the attention was therefore focused on the development of the snow pack, and the moment of disappearance of the snow cover.

The snow model TANASNOW represents the growth of the snow pack realistically, and is able to predict the disappearance of the snow cover within an accuracy of several days (figure 7.4). On average, the simulated snow cover disappears about 2 to 7 days too late. This delay is smallest at the two more inland stations, Karasjok and Sihcajavri, that generally have a thinner snow cover than the other two stations. The decline in measured snow depth in figure 7.4 starts earlier than the onset of melt that is simulated by the model. However, this is not very disturbing, because at the end of the winter season the thickness of a snow pack may decrease before the actual melting starts, as explained above. In individual years, both the development and the disappearance of the snow cover are simulated very well, but in other years the snowmelt appears to be too late (figure 7.5). Occasionally, the model has difficulty in building up a stable snow cover at the beginning of the winter season (figure 7.5.c). Nevertheless, these results are very encouraging, especially when realising that the input variables were partly derived from a RCM.
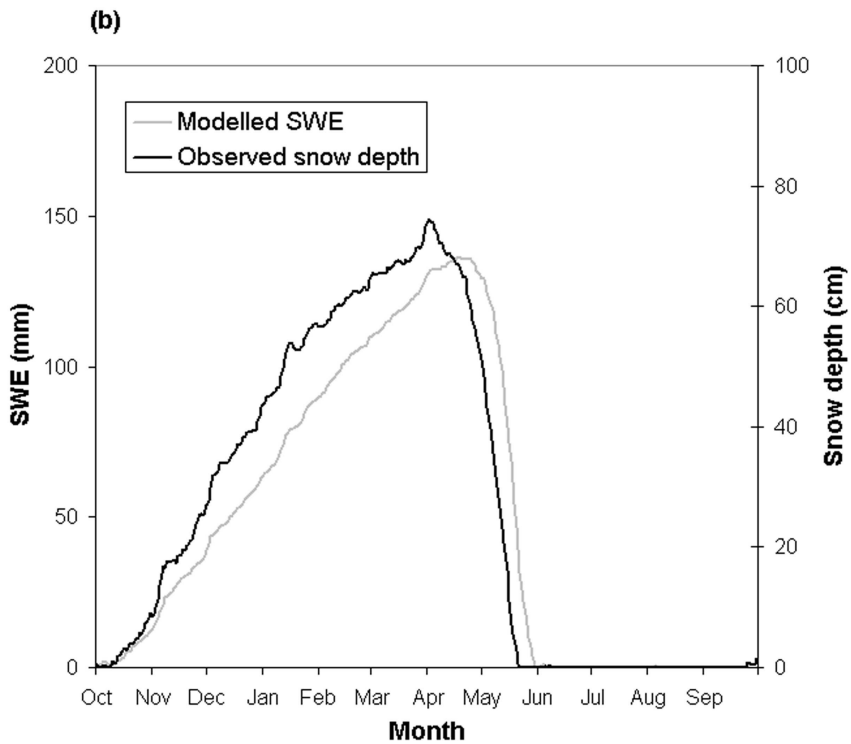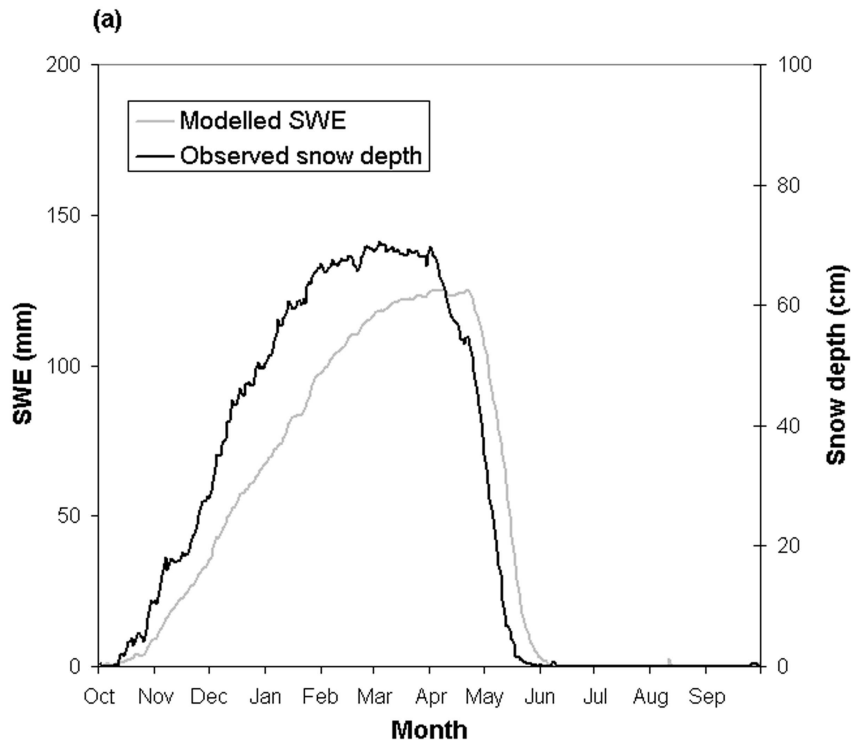
Figure 7.4 Simulated snow water equivalent (SWE) and observed snow depth at four meteorological stations in the Tana Basin, averaged over 1980-1993: (a) Rustefjelbma, (b) Kevo, (c) Karasjok, (d) Sihcajavri. Note the different scales for SWE and snow depth
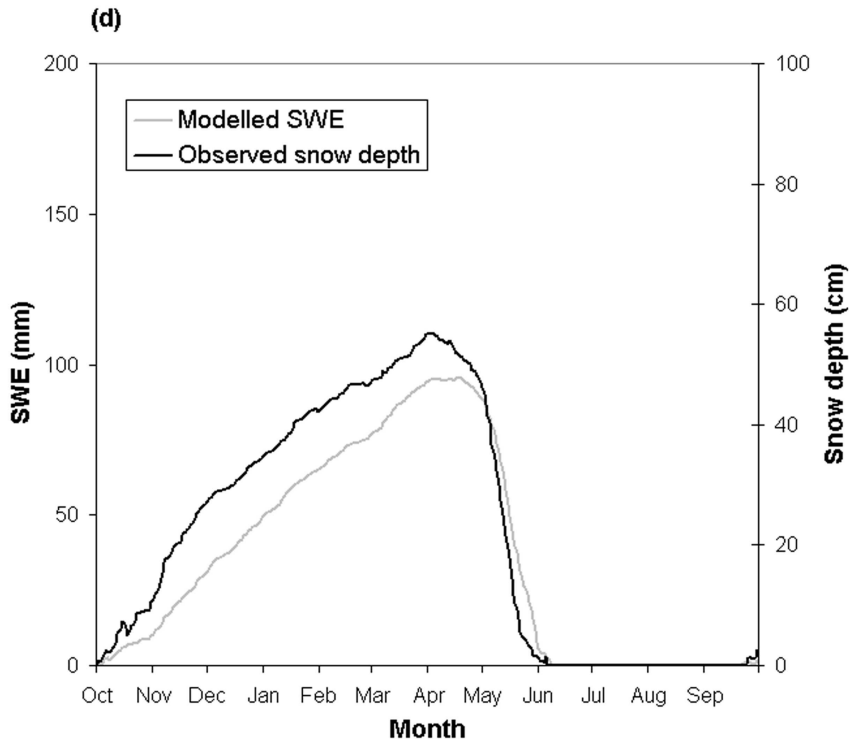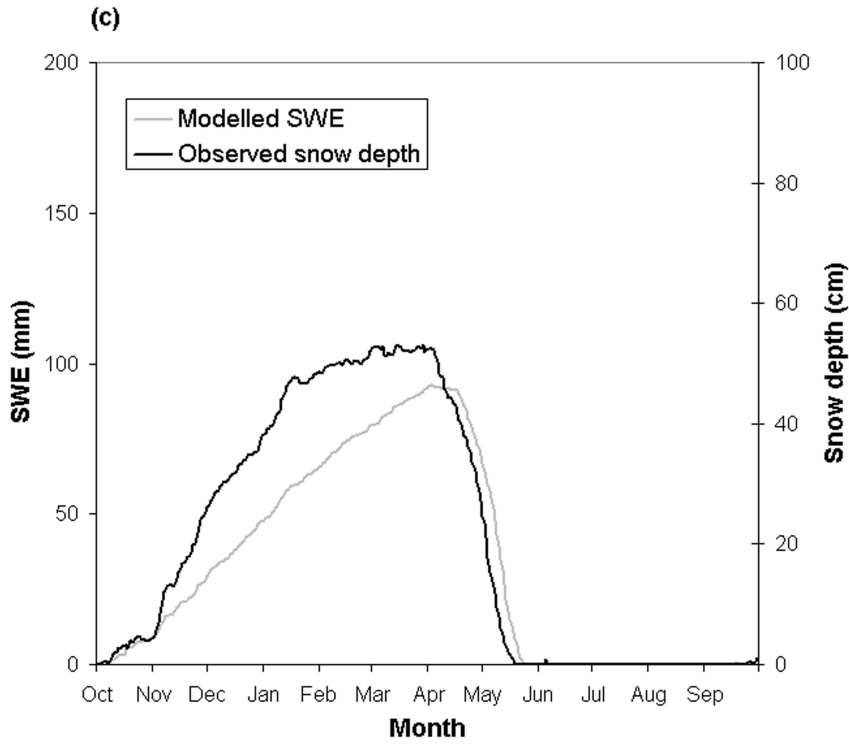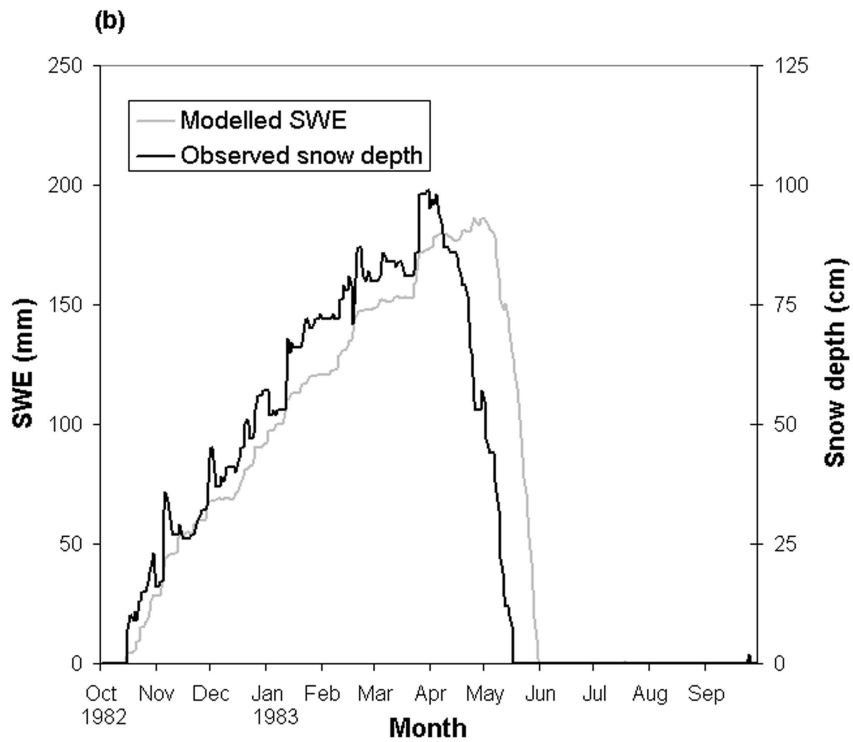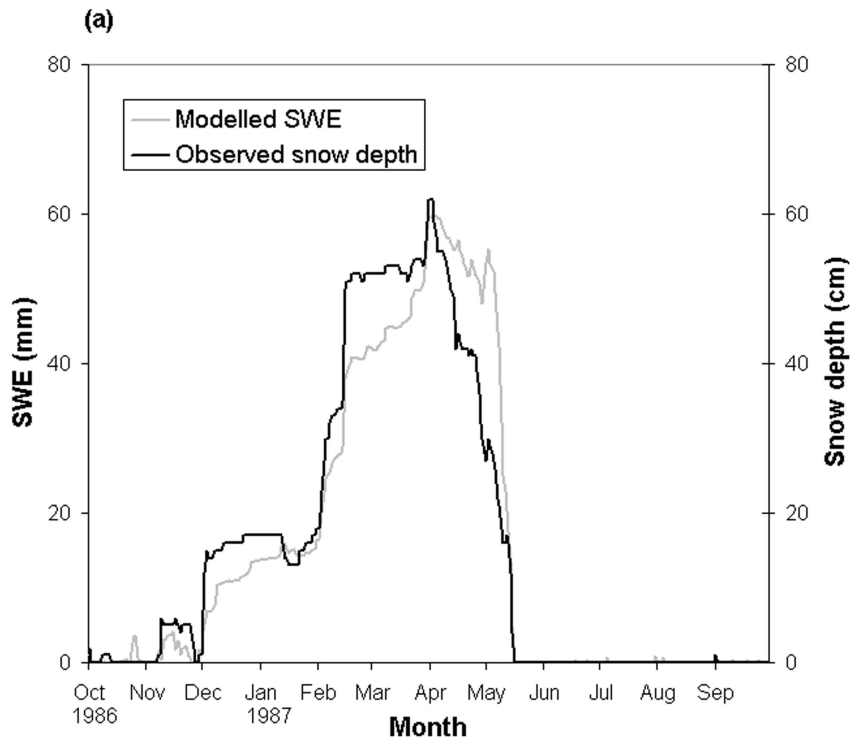
152

(c)

(d)

Figure 7.4 (continued)

153

Figure 7.5 Simulated snow water equivalent (SWE) and observed snow depth at (a) Karasjok, 1987; (b) Kevo, 1983; and (c) Sihcajavri, 1981

154

(c)
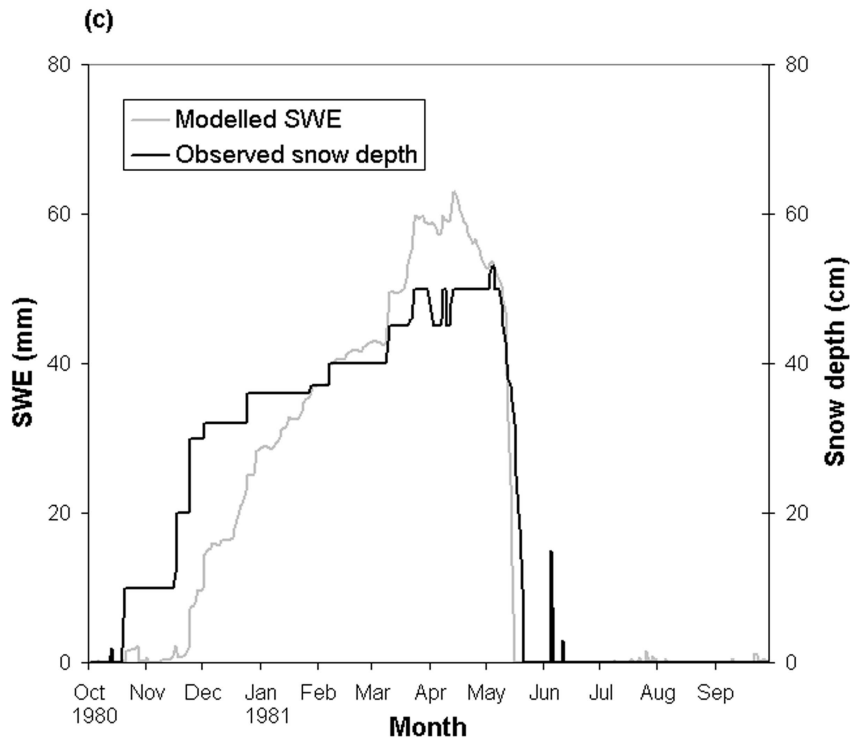
Figure 7.5 (continued)

7.7.2   Calibration of TANAFLOW

In the calibration of TANAFLOW, a similar approach was followed as described in chapter 5. The model was calibrated by adjusting the values of the seepage coefficient *S* (equation 7.21) and the recession parameter *C* (equation 5.11), and comparing the model-generated runoff with observed discharge at several locations in the Tana Basin (figure 7.1; table 5.6). All possible combinations of these two parameters were calculated within a predefined range of 0.1 to 0.7 for the seepage coefficient, and 50 to 600 days for the recession parameter. It was believed that higher values of *S* and lower values of *C* would lead to too little rapid runoff, and a too rapid response to rainfall events of the groundwater discharge, which would therefore lose its baseflow character. Compared with the previous version of TANAFLOW, one calibration parameter (the degree-day factor) has been omitted from the model. On the other hand, the snow module TANASNOW is dependent on a number of assumptions with regard to the actual values of a number of parameters (table 7.1). Moreover, the value of the precipitation lapse rate that was introduced into the model, had to be obtained by comparing long-term observed and simulated runoff.

Smith (1979) and Linacre (1992) mention various lapse rates for several locations, ranging from 3 to 20 % or more increase in precipitation per 100 m elevation rise. For a site in Northern Sweden, Ryden (1972) reports an increase of 6-7 % per 100 m. In the

present study, a much higher value of 15% was found by comparing observed and simulated discharge at Polmak, Norway. The spring months April to June were not included in this comparison, in order to minimise the effects of discharge measurement errors, that presumably are largest at high discharges. A lapse rate of 15 % results in a ratio of simulated to observed runoff in the period July to March of close to 1.00. On an annual basis, this ratio is only 0.85, meaning that the total volume of simulated runoff at Polmak is only 85 % of the observed discharge. Higher lapse rates however, result in a considerable overestimation of runoff in summer, and also yield lower modelling efficiencies. For these reasons, a lapse rate of 15 % increase in precipitation per 100 m was maintained in the model.

The decreasing model performance when using lapse rates higher than about 15 %, can be explained by the increase in snow mass, which consequently takes more time to melt completely, and results in a snowmelt discharge peak that is too late in comparison with the observed one. In this respect, it is interesting to note that in some of the sub-catchments the highest model performance is obtained with lower lapse rates than the 15 % found for Polmak, Norway. The best results for the calibration period in terms of the Nash & Sutcliffe (1970) efficiency coefficient are listed in table 7.2. At most stations the highest model performance is obtained with low values for the seepage coefficient S, and relatively high values for the recession parameter C (table 7.2, figure 7.6). This may not be surprising, since a low S leads to high soil moisture contents, and accordingly to more rapid runoff. When looking at the different seasons, it appears however that the smallest mean absolute bias error (MABE) (equation 5.12) in the spring (May and June) period is obtained with higher values of S, in combination with a higher recession parameter (table 7.3). In summer, the smallest error is obtained with a lower recession parameter, which leads to a faster drainage of the groundwater reservoir, and consequently higher discharge in summer. The same parameter combination gives also the smallest error in the winter period, if a much lower precipitation lapse rate is assumed as well. As can be seen in

Table 7.2 Best parameter combinations in the calibration period in terms of the Nash-Sutcliffe coefficient, for the Tana River and several subbasins. Explanation: S = seepage coefficient, C = recession parameter, P = precipitation, Q_s = simulated discharge, Q = observed discharge. For locations, see figure 7.1

| Discharge station	River	S	C	P lapse rate	Nash-Sutcliffe	Q_s/Q	Q_s/Q
		days^{-1}	days	%		July-April	Annual
Polmak	Tana	0.1	350	15	0.57	1.09	0.91
Alaköngäs	Tana	0.1	350	15	0.51	1.03	0.81
Onnelansuvanto	Tana	0.1	550	15	0.52	1.04	0.83
Patoniva	Utsjoki	0.5	150	5	0.51	0.92	0.77
Karigasniemi	Inarijoki	0.1	550	5	0.50	0.93	0.74
Vækkava	Jiesjåkka	0.1	350	15	0.48	1.10	0.85
Njalmigoaika	Karasjåkka	0.1	350	5	0.51	1.01	0.78

156

(a)
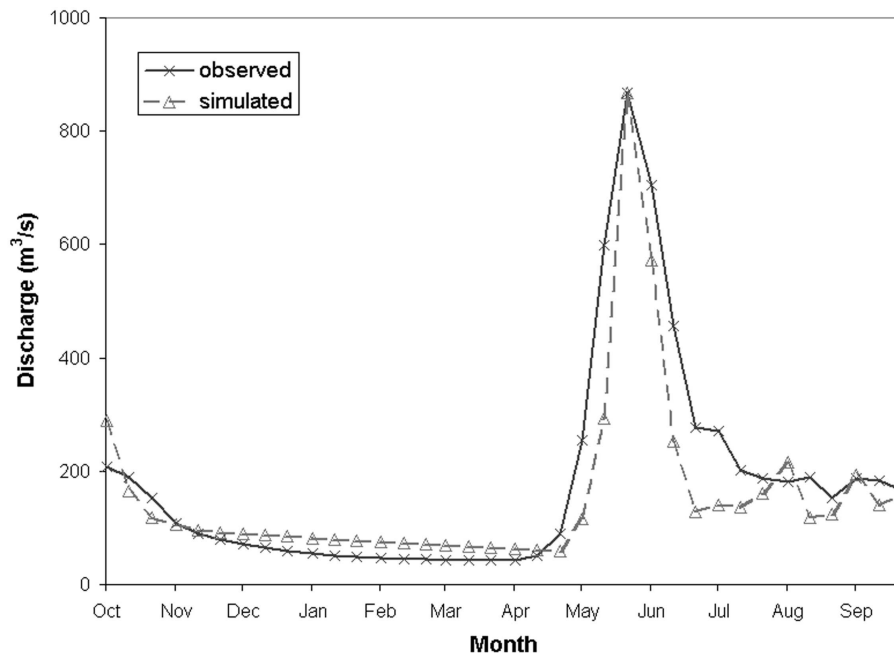
(b)
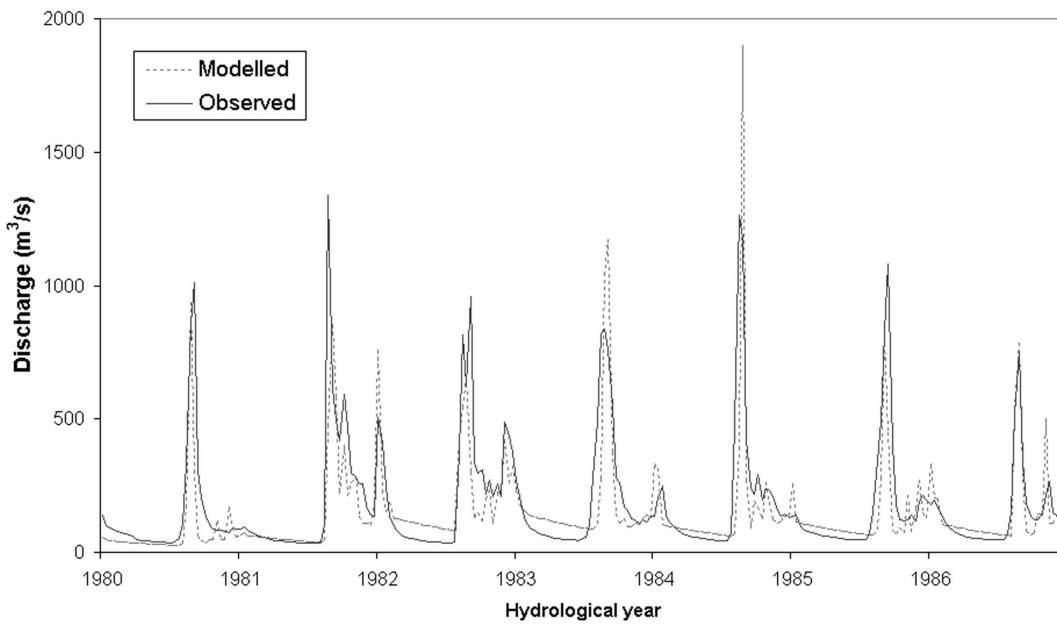
Figure 7.6 Simulated and observed runoff at Polmak, Norway, in the calibration period: (a) average over 1980-1986, (b) in individual years

157

Table 7.3 Best parameter combinations at Polmak in the calibration period, in terms of the mean absolute bias error (MABE), for the spring (May and June), summer (July-September) and winter (October-April) seasons, as well as the combined summer-winter season (July-April)

|	S	C	P lapse rate	MABE
	days^{-1}	days	%	
Spring	0.5	550	15	0.44
Summer	0.1	150	15	0.29
Winter	0.1	150	5	0.37
Summer + winter	0.1	150	8	0.36

figure 7.6, a lapse rate of 15 % results in a recession limb of the simulated hydrograph that is often higher than observed during the winter periods.

Figure 7.6 also shows that, on average, the model simulates both the timing and magnitude of the annual discharge peak well. However, shortly after snowmelt the simulated discharge is too low. This is a direct consequence of the assumption that infiltration is impeded during snow coverage, which means that the groundwater reservoir is only partially replenished. On the other hand, if there are no restrictions on infiltration during snow coverage, the snowmelt runoff peak becomes much too low, with a negative influence on the overall model performance. Later in summer, it appears that the simulated discharge peaks are sometimes higher than observed (figure 7.6.b), and also the baseflow is too high in some of the winters. Nevertheless, the overall discharge regime is fairly well simulated.

7.7.3   Validation

In Polmak, Norway, the discharge measurements stopped in 1992. The model was therefore validated at Alaköngäs, Finland, several kilometres upstream of Polmak. In the validation period 1987-1993 the model performs considerably better than in the calibration period. In Alaköngäs the parameter combination $S = 0.1$, $C = 350$, results in a Nash-Sutcliffe efficiency coefficient of 0.64 in the validation period (figure 7.7). Also the MABE values in the spring and summer season have decreased, but the MABE for the winter season has increased (table 7.4). The overall water balance for the period 1980-1993 is summarised in table 7.5. The Penman-based estimate of reference crop evapotranspiration is 160 mm year^{-1}. The spatial patterns (figure 7.8.a) appear to be dominated by differences in elevation and, accordingly, temperature. The actual evapotranspiration is influenced by the seepage coefficient S, but ranges between 50 and 60 mm year^{-1}, with the highest values obtained with low values for S. Consequently, the spatial distribution (figure 7.8.b) is more complex than in figure 7.8.a. Also the length of the snow-free season is clearly related to elevation (figure 7.9). According to the model,
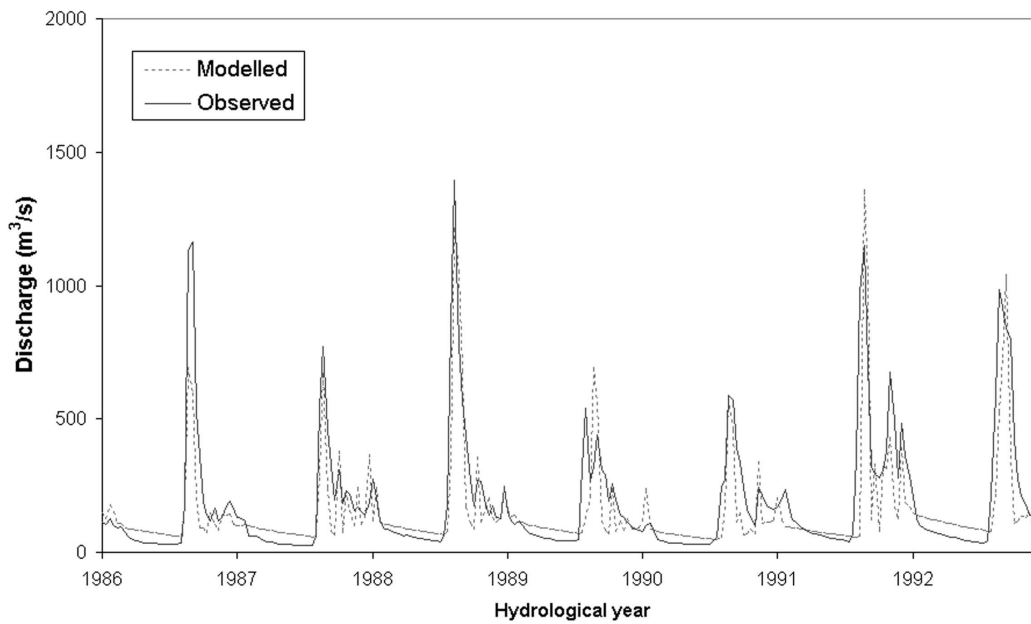
(a)
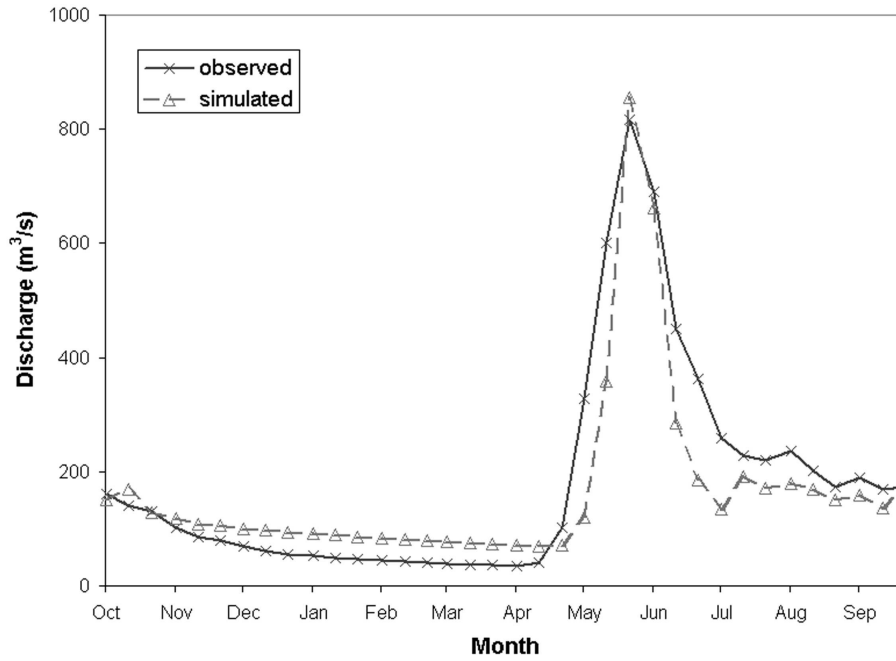
(b)

Figure 7.7 Simulated and observed runoff at Alaköngäs, Finland, in the validation period: (a) average over 1987-1993, (b) in individual years

Table 7.4 Model performance at Alaköngäs, Finland, in the calibration (1980-1986), validation (1987-1993) and total (1980-1993) simulation period

Parameter combination			Period	Error statistics			
S	C	P lapse rate		Nash-Sutcliffe	MABE spring	MABE summer	MABE winter
days^{-1}	days	%					
0.1	350	15	1980-86	0.51	0.51	0.36	0.56
			1987-93	0.64	0.44	0.36	0.51
			1980-93	0.56	0.48	0.36	0.54

the length of the snow-free season ranges from less than 80 days on some of the mountain peaks in the North, to more than 155 days in the valley of the Tana in the Northeast.

7.7.4   Spatial model performance

Considering the importance of snow coverage in sub-arctic ecosystems, one of the goals of the TANAFLOW is to simulate spatial snow cover patterns, in addition to river runoff. In the previous chapter is was demonstrated how satellite images can be used to validate the spatial performance of the model in simulating the snow cover depletion in spring. SPOT VEGETATION images appeared to be very useful for this, since this sensor makes observations in the mid-infrared part of the spectrum, which allows easy discrimination of clouds and snow. Unfortunately, the SPOT4 satellite was launched only in 1998, while the current simulation period ends in 1993, which is determined by the ECMWF reanalysis that was used in HIRHAM4. For this reason, the spatial performance of TANAFLOW was evaluated by comparing the simulated patterns of snow cover depletion with the previous version of the model, that was described in chapters 5 and 6. As was demonstrated in chapter 6, this model version realistically simulates the rate of snow cover depletion in the Tana Basin (figure 6.6), but the actual moment of snow disappearance is several days too late.

Compared with these results, the timing of snow cover depletion in the current model version, using a more sophisticated energy-balance model for snowmelt, is very similar (figure 7.10). As noted before, compared with the observed snow depths at meteorological stations in the area, the simulated moment of snow disappearance was on average 2 to 7 days too late (section 7.7.1). On average, the current model version generates a larger snow mass in the Tana Basin than the previous one (figure 7.11), which due to the precipitation lapse rate of 15 %. The onset of snowmelt is also somewhat later. However, the decline in snow water equivalent is faster, and therefore the moment of snow disappearance is more or less similar.

160

a) Reference ET

N

	50 - 100 mm/year
	100 - 150
	150 - 160
	160 - 170
	170 - 180
	180 - 205

b) Actual ET

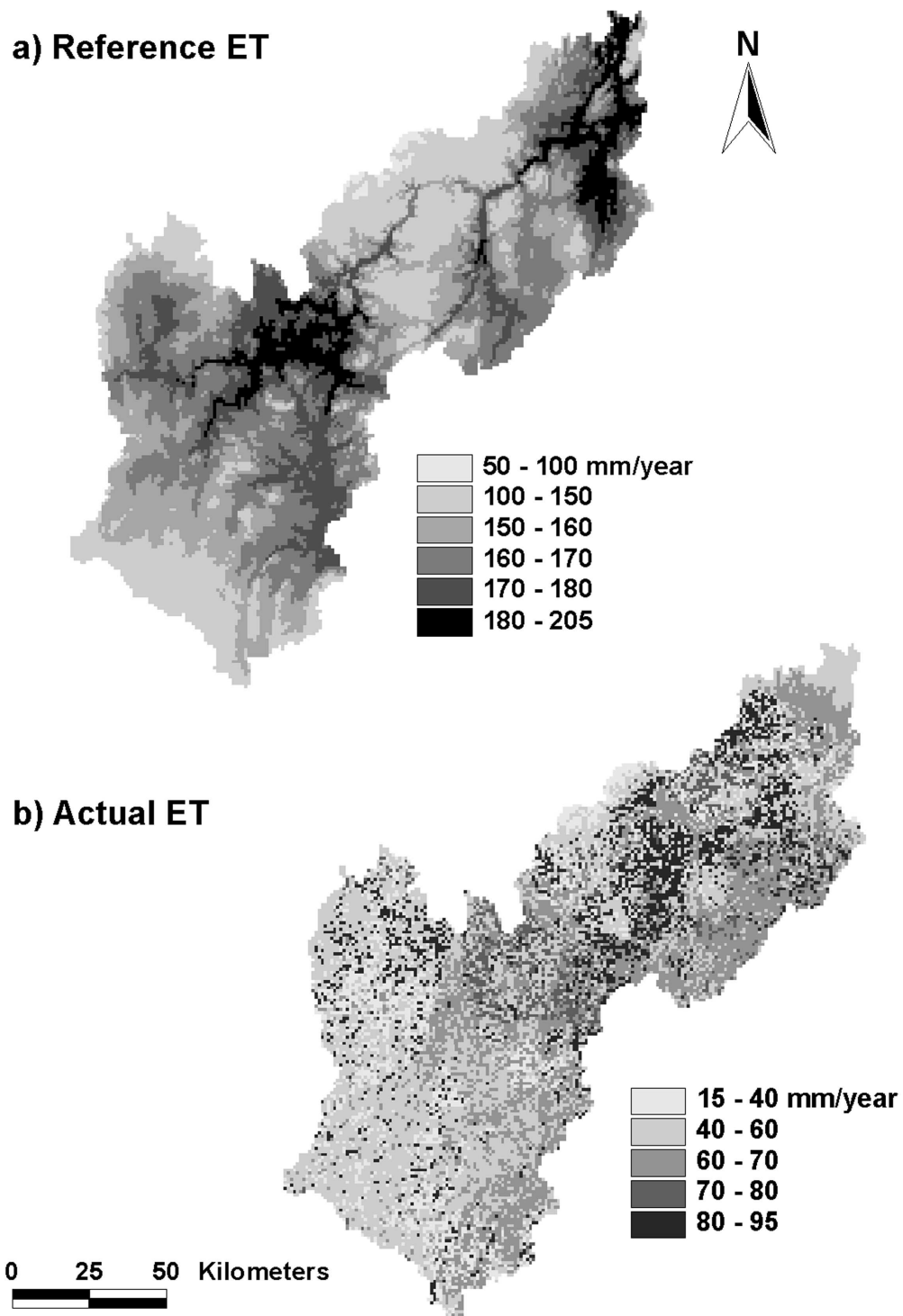|	
	15 - 40 mm/year
	40 - 60
	60 - 70
	70 - 80
	80 - 95

0   25   50   Kilometers

Figure 7.8 (a) Reference crop evapotranspiration, and (b) actual evapotranspiration in the Tana Basin in mm year^{-1}. See the appendix for a colour version
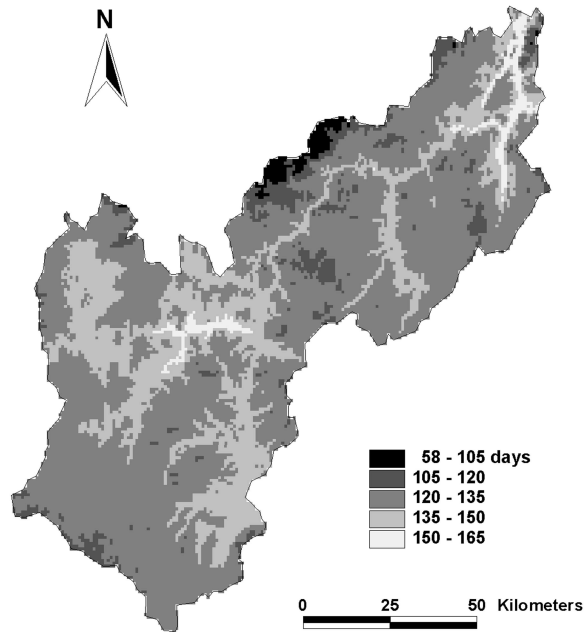
Figure 7.9 Length of the snow-free season in the Tana Basin, as simulated by TANASNOW / TANAFLOW for the period 1980-1993. See the appendix for a colour version

Table 7.5 Water balance of the Tana Basin upstream of Alaköngäs in the simulation period (1980-1993), for the parameter combination $S = 0.1$ days^{-1} and $C = 350$ days, and a precipitation lapse rate of 15 % increase per 100 m rise in elevation. Explanation: P = precipitation, E_s = sublimation, E_a = actual evapotranspiration, Q = observed discharge, Q_s = simulated discharge, ΔS = change in soil and groundwater storage

	1980-1986	1987-1993	1980-1993
P (mm/year)	490.4	517.5	503.9
E_s (mm/year)	65.4	90.4	77.9
E_a (mm/year)	59.7	59.5	59.6
Q (m^3/s)	190.0	181.8	185.9
Q (mm/year)	448.6	429.3	438.9
Q_s (m^3/s)	155.3	154.7	150.0
Q_s (mm/year)	362.2	363.0	362.6
Q_s / Q ratio	0.81	0.84	0.83
Q_s / P ratio	0.75	0.71	0.73
$(Q_s+E_s+E_a) / P$ ratio	0.99	0.99	0.99
ΔS (mm/year)	3.1	4.6	3.8

162

7.8 Discussion

In this chapter it was demonstrated that data from a regional climate model (RCM) can be used to drive physically-based models of snowmelt and evapotranspiration for use in large-scale hydrological models. By combining TANASNOW, a simplified energy-budget model of snow accumulation and melt, and the evapotranspiration model of Penman-Monteith (Monteith, 1965), in the water balance model TANAFLOW, the general runoff regime of the Tana River is well reproduced (figure 7.7). However, the model performance seems not to have improved in comparison with the "old" version of TANAFLOW. This model used a temperature-index approach to simulate snowmelt, and the highly empirical Thornthwaite model for evapotranspiration (Thornthwaite & Mather, 1957), adjusted with a reduction factor to meet the observed water balance characteristics. For completeness, the performance of the old model version is summarised in table 7.6 for the model runs that yielded the best results in the spring (May and June), summer (July-September) and winter (October-April) seasons (see chapter 5). The error statistics are different from table 5.8, because they have now been calculated for the modelling period used in this chapter. It appears that the performance of the old model was better in the calibration period, but worse in the validation period, when compared with the adjusted model (table 7.4). This difference between calibration and validation period is not completely understood.

Table 7.6 Model performance of the old model version (see chapter 5) at Alaköngäs, Finland, for the calibration (1980-1986), validation (1987-1993) and total (1980-1993) simulation period, for the parameter combinations in table 5.9

Parameter combination			Period	Error statistics			
DDF [a]	χ	C [b]		Nash-Sutcliffe	MABE spring	MABE summer	MABE winter
14	0.8	5	1980-86	0.62	0.41	0.52	0.86
			1987-93	0.61	0.37	0.55	0.84
			1980-93	0.62	0.39	0.54	0.85
20	0.3	40	1980-86	0.38	0.64	0.31	0.59
			1987-93	0.44	0.57	0.28	0.66
			1980-93	0.41	0.61	0.29	0.62
14	0.5	20	1980-86	0.55	0.54	0.33	0.36
			1987-93	0.62	0.45	0.36	0.32
			1980-93	0.58	0.49	0.35	0.34

[a] Units mm °C^{-1} period^{-1}
[b] Units 10-day periods

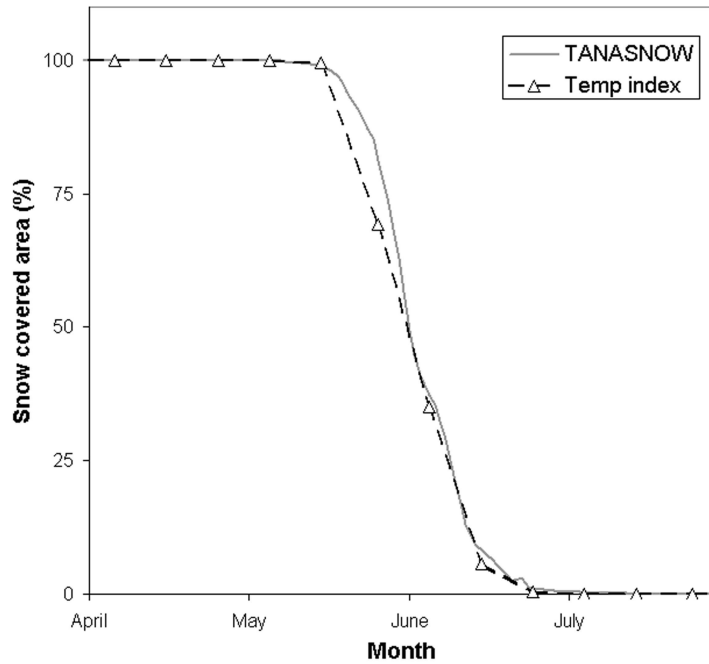**Figure 7.10** Snow cover depletion in the Tana Basin, averaged over 1980-1986, for the current model version using an energy-balance approach (TANASNOW) for snowmelt, and for the previous model version (see chapter 5 and 6) using a temperature-index approach
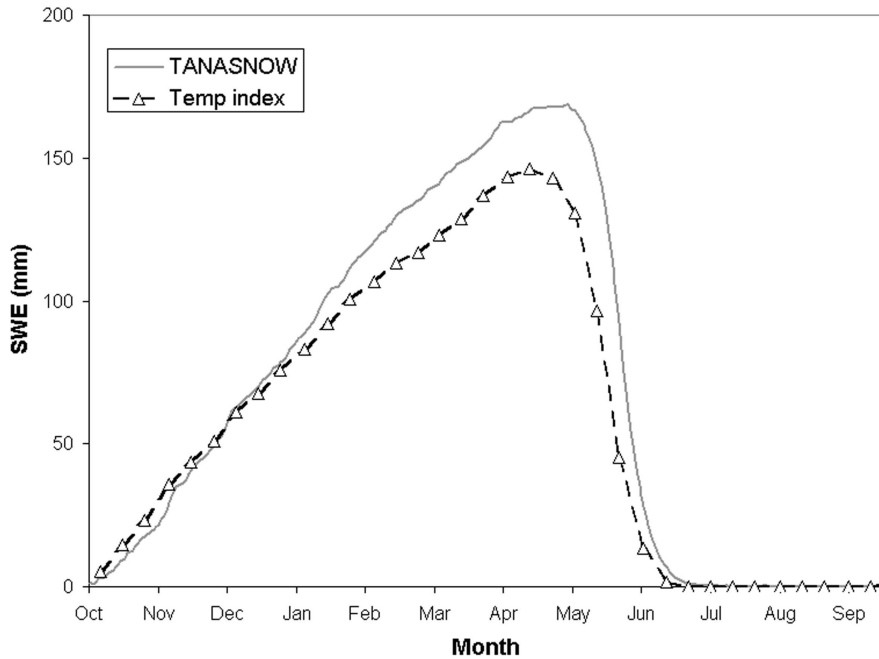

Figure 7.11 Basin-averaged snow water equivalent (SWE), averaged over 1980-1993, for both the current and the previous model version

164

With regard to the simulation of river discharge at the catchment outlet, the introduction of advanced models of snowmelt and evapotranspiration did not change the model performance significantly. At the same time, the current version of the model not only uses better process descriptions, but is also less dependent on calibration. As noted in chapter 5, the degree-day factor that is used in the temperature-index approach, is a powerful control on the timing of snowmelt in the model. In the current model, both TANASNOW and the Penman-Monteith evaporation model were applied without calibration. Moreover, radiation, humidity and wind speed data were not derived from observations, but from a regional climate model operating on a much larger grid scale than the TANAFLOW model itself. The results obtained in the present study are therefore encouraging. A major advantage of the current model is that it uses physically-based routines for snowmelt and evapotranspiration, that should be more robust when applied to different climatic conditions. At the same time, the model yields much more spatial detail than what is usual for climate models. By using observed precipitation from meteorological stations in the area, also the water balance is considerably more realistic (cf. figure 7.2.b). The "hybrid" approach that was followed in this chapter, therefore appears to be highly successful.

To account for the underestimation of precipitation at meteorological stations in the Tana Basin, as discussed in chapter 5, a precipitation lapse rate was introduced in the model. A lapse rate of 15 % increase in precipitation per 100 m elevation rise was found by comparing observed and simulated runoff in the summer and winter seasons, since it was believed that discharge measurement errors will be largest in spring. This value is considerably higher than that found by Ryden (1972) in Northern Sweden. However, a large part of the increase in precipitation is lost, due to higher evapotranspiration rates, as well as the sublimation that is calculated in winter (table 7.5). However, leaving sublimation out of TANASNOW, leads to a considerably worse simulation of the snow cover at the four meteorological stations where it was tested. Apparently, the model significantly benefits from the simulation of sublimation. For this reason, it was decided to include it in the model.

7.9   Conclusions

Two physically-based models of snowmelt and evapotranspiration were developed for use in the large-scale water balance model TANAFLOW. For evapotranspiration, the well-known model of Penman-Monteith (Monteith, 1965) was used. In order to simulate snow accumulation and snowmelt, a simplified energy-balance model named TANASNOW was developed. Both models were embedded in TANAFLOW and applied to the Tana Basin. Data on temperature and precipitation were obtained from meteorological stations in the area, while radiation, humidity and wind speed data were derived from the regional climate model HIRHAM4 (Christensen et al., 1998). It was shown that the model is able to simulate the hydrological regime of the Tana River realistically. With respect to the simulation of river discharge and snow cover depletion, the model performance is similar to the old model version, that used more empirical routines for snowmelt and evapotranspiration. At the same time, the current model uses

more detailed process descriptions, and is less dependent on calibration. Being physically-based, the model is believed to be more reliable when applied to different climatic conditions. The impact of climate change scenarios on the model simulations will be explored in the next chapter. In any case, it seems that the "hybrid" approach of combining observations and RCM data in a physically-based hydrological model, is effective in large-scale impact studies in northern environments.

7.10   References

Anderson, E.A. (1976): A point energy and mass balance model of a snow cover. Silver Spring, Maryland: U.S. Department of Commerce, National Oceanic and Atmosphere Administration, National Weather Service (NOAA Technical Report NWS 19).

Arnell, N.W. (1996): Global warming, river flows and water resources. Chichester: Wiley.

Arnell, N.W. (1999): A simple water balance model for the simulation of streamflow over a large geographic domain. Journal of Hydrology 217, pp. 314-335.

Christensen, O.B., J.H. Christensen, B. Machenhauer & M. Botzet (1998): Very high-resolution regional climate simulations over Scandinavia - Present climate, Journal of Climate 11, pp. 3204-3229.

Dingman, S.L. (1994): Physical Hydrology. New York: Macmillan.

Ferguson, R.I. (1999) Snow melt runoff models, Progress in Physical Geography 23, pp. 205-227.

Gray, D.M. & T.D. Prowse (1993): Snow and Floating Ice. In: D.R. Maidment (ed.): Handbook of Hydrology. New York: McGraw-Hill, pp. 7.1-7.58.

Harding, R.J., N.A. Jackson, E.M. Blyth & A. Culf (2002): Evaporation and energy balance of a sub-Arctic hillslope in northern Finland. Hydrological Processes 16, pp. 1419-1436.

Houghton, J. T., Y. Ding, D.J. Griggs, M. Noguer, P.J. van der Linden & D. Xiaosu (eds.) (2001): Climate Change 2001: The Scientific Basis. Cambridge: Cambridge University Press..

Källén E., (1996): HIRLAM documentation manual, system 2.5. Norrköping: Swedish Meteorological and Hydrological Institute (SMHI).

Kite, G.W., E. Ellehoj & A. Dalton (1996): GIS for large-scale watershed modelling. In: V.P. Singh & M. Fiorentino (eds.): Geographical Information Systems in Hydrology. Dordrecht, The Netherlands: Kluwer Academic Publishers, pp. 237-268.

Kite, G.W. & U. Haberlandt (1999): Atmospheric model data for macroscale hydrology. Journal of Hydrology 217, pp. 303-313.

Koivusalo, H., M. Heikinheimo & T. Karvonen (2001): Test of a simple two-layer parameterisation to simulate the energy balance and temperature of a snow pack. Theoretical and Applied Climatology 70, pp. 65-79.

Kustas, W.P., A. Rango & R. Uijlenhout (1994): A simple energy budget algorithm for the snowmelt runoff model. Water Resources Research 30, pp. 1515-1527.

Kuusisto, E. (1984): Snow Accumulation and Snowmelt in Finland. Helsinki: National Board of Waters (Publications of the Water Research Institute 55).

Kwadijk, J.C.J. (1993): The impact of climate change on the discharge of the River Rhine. Utrecht: Koninklijk Aardrijkskundig Genootschap / Faculteit Ruimtelijke Wetenschappen Universiteit Utrecht (Netherlands Geographical Studies 171).

Linacre, E. (1992): Climate data and resources: a reference guide. London: Routledge.

Melloh, R.A. (1999): A synopsis and comparison of selected snow melt algorithms. Hanover, New Hampshire: US Army Corps of Engineers, Cold Regions Research and Engineering Laboratory (CRREL report 99-8).

Monteith, J.L. (1965): Evaporation and environment. In: G.E. Fogg & P.G. Kohn (eds.): The state and movement of water in living organisms (Proceedings of the 19th Symposium of the Society for Experimental Biology). London: Cambridge University Press, pp. 205-234.

Nash, J.E. & J.V. Sutcliffe (1970): River flow forecasting through conceptual models; Part 1 -a discussion of principles. Journal of Hydrology 10, pp. 282-290.

Penman, H.L. (1948): Natural evaporation from open water, bare soil, and grass. Proceedings of the Royal Society of London Series A 193, pp. 120-145.

Price, A.G. & T. Dunne (1976): Energy balance computations of snowmelt in a subarctic area. Water Resources Research 12, pp. 686-694.

Roeckner, E., K. Arpe, L. Bengtsson, M. Christoph, M. Claussen, L. Dümenil, M. Esch, M. Giorgetta, U. Schlese & U. Schulzweida (1996): The atmospheric general circulation model ECHAM-4: Model description and simulation of present-day climate. Hamburg: Max-Planck-Institute (MPI Report 218).

Ryden, B.E. (1972): On the problem of vertical distribution of precipitation especially in areas with great height differences. In: WMO: Distribution of precipitation in mountainous areas: Geilo Symposium, Norway, 31 July - 5 August 1972, Vol. II: technical papers. Geneva: World Meteorological Organization (WMO/OMM Report 326).

Shuttleworth, W.J. (1993): Evaporation. In: D.R. Maidment (ed.): Handbook of Hydrology. New York: McGraw-Hill, pp. 4.1-4.53.

Smith, R.B. (1979): The influence of mountains on the atmosphere. Advances in Geophysics 21, pp. 87-230.

Tarboton, D.G. & C.H. Luce (1996): Utah Energy Balance Snow Accumulation and Melt Model (UEB), Computer model technical description and users guide. Logan / Ogden: Utah Water Research Laboratory and USDA Forest Service Intermountain Research Station, available from http://www.engineering.usu.edu/dtarb, accessed on 1 August 2002.

Tetens, O. (1930): Uber einige meteorologische Begriffe. Zeitschrift fur Geophysik. 6, 297-309.

Thornthwaite, C.W. & J.R. Mather (1957): Instructions and tables for computing potential evapotranspiration and the water balance. Centerton: Drexel Institute of Technology, Laboratory of Climatology (Publications in Climatology 10), pp. 183-243.

USACE (1956): Snow hydrology: summary report of the snow investigations [by the] North Pacific Division. Portland: U.S. Army Corps of Engineers.

USACE (1998): Engineering and Design: Runoff from Snowmelt. Washington: U.S. Army Corps of Engineers (Engineer manual EM 1110-2-1406).

Van Blarcum, S.C, J.R. Miller & G.L. Russell (1995): High latitude runoff in a doubled CO_2 climate. Climatic Change 30, pp. 7-26.

Van Dam, O. (2000): Modelling incoming Potential Radiation on a land surface with PCRaster. POTRAD5.MOD manual. Utrecht: Utrecht Centre for Environment and Landscape dynamics, Utrecht University.

Van Deursen, W.P.A. (1995): Geographical Information Systems and Dynamic Models. Development and application of a prototype spatial modelling language. Utrecht: Koninklijk Aardrijkskundig Genootschap / Faculteit Ruimtelijke Wetenschappen Universiteit Utrecht (Netherlands Geographical Studies 190).

Ward, R.C. & M. Robinson (1990): Principles of Hydrology. Third Edition. London: McGraw-Hill.

Williams, K.S. & D.G. Tarboton (1999): The ABC's of snowmelt: a topographically factorized energy component snowmelt model. Hydrological Processes 13, pp. 1905-1920.

8 IMPACT OF CLIMATE CHANGE ON THE HYDROLOGY OF THE SUB-ARCTIC TANA BASIN

8.1 Introduction

Due to the enhanced greenhouse effect, the global temperature is expected to increase by 1.4 to 5.8 degrees Celsius in the coming century. Among climate models, there is furthermore agreement that the greatest warming will occur at northern high latitudes, and in particular in the winter season. Also precipitation over high latitude regions is expected to increase, both in summer and in winter (Houghton et al., 2001). Although the combined effect of higher temperatures and precipitation is still uncertain, it seems likely that the snow cover in these areas will decrease, and evapotranspiration will increase (Everett & Fitzharris, 1998). Regional climate simulations for the Nordic region have been performed by the Swedish Meteorological and Hydrological Institute (SMHI, 1998). For Northern Fennoscandia, these come down to an increase in mean annual temperature of 3 to 4 degrees Celsius by the end of this century. As a consequence, the growing season – defined as the number of days with daily mean temperatures above 5ºC – will be extended by 30 to 60 days. Also the mean annual precipitation in Northern Fennoscandia is expected to increase by 10 to 40 %, and the snow season may be shortened by 50 days (SMHI, 1998).

In the sensitivity analysis (chapter 6) it was demonstrated that snow coverage and river discharge in the Tana Basin in northernmost Finland and Norway (figure 2.1) are indeed sensitive to changes of these magnitudes. In some parts of the Tana Basin, a rise in temperature of 5 ºC resulted in an extension of the snow-free season by more than 80 days (figure 6.8). These results were however obtained with a highly empirical model snowmelt. For current climate conditions, the temperature-index approach describes snowmelt in the Tana Basin adequately, but it remains uncertain whether the empirical relation with temperature still holds if the snowmelt season begins earlier. At these latitudes, the potential solar radiation in mid-April is only 58 % of that in mid-May (figure 6.10). Likewise, the empirical Thornthwaite & Mather (1955; 1957) model of evapotranspiration that was employed may not be valid in different climate conditions. In the sensitivity analysis (chapter 6) only arbitrary changes in temperature and precipitation were considered, and differences among the seasons were not taken into account.

The aim of the present chapter is to present a more reliable assessment of the impact of climate changes on the hydrological system of the Tana Basin. For this purpose, climate change scenarios, produced by the regional climate model (RCM) HIRHAM4 (Christensen et al., 1998), were used as input in the modified version of the TANAFLOW model, that was introduced in chapter 7. Since it is based on physically-based descriptions of snow accumulation, snowmelt, and evapotranspiration, this model is believed to be more robust, and should be able to simulate these processes realistically, also under different climate and radiation conditions. What is more, since the model is fully distributed and runs at a higher spatial resolution than any climate model, it is able

to give detailed information at a spatial scale that is more relevant to the ecological and hydrological processes in the landscape.

8.2   Methodology

Climate change scenarios were derived from the RCM HIRHAM4 (Christensen et al., 1998), that was driven by the global model ECHAM/OPYC (Roeckner et al., 1999). This model was forced according to the emission scenarios A2 and B2 of the Intergovernmental Panel on Climate Change (IPCC) Special Report on Emission Scenarios (SRES) (Nakicenovic & Swart, 2000). The simulations encompass 30 years corresponding to the period 2071-2100, as well as a 30-year control run that corresponds to a greenhouse gas forcing of 1961. In the present study, the SRES scenario A2 was used, since this scenario results in larger climate changes at the end of the 21st century than the other marker scenarios of the IPCC (Houghton et al., 2001). In the A2 scenario the global population increases continuously, and economic development is primarily regionally oriented. This scenario foresees a high use of fossil fuels, and the emissions of carbon dioxide and other greenhouse gases are the highest of all scenario families considered by the SRES (Nakicenovic & Swart, 2000). The global average temperature change for this scenario ranges from +1.3 to 4.5°C (Houghton et al., 2001).

The RCM estimates of precipitation, temperature, radiation, humidity and wind speed were used as input into the modified version TANAFLOW (see chapter 7). This model simulates snow accumulation and snowmelt using a simplified energy budget module (TANASNOW), that represents the snow pack as a single layer, with energy content and water equivalent as the main state variables. The energy exchange at the snow surface is simulated using physically-based descriptions, and an equilibrium approach is used to solve for the snow surface temperature. Evapotranspiration is calculated with the Penman-Monteith model (Monteith, 1965), that takes account of both the meteorological influences on evaporation, and the aerodynamic and physiological influences of the vegetation cover (Ward & Robinson, 1990). In TANAFLOW, this model is used to calculate a reference crop evapotranspiration, that is adjusted for the specific vegetation types in the Tana Basin by using a crop factor.

The HIRHAM4 model operates on a grid of 110 by 104 points with a distance of about 50 km. For the 30 years of each model run, the results were interpolated from the grid points within the Tana Basin to the entire catchment area using an inverse distance interpolation technique. If no correction for elevation is applied, the HIRHAM-based estimate of the average temperature in the Tana Basin is equal to the estimate based on interpolation from meteorological stations in the area (table 8.1). In the previous chapter a temperature lapse rate was used in order to take elevation differences into account, which lowered the basin-average temperature by almost one degree Celsius. The difference between elevation-corrected and uncorrected temperature at each pixel was therefore applied to the interpolated HIRHAM data as well.

170

Table 8.1 Estimates of mean annual temperature in the Tana Basin with different extrapolation methods. Explanation: Th. = Thiessen polygons, Id. = inverse distance interpolation

Source	Period	Interpolation technique	Correction for elevation?	Mean annual temperature (ºC)
Met stations	1980-1999	Th.	no	–2.0
	1980-1999	Th.	yes	–2.9
	1980-1993	Id.	no	–1.9
	1980-1993	Id.	yes	–2.9
HIRHAM4	control run	Id.	no	–2.0
	control run	Id.	yes[a]	–3.0
	scenario run	Id.	no	+3.2
	scenario run	Id.	yes[a]	+2.2

[a] correction based on differences between corrected and uncorrected temperature after interpolation from meteorological stations

A similar approach was used for the precipitation data. In chapter 7, a precipitation lapse rate was introduced into the model, as there was strong evidence that the recordings at the meteorological stations in the river valleys significantly underestimate the amount of precipitation over the surrounding uplands. However, the HIRHAM precipitation over the Tana Basin is considerably higher than the precipitation sum recorded at the meteorological stations in the area. Therefore, two different model experiments were performed. In experiment A, the RCM precipitation was taken as input into TANAFLOW without any adjustment, and no lapse rate was applied to the data. In the second experiment B, the data from HIRHAM were scaled in order to meet the observed mean annual precipitation. After interpolation, a lapse rate was applied to these data in order to preserve the relation with altitude. Furthermore, as described in section 8.3.1, it appeared that the HIRHAM temperature data in the control run are lower than observed in the spring period, resulting in a delay in the simulation of snowmelt. For this reason, a third experiment C was calculated, in which the average differences in temperature and precipitation between the control and scenario run were calculated, and applied to the meteorological station data in the period 1980-1993. In order to maintain the seasonality, these differences were calculated on a monthly basis. The monthly changes in radiation, humidity and wind speed were applied to the observation-based HIRHAM4 data covering the same period (section 7.3).

8.3   Results

In the following sections, the consequences of the SRES scenario A2 for the climate, snow cover dynamics, evapotranspiration and runoff in the Tana Basin are discussed. In doing so, special attention is paid to the spatial patterns. The results in the following

sections were obtained from experiment B, which used a more realistic estimate of the precipitation than experiment A. The differences with experiment A and C are discussed afterwards.

8.3.1   Temperature

After interpolation and correction for elevation differences, the model estimate of the mean annual temperature in the Tana Basin in the control run was almost equal to the estimate based on interpolation of observed temperature data (table 8.1). On a seasonal basis, the HIRHAM data appear to be very similar to the observed temperatures, except in spring, when the temperature curve rises above zero about 10-20 days too late (figure 8.1). Also the low temperatures that are observed in mid-winter, are not well reproduced. In the control run, the mean annual temperature ranges from about –1.5 ℃ in the northeast, close to the Barents Sea, and in the river valleys in the south, to less than –6 ℃ at the highest mountaintops (figure 8.2.a). For the Tana Basin, the A2 scenario implies a rise in mean annual temperature of more than 5 degrees Celsius, from –3.0 to +2.2 ℃ (figure 8.3). This warming is largest in the winter months (+6.3 degrees in December – February), and somewhat less in summer (+3.5 degrees in June – August). In May, when under current conditions snowmelt usually takes place, the average temperature rises from 0.4 to 6.1 ℃. Likewise, the temperature in April rises from –5.7 degrees to close to zero (-0.9 ℃). Almost everywhere in the Tana Basin the mean annual temperature has come above 0 ℃, except for the highest mountaintops in the north (figure 8.2.b).
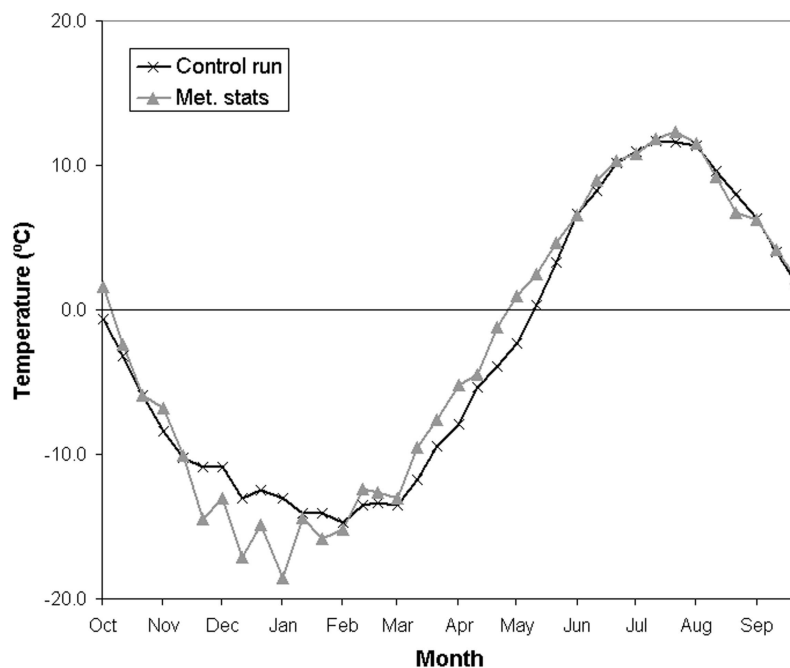

Figure 8.1 Basin-averaged temperature in the Tana Basin, expressed as 10-day means, in the control run (average over 30 years), compared with the interpolated temperatures from meteorological stations (averaged over 1980-1993)
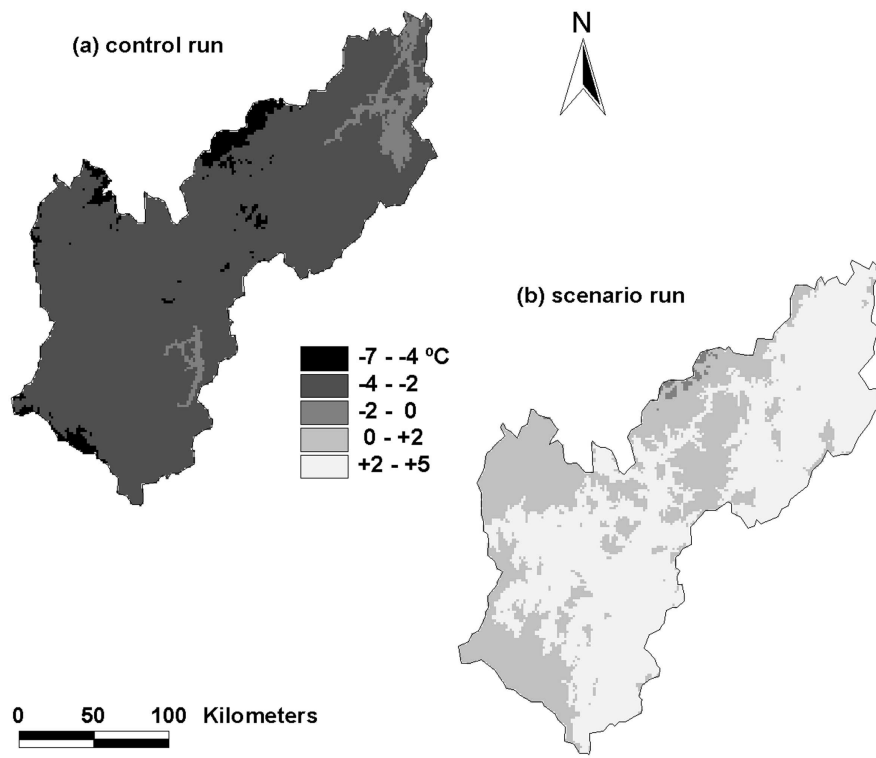
172

Figure 8.2 Mean annual temperature in the Tana Basin in the control run (a) and the scenario run (b). See the appendix for a colour version
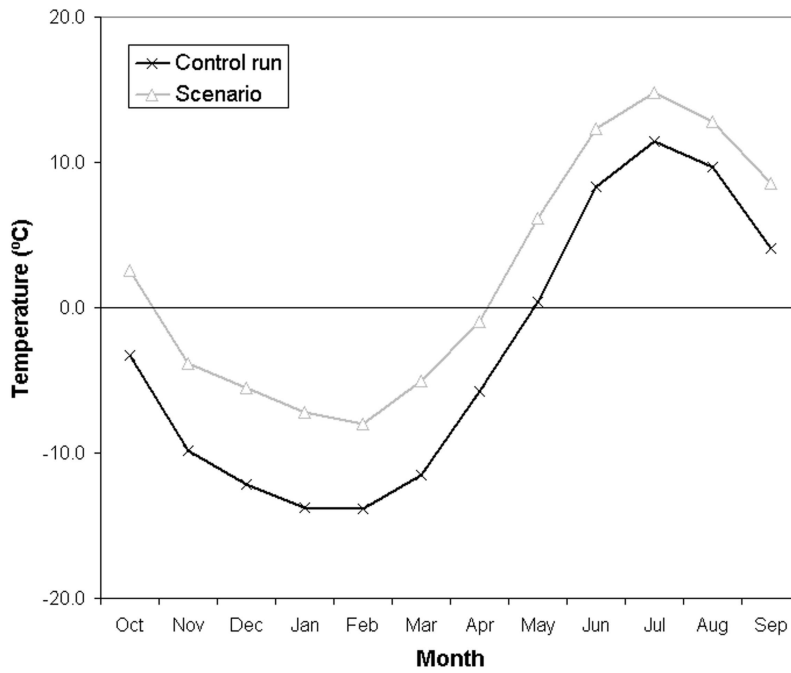

Figure 8.3 Basin-averaged temperature in the Tana Basin in the control and the scenario run

173

8.3.2   *Precipitation*

Precipitation is also projected to increase in the scenario run. The model estimate in experiment B of the mean annual precipitation amount is 508 mm. This value is very close to the 504 mm that was obtained by interpolation from the meteorological stations with a lapse rate of 15 % (table 7.5). The HIRHAM model also reproduces the observed seasonal patterns in precipitation (figure 8.4), although the precipitation is considerably higher than observed in the spring months, and lower in summer. Due to the lapse rate, the spatial distribution in precipitation is largely controlled by topography (figure 8.5). According to the model, mean annual precipitation is highest in the mountainous areas in the north, as well as in the southernmost part of the Tana Basin, where it amounts to more than 700 mm per year. Meanwhile the total annual precipitation is estimated at only 300 mm per year in some of the river valleys, which is lower than observed at most meteorological stations (see for example table 2.2). In the scenario run, precipitation has increased by 25 % to 634 mm per year on average (table 8.2). In all months precipitation is higher, except for August, that shows a slight decrease (figure 8.6). As for temperature, the increase is largest in the winter months (+37.6 % in December – February), and smallest in summer (+6 % in summer).
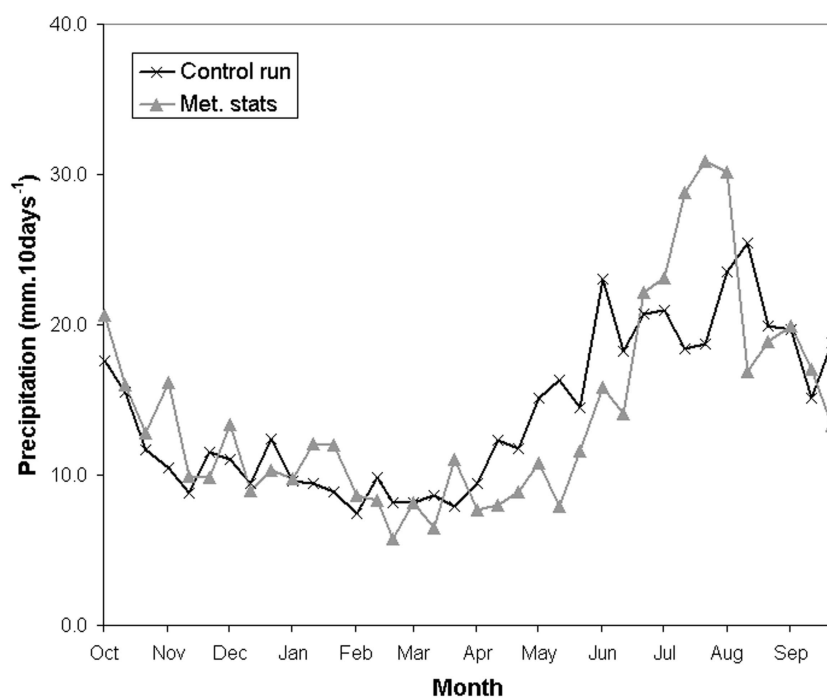

Figure 8.4 Precipitation in the Tana Basin, expressed as 10-day sums, in the 30-year control run, compared with the observations at meteorological stations, interpolated with a lapse rate of 15% per 100 m, and averaged over 1980-1993
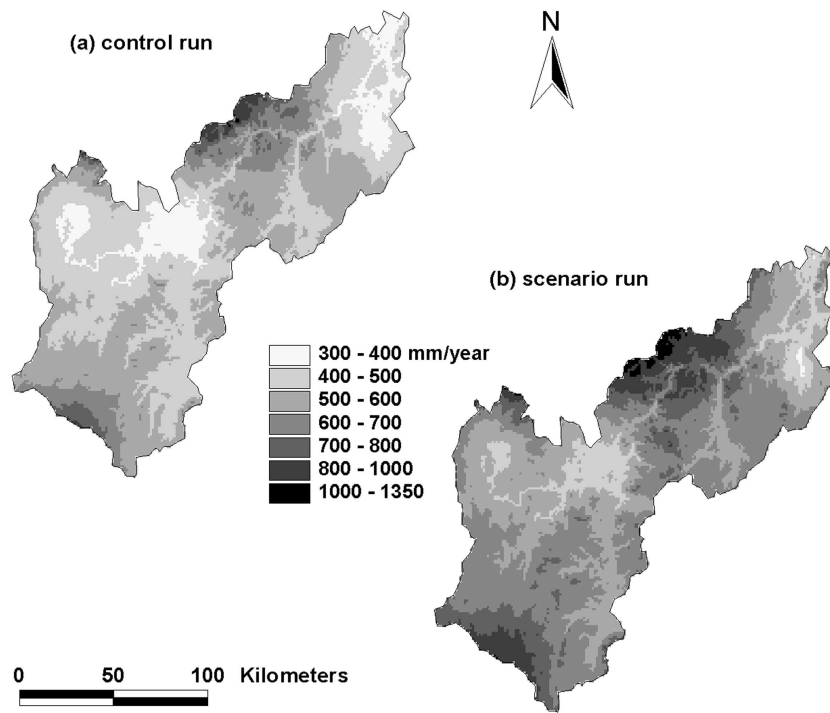
174

Figure 8.5 Annual precipitation in the Tana Basin in the control run (a) and the scenario run (b). See the appendix for a colour version
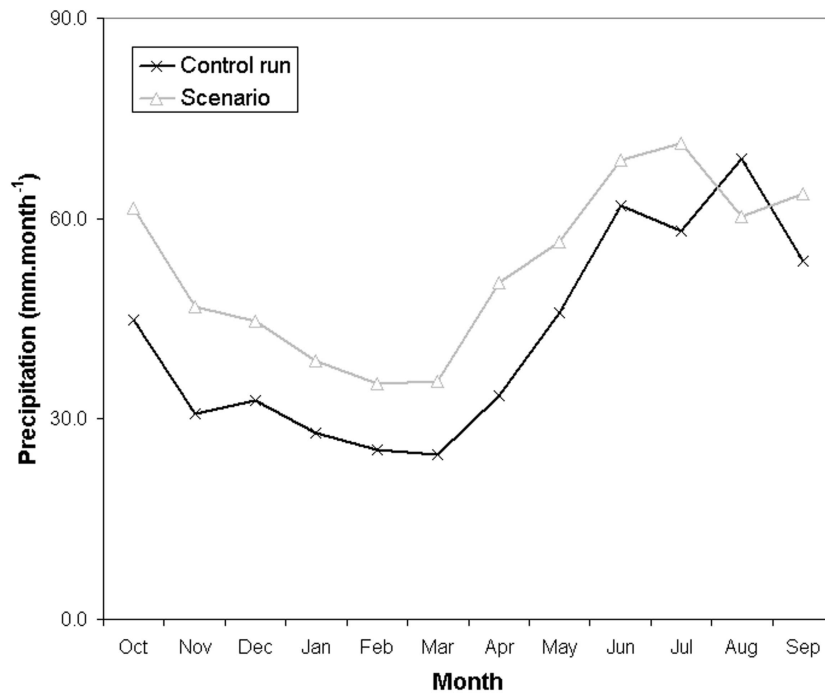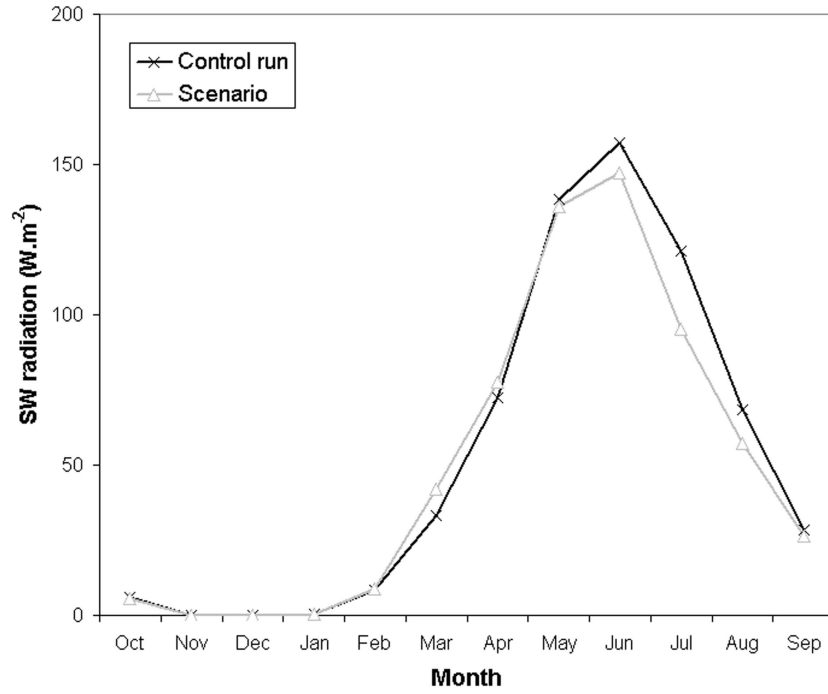

Figure 8.6 Basin-averaged precipitation in the Tana Basin in the control and scenario run
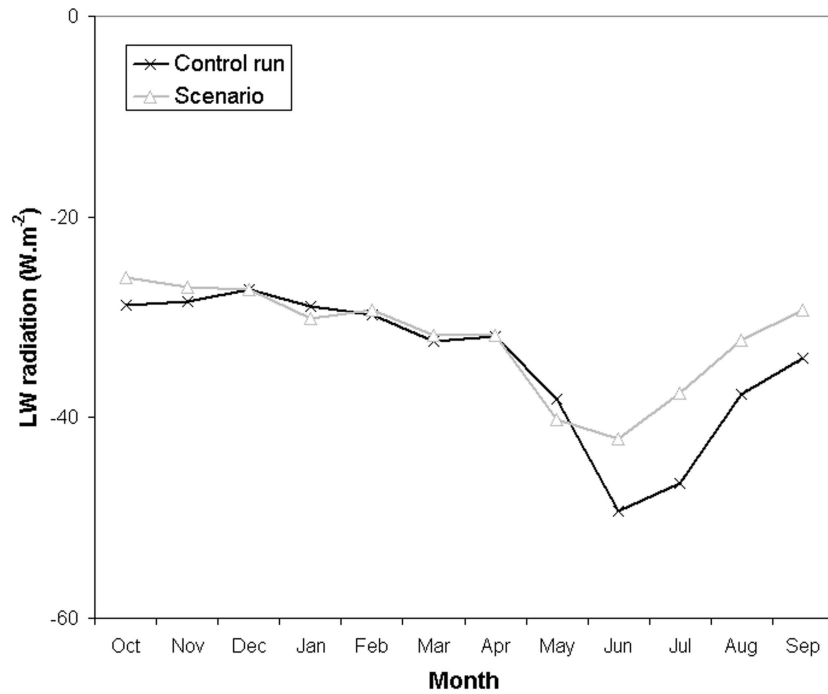
175

(a)

(b)

Figure 8.7 (a) Basin-averaged shortwave (SW) radiation, (b) longwave (LW) radiation, and (c) net radiation in the control and the scenario run
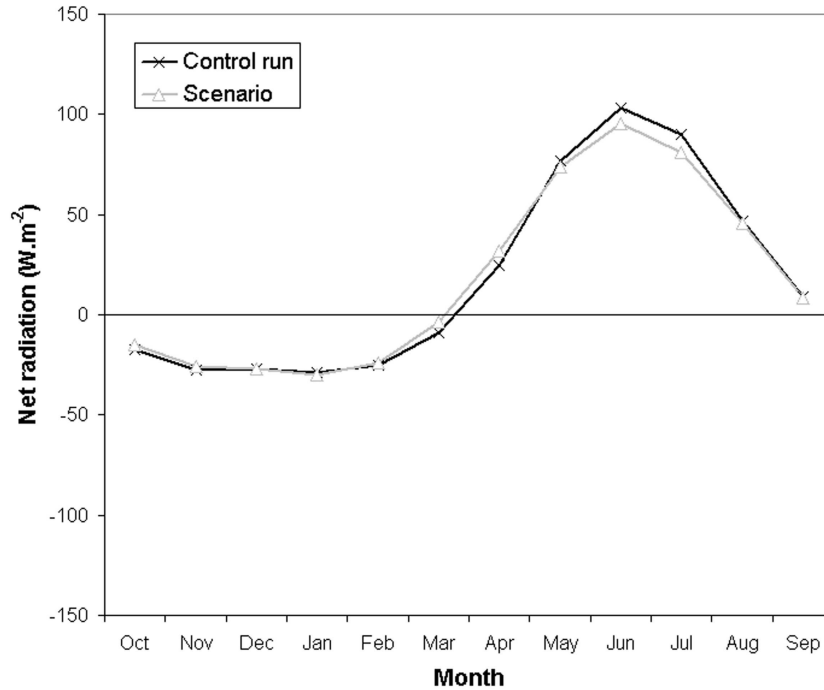
176

(c)

Figure 8.7 (continued)

8.3.3   Radiation, humidity and wind speed

In addition to temperature and precipitation, the HIRHAM estimates of shortwave and longwave radiation, humidity and wind speed were interpolated from the data points, and used as input into the hydrological model as well. No observations were available to validate these data. The annual average net radiation, that is calculated in the control run at 18 W.m^{-2}, is however within the range of net radiation simulated by 21 land surface models for a high-latitude area in northernmost Sweden (Bowling et al., 2001). Due to the larger amount of water vapour in the atmosphere, there is a 5 % decrease in shortwave radiation in the scenario run, especially in the summer months (figure 8.7.a). However, since the longwave radiation loss in the scenario run is also less in summer, the resulting net radiation remains more or less the same (figure 8.7.c).

The basin-averaged relative humidity is 88 %, which is higher than the 79 % reported by Seppälä (1976) for the meteorological station of Kevo, Finland. The seasonal pattern is however in line with Seppälä (1976), with a minimum in June and a maximum in October – November (figure 8.8). There are only minor differences between control and scenario run. On average the relative humidity is slightly higher in the scenario run, except for the spring months because the decline in humidity starts earlier. Also the differences in average wind speed are small (figure 8.9). The average wind speed in the control run is 4.0 m.s^{-1}, which is higher than the 3.3 m.s^{-1} reported by Seppälä (1976) after omitting the
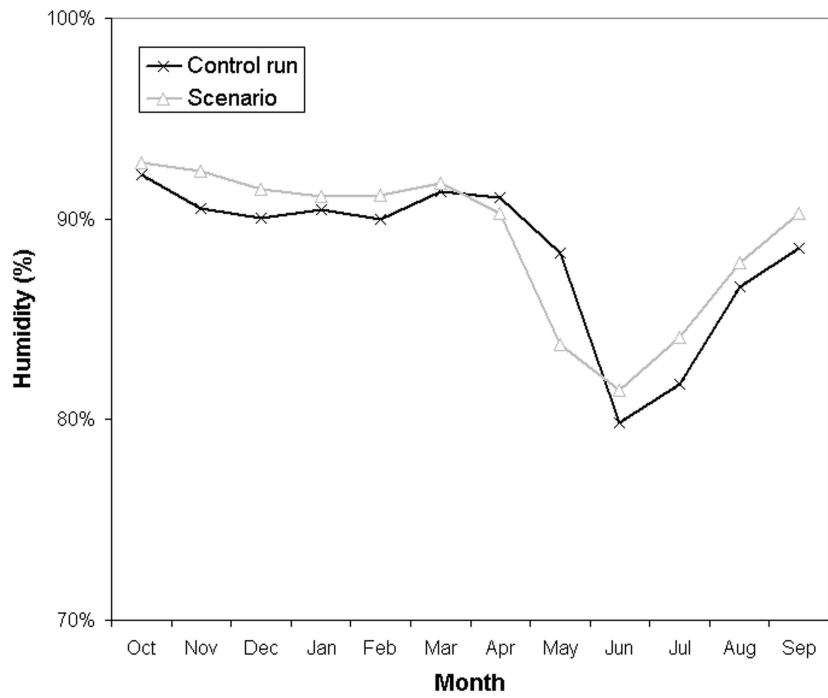
177

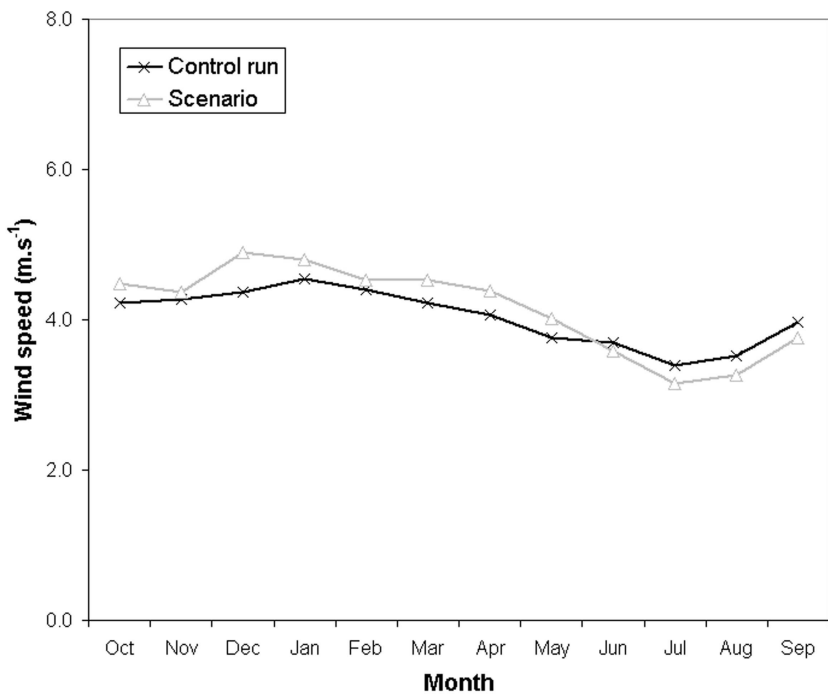**Figure 8.8** Basin-averaged relative humidity in the control and the scenario run

Figure 8.9 Basin-averaged wind speed in the control and the scenario run

178

windless periods. Kevo is however located in the valley of the Utsjoki, where winds may be reduced compared with the surrounding fell areas (Mansikkaniemi & Laitinen, 1990).

8.3.4   Snow

Due to the lower temperatures in the HIRHAM output, and perhaps also the higher precipitation in spring, the snow is melted several days later in the control run of experiment B than in the model runs of chapter 7, where observed temperature and precipitation were used (figure 8.10). The mean maximum amount of snow in the Tana Basin is higher as well (183 vs. 169 mm). In the control run, most of the snowmelt occurs in June. As a consequence, the snow cover depletion is delayed as well (figure 8.11). In the control run, the length of the snow season, defined as the mean annual number of days on which the ground is covered with snow, is on average about 10 days longer than in the model runs of chapter 7 that used meteorological data as input (cf. figure 7.9). It should be noted here that when observed temperature and precipitation data were used, the simulation of snow cover depletion in the Tana Basin was already later than observed by satellite (figures 6.6 and 7.10).Compared with these estimates, snowmelt in the control run is particularly delayed in the northern, western and southwestern parts of the Tana Basin; in the northeastern Tana Valley the snow season has even become shorter, which is attributed to the lower precipitation amount in this region. Nevertheless, the overall spatial pattern is very similar. According to the current
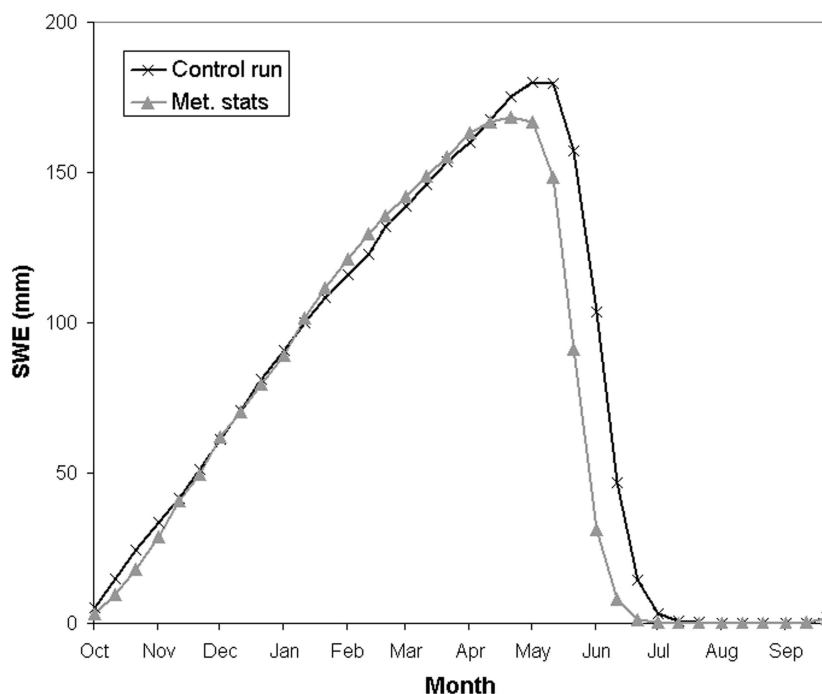

Figure 8.10 Simulated snow water equivalent (SWE) in the Tana Basin, using RCM data for the 30-year control run, and using observed temperature and precipitation at meteorological stations for the period 1980-1993. The latter model run is described in chapter 7
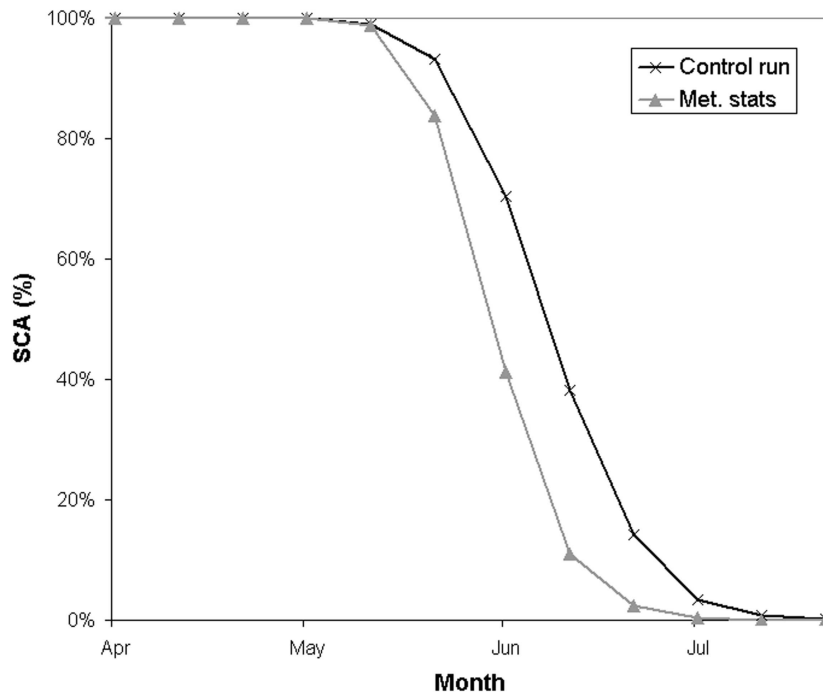
Figure 8.11 Snow covered area (SCA) in the Tana Basin expressed as percentage of the total catchment area, simulated using RCM data for the 30-year control run, and using observed temperature and precipitation at meteorological stations for the period 1980-1993

model the snow season lasts from less than 200 days in the Tana Valley close to the Barents Sea, to over 300 days at some of the mountaintops (figure 8.12.a).

The SRES A2 scenario has a significant impact on the snow coverage in the Tana Basin. The snow cover starts to accumulate about 2 – 3 weeks later, while snowmelt begins about 3 weeks earlier than in the control run (figure 8.13). Due to the higher precipitation in winter, the maximum snow water equivalent has nevertheless increased slightly. As a consequence of the earlier snowmelt in spring, when temperature and radiation are high, the total amount of sublimation is considerably lower in the scenario run (figure 8.14; table 8.2). The total amount of meltwater that is generated during spring and early summer, has accordingly increased by about 16 %. The melt season in the scenario run lasts somewhat longer as well. In addition, more melt is generated in late summer (at high elevations) and in autumn (figure 8.15). The snow-free season is accordingly extended by about 41 days, with the largest increase in the northeast, near the Barents Sea, and in particular in the river valleys where in places the snow season is shortened by more than 50 days (figures 8.12.b and 8.12.c). This shortening is similar in magnitude to the predictions by the SMHI (1998) for northern Fennoscandia. Averaged over the entire basin, there is little difference in the rate of snowmelt, in spite of the lower radiation due to the earlier snowmelt. The latter effect appears to be counterbalanced by a reduction of the "cold content" (i.e. the heat deficit) of the snow pack, caused by the higher temperatures in winter.
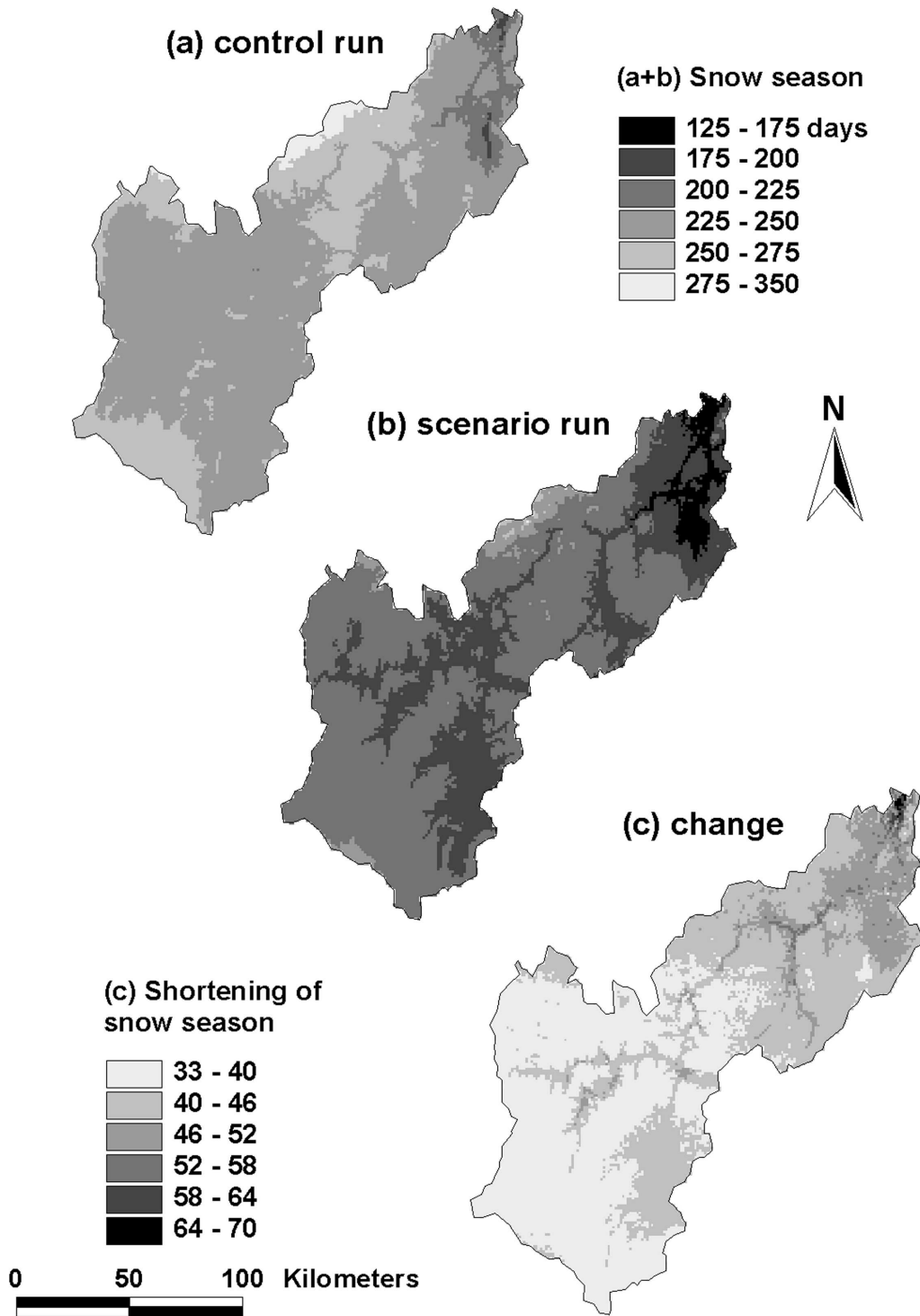
180

Figure 8.12 Period of snow coverage in the control run (a) and the scenario run (b), and shortening of the snow season in the scenario run (c). See the appendix for a colour version
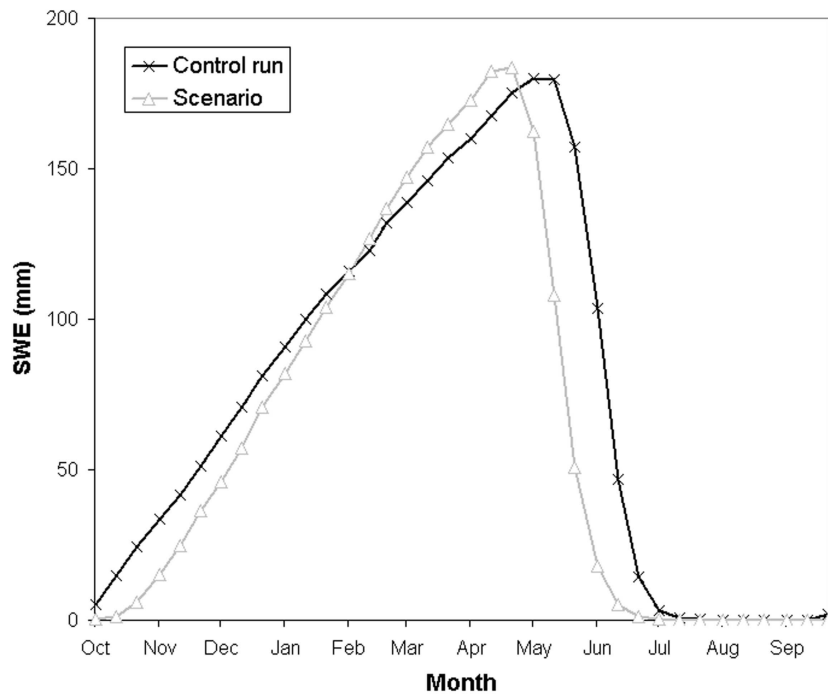
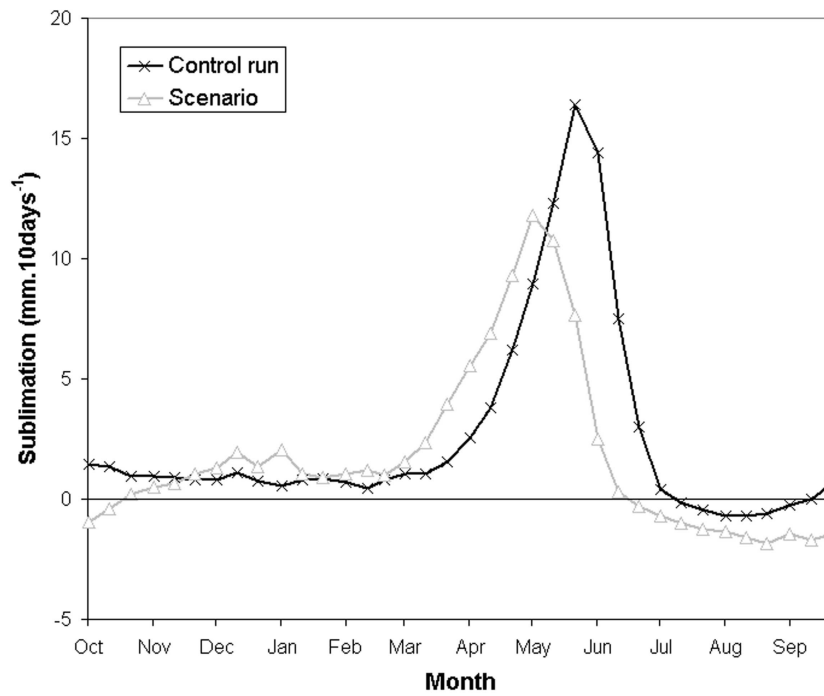**Figure 8.13** Basin-averaged snow water equivalent (SWE) in the control and the scenario run

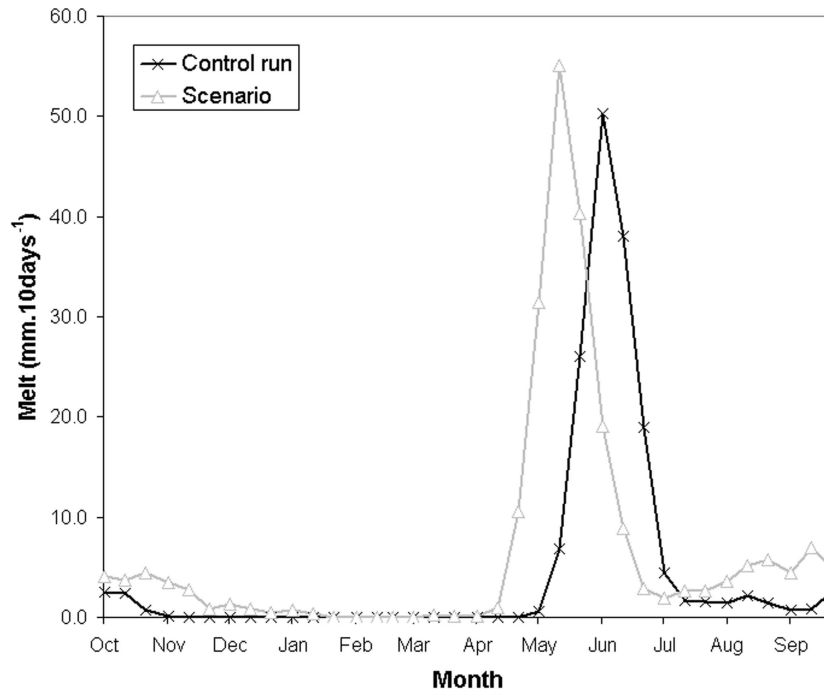**Figure 8.14** Basin-averaged sublimation in mm per 10 days, in the control and scenario run

182

Figure 8.15 Simulated snowmelt runoff upstream of Polmak, Norway, in the control and scenario run

8.3.5   *Evapotranspiration*

The annual amount of evapotranspiration in the control run amounts to 58 mm, which is close to the estimate of 60 mm.year^{-1} in chapter 7. The spatial patterns in evapotranspiration are complex, but it is clearly lowest at high elevations. In the rest of the Tana Basin the amount of evaporation is significantly higher, and in particular at those places where it is promoted by relatively high temperatures, vegetation type and soil storage (figure 8.16.a). In the scenario run, the annual evaporation increases by about 15 % to 67 mm. This difference is largely due to the earlier snowmelt, which allows evapotranspiration to start earlier (figure 8.17). During the rest of the summer, the differences with the control run are remarkably small, and in fact the evaporation rates are even somewhat lower. The reason for this is the lower precipitation in August, in combination with the higher humidity and slightly lower wind speeds in the scenario run (figure 8.8 and 8.9). Interestingly, the increase in annual evaporation is largest at higher elevations, and very small in some of the river valleys in the south (figure 8.16.c). A possible explanation may be that at higher elevations the snow-free season is extended in a period when solar radiation is at maximum.
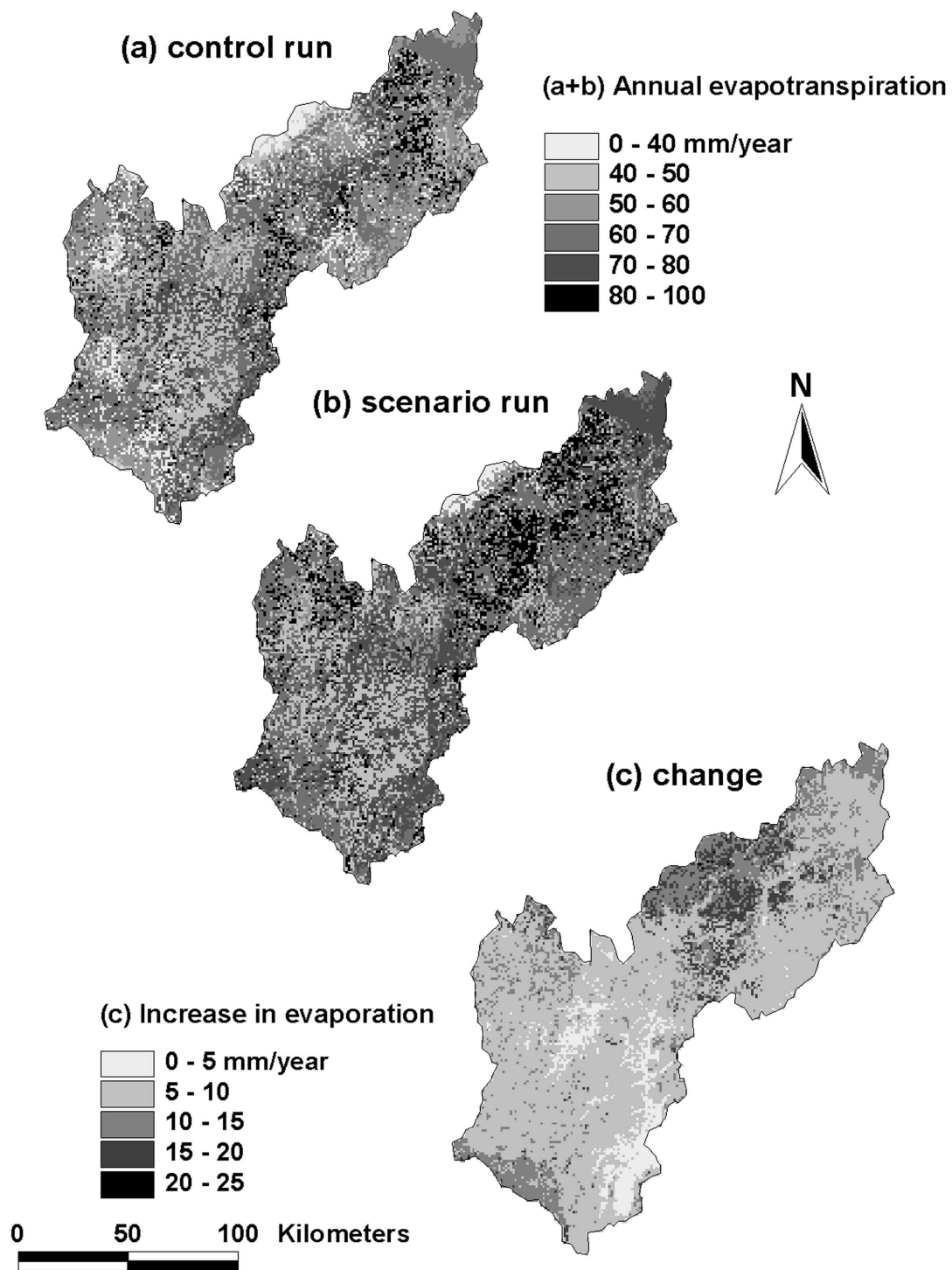
Figure 8.16 Annual evapotranspiration in the Tana Basin, in the control run (a) and the scenario run (b), and the increase in evaporation in the scenario run (c). See the appendix for a colour version
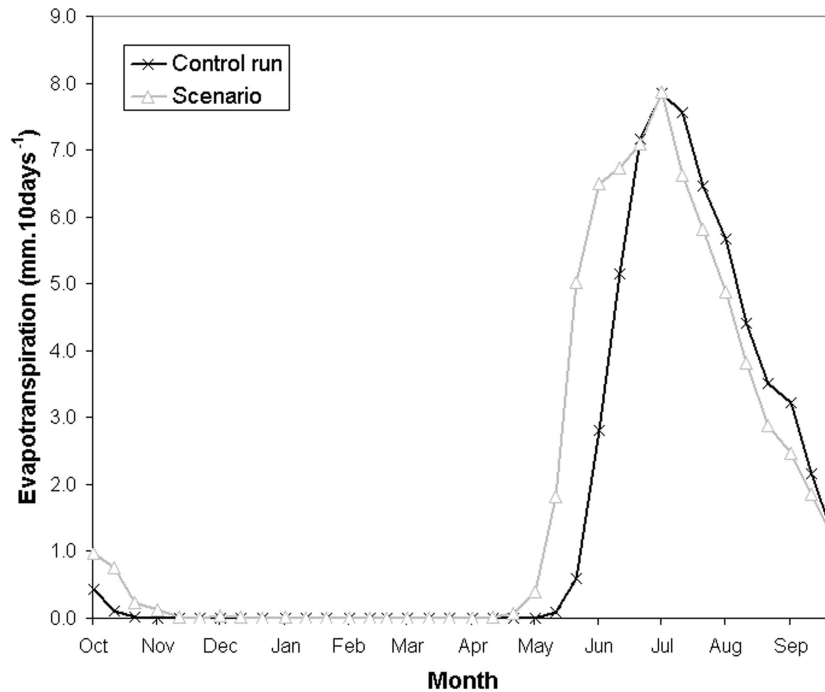
184

Figure 8.17 Basin-averaged evapotranspiration in the control and the scenario run

8.3.6   Discharge

The simulation of runoff in experiment B is also affected by the delay in snowmelt, caused by the lower temperatures in HIRHAM in spring. In the control run, the annual discharge peak is on average exactly one timestep of 10 days too late, compared with the observed long-term average, or the model runs of chapter 7, that used observed temperature and precipitation data (figure 8.18). On average, the actual discharge peak occurs in the last 10 days of May, but in the current simulation it is delayed until early June. Due to the higher precipitation in the spring months, the peak runoff is also slightly higher. Apart from these shortcomings, the average discharge pattern of the Tana River is well represented.

In the scenario run, the annual discharge peak at Polmak, Norway, has shifted by about 20 days to mid-May (figure 8.18.b). What is more, the peak runoff has increased from 923 to 1024 $m^3.s^{-1}$ (+11 %) on average. This increase is due to the slightly larger snow mass and the reduced sublimation, that together produce more meltwater runoff. Although smaller in absolute numbers, the relative increase in runoff is even larger in the rest of the year. In July – September, the mean discharge at Polmak rises from 149 $m^3.s^{-1}$ in the control run, to 218 $m^3.s^{-1}$ in the scenario run (+46 %). The simulated discharge in the control run is however smaller than the observed average over 1961-1990, which amounted to 180 $m^3.s^{-1}$. Due to a higher baseflow, runoff in winter (October – March) has increased in the scenario run as well, from 92 to 143 $m^3.s^{-1}$, an increase of 55 %. Similar changes occur in all other sub-basins.
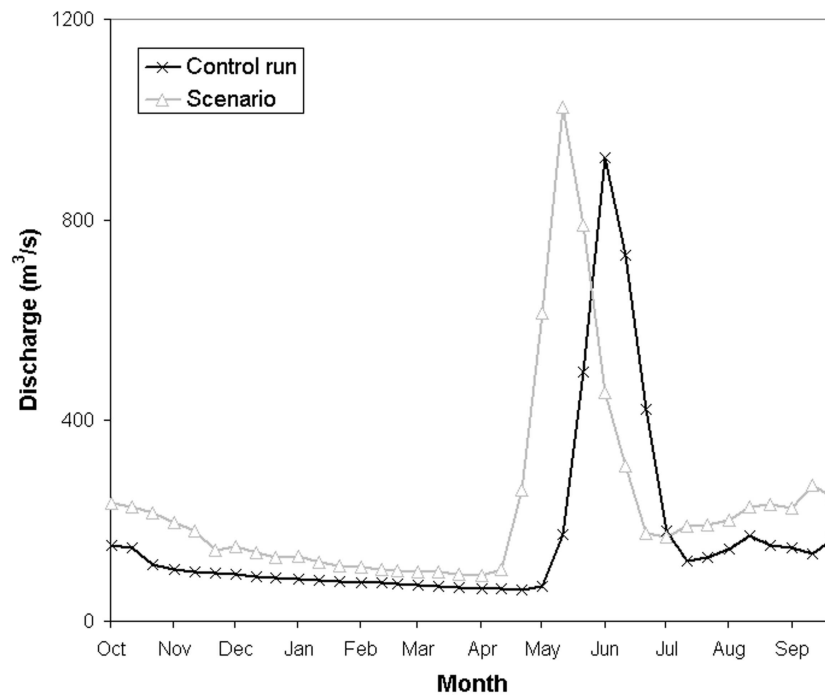
(a)
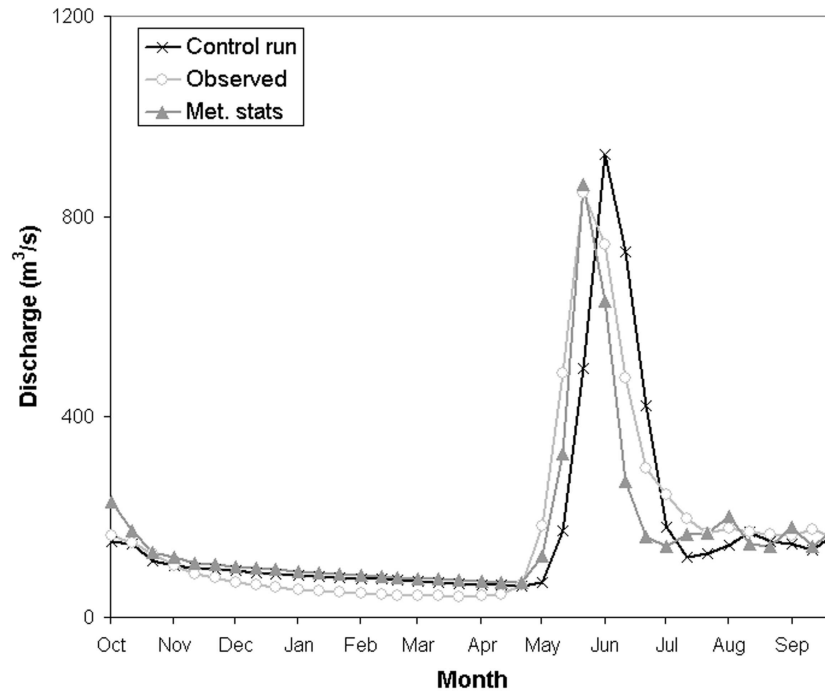
(b)

Figure 8.18 (a) Discharge of the Tana River at Polmak, Norway, in the control run, compared with observed discharge in 1961-1990. Also shown is the runoff simulated using observed temperature and precipitation at meteorological stations for the period 1980-1993 (chapter 7); (b) Discharge of the Tana River at Polmak in the control run and the scenario run

186

Table 8.2 Water balance of the Tana Basin in the control and scenario experiment B. Explanation: P = precipitation, E_s = sublimation, E_a = actual evapotranspiration, Q = observed discharge at Polmak (Norway) in 1961-1990, Q_s = simulated discharge at Polmak

	Control run	Scenario run	Change %
P (mm/year)	508.4	633.7	*+24.6*
E_s (mm/year)	90.1	62.7	*–30.3*
E_a (mm/year)	58.5	67.3	*+15.0*
Q (m³/s)	170.2		
Q (mm/year)	368.0		
Q_s (m³/s)	166.8	232.3	*+39.3*
Q_s (mm/year)	360.6	502.3	*+39.3*
Q_s / Q ratio	0.98		
Q_s / P ratio	0.71	0.79	*+11.7*
$Q_s+E_s+E_a$	509.1	632.3	*+24.2*

8.3.7   *Ecological impacts*

Apart from the water balance components discussed in the previous chapter, a number of related parameters was calculated that give an indication of the consequences of the changed climatic and snow conditions for the ecology of the Tana Basin. In the Nordic countries the growing season is generally defined as the period in which the daily mean temperature is above 5 ℃ (Tveito et al., 2001). Not surprisingly, the climate change scenario has a serious impact on the length of the growing season in the Tana Basin. According to the model, the growing season lasts from about 50 days on the mountains, to almost 120 in the river valleys under current climate conditions (figure 8.19). This is in good agreement with the calculations of Tveito et al. (2001) for this part of Northern Fennoscandia in 1961 – 1990. In the scenario run, the growing season is extended by 40 to 50 days to a maximum of 164 days. Instead of the length of the growing season, the degree-days or degree sum above 5 ℃ gives an indication of the total energy that is available to the vegetation. It is calculated as follows (Tveito et al., 2001):

$$T_D = \sum_{i=1}^{365} T_i - T_0 \quad \text{if } T_i \geq T_o \tag{8.1}$$

where T_D = number of degree-days
           T_i = daily mean temperature
           T_0 = reference temperature (5 ℃)

Figure 8.19 Length of the growing season in the Tana Basin in the control run (a) and the scenario run (b), and the increase in the scenario run in days (c). See the appendix for a colour version

188

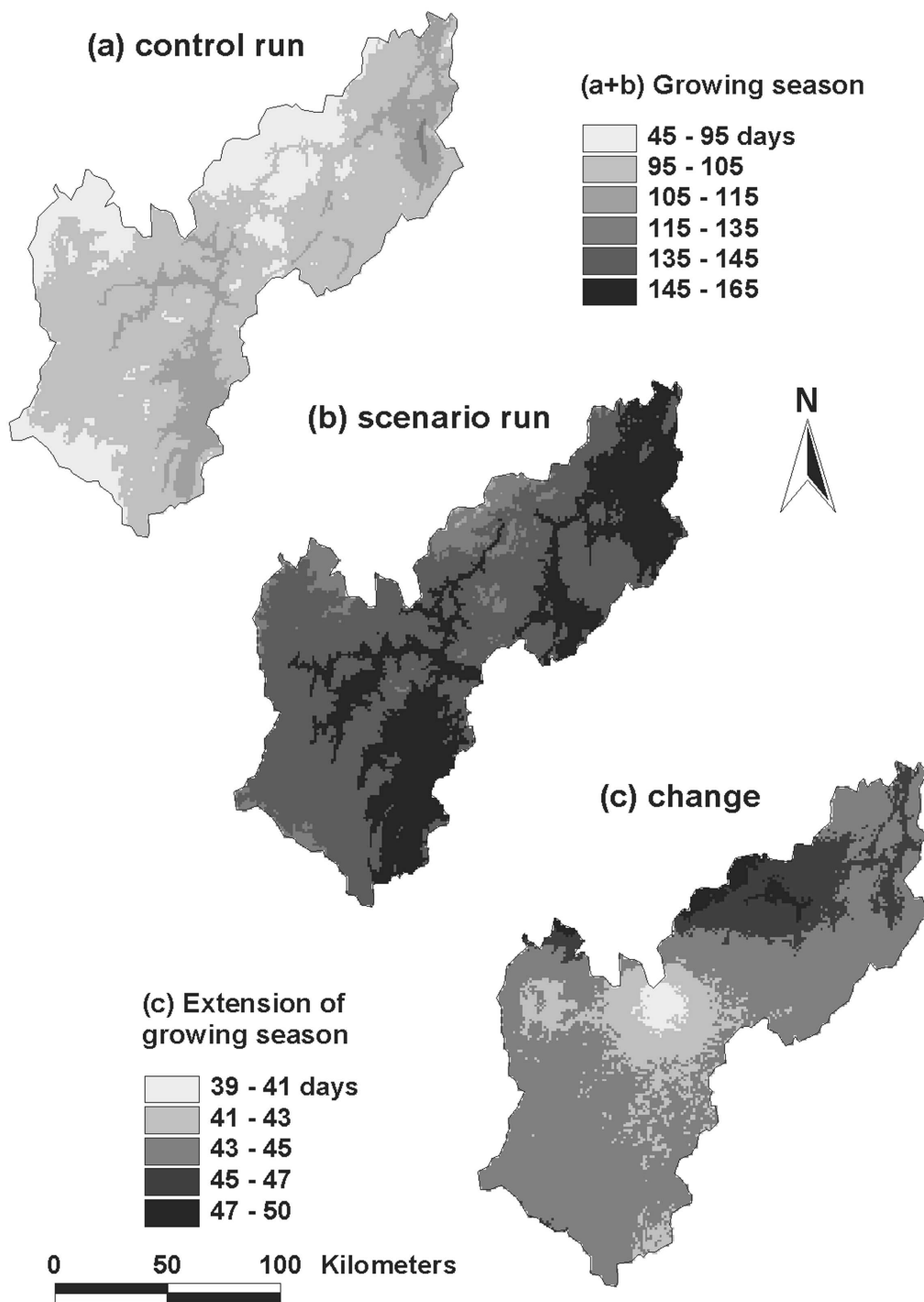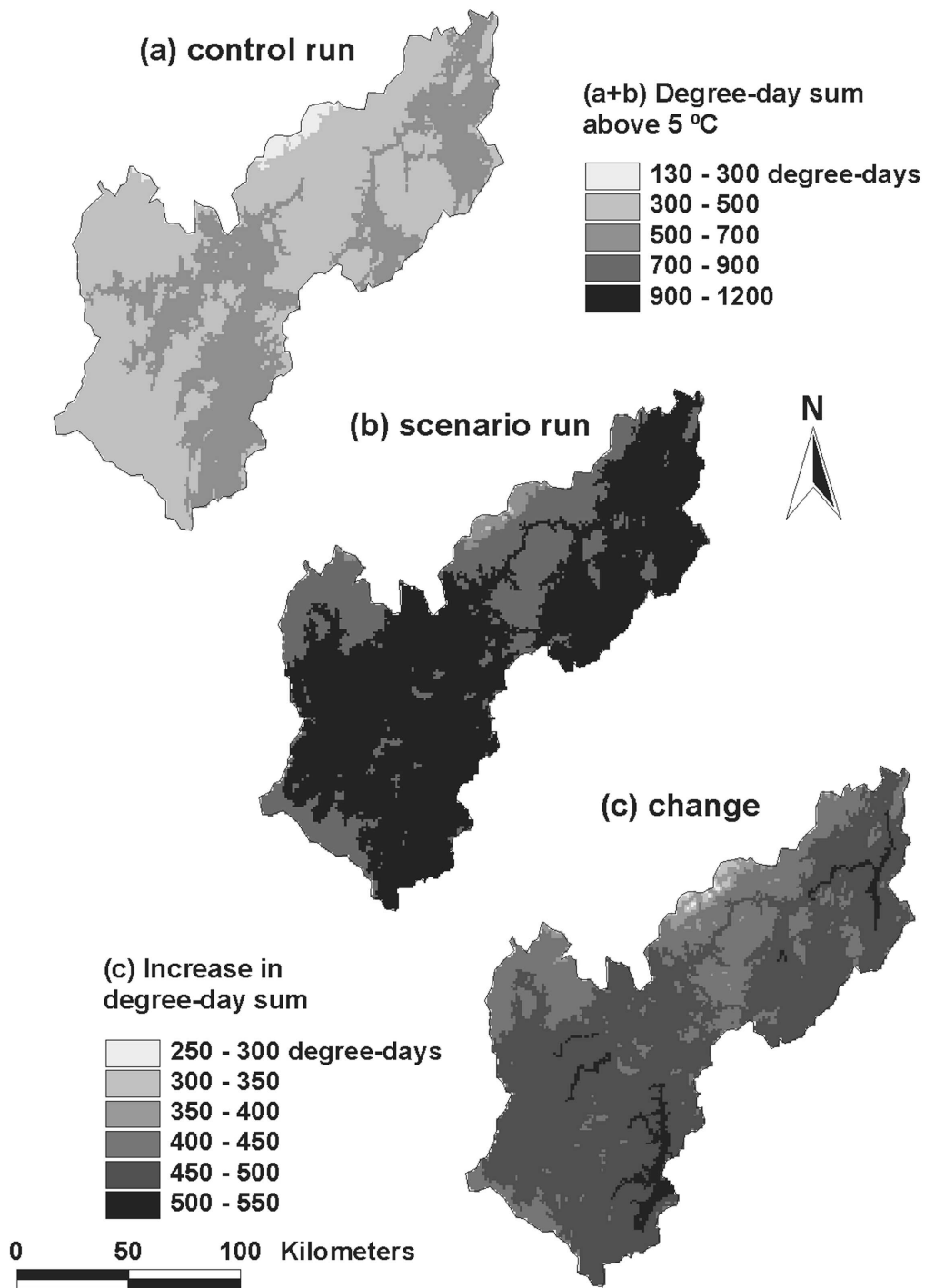**Figure 8.20** Number of degree-days in the Tana Basin in the control run (a) and the scenario run (b), and the increase in the scenario run in degree-days (c). See the appendix for a colour version
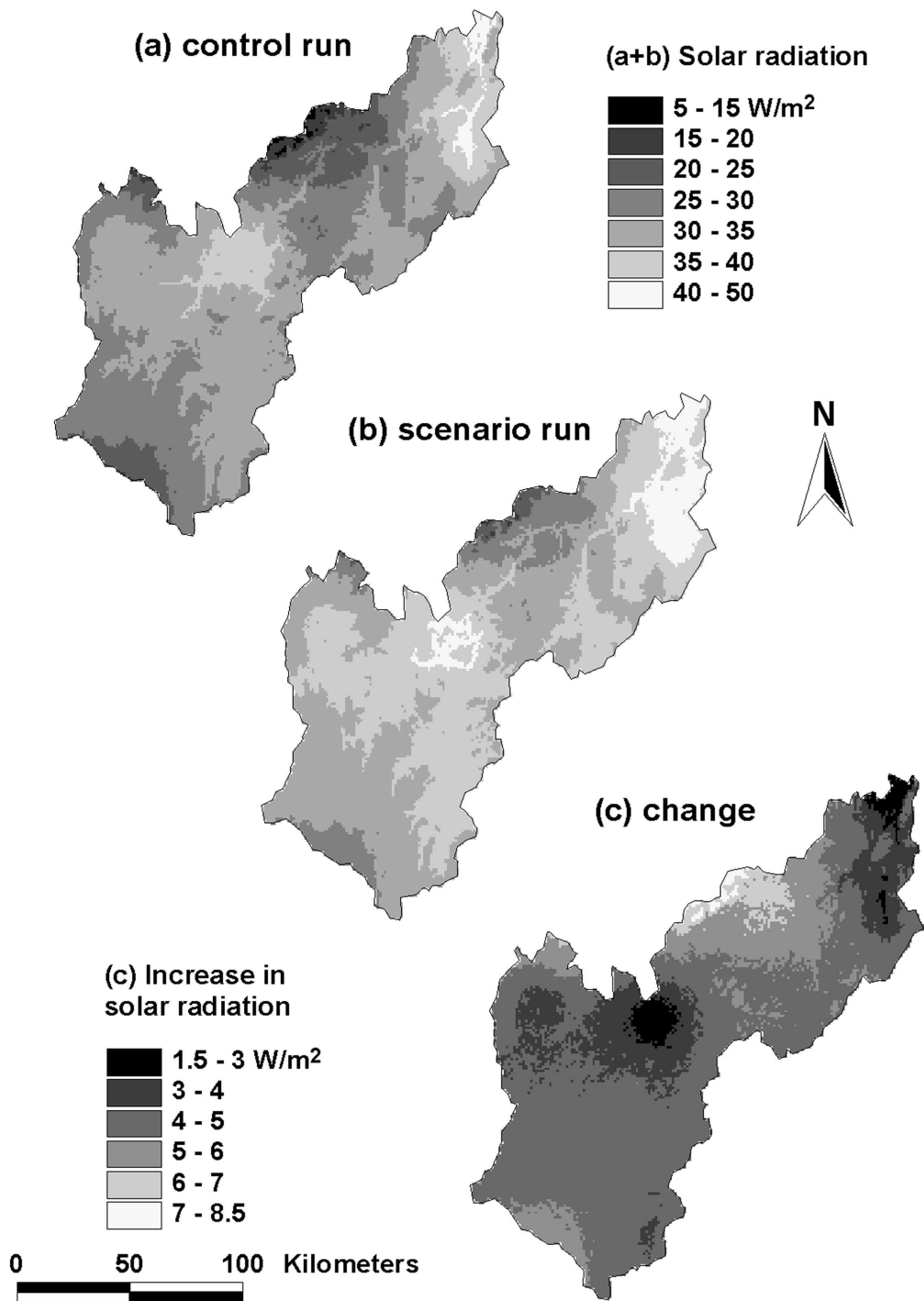
189

Figure 8.21 Solar radiation during the snow-free season in the control run (a) and the scenario run (b), and the increase in the scenario run in W.m^{-2} (c). See the appendix for a colour version

190

According to Tveito et al. (2001), the mean degree sum above 5 ºC in Northern Fennoscandia is 200 – 600 degree-days for the period 1961-1990. The mean degree sum in the control run corresponds with their calculations, and ranges from less than 150 at the highest parts, to more than 650 in the Tana Valley, with an average value of 480 degree-days for the entire basin (figure 8.20). In the scenario run, the mean number of degree-days has almost doubled to 940. In absolute numbers this increase is largest in the river valleys, in relative terms it is largest at high elevations, where the number of degree-days has sometimes more than doubled (figure 8.20).

A more direct measure of the energy available to the vegetation is the total amount of solar radiation that is received during the year. In particular for tundra vegetation, consisting of shrubs and heath, the annual radiation sum is to a large extent controlled by the persistence of the winter snow cover. In the control run, the amount of solar radiation received during the snow-free season, is therefore largest in the valley of the Tana River, close to the mouth, where it amounts to more than 40 $W.m^{-2}$ (figure 8.21). At the highest mountain tops, the annual amount of solar radiation during the snow-free season is even less than 10 $W.m^{-2}$, and the basin average is 30 $W.m^{-2}$. Due to the shorter snow season in the scenario run, the total radiation amount increases on average by about 16 % to 35 $W.m^{-2}$. The largest changes occur at high altitudes, since in these areas snow coverage lasts longest in the control run, and the snow pack melts away even after the moment of maximum radiation.

8.3.8   Differences with model experiments A and C

In experiment A, the HIRHAM precipitation was not scaled to meet the observed annual precipitation. Consequently, the magnitudes of the various water balance components are different from experiment B. The patterns of change from control to scenario run, are however very similar. In the control run for example, spring discharge of the Tana is considerably overestimated, compared with observed discharges (figure 8.22). Similar to experiment B however, the discharge peak in the scenario run has been shifted for about 20 days, and has become slightly higher as well. In the same way, the snow season is in general longer in experiment A than in experiment B, except for the higher elevations, which is due to the use of a lapse rate in experiment B. However, since this is true for both the control and scenario runs, the difference between the two is very similar. As in experiment B, snowmelt in the scenario run A starts about 20 days earlier. In summer, the evapotranspiration rates are slightly higher in experiment A than in experiment B. Again, the patterns of change are very similar, meaning more evaporation in the scenario run in early summer, due to the shorter snow season, and slightly less evaporation in the rest of the summer.

The differences with experiment C are more significant. Since this experiment used meteorological observations from the period 1980-1993 as a baseline, the temperature in springtime is higher, and precipitation is lower than in experiment B (figure 8.1 and 8.4). This is also true for the scenario run, in which the average difference between the HIRHAM control and scenario data was added to the station data on a monthly basis. In

(a)
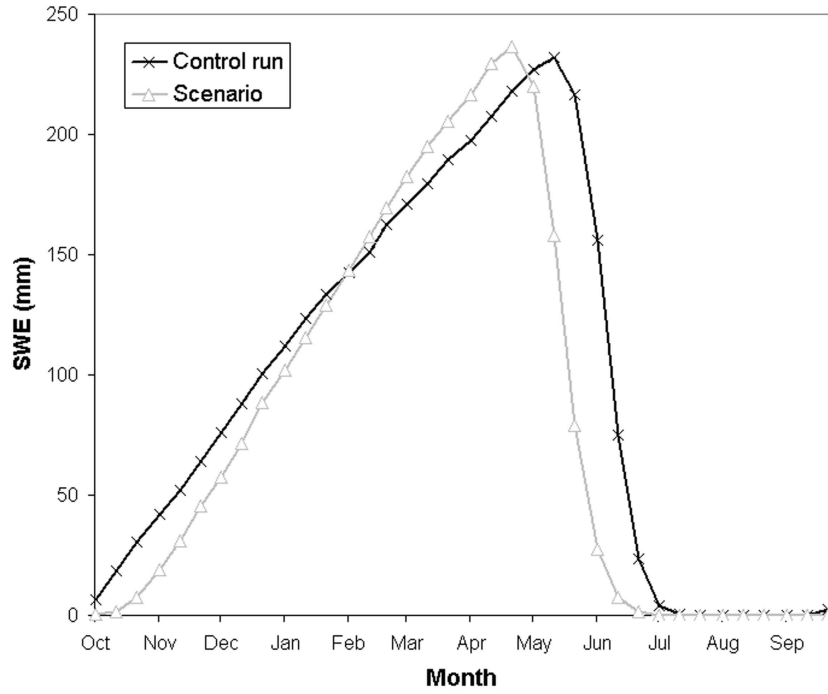
(b)

Figure 8.22 Basin-averaged snow water equivalent (SWE) (a), evapotranspiration (b), and discharge of the Tana at Polmak (c) in the control and scenario run of experiment A

192

(c)
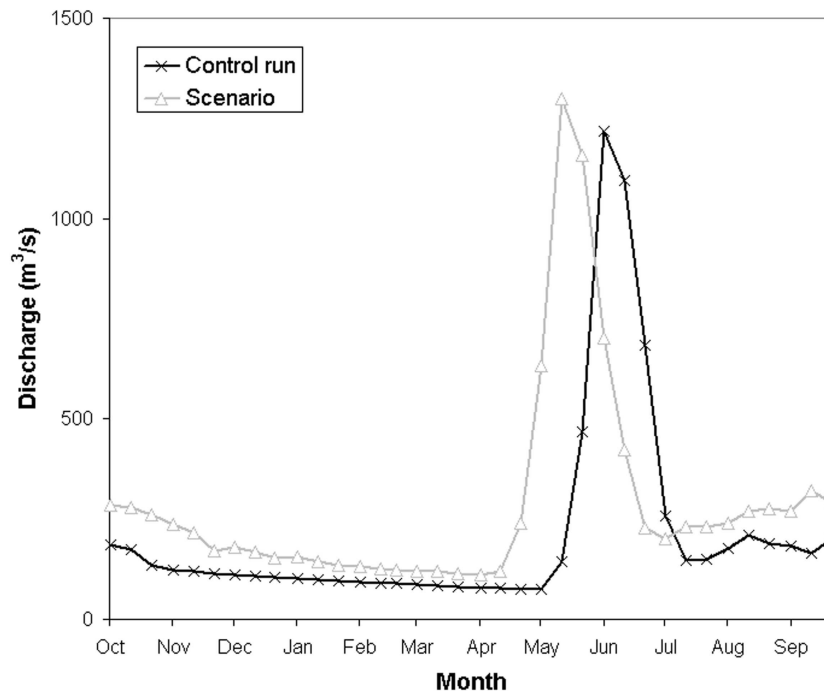
Figure 8.22 (continued)

the scenario run C, the precipitation in April and May is even 31 % lower than in the scenario run B. As a result, the maximum amount of snow water equivalent in the scenario run C has now decreased (figure 8.23). The snow-free season in experiment C is extended with 56 days on average (against 41 in experiment B), while it was already about 10 days longer in the control run. The spatial pattern is however similar, with the largest extension of more than 70 days taking place in the Tana Valley, close to the river mouth. Since the snow season is shorter, the annual evapotranspiration increases with 28 % to 76 mm.year^{-1}. Like in experiment B, there is however little difference in evaporation later in summer (figure 8.23.b). Due to the smaller amount of snow, the annual peak discharge in the scenario run is now considerably lower. In the control run, the runoff peaks on average in late May, which is in agreement with the observations of the Tana River. In the scenario run the discharge peak has shifted to the beginning of May, and runoff starts to rise already in April (figure 8.23.c). In experiment C, the relative increase in runoff in summer and winter, is also somewhat higher.

8.4 Discussion

Generally speaking, the results presented above confirm the predictions of previous studies about the consequences of climate change for hydrological processes in the Arctic and sub-Arctic: a shorter snow season, earlier snowmelt, a shift in the annual runoff
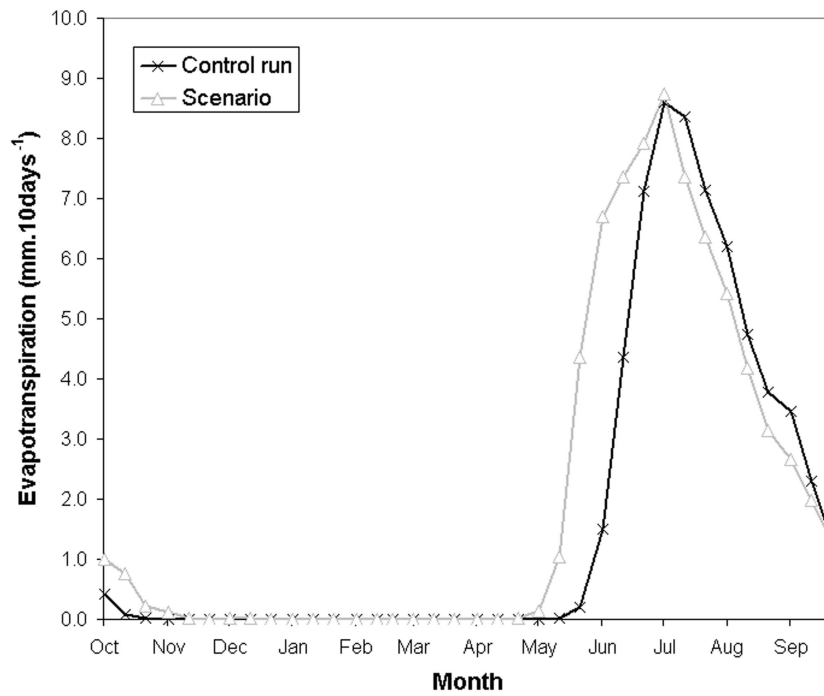
(a)

(b)
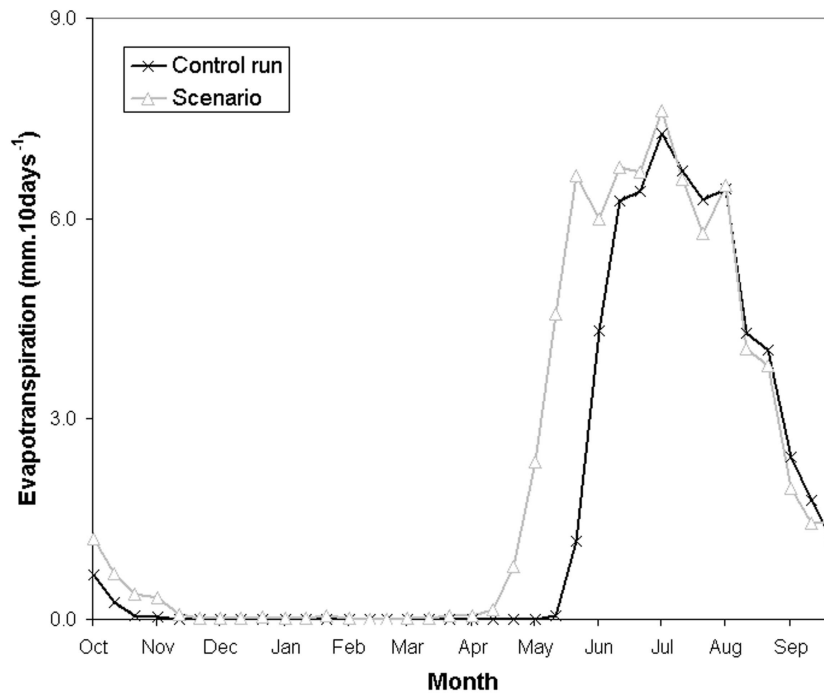
Figure 8.23 Basin-averaged snow water equivalent (SWE) (a), evapotranspiration (b), and discharge of the Tana at Polmak (c) in the control and scenario run of experiment C

194
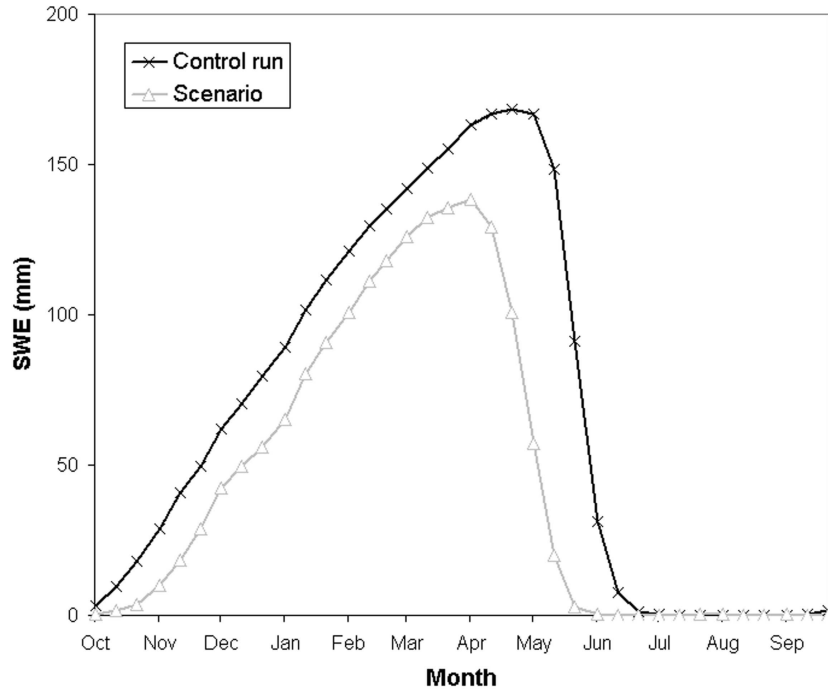
(c)
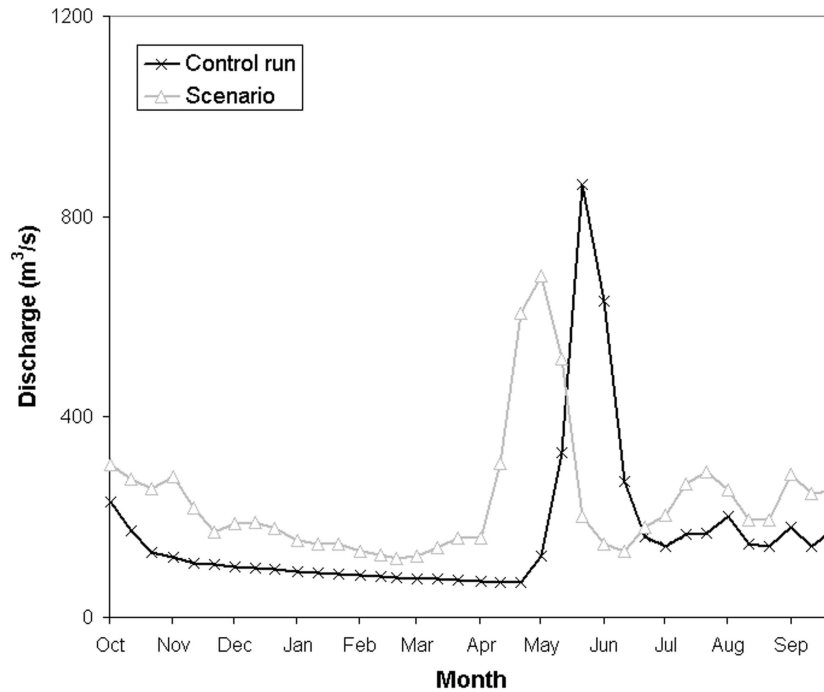
Figure 8.23 (continued)

peak, and more evapotranspiration in summer (see e.g. Vehviläinen & Lohvansuu, 1991; Van Blarcum et al., 1995; Everett & Fitzharris, 1998; SMHI, 1998; Nijssen et al., 2001). This study gives more insight into the local changes in the various processes that are of importance in sub-arctic environments, and provides some interesting details. Although the snow season in the scenario run B was considerably shorter, the maximum snow water equivalent had not decreased, but was in fact slightly higher (figure 8.13). This is explained by the higher precipitation that accumulated throughout the winter season. In experiment C, where the amount of precipitation in spring was considerably lower, and temperatures were higher than in experiment B, the maximum snow amount did show a decrease. In addition, due to the earlier melt season, the mean annual amount of sublimation in experiment B reduced significantly (figure 8.14). The amount of meltwater runoff that is produced in spring, and the annual peak discharge were consequently higher in the scenario run as well (figures 8.15 and 8.18). Apart from that, the runoff peak was also shifted and occurred on average about 20 days earlier in the season. Also the amount of evapotranspiration had increased in the scenario run, which is primarily caused by the extension of the snow-free season. Despite the higher temperatures, evapotranspiration rates were not higher in the rest of the summer (figure 8.17), which may be explained by the higher humidity and slightly lower wind speeds, in combination with the lower amount of precipitation in August.

(a)
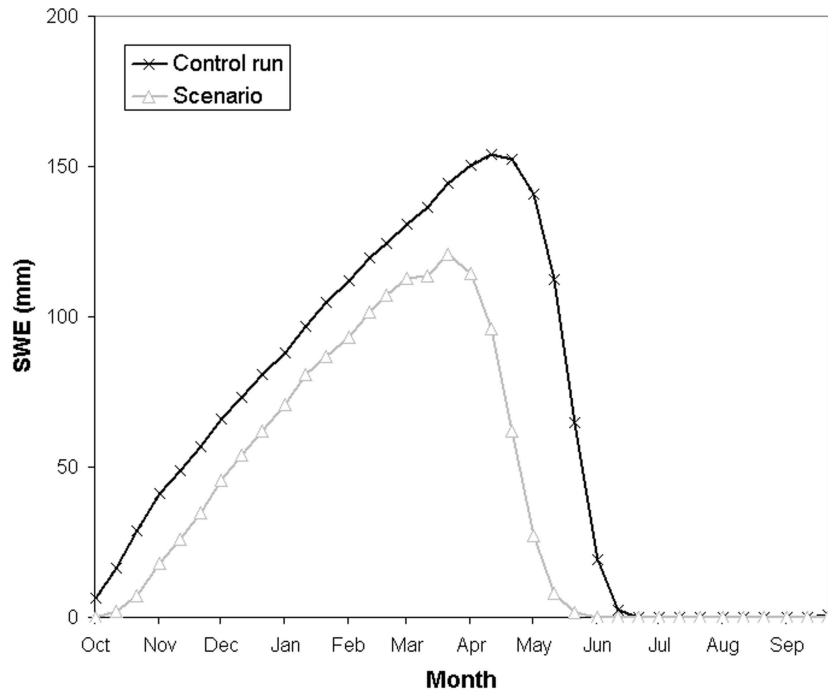
(b)
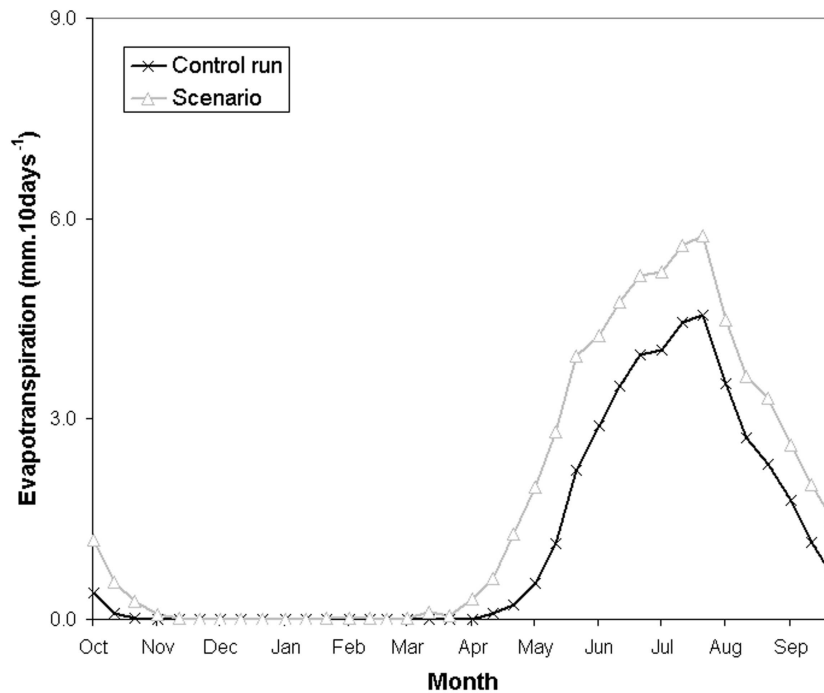
Figure 8.24 Results of the sensitivity analysis (chapter 6) for a rise in temperature of 5 ºC, and an increase in precipitation of 20 % for the basin-averaged snow water equivalent (SWE) (a), evapotranspiration (b) and discharge of the Tana river at Polmak (c)

196

(c)
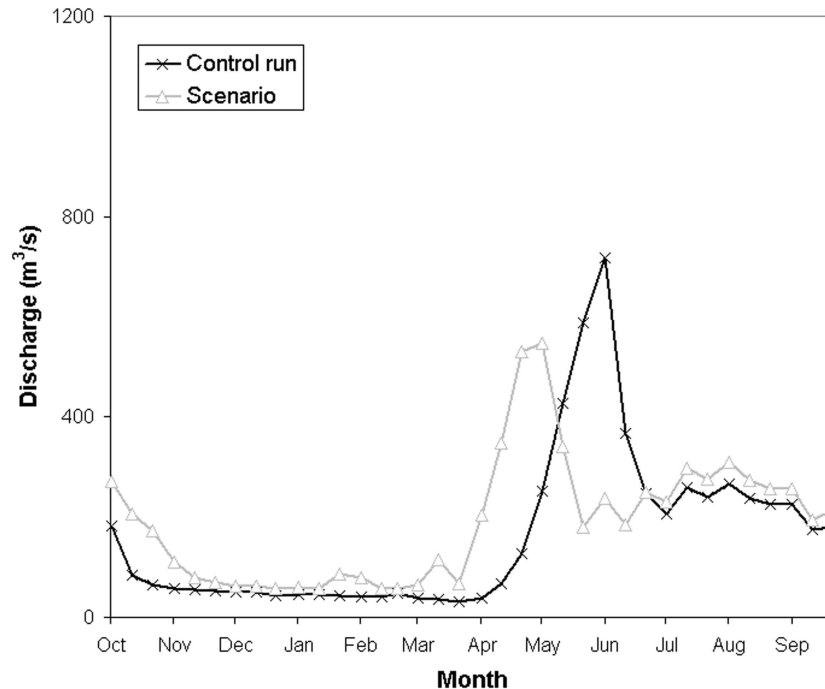
Figure 8.24 (continued)

This study also demonstrates that there are important local differences in climate change impact within the Tana Basin. The most dramatic decrease in snow cover duration occurred in the valley of the Tana River, close to the Barents Sea (figure 8.12.c). However, the largest increase in evapotranspiration, as well as the amount of solar radiation that is received during summer, was modelled at high altitudes (figure 8.16.c, 8.21) . Here, the extension of the snow-free season takes place in a period in which the solar radiation is high. The impact of a shorter snow season is therefore larger than at lower altitudes, where the snow-free season is extended with a period of lower radiation.

It is interesting to compare the results of the modelling study in this chapter with the sensitivity analysis of chapter 6. In the latter, simpler models of snowmelt and evapotranspiration were used in TANAFLOW, and temperature and precipitation were arbitrarily increased with fixed amounts. Here, the results are summarised in figure 8.24 for a rise in temperature of 5 °C, in combination with an increase in precipitation of 20 %. These amounts correspond well with the predictions of HIRHAM4 for the SRES scenario A2 in the Tana Basin, that come down to +5.2 °C and +25 %. In details the sensitivity analysis differs from experiment A and B, but the results are similar to those of experiment C. In the sensitivity analysis, the changes in temperature and precipitation not only resulted in a considerably shorter snow season, but also in a decrease in the maximum amount of snow water equivalent (figure 8.24.a). In contrast, experiment A and B showed even a slight increase in maximum snow amount due to higher

197

precipitation amounts and reduced temperatures. What is more, in the scenario runs the annual amount of sublimation had decreased significantly; in the old version of TANAFLOW this process was completely ignored.

As a result of the decreased snow mass in the sensitivity analysis, the discharge peak was not only shifted by about one month, but also reduced in magnitude in comparison with the baseline run, that on average already underestimated the observed peak runoff (see chapter 6). Again, this reduction was also observed in experiment C, but not in experiment A and B. Similar to the present study, in the sensitivity analysis runoff was predicted to increase in summer (figure 8.24.c). There is also agreement on the earlier beginning of evapotranspiration (figure 8.24.b). However, in the sensitivity analysis evaporation rates remain higher throughout the summer, since they are directly dependent on temperature, while in the present study evaporation rates remained more or less the same (figure 8.17, 8.23). In summary, the patterns of change in the sensitivity analysis are similar in general, but they differ in details from the results in this chapter. Being based on physically-based algorithms of snowmelt and evapotranspiration, the reliability of the conclusions has however been increased.

The magnitudes of changes in snow coverage, evaporation and runoff that were found in the present study, will certainly be relevant to the ecology of the study area. At a much larger scale, changes in the extent and duration of snow coverage will affect the radiation balance of northern latitudes (Harding et al., 2002). In the Tana Basin, the shorter snow season resulted in an increase of 16 % in the amount of solar radiation available to shrubs and tundra vegetation after depletion of the snow cover. Moreover, changes in the amount of freshwater runoff to the Arctic Ocean may influence the formation of sea ice (Lewis et al., 2000; Miller & Russell, 2000). However, in the present study, several possible feedback effects have not been taken into account. Changes in climate and snow conditions will affect plant growth, and may ultimately lead to changes in vegetation structure and composition. Increased shrub height may augment the snow depth accumulated in winter, and diminish the sublimation of snow transported by wind (Sturm et al., 2001). In a modelling study by Liston et al. (2002), increased shrub height delayed the time of final melt by several days. In summer, changes in biomass will affect the amount of transpiration; however, higher CO_2 concentrations tend to reduce the water use efficiency of plants, which may counterbalance the increase in evapotranspiration (Dingman, 1994). In TANAFLOW, these processes and several others, such as the effect of soil frost on infiltration of rain and meltwater, or the dynamics of soil moisture, are still poorly represented. Moreover, in the present study only one scenario of climate change has been considered. In order to analyse the effects of uncertainties associated to the predictions, it may be useful to assess the impacts for a range of scenarios. Nevertheless, the changes that were found in snow coverage, evapotranspiration and runoff, were consistent between the various model experiments, and are a strong indication of the sensitivity of the sub-arctic hydrological system to human-induced changes in climate.

198

8.5   Conclusions

In the Tana Basin in the northernmost part of Fennoscandia, the IPCC SRES scenario A2 may cause the mean annual temperature to rise by more than 5 degrees Celsius, and the annual precipitation to increase with 25 %. In this chapter, the impact of these changes on the hydrological system of the Tana Basin was investigated by using a large-scale hydrological model with physically-based algorithms for snowmelt and evaporation. Input data were derived directly from the regional climate model HIRHAM4 (Christensen et al., 1998), but the differences in temperature and precipitation between the control and scenario runs were also applied to meteorological observations from the period 1980-1993.

In all model experiments considered in this chapter, the length of the snow-free season in the scenario run was considerably extended with more than 30 days at higher elevations, to 70 days or more in the valley of the Tana River, close to the Barents Sea. Due to the shorter snow season, the annual amount of sublimation decreased by 30 %, and in the model experiment using observed temperature and precipitation data even by more than 50 %. The amount of solar radiation received during the snow-free season, increased accordingly by about 16 %. The annual maximum amount of snow and the annual peak discharge increased in two of the three model experiments, which is the result of the lower temperatures and higher precipitation in springtime in the HIRHAM data. The annual amount of evapotranspiration also increased significantly in all model experiments, but this is mainly the result of the longer snow-free season. During the rest of the summer, evaporation rates in the scenario run were similar to, or even slightly lower than in the control run. As a result of the increased precipitation and groundwater storage, river discharge increased both in summer and in winter. Although the representation of some processes in the current model is still rather poor, and several possible feedback effects have not been taken into account in the present analysis, it is believed that these results provide a realistic assessment of possible future conditions in the Tana Basin.

8.6   References

Bowling, L.C., D.P. Lettenmaier, B. Nijssen, L.P. Graham, D.B. Clark, M. El Maayar, R. Essery, S. Goers, Y.M. Gusev, F. Habets, B. Van den Hurk, J. Jin, D. Kahan, D. Lohmann, X. Ma, S. Mahanama, D. Mocko, O. Nasonova, G.-Y. Niu, P. Samuelsson, A.B. Shmakin, K. Takata, D. Verseghy, P. Viterbo, Y. Xia, Y. Xue & Z.-L. Yang (2001): Simulation of high latitude hydrological processes in the Torne-Kalix basin: PLIPS Phase2(e). 1: Experiment description and summary intercomparisons. Global and Planetary Change, to be submitted.

Christensen, O.B., J.H. Christensen, B. Machenhauer & M. Botzet (1998): Very high-resolution regional climate simulations over Scandinavia - Present climate. Journal of Climate 11, pp. 3204-3229.

Dingman, S.L. (1994): Physical Hydrology. New York: Macmillan.

Everett, J.T. & B.B. Fitzharris (1998): The Arctic and Antarctic. In: R.T. Watson, M.C. Zinyowera & R.H. Moss (eds.): The regional impacts of climate change: an assessment of vulnerability. Special report of IPCC Working Group II. Cambridge: Cambridge University Press, pp. 85-103.

Harding, R.J., P. Kuhry, T.R. Christensen, M.T. Sykes, R. Dankers & S. van der Linden (2002): Climate feedbacks at the taiga / tundra interface. Ambio, in press.

Houghton, J. T., Y. Ding, D.J. Griggs, M. Noguer, P.J. van der Linden & D. Xiaosu (eds.) (2001): Climate Change 2001: The Scientific Basis. Cambridge: Cambridge University Press.

Lewis, E.L., E.P. Jones, P. Lemke, T.D. Prowse & P. Wadhams (eds.) (2000): The Freshwater Budget of the Arctic Ocean. Dordrecht: Kluwer Academic Publishers.

Liston, G.E., J.P. McFadden, M. Sturm & R.A. Pielke, Sr. (2002): Modeled changes in arctic tundra snow, energy and moisture fluxes due to increased shrubs. Global Change Biology 8, pp. 17-32.

Miller, J.R. & G.L. Russell (2000): Projected impact of climate change on the freshwater and salt budgets of the Arctic Ocean by a global climate model. Geophysical Research Letters 27, pp. 1183-1186.

Mansikkaniemi, H. & T. Laitinen (1990): Pattern of local wind changes in a fell region, northern Finland. Reports from the Kevo Subarctic Research Station. 21, pp. 11-20.

Monteith, J.L. (1965): Evaporation and environment. In: G.E. Fogg & P.G. Kohn (eds.): The state and movement of water in living organisms (Proceedings of the 19th Symposium of the Society for Experimental Biology). London: Cambridge University Press, pp. 205-234.

Nakicenovic, N & R. Swart (eds.) (2000): Special Report on Emissions Scenarios. Cambridge: Cambridge University Press.

Nijssen, B., G.M. O'Donnel, A.F. Hamlet & D.P. Lettenmaier (2001): Hydrological sensitivity of global rivers to climate change. Climatic Change 50, pp. 143-175.

Roeckner E., L. Bengtsson, J. Feichter, J. Lelieveld & H. Rohde (1999): Transient climate change simulations with a coupled atmosphere-ocean GCM including the tropospheric sulfur cycle. Journal of Climate 12, pp. 3004-3032.

Seppälä, M. (1976): Periglacial character of the climate of the Kevo region (Finnish Lapland) on the basis of meteorological observations 1962-71. Reports from the Kevo Subarctic Research Station 13, pp. 1-11.

Sturm, M., J.P. McFadden, G.E. Liston, F. Stuart Chapin III, C.H. Racine & J. Holmgren (2001): Snow-shrub interactions in Arctic tundra: a hypothesis with climatic implications. Journal of Climate 14, pp. 336-344.

SMHI (1998): Regional climate simulations for the Nordic region - First results from SWECLIM. Norrköping: Swedish Meteorological and Hydrological Institute.

Thornthwaite, C.W. & J.R. Mather (1955): The water balance. Centerton: Drexel Institute of Technology, Laboratory of Climatology (Publications in Climatology 8).

Thornthwaite, C.W. & J.R. Mather (1957): Instructions and tables for computing potential evapotranspiration and the water balance. Centerton: Drexel Institute of Technology, Laboratory of Climatology (Publications in Climatology 10), pp. 183-243.

Tveito, O.E., E.J. Førland, H. Alexandersson, A. Drebs, T. Jónsson, H. Tuomenvirta & E. Vaarby Laursen (2001): Nordic Climate Maps. Oslo: Norwegian Meteorological Institute (DNMI report no. 06/01).

Van Blarcum, S.C., J.R. Miller & G.L. Russell (1995): High latitude river runoff in a doubled CO_2 climate. Climatic Change 30, pp. 7-26.

Vehviläinen, B. & J. Lohvansuu (1991): The effects of climate change on discharges and snow cover in Finland. Hydrological Sciences Journal 36, pp. 109-121.

Ward, R.C. & M. Robinson (1990): Principles of Hydrology. Third Edition. London: McGraw-Hill.

9   DISCUSSION, CONCLUSIONS, AND RECOMMENDATIONS FOR FURTHER RESEARCH

9.1   Introduction

In the previous chapters, a series of studies was presented that aimed at assessing the possible impacts of climate change on the sub-arctic hydrology of the Tana River Basin in Northern Fennoscandia. This final chapter evaluates the results of these studies, draws some general conclusions, and makes some recommendations for further research. It consists of three parts: the first part discusses the large-scale hydrological characteristics of high-latitude environments, such as the Tana Basin, and the potential impacts of climate change in the coming century. The second part evaluates the approach that was followed in this thesis, and emphasises it strengths and limitations. Finally, in the third part some recommendations for future research are presented.

9.2   Sub-arctic hydrology and climate change

The hydrology of areas at high latitudes is dominated by the presence of a seasonal snow cover, that may last for eight months a year or more. Usually, this snow cover melts away in May or June, when the intensity of solar radiation is almost at maximum. Snowmelt is therefore in general a very rapid process. In chapter 4, snow cover depletion in the Tana Basin was monitored using time series of satellite images acquired in 1998 and 1999. In both years, most of the catchment area became free of snow within a period of 4 to 6 weeks (figure 4.8). Melting of snow releases a large volume of precipitation, that has accumulated during winter. Due to the presence of ice layers in the snow pack and frozen soils, that may inhibit infiltration, a major part of this volume is discharged right away. A field study in the catchment of the Kidisjoki near Kevo, Finland, in 2001, suggested that approximately 30 % of the total amount of snow that was stored in the area at the end of the winter, was discharged in the first few days of snowmelt, and almost half of it ran off within one month (chapter 3). There is however strong evidence that these proportions vary from year to year, depending on the extent of soil frost and the conditions during snowmelt. Part of the amount of meltwater that is produced in spring, will infiltrate, and may have a long-lasting influence on evapotranspiration and runoff in summer. Measurements in the same Kidisjoki catchment in 1999 and 2000, also indicated that evapotranspiration may dominate the water balance during summer (table 3.1). In both study periods, evapotranspiration accounted for 60 % or more of the total precipitation input. It seems that evaporation is promoted by high moisture contents that are maintained throughout the summer season. Except for extreme rainstorms, it seems that direct runoff is only generated in wetland areas, that remain near saturation all summer, and therefore offer little storage capacity.

Climate models generally predict that the greatest warming in the coming century, due to the so-called enhanced greenhouse effect, will occur at northern high latitudes (Houghton

201

et al., 2001). Being covered with snow for over half a year, sub-arctic environments are just at the edge of the cryosphere and hydrosphere, and therefore particularly sensitive to changes in climate. In this thesis, the impact of climate change on sub-arctic hydrology was studied using an advanced hydrological model employing physically-based descriptions of snow accumulation, snowmelt and evapotranspiration (chapter 8). The results were consistent between the various model runs and corresponded well with a sensitivity analysis of a simpler, empirical model in chapter 6. Previous suppositions on the impacts of climate change (e.g. Rouse et al., 1997; Anisimov & Fitzharris, 2001) have now been confirmed and quantified. What is more, by using a distributed hydrological model, changes in snow coverage and evapotranspiration could be studied at a high spatial resolution, and differences between the various parts of the Tana Basin could be identified.

As a result of global warming, significant changes can be expected in the length of the snow season at high latitudes. In the Tana Basin, the snow season would be shortened by 30 to 70 days, following a rise in mean annual temperatures of more than 5 ℃ and an increase in total annual precipitation of 25 % (figure 8.12). The most dramatic decrease in snow cover duration was found in those areas that are already warmest under current conditions. Extension of the snow-free season may increase the total amount of solar radiation that is available to shrubs and tundra vegetation by 16 %. Since the presence of snow modifies the surface albedo substantially, changes in the extent and duration of snow cover at high latitudes may ultimately affect the global radiation budget, and provide a positive feedback to global warming (Anisimov & Fitzharris, 2001; Harding et al., 2002).

Despite a reduction in snow coverage, the maximum amount of snow that accumulates in winter may still increase, depending on the changes in winter precipitation and temperatures in spring. It is sometimes supposed that higher precipitation would increase snow depth and delay the onset of snowmelt in spring (e.g. Callaghan et al., 1998). In none of the model experiments in the present study (chapter 8), nor in the sensitivity analysis in chapter 6, it was found that more precipitation leads to a delay in snowmelt, provided that it is accompanied by a temperature rise. It seems therefore likely that a rise in temperature will lead to a shorter snow season, regardless of a significant increase in precipitation in winter.

As a consequence of the reduced snow coverage, the importance of sublimation in the annual water balance diminishes. Extension of the snow-free season means however that the total amount of evapotranspiration increases by about 15 % (table 8.2). In the Tana Basin this increase was only observed in spring; during the rest of the summer, evapotranspiration rates remained more or less unchanged (figure 8.17). The relative importance of evaporation in the water balance therefore decreased, despite the higher temperatures in the scenario run. In absolute terms, evapotranspiration increased mostly at high elevations (figure 8.16.c).

Due to the earlier snowmelt the spring peak in river discharge is moved forward by about 3 weeks. Depending on the amount of snow that accumulates in winter, peak flows may

202

also be lower than at present (figures 8.18, 8.23). Both in summer and in winter, river discharge is expected to increase. However, the snowmelt runoff peak still dominates the hydrological regime, and there was no evidence of a substantial decrease in the seasonality of sub-arctic runoff, as was supposed by Rouse et al. (1997) and Anisimov & Fitzharris (2001). In the Tana Basin, an increase in precipitation of 25 % resulted in almost 40 % more discharge (table 8.2). A circumpolar increase in runoff to the Arctic Ocean might have an effect on the freshwater budget of the Arctic Ocean, and ultimately on the thermohaline circulation in the North Atlantic (Lewis et al., 2000).

Changes in climate, snow coverage and hydrology, as outlined above, are substantial, and will influence the ecological processes in the sub-arctic landscape; however, the response of the vegetation to these changes may in turn modify the impacts of climate change on the hydrology. As noted in chapter 8, it is possible that increased shrub height will enhance snow accumulation, which leads to a delay in snow cover depletion (Sturm et al., 2001; Liston et al., 2002). Although snow depth measurements in the Kidisjoki catchment did not reveal any significant correlation between snow depth and vegetation type (chapter 3), this issue may certainly be relevant, and needs more attention in hydrological impact studies. On the other hand, the large-scale snow cover depletion in the Tana Basin, as observed by satellites (chapter 4), is primarily controlled by elevation and, accordingly, temperature. According to Kallio et al. (1969) and others, the snow cover in the Kevo region may disappear much earlier on the barren fell summits, where snow is more exposed to wind transport. However, in both years in which the patterns of snow cover depletion in the Tana Basin were studied, there were no indications that this phenomenon was very important at the scale of 1 km^2 pixels of the SPOT VEGETATION sensor.

Increased plant growth will also change the amount of transpiration in the summer season. At high latitudes, vegetation growth rarely starts until the snow has melted (Harding et al., 2002), and in the first few weeks the canopy is still developing, which may limit the transpiration in this period. Both processes have been ignored in the hydrological model that was used in the scenario study, as for practical reasons a constant crop factor was adopted to simulate vegetation controls on evaporation (chapter 7). Obviously, there is a need for a better representation of vegetation properties in hydrological models such as TANAFLOW.

Furthermore, changes in the distribution of permafrost may influence the hydrology in many arctic and sub-arctic environments as well. However, since Northern Fennoscandia already belongs to the sporadic or discontinuous permafrost zone (King & Seppälä, 1988), a further reduction in permafrost extent will most likely have little influence on infiltration and groundwater storage. Changes in permafrost occurrence have therefore been ignored in the present analysis, but they will be of importance in other areas (cf. Van der Linden et al., 2002).

9.3 Large-scale hydrological modelling in sub-arctic environments

The impact of changes in climate on sub-arctic hydrology and river runoff can be studied in different ways. First of all, one may want to have a look at historical records and to analyse the changes over the past centuries. Although in most northern areas measurements on climate and river discharge started relatively late, temperature and precipitation in the Tana Basin have been monitored since 1876, and river discharge since 1911. However, the range of climatic change in the past century is much smaller the range expected for the future. Although there has been a significant increase in precipitation over the past 100 years (Lee et al., 2000), a significant trend in the discharge of the Tana River could not be found (chapter 2). Also in other rivers flowing to the Arctic Ocean there is no discernible long-term trend in discharge (Shiklomanov et al., 2000). It is possible that the magnitude of the response of rivers to changes in climate is too small to be recognised, given the natural variability of the process and the quality of the data. In other words, there may be a signal to noise problem (cf. Rastetter, 1996). Other observations are only available for an even shorter period. Satellite observations on snow cover extent have only been made since the 1970s, and only in recent years several sensors have been launched that are optimised for frequent snow mapping (chapter 4). Analogue studies of past climatic change in, for example, the Holocene, provide the opportunity to study the impacts in an integrated way. However, although the magnitude of change has been much larger than in the past century, many environmental variables are only known by proxy, and uncertainties can be large. Moreover, it is unknown whether the rate of change in the past has been similar to what is expected for the future.

For these reasons, this study used a large-scale hydrological model to simulate the response of sub-arctic hydrology to climate change. A main objective of this model was to simulate the hydrological processes in a spatially distributed way, in order to analyse the changes in snow coverage and evapotranspiration, in addition to river discharge. Hydrological modelling, and especially distributed modelling, is however severely limited by the proper representation of processes at the appropriate scale, the heterogeneity of catchments, and the availability of sufficient input data (Beven, 1989; Blöschl & Sivapalan, 1995; Beven, 2000). This is especially true for northern environments, where data are usually sparse. Despite the relatively large number of meteorological stations in the Tana Basin, the quality of the data was insufficient to make a proper estimate of the actual amount of precipitation in the catchment area, as demonstrated in chapter 5. In addition to uncertainties about the exact amount and distribution of precipitation, there is a tremendous variation in topography, vegetation, soil type, and other factors that control the hydrology of large areas, such as the Tana Basin. Many previous studies rely therefore on simple, empirical models to describe the relationship between precipitation and runoff (e.g. Kwadijk, 1993). These simple relationships often work tolerably well, partly because the natural variability averages out at a larger scale, partly because precipitation is by far the most important factor controlling runoff within a given setting (Phillips, 1999). In chapter 5 it was demonstrated that such an empirical model can be applied to the sub-arctic Tana Basin with reasonable results.

Empirical models give however little information about the hydrological processes acting within the catchment. Moreover, the empirical relationships that are found, may not be valid for a different climate. If global warming results in an earlier snowmelt, the radiation intensity during snowmelt will be different from current conditions (figure 6.10). Evapotranspiration is controlled by a multitude of factors, and the response to global warming is therefore not necessarily linearly related to temperature. For these reasons, the relatively simple model of chapter 5 has been extended with physically-based algorithms for evapotranspiration, snow accumulation and snowmelt (chapter 7). The introduction of more detailed process descriptions did not significantly improve the model performance, but perhaps this should not be expected if the amount and quality of the input data have not improved (cf. De Wit, 1999). What is more, it should be noted that the complex models of snowmelt and evapotranspiration were applied to the Tana Basin without calibration, and in this respect the similar overall model performance is in fact encouraging. As noted in chapter 5, the degree-day factor, that was used in the simple model to simulate snowmelt, and that was obtained by calibration against river discharge, had an important influence on the timing of the simulated annual runoff peak. By omitting this factor, a powerful control on the modelling efficiency has been omitted as well. Nevertheless, the model performance, as expressed by several error statistics, remained more or less the same (chapter 7). This supports the conclusion that the "hybrid" approach that has been followed in this study, in which observations and data from a regional climate model are combined to drive a physically-based hydrological model, is effective in large-scale impact studies.

In the end, there was no evidence for a marked change in snowmelt rates in the scenario runs, despite the fact that the intensity of solar radiation is significantly reduced earlier in spring (figure 6.10). Apparently, this effect is counterbalanced by a decrease in the "cold content" of the snow pack, which is due to higher temperatures in winter. However, although the temperature was significantly higher, evaporation rates in summer remained more or less similar or even reduced slightly, something that was not foreseen by the simpler model (figures 8.17 and 8.24.b). This illustrates the usefulness of physical, process-based models in global change studies. The fact that there was, in general, not too much difference between the scenario study in chapter 8, and the sensitivity analysis of the simple, empirical model in chapter 6, increases the confidence in the results of the latter. For the range of changes in temperature and precipitation that have been considered in chapter 6, the results may be a sound indication of the changes in snow coverage and river discharge that can be expected.

One of the objectives of the model that was developed in this thesis, was to simulate the spatial patterns in snow cover dynamics and evapotranspiration. However, a model that is able to estimate river discharge at the catchment outlet reasonably well, does not necessarily simulate the spatial processes within the catchment correctly. Before the spatial patterns simulated by the model can be accepted, they need to be validated. For this reason, remote sensing techniques have shown to be useful not only in providing spatially distributed input data, but also in evaluating the model results in a spatial way. In this study, moderate-resolution sensors such as SPOT VEGETATION, appeared to be useful in monitoring snow cover dynamics, because of their high imaging frequency, as

well as their mid-infrared spectral band, that allows easy discrimination between clouds and snow (chapter 4). Satellite observations on snow coverage provided insight in the large-scale patterns of snow cover depletion, that could not be inferred from observations at meteorological stations in the Tana Basin. With the arrival of new sensors, global datasets on snow cover extent, vegetation development, and many other ecosystem properties will become increasingly available in the coming years. Hydrologists should take advantage of these developments, not only by looking for trends in – for example – snow coverage, but also by using these observations to validate the models that are used in climate change studies. This thesis is one of the few studies in which this approach has been followed (but see for example Blöschl et al., 1991), although the spatial validation of the modified model version in chapter 7 was unfortunately hindered in the absence of appropriate satellite images in the simulation period. Nevertheless, it was demonstrated in chapter 6 that such a spatial validation provides additional information on the model performance. Obviously, there is a need for image processing techniques that are able to map the snow cover extent with a high degree of accuracy, and methods such as the one employed in chapter 4, should therefore be tested thoroughly, and be developed further.

As discussed in the previous section, several possible feedback effects, such as the response of vegetation, have not yet been taken into account in the present study. Changes in snow coverage or in the flux of water vapour to the atmosphere may also provide a profound feedback on the climate system itself. In this thesis, a large-scale hydrological model was coupled to a regional climate model in only one direction. In order to come to a complete, integrated assessment of the impact of climate change on northern ecosystems, it is necessary to couple atmospheric models with hydrological and vegetation models in a full, two-way linking (Kite & Haberlandt, 1999). Clearly, this will be an even more complex task than the coupling of atmospheric and oceanic models, and it may still take several years to accomplish. Studies like the present are only a first step, but demonstrate the advantages of such an approach.

9.4   Recommendations for further research

From the discussions above, a number of recommendations for further research can be deduced:

- First of all, several processes are still poorly represented in TANAFLOW. In particular the simulation of evapotranspiration needs more attention. In order to include the effects of vegetation development, transpiration rates should be simulated using more physical vegetation parameters, such as leaf area index, instead of a single crop factor. Moreover, it should be tried to relate these parameters to indices that can be calculated from satellite data, which could improve the spatial simulation of evapotranspiration considerably.
- In addition, the representation of soil processes is still relatively simple in the current model. This relates to the simulation of evapotranspiration by making allowances for soil moisture constraints. However, also the effects of frozen

soils on the infiltration of snow meltwater should be represented more realistically, so that differences between individual years will be properly simulated.

- On a more general level, research in arctic and sub-arctic ecosystems should focus on the interactions between hydrology and vegetation, and in particular between snow and vegetation. In order to analyse scaling effects, these interactions should not only be studied at the local scale of a field plot, but also at a larger regional or landscape scale. Satellite remote sensing techniques may prove to be useful also for this purpose.

- In order to take account of all feedback effects, studies of the impact of climate change on arctic and sub-arctic hydrology should include the response of the vegetation to global warming and changed snow cover dynamics, and this should be done in a transient way. For this purpose, hydrological models need to be coupled to vegetation models.

- Finally, it is believed that hydrological and vegetation models should also be linked with atmospheric models, in order to come to a full, integrated analysis of the magnitudes and impacts of global change on high latitude environments.

9.5   Final comments

Due to the problem of induction (Popper, 1959), the general validity of any model can never be established. By subjecting a model or hypothesis to thorough testing, with the possibility of refutation, we may however gain confidence in its validity. Models that simulate the response of ecosystems to global change can however not be tested unequivocally – unless enough time is allowed for the full ecosystem response to develop (Rastetter, 1996). The results presented in this thesis concerning changes in sub-arctic hydrology, should therefore not be regarded as predictions about what is going to happen in the coming century, but rather as an analysis of sensitivities. Nevertheless, it seems certain that climate change will have a major impact on the hydrology of areas at high latitudes, with potentially considerable feedback effects on the global climate system.

9.6   References

Anisimov, O. & B. Fitzharris (2001): Polar Regions (Arctic and Antarctic). In: J.J. McCarthy, O.F. Canziani, N.A. Leary, D.J. Dokken & K.S. White (eds.): Climate Change 2001: Impacts, Adaptation and Vulnerability. Cambridge: Cambridge University Press, p. 801-841.

Beven, K. (1989): Changing ideas in hydrology – the case of physically-based models. Journal of Hydrology 105, pp. 157-172.

Beven, K. (2000): On the future of distributed modelling in hydrology. Hydrological Processes 14, pp. 3183-3184.

Blöschl, G. & M. Sivapalan (1995): Scale issues in hydrological modelling: a review. In: J.D. Kalma & M. Sivapalan (eds.): Scale Issues in Hydrological Modelling. John Wiley & Sons, Chichester, United Kingdom, pp. 9-48.

Blöschl, G., R. Kirnbauer & D. Gutknecht (1991): Distributed snowmelt simulations in an Alpine catchment 1. Model evaluation on the basis of snow cover patterns. Water Resources Research 27, pp. 3171-3179.

Callaghan, T.V., C. Körner, O.W. Heal, S.E. Lee & J.H.C. Cornelissen (1998): Scenarios for ecosystem response to global change. In: O.W. Heal, T.V. Callaghan, J.H.C. Cornelissen, C. Körner & S.E. Lee (eds.): Global Change in Europe's cold regions. Luxembourg: Office for Official Publications of the European Communities (Ecosystems Research Report No. 27), p. 11-63.

De Wit, M.J.M. (1999): Nutrient fluxes in the Rhine and Elbe basins. Utrecht: Koninklijk Aardrijkskundig Genootschap / Faculty of Geographical Sciences, University of Utrecht (Netherlands Geographical Studies 259).

Harding, R.J., P. Kuhry, T.R. Christensen, M.T. Sykes, R. Dankers & S. van der Linden, S. (2002): Climate feedbacks at the taiga / tundra interface. Ambio, in press.

Houghton, J. T., Y. Ding, D.J. Griggs, M. Noguer, P.J. van der Linden & D. Xiaosu (eds.) (2001): Climate Change 2001: The Scientific Basis. Cambridge: Cambridge University Press.

Kallio, P., U. Laine & Y. Mäkinen (1969): Vascular flora of Inari Lapland 1: Introduction and Lycopodiaceae. Reports from the Kevo Subarctic Research Station 5, pp. 1-108.

King, L. & M. Seppälä (1988): Permafrost thickness and distribution in Finnish Lapland – results of geoelectrical soundings. Polar-Forschung 57, pp. 127-147.

Kite, G.W. & U. Haberlandt (1999): Atmospheric model data for macroscale hydrology. Journal of Hydrology 217, pp. 303-313.

Kwadijk, J.C.J. (1993): The impact of climate change on the discharge of the River Rhine. Utrecht: Koninklijk Nederlands Aardrijkskundig Genootschap / Faculty of Geographical Sciences, University of Utrecht (Nederlandse Geografische Studies 171).

Lee, S.E., M.C. Press & J.A. Lee (2000): Observed climate variations during the last 100 years in Lapland, Northern Finland. International Journal of Climatology 20, pp. 329-346.

Lewis, E.L., E.P. Jones, P. Lemke, T.D. Prowse & P. Wadhams (eds.) (2000): The Freshwater Budget of the Arctic Ocean. Dordrecht: Kluwer Academic Publishers.

Liston, G.E., J.P. McFadden, M. Sturm & R.A. Pielke, Sr. (2002): Modeled changes in arctic tundra snow, energy and moisture fluxes due to increased shrubs. Global Change Biology 8, pp. 17-32.

Phillips, J.D. (1999): Earth surface systems: complexity, order and scale. Malden, Massachusetts: Blackwell.

Popper, K.R. (1959): The logic of scientific discovery. London: Hutchinson.

Rastetter, E.B. (1996): Validating models of ecosystem response to global change. BioScience 46, pp. 190-198.

Rouse, W.R., M.S.V. Douglas, R.E. Hecky, A.E. Hershey, G.W. Kling, L. Lesack, P. Marsh, M. McDonald, B.J. Nicholson, N.T. Roulet & J.P. Smol (1997): Effects of climate change on the fresh waters of Arctic and sub-Arctic North America. Hydrological Processes 11, pp. 873-902.

Shiklomanov, I.A., A.I. Shiklomanov, R.B. Lammers, B.J. Peterson, A.I. Shiklomanov & C.J. Vorosmarty (2000): The dynamics of river water inflow to the Arctic Ocean. In: E.L. Lewis, E.P. Jones, P. Lemke, T.D. Prowse & P. Wadhams (eds.): The Freshwater Budget of the Arctic Ocean. Dordrecht: Kluwer Academic Publishers (NATO Science Series 2, Environmental Security 70), pp. 281-296.

Sturm, M., J.P. McFadden, G.E. Liston, F. Stuart Chapin III, C.H. Racine & J. Holmgren (2001): Snow-shrub interactions in Arctic tundra: a hypothesis with climatic implications. Journal of Climate 14, pp. 336-344.

Van der Linden, S., T. Virtanen, N. Oberman & P. Kuhry (2002): Sensitivity analysis of discharge in the arctic Usa basin, East-European Russia. Climatic Change, in press.
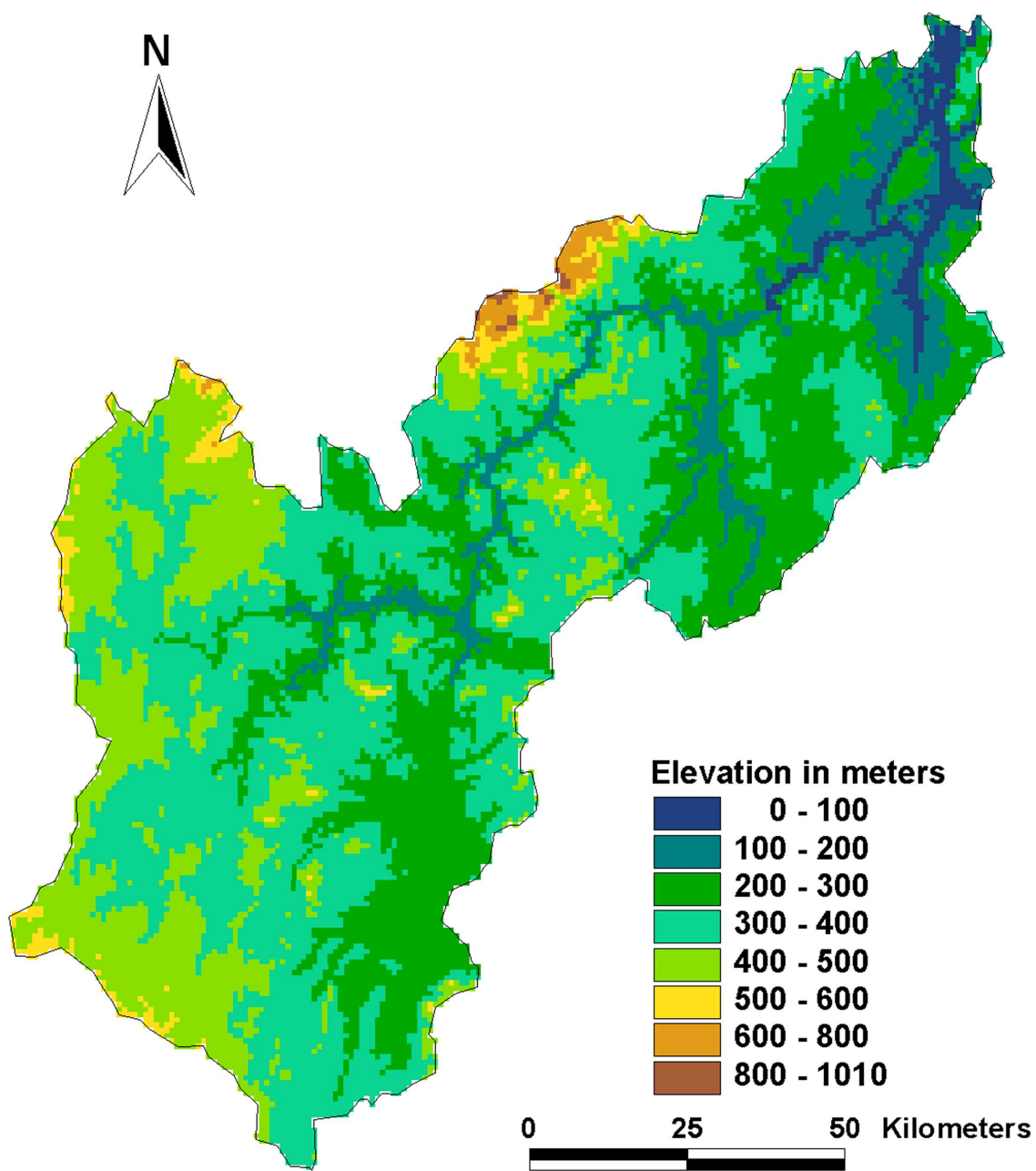
APPENDIX: COLOUR PLATES

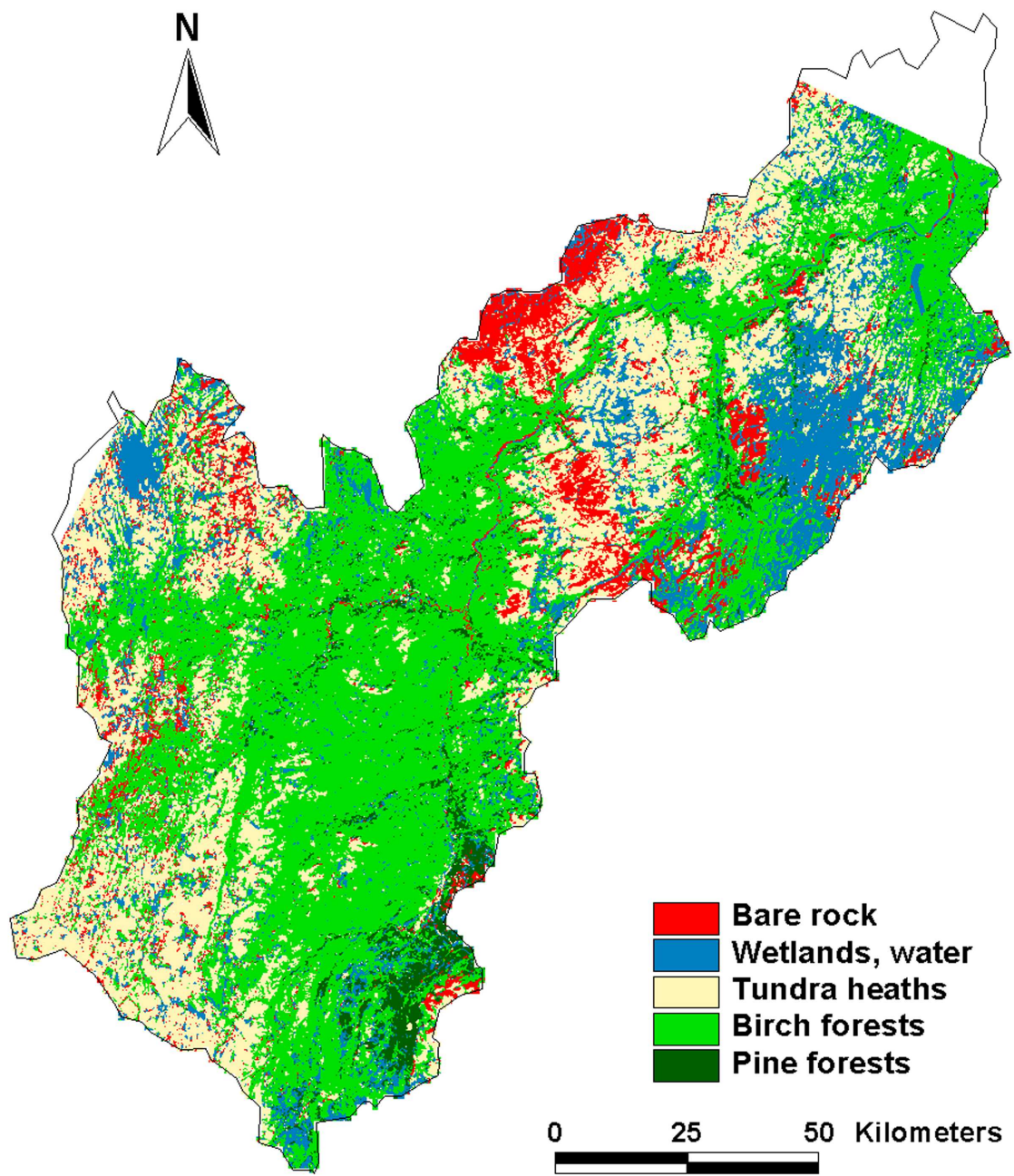**Figure 2.2** (a) Digital Elevation Model (DEM) of the Tana River Basin

Figure 2.5 Generalised vegetation map of the Tana Basin, based on a Landsat TM image of 18 July 1987
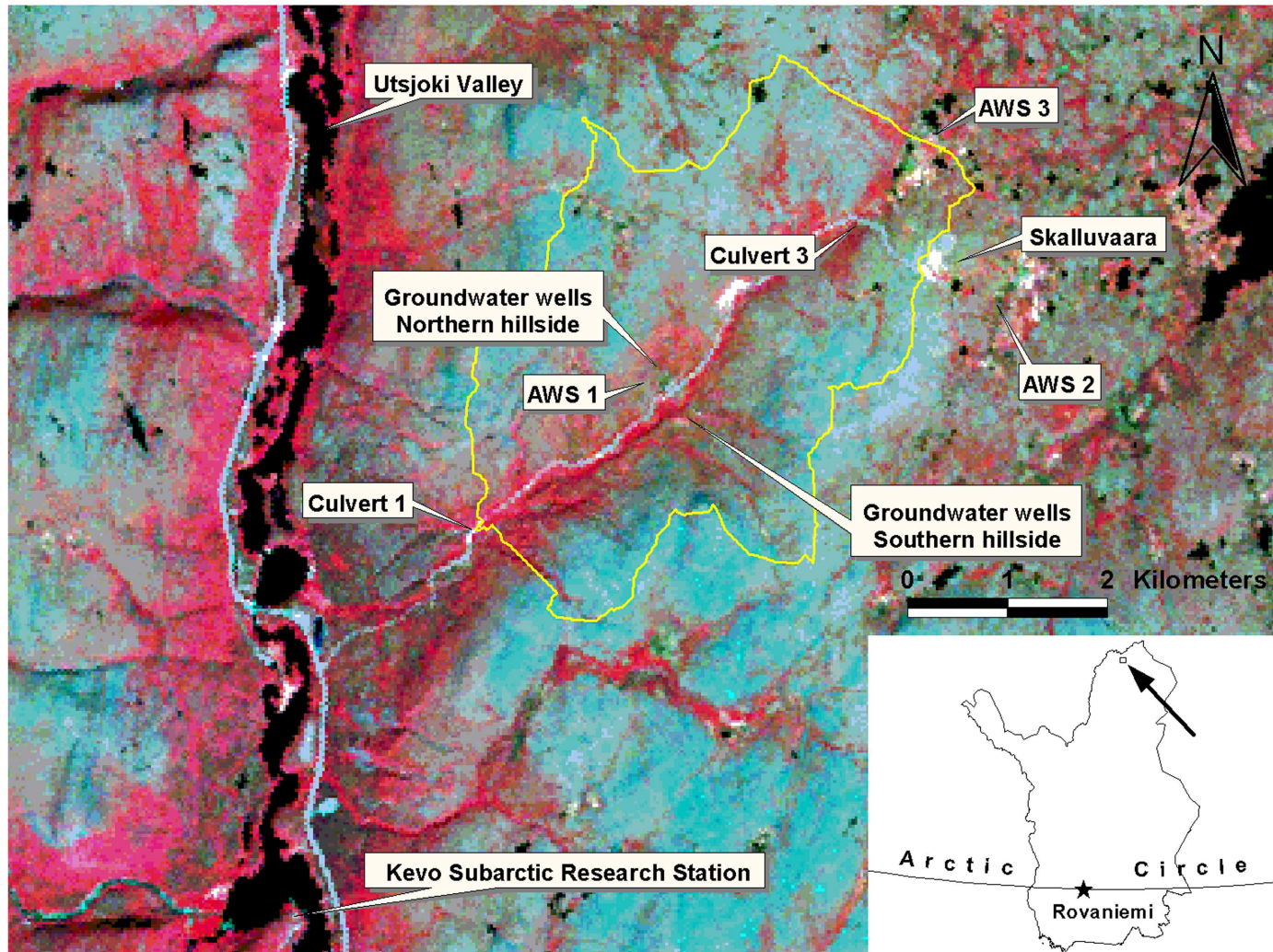
210

Figure 3.1 Location of the Kidisjoki catchment in northern Finnish Lapland. Background is a Landsat TM image of 30 June 1998 (R,G,B = band 4, 3, 2)
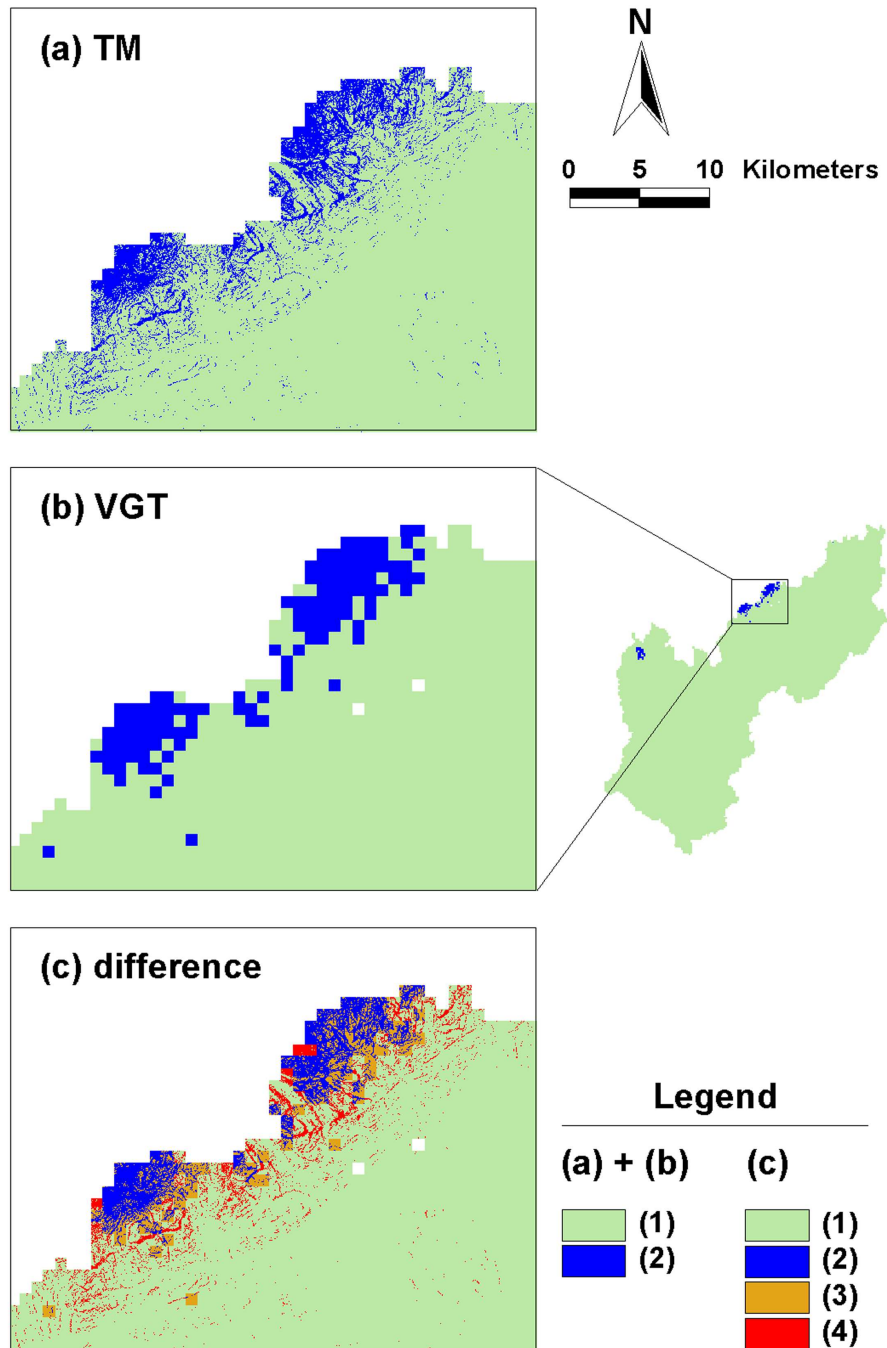
Figure 4.6 (a) Mapped snow cover in the TM image of 30-6-98; (b) mapped snow cover in the corresponding VGT image; (c) differences between (a) and (b). Legend: figure (a) + (b): 1 = snow-free, 2 = snow-covered; figure (c): 1 = snow-free in both images, 2 = snow-covered in both images, 3 = snow-free in TM and snow-covered in VGT image, 4 = snow-covered in TM and snow-free in VGT image
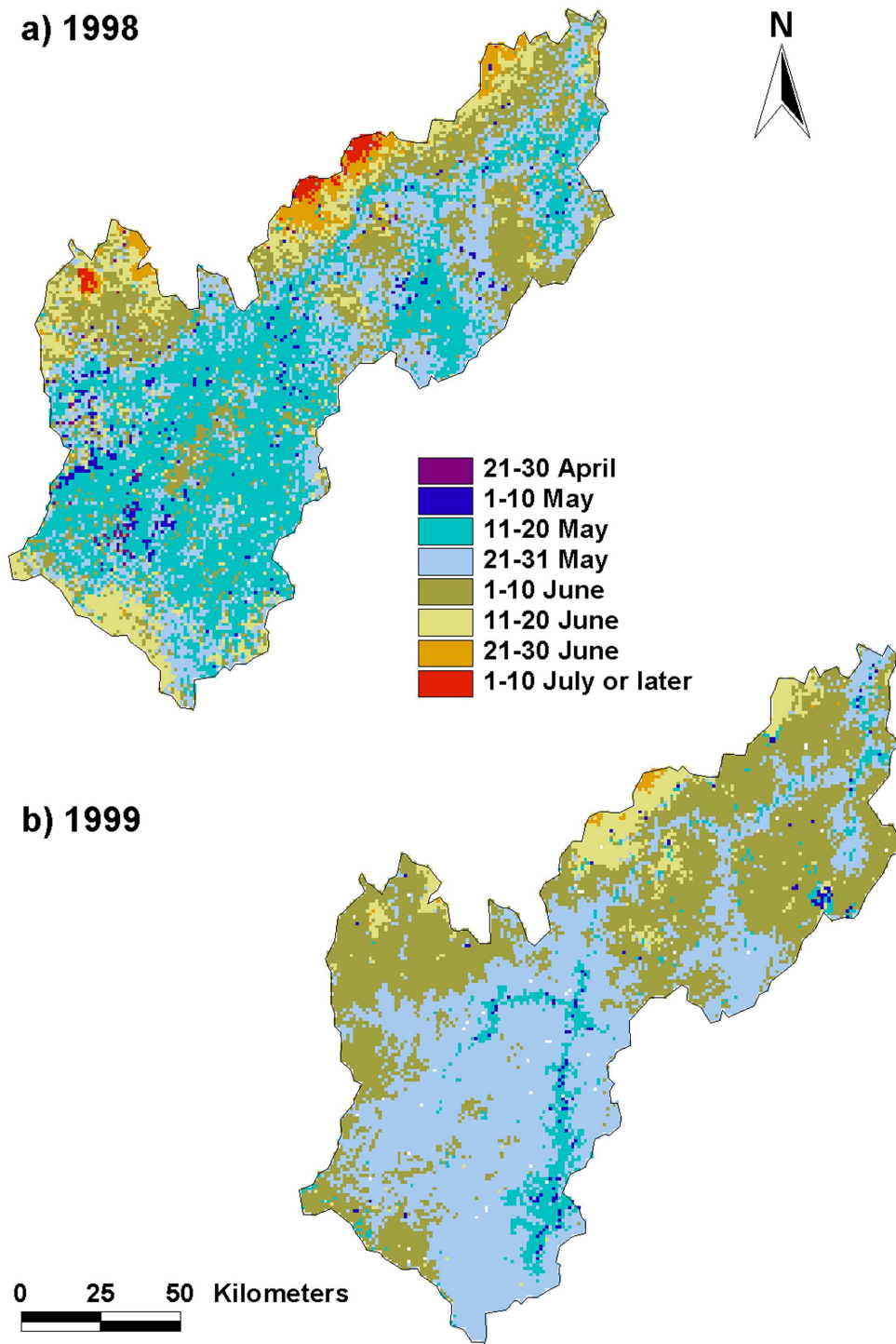
Figure 4.7 (also shown as **figure 6.3**) Disappearance of snow in the Tana Basin, based on 10-day VGT syntheses of (a) 1998 and (b) 1999
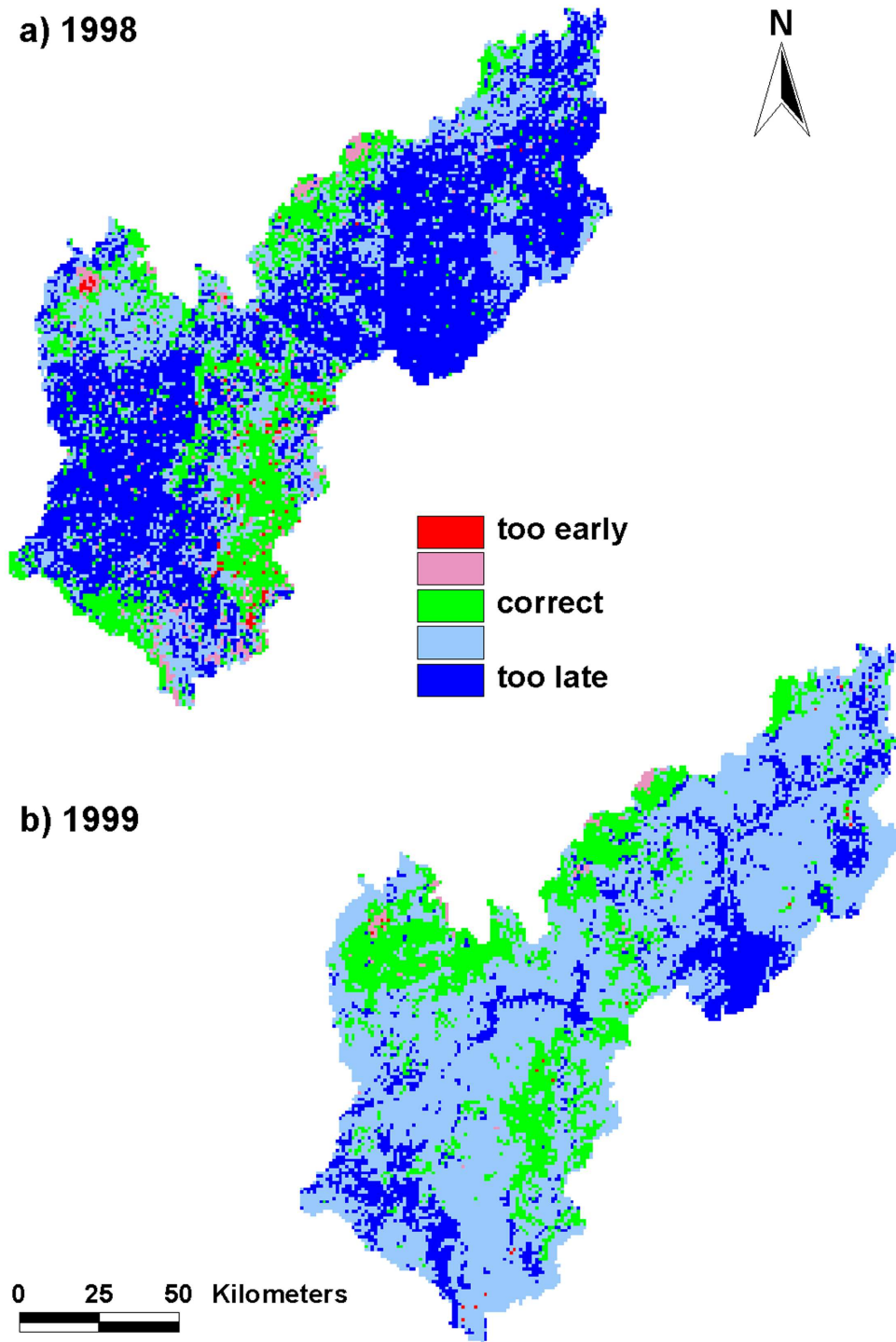
Figure 6.5 Disappearance of snow as predicted by TANAFLOW, compared with satellite observations of pixels covered by snow for more than 50%: (a) in 1998; (b) in 1999
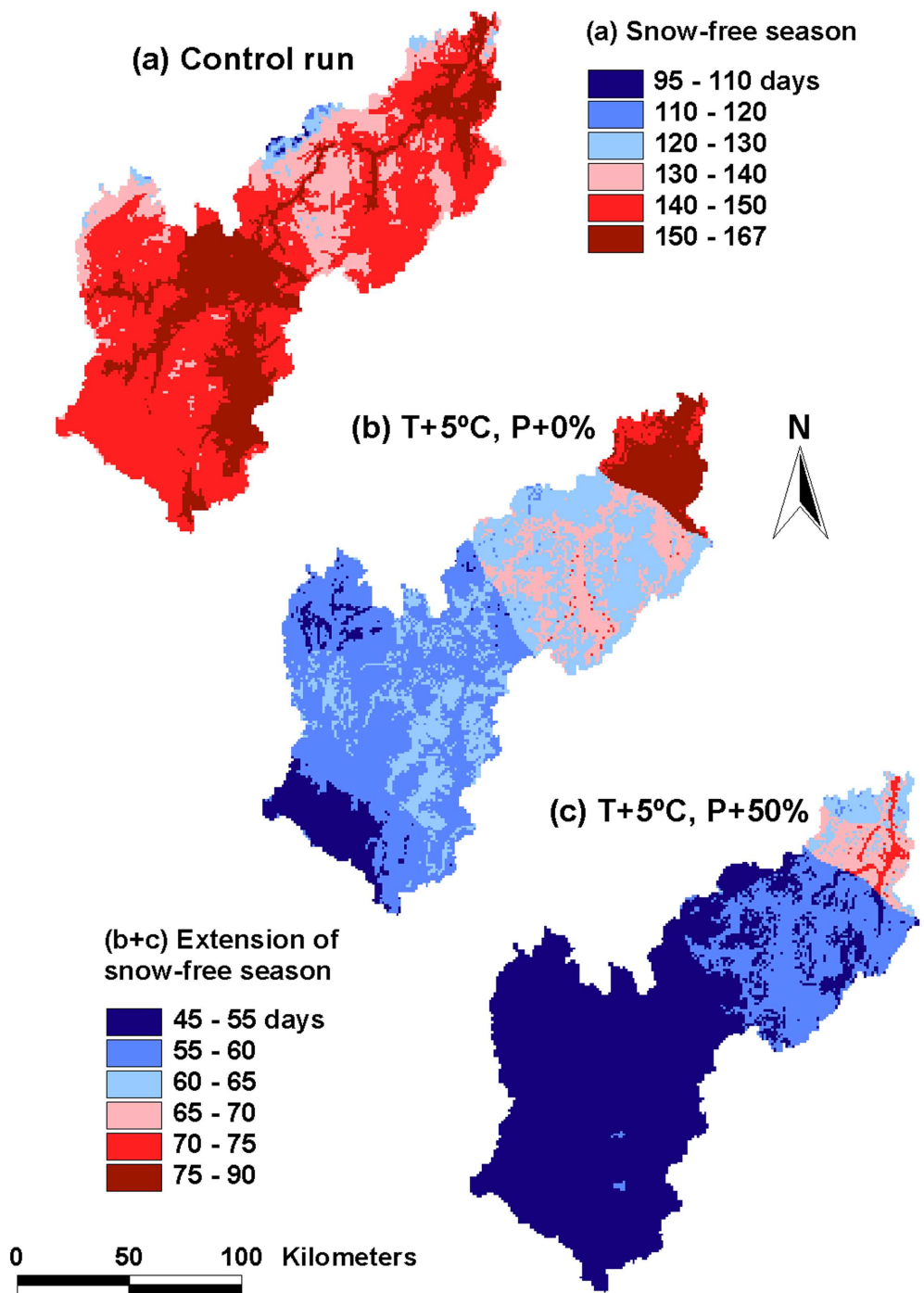
Figure 6.8 Length of the snow-free season in the Tana Basin, predicted by TANAFLOW: (a) for current climate conditions; (b) prolongation after a temperature rise of 5ºC; (c) prolongation after a combined increase in temperature and precipitation of 5ºC and 50 % respectively

a) Reference ET

N

50 - 100 mm/year
100 - 150
150 - 160
160 - 170
170 - 180
180 - 205

b) Actual ET

15 - 40 mm/year
40 - 60
60 - 70
70 - 80
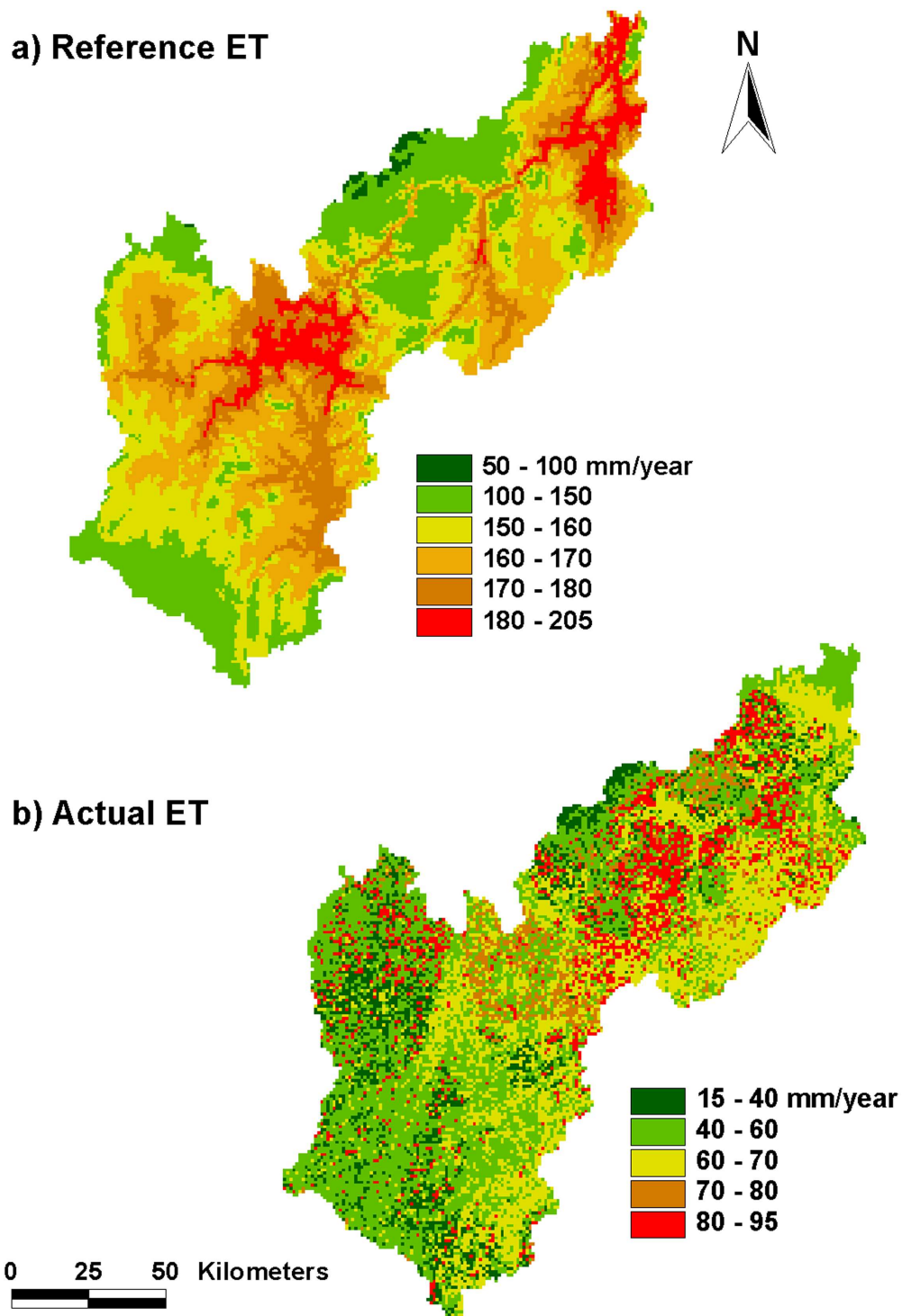80 - 95

0   25   50   Kilometers

Figure 7.8 (a) Reference crop evapotranspiration, and (b) actual evapotranspiration in the Tana Basin in mm year^{-1}

216
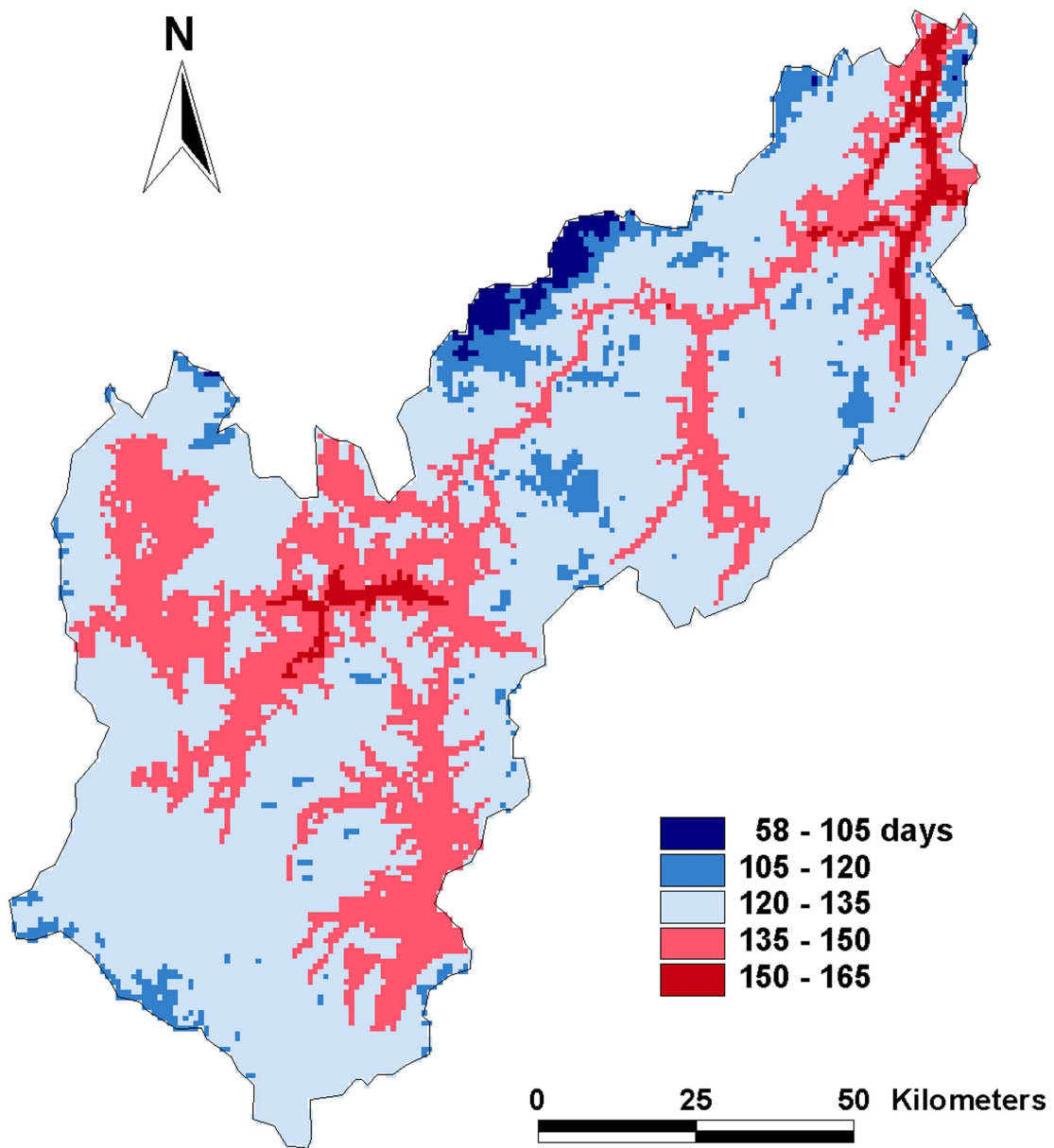
Figure 7.9 Length of the snow-free season in the Tana Basin, as simulated by TANASNOW / TANAFLOW for the period 1980-1993

Figure 8.2 Mean annual temperature in the Tana Basin in the control run (a) and the scenario run (b)

(a) control run

N

300 - 400 mm/year
400 - 500
500 - 600
600 - 700
700 - 800
800 - 900
900 - 1000
1000 - 1350

(b) scenario run

0   25   50 Kilometers

Figure 8.5 Annual precipitation in the Tana Basin in the control run (a) and the scenario run (b)

219

(a) control run

(a+b) Snow season

- 125 - 175 days
- 175 - 200
- 200 - 225
- 225 - 250
- 250 - 275
- 275 - 350

(b) scenario run

N

(c) change

(c) Shortening of snow season

- 33 - 40
- 40 - 46
- 46 - 52
- 52 - 58
- 58 - 64
- 64 - 70

0   50   100   Kilometers
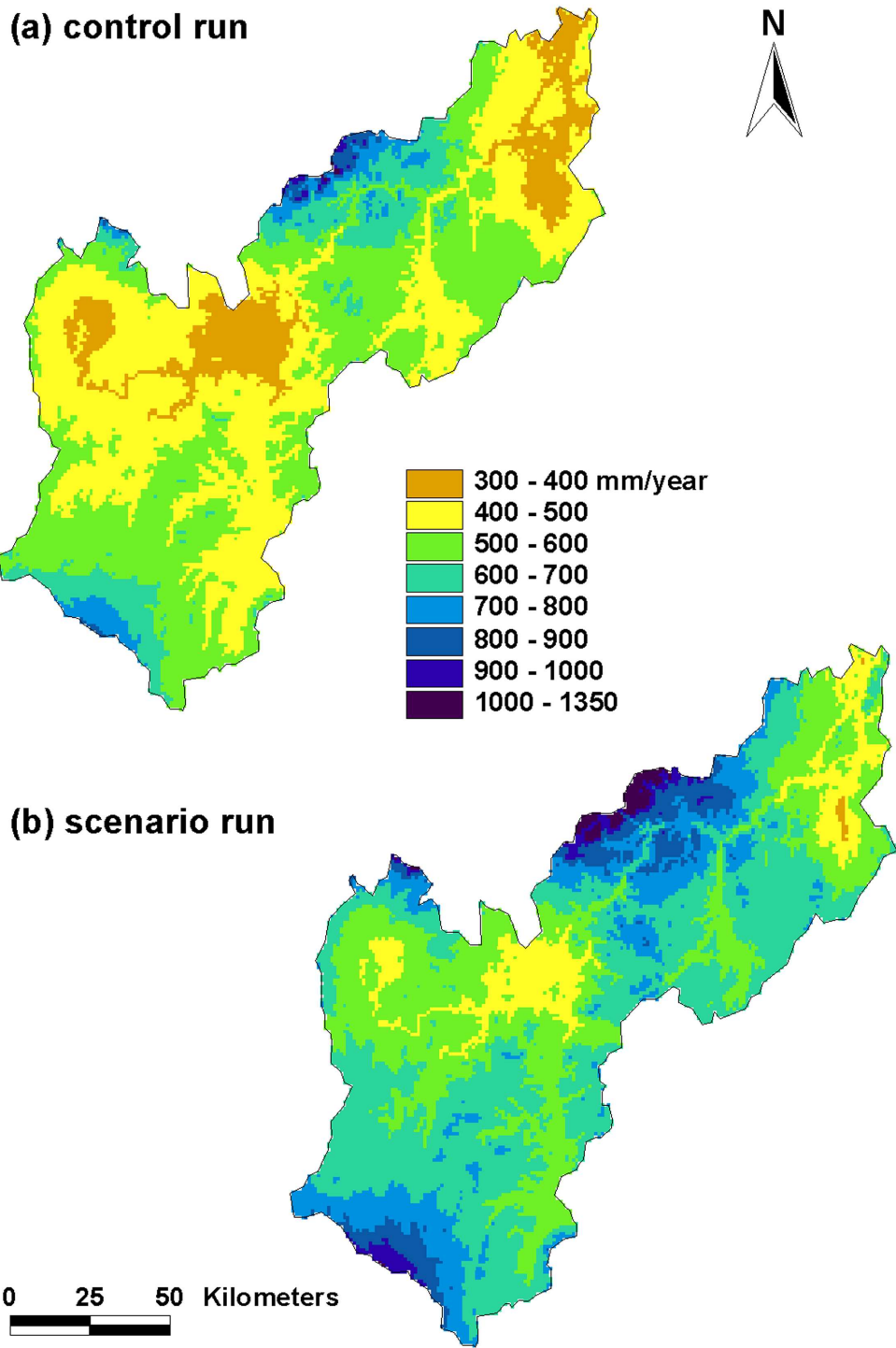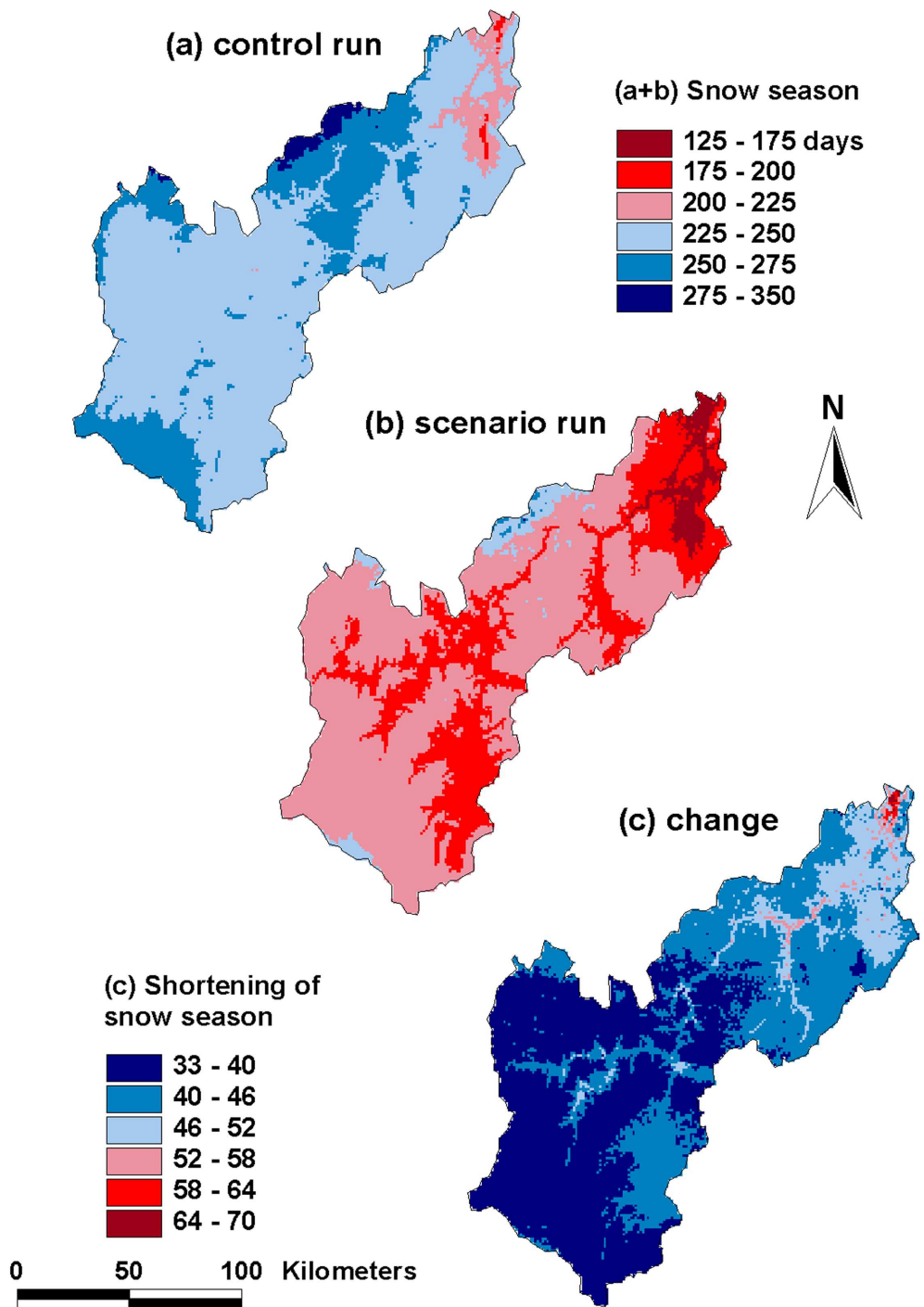
Figure 8.12 Period of snow coverage in the control run (a) and the scenario run (b), and shortening of the snow season in the scenario run (c)
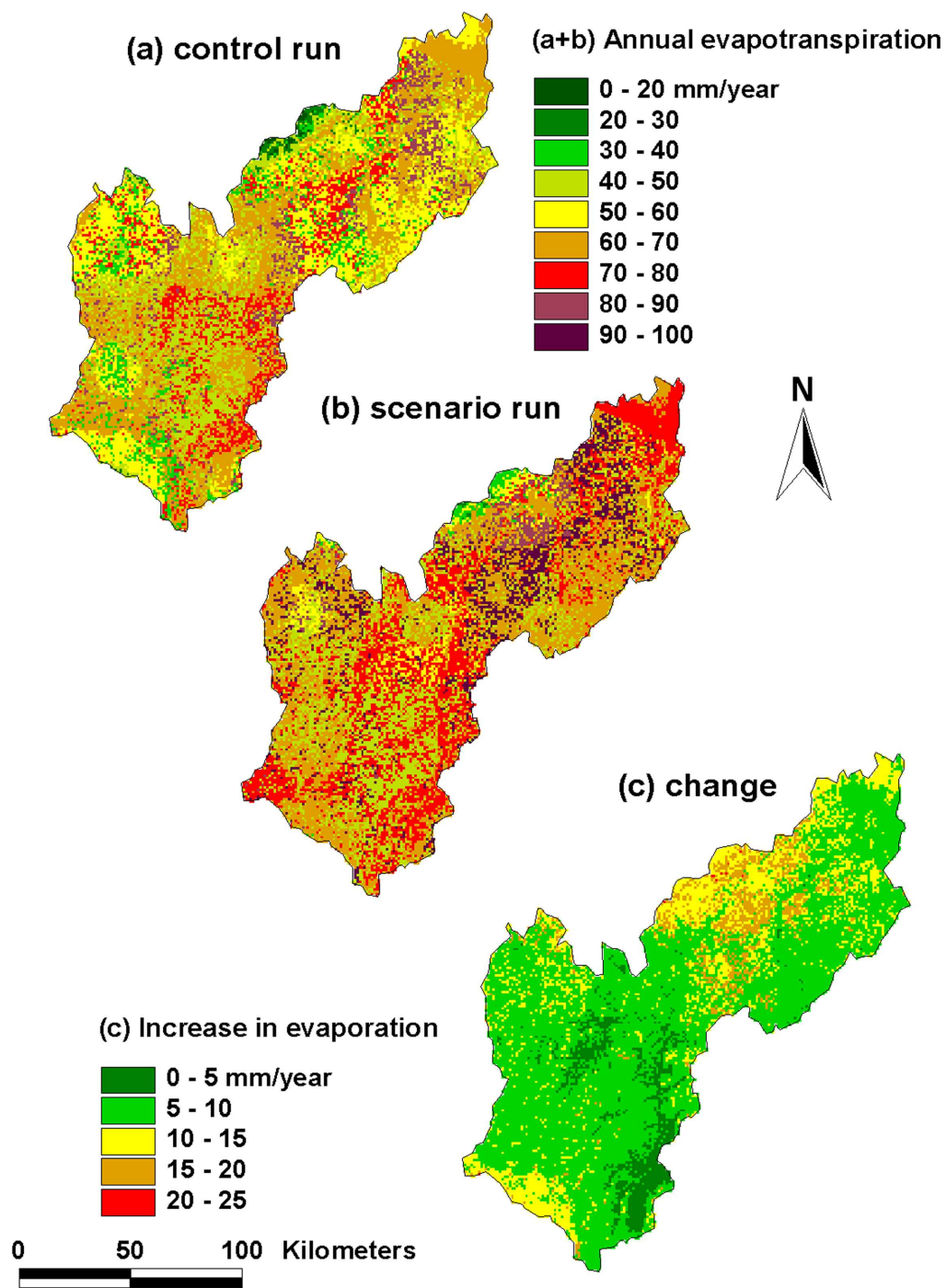
Figure 8.16 Annual evapotranspiration in the Tana Basin, in the control run (a) and the scenario run (b), and the increase in evaporation in the scenario run (c)

Figure 8.19 Length of the growing season in the Tana Basin in the control run (a) and the scenario run (b), and the increase in the scenario run in days (c)

Figure 8.20 Number of degree-days in the Tana Basin in the control run (a) and the scenario run (b), and the increase in the scenario run in degree-days (c)

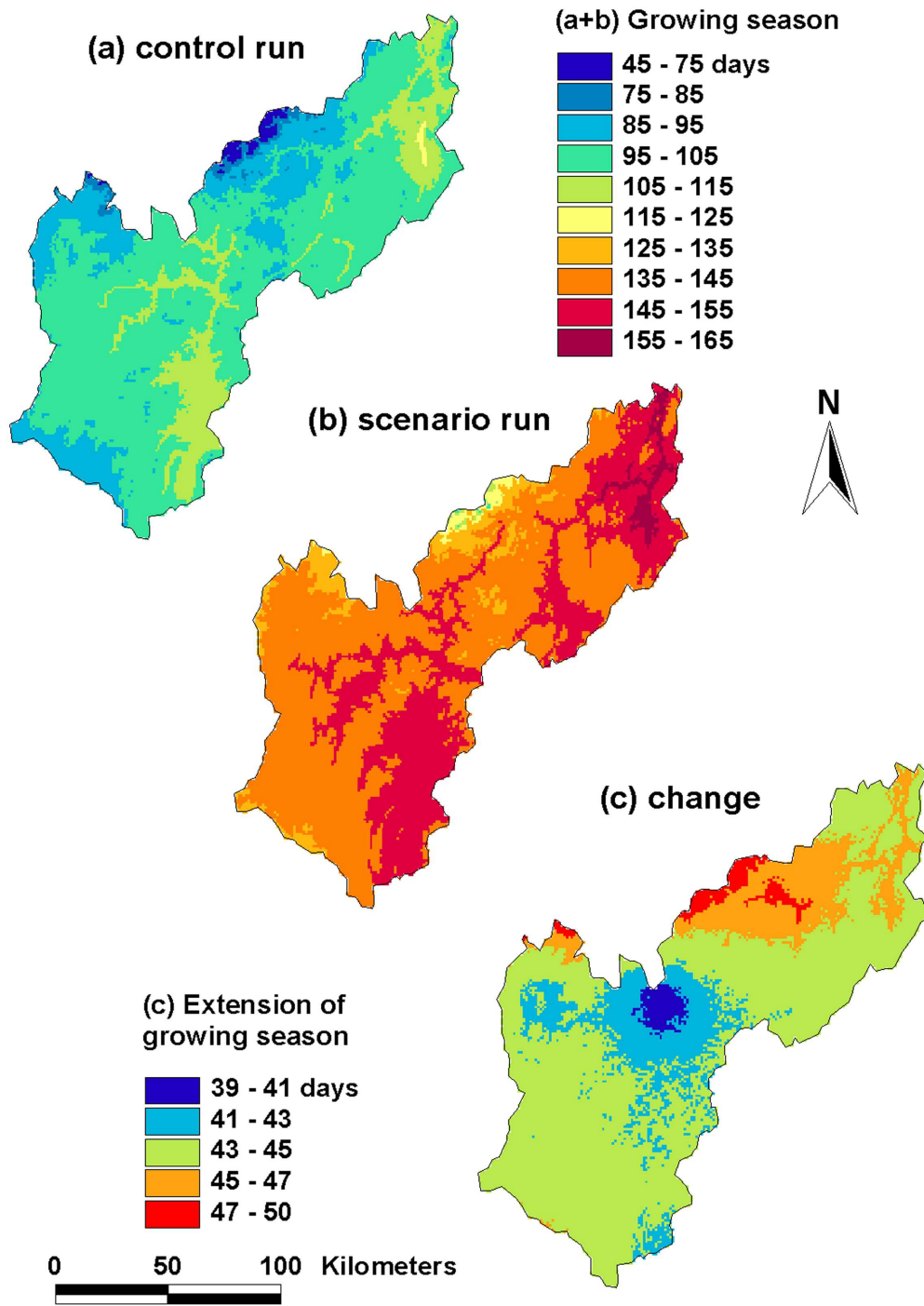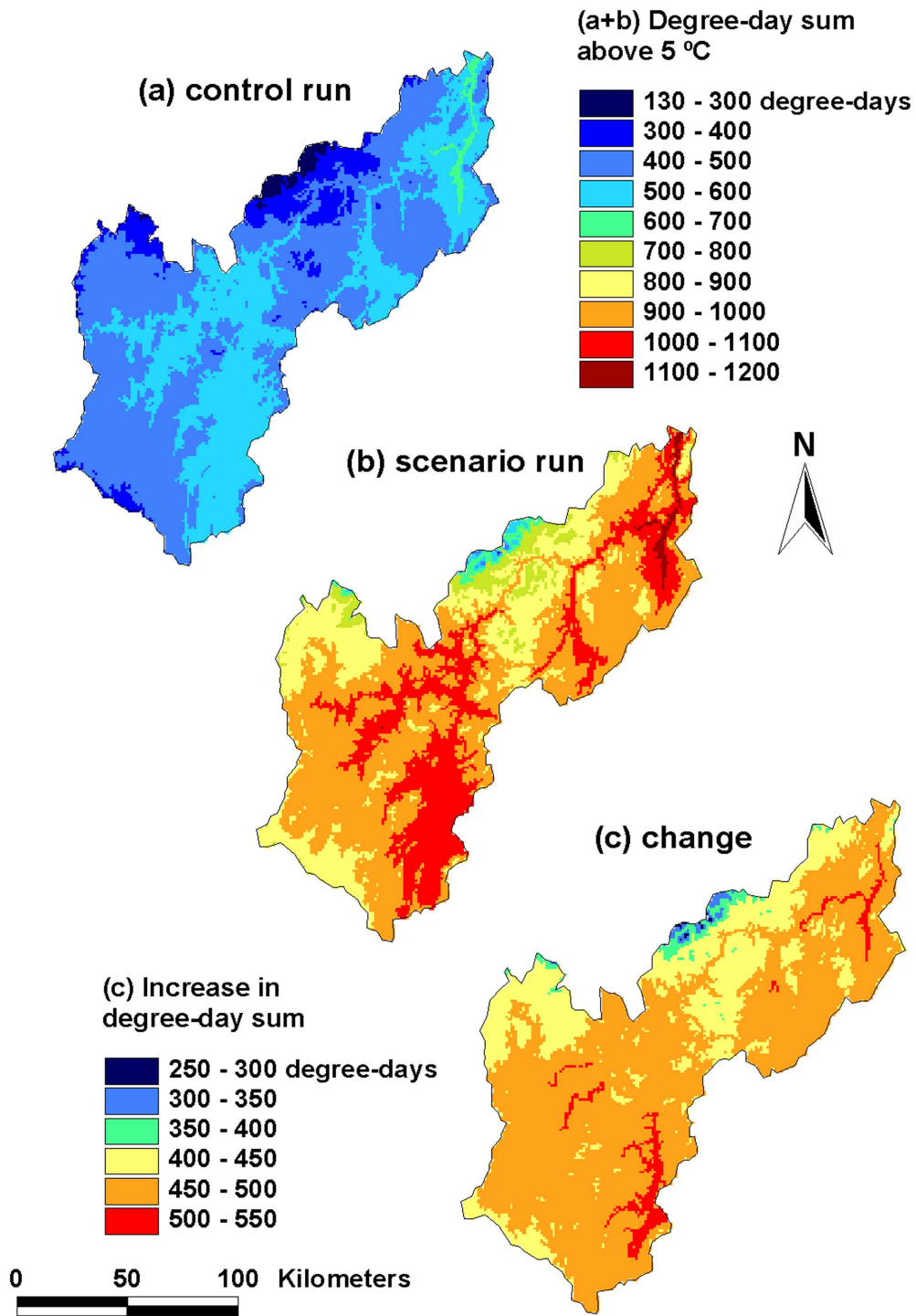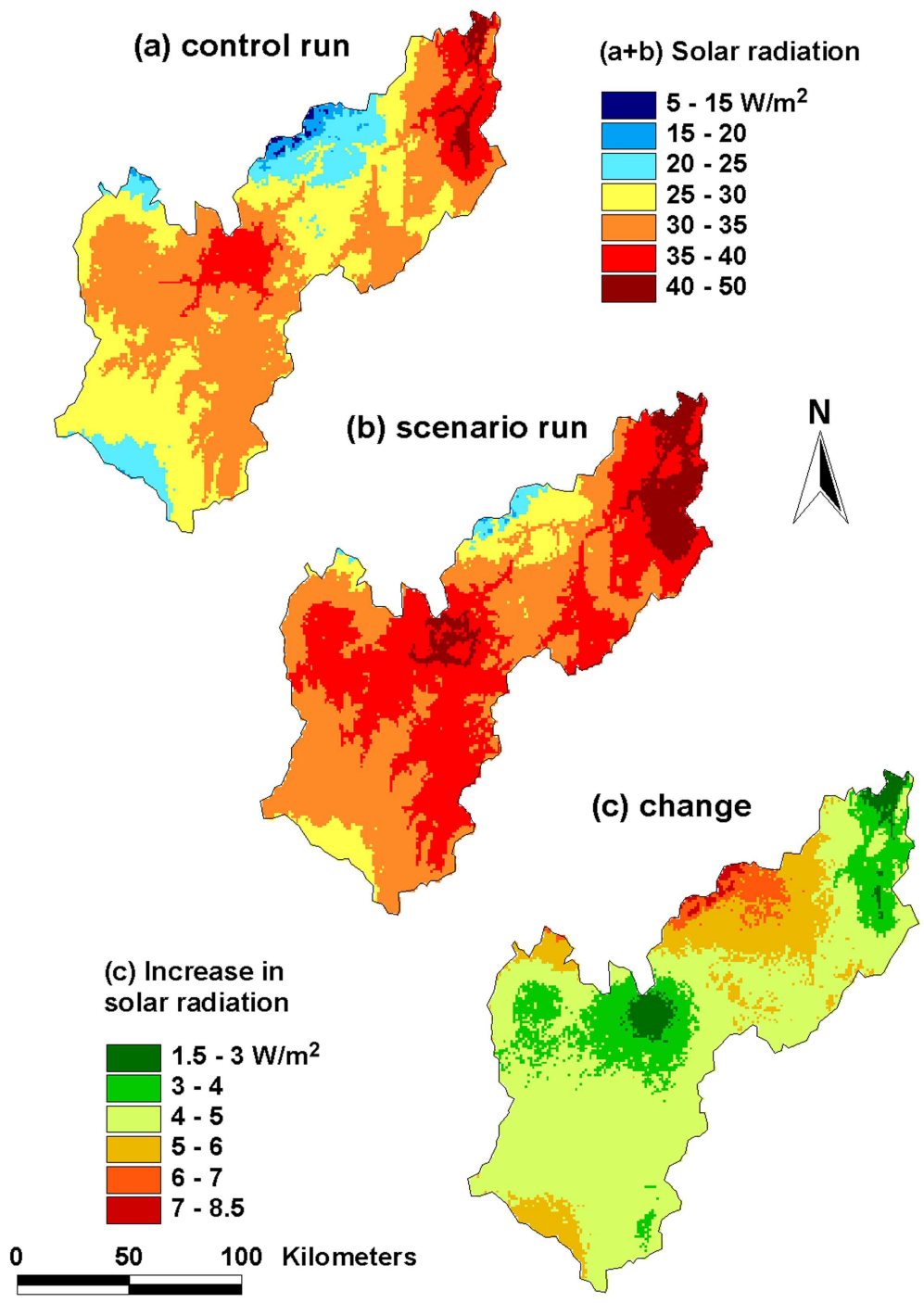**Figure 8.21** Solar radiation during the snow-free season in the control run (a) and the scenario run (b), and the increase in the scenario run in W.m^{-2} (c)

SUB-ARCTIC HYDROLOGY AND CLIMATE CHANGE:
A case study of the Tana River Basin in Northern Fennoscandia

SUMMARY

The most significant changes in climate, due to the well-known enhanced greenhouse effect, are generally expected to occur at northern high latitudes. Sub-arctic environments, that are dominated by the presence of a seasonal snow cover, may therefore be particularly sensitive to global warming. Due to changes in albedo and the amount of freshwater runoff towards the Arctic Ocean, changes in the hydrological cycle of sub-arctic areas may also provide a feedback to the global climate system. Understanding the hydrological processes operating in sub-arctic environments, and evaluating their sensitivity to climate change, is therefore an essential part of global change research. The main objective of the research presented in this thesis was to assess the sensitivity of the hydrological system of Northern Fennoscandia to human-induced climatic changes. Considering the importance of snow coverage, snowmelt and evapotranspiration in sub-arctic hydrology and ecology, special attention was paid to the spatial distribution of these components of the water balance, in addition to river discharge. To achieve this objective, a series of studies was undertaken in the Tana Basin in northernmost Finland and Norway. Central to the approach was a large-scale hydrological model of the study area. Development and application of this model involved four steps:

1   Analysis of the hydrological system of the Tana Basin, at both small and large scales, using field measurements and satellite observations (chapters 2 to 4).
2   Application of an existing water balance model, developed for the River Rhine, to the sub-arctic Tana Basin, and evaluation of the model performance (chapters 5 and 6).
3   Development of physically-based process descriptions of snowmelt and evapotranspiration, that replaced the previous, empirical formulations in the model (chapter 7).
4   Simulation of the hydrological behaviour of the Tana Basin under conditions of climate change, by using this improved model version (chapter 8).

The following sections summarise the main findings of these four different parts.

1   Hydrological processes in the sub-arctic Tana Basin

In the Tana Basin (figure 1.2), observations on climate have been made since 1876, and discharge of the Tana has been measured since 1911. Over the past century, precipitation at Karasjok, Norway, increased significantly, but at Polmak, Norway, there was no concurrent significant increase in river discharge. The only significant trend in runoff that could be found, was decreasing, and occurred in the first half of the 20th century. In the

same period, there was a significant annual warming trend at Karasjok, mainly due to higher winter temperatures (chapter 2). Apparently, there are several processes that determine the catchment response to rainfall, which may have been counteracting. It is therefore not feasible to draw any conclusions on the hydrological response to future climatic changes on the basis of historical data.

The processes of runoff generation were studied in more detail in a small (16 km^2) study area in Northern Finland (chapter 3). In this area, the components of the water balance were measured during two study periods in summer, and one in spring during snowmelt. In both summer periods, a large part of the precipitation input into the catchment was lost to evapotranspiration (table 3.1). Evaporation was promoted by the relatively high moisture contents of the soil, that also gave rise to rapid fluctuations in groundwater level. During the summer study periods, direct runoff played only a minor part in the water balance, and originated in the wetland areas only. Due to the presence of surface ice and frozen ground, direct runoff was much more important in the snowmelt period. A significant part of the volume of water that was stored in the snow pack at the end of the winter, was discharged in the first few days of the snowmelt season. This pattern may however differ from year to year, depending on the extent of soil frost.

At a much larger scale, the patterns of snow cover depletion in the Tana Basin during two snowmelt seasons were monitored by using images of the SPOT VEGETATION (VGT) sensor (chapter 4). Snow covered areas were identified by modifying an algorithm that has originally been developed for data from the Moderate Resolution Imaging Spectroradiometer (MODIS). For each 1 by 1 km pixel in the Tana Basin, the moment of snow disappearance could be registered by applying the algorithm to 10-day syntheses of VGT images. The results (figure 4.7) were largely consistent with the observed first snow-free date at meteorological stations in the area, confirming the effectiveness of moderate resolution sensors such as VGT in monitoring snow cover dynamics. In this way, large-scale patterns of snow cover depletion were observed, that could not be inferred from observations at meteorological stations in the Tana Basin.

2   Application of an existing, large-scale water balance model

This study used a hydrological model, that was based on a conceptual water balance model originally developed for the River Rhine. Being fully distributed and embedded in a Geographical Information System (GIS), this model calculates the water balance on a 10-day basis for grid cells of 1 km by 1 km. The performance of the original model in the sub-arctic environment of the Tana Basin, was evaluated in chapter 5. It was demonstrated that such a model can successfully be applied to a sub-arctic river basin, resulting in a model performance that is comparable with more temperate conditions. However, for application in impact studies of climate change, it was concluded that there was room for improvement. First of all, the simulations were complicated by uncertainties about the actual amount of precipitation over the catchment. In addition, both snowmelt and evapotranspiration were simulated by using highly empirical

methods. Accordingly, the relations that were found by calibration of the model against river discharge data, may not remain valid under changed climatic conditions.

A first indication of the magnitude of changes in the water balance, and in particular in snowmelt, that may be expected due to climate change, was obtained in chapter 6. Because of the emphasis in this study on spatial patterns in snow coverage and snowmelt, the spatial model performance was first tested by comparing the simulations with the satellite-based observations on snow cover depletion, discussed in chapter 4. Although the model was able to simulate the timing of the annual discharge peak resulting from snowmelt correctly, the depletion of the snow cover was generally too late when compared to satellite observations (figure 6.5). Nevertheless, the sensitivity analysis clearly showed that a rise in temperature may result in a considerably earlier snowmelt. A concurrent increase in precipitation may compensate for the reduction in winter snow mass, but showed little effect on the timing of snowmelt (figure 6.7). In other words, snow accumulation and snowmelt, being dependent on both temperature and precipitation, are indeed highly sensitive to changes in climate.

3   Development of physically-based process descriptions

In order to be able to make proper estimates of the consequences of climate change for the hydrology of the Tana Basin, the empirical methods of estimating snowmelt and evapotranspiration in the water balance model were replaced by two physically-based models (chapter 7). For the simulation of snow accumulation and snowmelt, a simplified energy-balance model was developed that considers the snow pack as a single layer. The well-known model of Penman-Monteith (Monteith, 1965) was chosen to simulate evapotranspiration. Both models were embedded in the water balance model and applied to the Tana Basin. Input data on temperature and precipitation were obtained from meteorological stations in the area, while radiation, humidity and wind speed data were derived from a regional climate model (RCM). The model performance was evaluated by using river discharge data and satellite observations on snow coverage. The snow module was tested separately by comparing the simulated snow water equivalent with observed snow depths at four meteorological stations in and around the Tana Basin. At these locations, the growth of the snow pack was represented realistically, and the disappearance of the snow cover was predicted with an accuracy of several days (figure 7.4). With respect to the simulation of river discharge and large-scale snow cover depletion, the model performance is described by an efficiency coefficient of 0.64 in the validation period, which is similar to the "old" model version, that used empirical routines for snowmelt and evapotranspiration. However, in its modified form, the model uses more detailed process descriptions and is less dependent on calibration. In addition, the model has become robust and should be more reliable when applied to different climatic conditions.

4   Assessing the impacts of climate change

Due to the enhanced greenhouse effect, the mean annual temperature in the Tana Basin may rise by more than 5 degrees Celsius in the coming century, and precipitation may increase by 25 %. The impacts of these changes on the hydrology of the Tana Basin were investigated in chapter 8. The improved, physically-based model version was used to simulate the hydrological behaviour of the Tana Basin under conditions of climate change. Climate change scenarios were derived from a RCM, driven by a general circulation model (GCM). All input data were obtained directly from the RCM, but the differences in temperature and precipitation between the control and scenario runs were also applied to meteorological observations. In all model experiments that were considered, the snow-free season in the scenario run was extended by more than 30 days at higher elevations, to 70 days or more days close to the Barents Sea (figure 8.12). Consequently, the amount of solar radiation that is received during the snow-free season, increased by about 16 %. This increase in the annual radiation sum may be of importance for the tundra vegetation, that consists mainly of low shrubs and heath. Due to the shorter snow season, the annual amount of sublimation decreased by 30 %, while the amount of evapotranspiration in summer increased by about 15 % (figure 8.17). River discharge increased as well, by almost 40 % on an annual basis (table 8.2).

This study demonstrates that changes in climate, as predicted for the coming century, will have a significant impact on snow coverage, evapotranspiration and freshwater runoff in the Tana Basin. These changes will influence the ecological processes in the sub-arctic landscape. However, the response of the vegetation to different climate and snow conditions may in turn modify the hydrological response to climate change. In the present study this possible feedback effect has not yet been taken into account. Further research in arctic and sub-arctic ecosystems should therefore focus on the interactions between hydrology and vegetation, and in particular between snow and vegetation. In order to take account of all feedback effects, hydrological models need to be adapted and linked to climate and vegetation models. Only in this way, it may be possible to obtain a full, integrated analysis of the impacts of global change on high latitudes, and the potential feedback effects on the global climate system.

SUBARCTISCHE HYDROLOGIE
EN KLIMAATSVERANDERINGEN:
Een studie in het stroomgebied van de Tana Rivier
in het noorden van Fennoscandië

SAMENVATTING

De grootste veranderingen in klimaat, veroorzaakt door het welbekende versterkte broeikaseffect, worden in het algemeen verwacht op hoge breedten op het noordelijk halfrond. Subarctische milieus, die worden gekenmerkt door een langdurige bedekking met sneeuw in het winterseizoen, zijn daarom mogelijk bijzonder gevoelig voor klimaatsveranderingen. Door veranderingen in albedo en de hoeveelheid zoet water die naar de Arctische Oceaan wordt afgevoerd, kunnen veranderingen in de hydrologische kringloop van subarctische gebieden op hun beurt zelfs weer van invloed zijn op het wereldwijde klimaatsysteem. Het begrijpen van de hydrologische processen die werkzaam zijn in subarctische milieus, en het beoordelen van hun gevoeligheid voor veranderingen in het klimaat, zijn daarom een essentieel onderdeel van het onderzoek naar klimaatsverandering. Het belangrijkste doel van het onderzoek in dit proefschrift was om de gevoeligheid vast te stellen van het hydrologische systeem van Noord-Fennoscandië voor veranderingen in het klimaat die door de mens worden veroorzaakt. Gezien het belang van bedekking met sneeuw, sneeuwsmelt en evapotranspiratie in de hydrologie en ecologie van subarctische gebieden, is er, naast rivierafvoer, speciale aandacht besteed aan de ruimtelijke verdeling in deze componenten van de waterbalans. Om dit doel te bereiken, zijn een aantal studies ondernomen in het stroomgebied van de rivier de Tana, in het uiterste noorden van Finland en Noorwegen. Het onderzoek is opgezet rond een grootschalig hydrologisch model van het studiegebied. Het ontwikkelen en toepassen van dit model gebeurde in vier stappen:

1   Een analyse van het hydrologische systeem van het Tana stroomgebied, zowel op kleine als op grote schaal, waarbij gebruik werd gemaakt van veldmetingen en satellietwaarnemingen (hoofdstuk 2 tot en met 4).
2   Toepassing van een bestaand waterbalansmodel, ontwikkeld voor de Rijn, op het subarctische stroomgebied van de Tana, en evaluatie van de modelprestaties (hoofdstukken 5 en 6).
3   Ontwikkeling van fysische procesbeschrijvingen van sneeuwsmelt en evapotranspiratie, ter vervanging van de oude, empirische formules in het model (hoofdstuk 7).
4   Simulatie van het hydrologische gedrag van het Tana stroomgebied onder veranderde klimaatscondities, gebruik makend van deze verbeterde versie van het model (hoofdstuk 8).

In de volgende paragrafen worden de belangrijkste bevindingen van deze vier onderdelen samengevat.

1   Hydrologische processen in het subarctische stroomgebied van de Tana

In het stroomgebied van de Tana (figuur 1.2) worden sinds 1876 waarnemingen gedaan van het klimaat, en de afvoer van de Tana wordt gemeten sinds 1911. Over de afgelopen eeuw is de neerslag in Karasjok (Noorwegen) significant toegenomen, maar er was geen gelijktijdige toename van de afvoer bij Polmak (Noorwegen). De enige significante trend in afvoer die kon worden gevonden, vond plaats in de eerste helft van de 20^e eeuw, en was dalend. In dezelfde periode was er een significante stijging van de jaarlijkse temperatuur in Karasjok, hoofdzakelijk veroorzaakt door hogere temperaturen in de winter (hoofdstuk 2). Klaarblijkelijk zijn er verschillende processen die de respons van het stroomgebied op neerslag bepalen, en die elkaar mogelijk hebben tegengewerkt. Het is daarom niet verstandig om op basis van historische gegevens conclusies te trekken over de gevolgen van toekomstige klimaatsveranderingen voor de hydrologie.

De processen die een rol spelen bij het ontstaan van afvoer zijn in detail bestudeerd in een klein (16 km^2) studiegebied in Noord-Finland (hoofdstuk 3). Gedurende twee onderzoeksperioden in de zomer, en één in de lente tijdens het smelten van de sneeuw, zijn de componenten van de waterbalans in dit gebied gemeten. In beide zomerperioden ging een groot deel van de totale input van neerslag in het gebied verloren aan verdamping (tabel 3.1). De verdamping werd bevorderd door het hoge vochtgehalte van de bodem, dat tevens aanleiding gaf tot snelle fluctuaties in de grondwaterstand. Directe afvoer was relatief onbelangrijk in de waterbalans van de beide zomerperioden, en ontstond alleen in de moeraslanden. In de sneeuwsmeltperiode was directe afvoer veel belangrijker door de aanwezigheid van ijs op de grond en bevroren bodems. Een aanzienlijk gedeelte van het volume water dat aan het eind van de winter was opgeslagen in het sneeuwdek, werd in de eerste paar dagen van het sneeuwsmeltseizoen afgevoerd. Dit beeld kan echter van jaar tot jaar verschillen, afhankelijk van de mate waarin de bodem bevroren is.

Op een veel grotere schaal zijn de patronen in het verdwijnen van het sneeuwdek waargenomen met behulp van beelden van de SPOT VEGETATION (VGT) sensor. Met sneeuw bedekte gebieden werden geïdentificeerd door gebruik te maken van een aangepast algoritme, dat oorspronkelijk is ontwikkeld voor data van de *Moderate Resolution Imaging Spectroradiometer* (MODIS). Door het algoritme toe te passen op 10-daagse syntheses van VGT-beelden, kon het moment van het verdwijnen van de sneeuw worden vastgesteld voor iedere pixel van 1 bij 1 km in het stroomgebied van de Tana. De resultaten (figuur 4.7) waren grotendeels in overeenstemming met de waargenomen eerste sneeuwvrije dag op de meteorologische stations in het gebied, wat de effectiviteit van sensoren als de VGT in het waarnemen van sneeuwdynamiek bevestigd. Op deze manier konden grootschalige patronen in het verdwijnen van de sneeuw worden waargenomen, die niet uit de waarnemingen op de meteorologische stations in het Tana stroomgebied konden worden gehaald.

230

2 Toepassing van een bestaand, grootschalig waterbalansmodel

In dit onderzoek is gebruik gemaakt van een hydrologisch model, dat is gebaseerd op een conceptueel waterbalansmodel dat oorspronkelijk is ontwikkeld voor de Rijn. Het model is volledig ruimtelijk gedistribueerd en ingepast in een geografisch informatie systeem (GIS), en berekent op 10-daagse basis de waterbalans van rastercellen van 1 bij 1 km. De prestaties van het oorspronkelijke model in het subarctische milieu van het Tana stroomgebied, zijn geëvalueerd in hoofdstuk 5. Dit toonde aan dat een dergelijk model succesvol kan worden toegepast op subarctische stroomgebieden, wat leidt tot vergelijkbare prestaties als in meer gematigde streken. De conclusie luidde echter dat er voor toepassing in klimaateffectstudies wel degelijk ruimte was voor verbetering. Ten eerste werden de simulaties bemoeilijkt door onzekerheden over de werkelijke hoeveelheid neerslag die in het stroomgebied valt. Daar komt bij dat zowel sneeuwsmelt als evapotranspiratie werden gesimuleerd door middel van zeer empirische methoden. De relaties die worden gevonden door het model te kalibreren met afvoerdata, zijn daarom mogelijkerwijs niet geldig onder andere klimaatcondities.

Een eerste indicatie van de grootte van de veranderingen in de waterbalans, en dan vooral in sneeuwsmelt, die kunnen optreden als gevolg van klimaatsveranderingen, werd verkregen in hoofdstuk 6. Vanwege de nadruk die er in dit onderzoek wordt gelegd op de ruimtelijke patronen in sneeuwbedekking en sneeuwsmelt, werden de ruimtelijke modelprestaties eerst getest door de simulaties te vergelijken met de waarnemingen gebaseerd op satellietbeelden, die zijn beschreven in hoofdstuk 4. Hoewel het model in staat bleek om het moment van de jaarlijkse afvoerpiek, die het gevolg is van sneeuwsmelt, correct weer te geven, was het moment van verdwijnen van de sneeuw in het algemeen te laat in vergelijking met de satellietwaarnemingen (figuur 6.5). De gevoeligheidsanalyse liet niettemin zien dat een stijging van temperatuur kan leiden tot een aanzienlijk vervroegde sneeuwsmelt. Een gelijktijdige toename van de neerslag zal mogelijkerwijs de afname in de hoeveelheid sneeuw compenseren, maar liet tegelijkertijd weinig invloed zien op het tijdstip waarop de sneeuwsmelt plaatsvindt (figuur 6.7). Met andere woorden, zowel de accumulatie als het smelten van de sneeuw zijn, door hun afhankelijkheid van temperatuur en neerslag, inderdaad erg gevoelig voor veranderingen in het klimaat.

3 Ontwikkeling van fysische procesbeschrijvingen

Om een juiste inschatting te kunnen maken van de gevolgen van klimaatsveranderingen voor de hydrologie van het Tana stroomgebied, werden de empirische formules van sneeuwsmelt en verdamping in het model vervangen door twee fysische modellen (hoofdstuk 7). Om de accumulatie en het smelten van de sneeuw te simuleren, werd een vereenvoudigd energiebalansmodel ontwikkeld dat het sneeuwdek beschouwt als één enkele laag. Het welbekende model van Penman-Monteith (Monteith, 1965) werd gebruikt om evapotranspiratie te simuleren. Beide modellen werden ingepast in het waterbalansmodel en toegepast op het stroomgebied van de Tana. De invoergegevens van temperatuur en neerslag werden verkregen van de meteorologische stations in het gebied,

terwijl straling, luchtvochtigheid en windsnelheid uit een regionaal klimaat model (RCM) werden gehaald. De prestaties van het model werden geëvalueerd met behulp van afvoergegevens en satellietwaarnemingen aan de sneeuwbedekking. De sneeuwmodule werd bovendien afzonderlijk getest door de gesimuleerde hoeveelheid sneeuw te vergelijken met waargenomen sneeuwdiktes op vier meteorologische stations in en nabij het Tana stroomgebied. Op deze locaties werd de groei van het sneeuwdek realistisch weergegeven, en het verdwijnen van de sneeuw werd voorspeld met een nauwkeurigheid van enkele dagen (figuur 7.4). Met betrekking tot de simulatie van de rivierafvoer worden de modelprestaties weergegeven door een "efficiëntie-coëfficiënt" van 0.64, wat vergelijkbaar is met de "oude" versie van het model waarin gebruik werd gemaakt van empirische routines voor sneeuwsmelt en verdamping. In zijn huidige, aangepaste vorm maakt het model echter gebruik van meer gedetailleerde procesbeschrijvingen, en is minder afhankelijk van kalibratie. Bovendien is het model robuust geworden en zou het betrouwbaarder moeten zijn wanneer het wordt toegepast onder andere klimaatcondities.

4   Inschatting van de gevolgen van klimaatsveranderingen

Als gevolg van het versterkte broeikaseffect kan in de komende eeuw de gemiddelde jaarlijkse temperatuur in het stroomgebied van de Tana met meer dan 5 graden Celsius stijgen, en de neerslag kan met 25 % toenemen. De gevolgen van deze veranderingen voor de hydrologie van het Tana stroomgebied werden onderzocht in hoofdstuk 8. De verbeterde, fysische versie van het model werd gebruikt om het hydrologische gedrag van het stroomgebied onder veranderde klimaatcondities te simuleren. De klimaatscenario's zijn afkomstig van een RCM dat is aangestuurd door een globaal klimaatmodel (GCM). Alle invoergegevens werden rechtstreeks ontleend aan dit RCM, maar daarnaast werden de verschillen in temperatuur en neerslag tussen de controle- en de scenariorun ook opgeteld bij de meteorologische waarnemingen. In alle modelexperimenten die zijn uitgevoerd, nam de lengte van het sneeuwvrije seizoen toe met meer dan 30 dagen op de hoger gelegen delen, tot 70 dagen of meer dicht bij de Barentszee (figuur 8.12). Als gevolg hiervan nam de hoeveelheid zonnestraling die gedurende het sneeuwvrije seizoen wordt ontvangen, toe met ongeveer 16 %. Deze toename in de jaarlijkse hoeveelheid straling kan van belang zijn voor de toendravegetatie, die voornamelijk bestaat uit lage struiken en alpiene heide. Dankzij het kortere sneeuwseizoen nam de jaarlijkse hoeveelheid sublimatie af met 30 %, terwijl de hoeveelheid evapotranspiratie in de zomer toenam met ongeveer 15 % (figuur 8.17). De rivierafvoer nam eveneens toe met bijna 40 % op jaarbasis (tabel 8.2).

Deze studie toont aan dat veranderingen in klimaat, zoals voorspeld voor de komende eeuw, belangrijke gevolgen zullen hebben op de bedekking met sneeuw, de verdamping en de zoetwaterafvoer in het stroomgebied van de Tana. Deze veranderingen zullen de ecologische processen in het subarctische landschap beïnvloeden. De respons van de vegetatie op veranderde klimaat- en sneeuwcondities kan op haar beurt echter de hydrologische respons op klimaatsveranderingen veranderen. In het huidige onderzoek is nog geen rekening gehouden met dit mogelijke terugkoppelingseffect. Verder onderzoek in arctische en subarctische ecosystemen moet zich dan ook richten op de interacties

232

tussen de hydrologie en de vegetatie, en dan met name tussen sneeuw en vegetatie. Om met alle feedbackeffecten rekening te houden, zouden hydrologische modellen aangepast moeten worden en gekoppeld moeten worden aan klimaat- en vegetatiemodellen. Mogelijkerwijs kan alleen op deze manier een volledige, geïntegreerde analyse worden verkregen van de gevolgen van klimaatsveranderingen voor hoge breedten, en de mogelijke terugkoppelingsmechanismen op het klimaatsysteem van de wereld.

ACKNOWLEDGEMENTS

CURRICULUM VITAE

Rutger Dankers was born on July 24, 1973 in Tilburg (The Netherlands), and grew up in Oisterwijk. Between 1985 and 1991 he attended classes at Maurick College in Vught, and after that he started studying Physical Geography at the University of Utrecht. During his studies he specialised in geomorphological and hydrological modelling, and remote sensing techniques, and had an internship at Candiensten in Amsterdam, in which he evaluated ER Mapper, a software package for image processing. Rutger graduated in 1997 on a study of landslide activity near Alcoy, Southeast Spain. In 1998 he started working in the EU-project BASIS (*Assessing the consequences of global changes for the Barents Sea Region: the Barents Sea Impact Study*) as an employed PhD student at the Faculty of Geographical Sciences of the University of Utrecht. As part of his PhD study he carried out several field studies in Northernmost Finland, in cooperation with the Kevo Subarctic Research Institute of the University of Turku, Finland, and the Centre for Ecology and Hydrology (formerly the Institute of Hydrology) at Wallingford, United Kingdom. In the coming years Rutger will continue to work in Northern environments as a post-doctoral researcher at the University of Utrecht within the framework of the EU-project BALANCE (*Global Change Vulnerabilities in the Barents Region: Linking Arctic Natural Resources, Climate Change and Economies*).